CRUISE REPORT: Tropical Atlantic

(Updated AUG 2013)

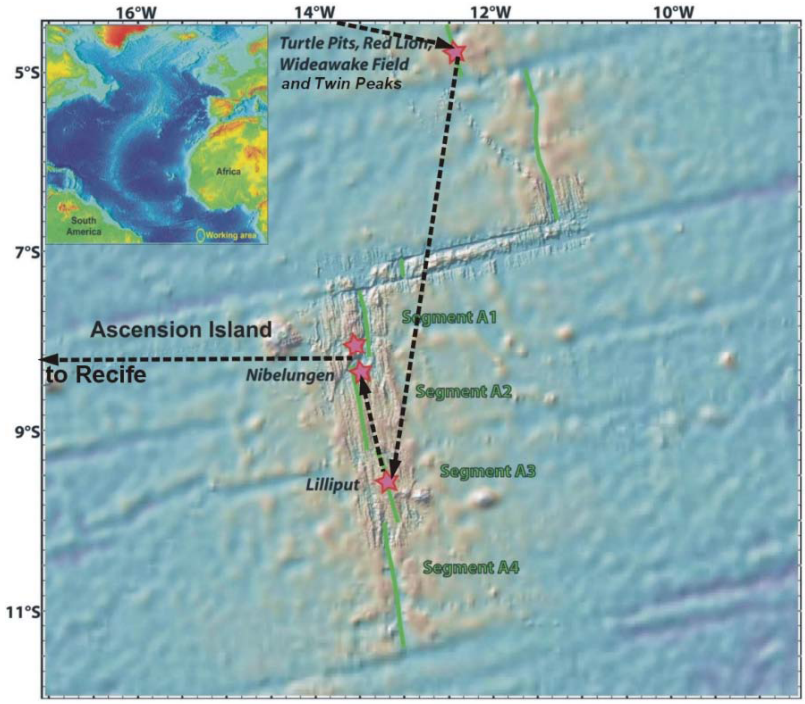

Highlights

Cruise Summary Information

WOCE Section Designation	Tropical Atlantic Leg 1
Expedition designation (ExpoCodes)	06MT20060427
Alias	M68/1
Chief Scientists	Dr. Andrea Koschinsky / IUB
Dates	2006 APR 27 – 2006 JUN 2
Ship	*r/v Meteor*
Ports of call	Bridgetown (Barbados) – Recife (Brazil)
Geographic Boundaries	4° 44' 18" S 13° 33' 19" W 12° 19' 30" W 9° 35' 30" S
Stations	27
Floats and drifters deployed	4 ARGO floats deployed
Moorings deployed or recovered	0

Contact Information:
Dr. Andrea Koschinsky
International University Bremen; now: Jacobs University Bremen
GmbH, Campus Ring 8, D-28759 Bremen, Germany
e-mail: a.koschinsky@iu-bremen.de

Links To Select Topics

Shaded sections are not relevant to this cruise or were not available when this report was compiled.

CRUISE REPORT: Tropical Atlantic

(Updated AUG 2013)

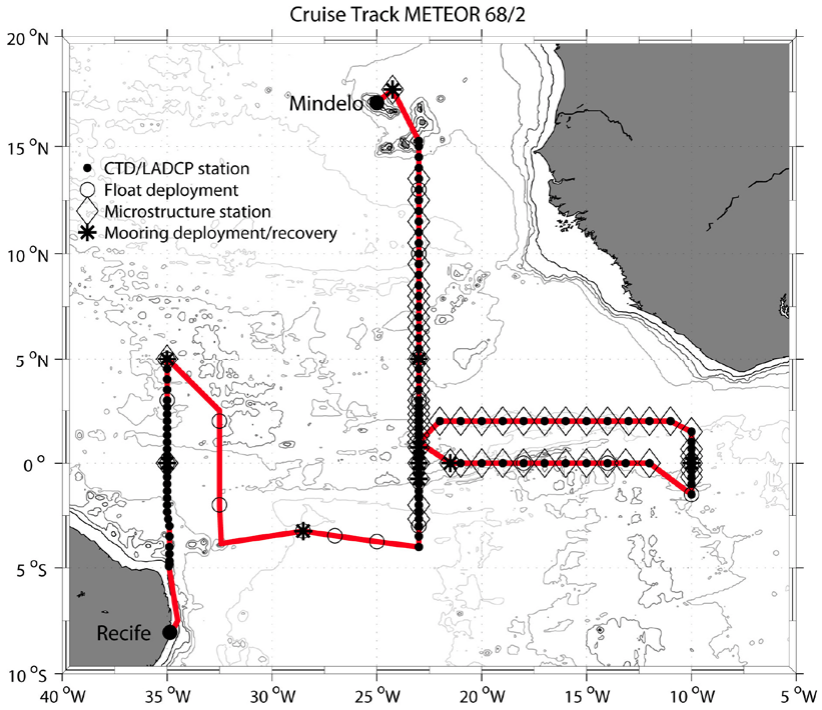

Highlights

Cruise Summary Information

WOCE Section Designation	Tropical Atlantic Leg 2
Expedition designation (ExpoCodes)	06MT20060606
Alias	M68/2
Chief Scientists	Dr. Peter Brandt / IMF-GEOMAR
Dates	2006 JUN 6 - 2006 JUL 9
Ship	*r/v Meteor*
Ports of call	Recife (Brazil) - Mindelo (Cape Verde)
Geographic Boundaries	17° 35' 27" N 35° W 9° 50' W 4° 54' 57" S
Stations	115
Floats and drifters deployed	18 isobaric profiling drifters (floats) deployed
Moorings deployed or recovered	2 recovered, 7 deployed

Contact Information:

Dr. Peter Brandt

Leibniz-Institut für Meereswissenschaften an der Universität Kiel

Düsternbrooker Weg 20, 24105 • Kiel - Germany

e-mail:pbrandt@ifmgeomar.de

Links To Select Topics

Shaded sections are not relevant to this cruise or were not available when this report was compiled.

CRUISE REPORT: Tropical Atlantic

(Updated AUG 2013)

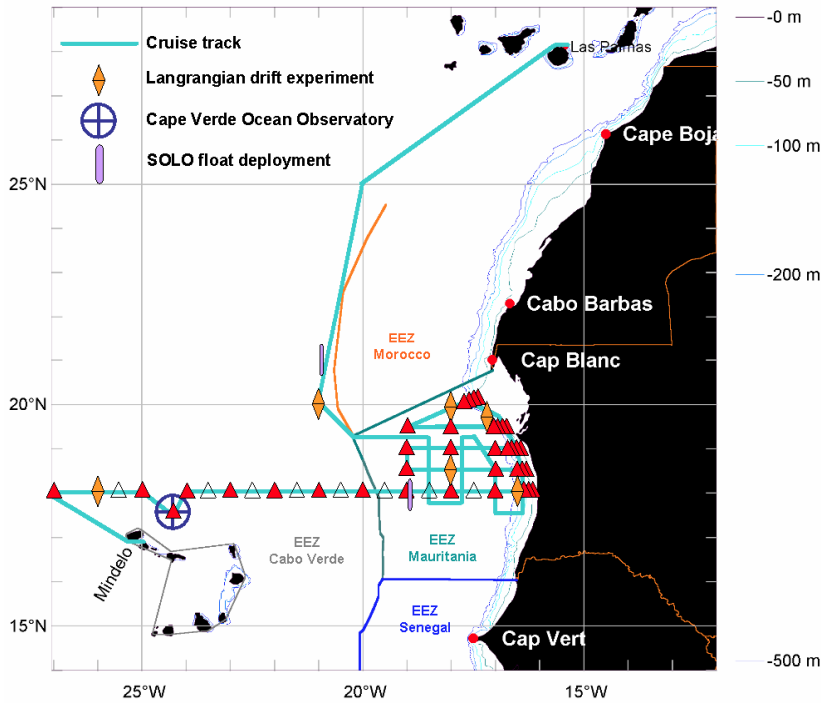

Highlights

Cruise Summary Information

WOCE Section Designation	Tropical Atlantic Leg 3
Expedition designation (ExpoCodes)	06MT20060712
Alias	M68/3
Chief Scientists	Dr. Arne Körtzinger / IMF-GEOMAR
Dates	2006 JUL 10 - 2006 AUG 6
Ship	*r/v Meteor*
Ports of call	Recife (Brazil) - Mindelo (Cape Verde)
Geographic Boundaries	20° 23' 24" N 27° W 16° 16' 12" W 16° 58' 12" N
Stations	96
Floats and drifters deployed	0
Moorings deployed or recovered	0

Contact Information:

Dr. Peter Brandt

Leibniz-Institut für Meereswissenschaften an der Universität Kiel

Düsternbrooker Weg 20, 24105 • Kiel - Germany

e-mail: akoertzinger@ifmgeomar.de

Links To Select Topics

Shaded sections are not relevant to this cruise or were not available when this report was compiled.

METEOR-Berichte 09-4

Tropical Atlantic 2006

Cruise No. 68

April 26 – August 7, 2006

Bridgetown – Recife – Mindelo – Las Palmas

Andrea Koschinsky, Peter Brandt, Arne Körtzinger

Editorial Assistance:

Sonja-B. Löffler

Alfred-Wegener-Institut für Polar- und Meeresforschung, Bremerhaven

Leitstelle METEOR/MERIAN

Institut für Meereskunde der Universität Hamburg

2009

The METEOR-Berichte are published at irregular intervals. They are working papers for people who are occupied with the respective expedition and are intended as reports for the funding institutions. The opinions expressed in the METEOR-Berichte are only those of the authors. The reports can be obtained from:

Universität Hamburg
Zentrum für Meeres- und Klimaforschung
Institut für Meereskunde
Leitstelle METEOR/MERIAN
Bundesstr. 53
20146 Hamburg
Germany

The reports are available in PDF format from http://www.dfg-ozean.de/.

The METEOR expeditions are funded by the *Deutsche Forschungsgemeinschaft* and the *Bundesministerium für Bildung und Forschung*.

Addresses of the editors:

Prof. Dr. Andrea Koschinsky
Jacobs University Bremen GmbH
Campus Ring 8
28759 Bremen
Germany
Tel.: +49-(0)421-200 3567
Fax: +49-(0)421-200 3229
e-mail: a.koschinsky@jacobs-university.de

Prof. Dr. Peter Brandt
Leibniz-Institut für Meereswissenschaften
IFM-GEOMAR
Düsternbrooker Weg 20
24105 Kiel
Germany
Tel.: +49-(0)431-600 4105
Fax: +49-(0)431-600 4102
e-mail: pbrandt@ifm-geomar.de

Prof. Dr. Arne Körtzinger
Leibniz-Institut für Meereswissenschaften
IFM-GEOMAR
Düsternbrooker Weg 20
24105 Kiel
Germany
Tel.: +49-(0)431-600 4205
Fax: +49-(0)431-600 4202
e-mail: akoertzinger@ifm-geomar.de

Citations:

Koschinsky A, Brandt P, Körtzinger, A (2009) (Eds) Tropical Atlantic 2006, Cruise No. 68, April 26 – August 7, 2006. METEOR-Berichte 09-4, 188 pp, Universität Hamburg.

ISSN 0 9 3 6 – 8 9 5 7

METEOR-Berichte 09-4

Tropical Atlantic 2006

Cruise No. 68

April 26 – August 7, 2006
Bridgetown – Recife – Mindelo – Las Palmas

Andrea Koschinsky, Peter Brandt, Arne Körtzinger

Editorial Assistance:
Sonja-B. Löffler
Alfred-Wegener-Institut für Polar- und Meeresforschung, Bremerhaven

Leitstelle METEOR/MERIAN
Institut für Meereskunde der Universität Hamburg

2009

Table of Contents

Table of Contents Part 1 (M68/1)

Table of Contents Part 2 (M68/2)

Table of Contents Part 3 (M68/3)

Abstract

R/V METEOR Cruise No. 68 was aimed at studying biogeochemical and physical processes in the tropical/subtropical Atlantic Ocean. Observations were carried out in the entire water column, from the sea floor to the sea surface and even above: Hydrothermal fields at the Mid-Atlantic Ridge (MAR) were investigated during leg M68/1. Subsequently, the role of ocean circulation variability in the equatorial Atlantic for tropical Atlantic climate variability was studied during leg M68/2, and, finally, during the third leg M68/3 near-surface biogeochemical processes and exchanges across the air-sea interface including the exchange of climate relevant gases were the focus of the research program.

M68/1 had the goal to investigate hydrothermal activity on the southern MAR (4-10°S). This cruise that is part of the SPP 1144 "From Mantle to Ocean: Energy, Material and Life Cycles at Spreading Axes" was aimed at (a) providing a quantitative estimate of the regional distribution of hydrothermal activity between 4°S and 10°S, (b) establishing the volcano-tectonic setting of this activity, (c) determining the factors that influence fluid and mineral compositions and temporal variability, and (d) evaluating the role of the large equatorial fracture zones as possible biogeographic filters between the northern and the southern MAR. Hydrothermal prospecting and plume mapping was carried out using the autonomous underwater vehicle (AUV) 'ABE' from WHOI. During ROV Quest (MARUM) dives, chemical, biological and geological samples were obtained. Combined measurements of gases and metals together with physical properties (T, S, turbidity, currents) were aimed at estimating the fluxes from hydrothermal vents. In the 4°48'S area, temporal and spatial changes in vent activity and chemistry were investigated in this young, hot, boiling system.

M 68/2 was directed at quantifying warm water transports within the shallow subtropical cell (STC) in the equatorial Atlantic and, in particular, within the supply pathways toward the equatorial and eastern Atlantic upwelling regions. The Equatorial Undercurrent (EUC) is the main source of the equatorial upwelling waters. Off-equatorial upwelling that partly occurs in the cyclonic gyres in the eastern tropical Atlantic (Angola Dome, Guinea Dome) is thought to be supplied by the South and North Equatorial Undercurrents (SEUC, NEUC). The observations of the major current bands in the equatorial region using shipboard hydrographic and current measurements were complemented by observations with moored current meters at 35°W, 23°W, and 10°W on the equator as part of the BMBF Verbundvorhaben Nordatlantik and in cooperation with the French EGEE and the multi-national PIRATA projects, as well as microstructure measurements (DFG – Emmy Noether-Program). Tracer (helium) observations were carried out to provide supplemental information regarding the strength of equatorial upwelling. In addition to the physical program, biogeochemical measurements were carried out during M68/2. These measurements that are part of the international SOLAS (Surface Ocean Lower Atmosphere) program were aimed at estimating the air-sea material exchange.

M68/3 was carried out in the programmatic frame of the international "Surface Ocean Lower Atmosphere Study" (SOLAS) and presents the 2nd German SOLAS Cruise. It combined a wide spectrum of biological, chemical and physical oceanography as well as atmospheric chemistry under a regional focus on the Mauritanian Upwelling. This region is characterized by important SOLAS-relevant phenomena and processes – most importantly atmospheric dust deposition and

coastal upwelling – which have a major influence on substances (iron, nutrients, CO_2, volatile halocarbons) and processes (nitrogen fixation, ocean-atmosphere exchange). Upwelling regions in major dust deposition areas can be viewed as biogeochemical reactors which are fuelled simultaneously by vertical supply of macro and micro nutrients from the mesopelagial below and the atmosphere above. At the same time, these regions provide means of ventilation of radiatively and chemically active trace gases (e.g., CO_2, nitrous oxide, bromoform) which are produced sub-surface. The resulting flux densities are at times several magnitudes larger than in the oligotrophic background waters.

Zusammenfassung

Die R/V METEOR Reise 68 diente der Untersuchung von biogeochemischen und physikalischen Prozessen im tropischen und subtropischen Atlantik. Dabei wurde in allen Teilen der Wassersäule, vom Meeresboden bis zur Grenzschicht Ozean-Atmosphäre und sogar darüber hinaus Hydrothermalfelder vermessen (M68/1), im äquatorialen Atlantik wurde anschließend die Rolle der Ozeanzirkulation für Klimaschwankungen im atlantischen Raum untersucht (M68/2) und im nördlichen tropischen und subtropischen Ozean standen schließlich Prozesse und Wechselwirkungen im Oberflächenozean und an der Grenzfläche zwischen Ozean und Atmosphäre einschließlich des Gasaustausches von klimarelevanten Gasen im Vordergrund (M68/3).

M68/1 hatte als übergeordnetes Ziel die Untersuchung hydrothermaler Aktivität am südlichen MAR (4-10°S). Diese Fahrt, die im Rahmen des SPP 1144 „Vom Mantel zum Ozean: Energie-, Stoff- und Lebenszyklen an Spreizungsachsen“ stattfand sollte (a) quantitative Abschätzungen der regionalen Verteilung hydrothermaler Aktivität im Bereich 4-10°S erzielen, (b) den vulkanisch-tektonischen Rahmen dieser Aktivität erfassen, (c) die wichtigen Faktoren für die Zusammensetzung der Fluide und Mineralien und zeitliche Variationen bestimmen, und (d) die Rolle der großen äquatorialen Bruchzonen als mögliche biogeographische Filter für die Faunenverbreitung zwischen dem nördlichen und südlichen MAR bewerten. Die Erkundung und Kartierung hydrothermaler Plumes wurde mit dem autonomen Unterwasserfahrzeug (AUV) “ABE” vom WHOI durchgeführt. Während der Tauchgänge mit dem ROV Quest (MARUM) wurden geologische, biologische und chemische Proben gesammelt. Hydrothermale Stoffflüsse sollten durch kombinierte Messungen von Gasen und Metallen zusammen mit physikalischen Daten (T, S, Trübung, Strömung) abgeschätzt werden. In dem jungen, hochaktiven, siedenden Hydrothermalfeld bei 4°48’S wurde außerdem die zeitliche und räumliche Variabilität von Fluidfluss und Fluidzusammensetzung untersucht werden.

M 68/2 legte den Schwerpunkt auf die Bestimmung der Wassermassentransporte innerhalb der flachen tropisch-subtropischen Zelle im äquatorialen Bereich und insbesondere der Versorgungspfade zu den Auftriebsgebieten im äquatorialen und östlichen Atlantik. Der äquatoriale Auftrieb wird im Wesentlichen durch den Äquatorialen Unterstrom (EUC) versorgt. Der außeräquatoriale Auftrieb, der innerhalb der zyklonal umströmten Dome (Angola Dome, Guinea Dome) stattfindet, scheint dagegen hauptsächlich durch die Süd- bzw. Nordäquatorialen Unterströme (SEUC, NEUC) versorgt zu werden. Die Erfassung des äquatorialen Stromsystems durch hydrographische Messungen und Strömungsmessungen vom fahrenden Schiff wurde ergänzt durch Beobachtungen mit am Äquator bei 35°W, 23°W und 10°W verankerten

Strömungsmessern (BMBF Verbundvorhabens „Nordatlantik“ und in Zusammenarbeit mit dem französischen EGEE und dem internationalen PIRATA Projekt) sowie Mikrostrukturmessungen (DFG – Emmy Noether-Programm). Die physikalischen Messungen wurden von Tracermessungen (Helium) begleitet, die zusätzliche Informationen zum äquatorialen Auftrieb liefern werden. Weiterhin enthielt die METEOR-Reise M68/2 auch eine SOLAS-Komponente, die eine Fortführung und Erweiterung der auf den METEOR -Reisen M55 und M60/5 begonnenen biogeochemischen Arbeiten zum Stoffaustausch zwischen Ozean und Atmosphäre darstellte.

M 68/3 stand als 2. Deutsche SOLAS-Expedition unter dem programmatischen Rahmen der internationalen „Surface Ocean Lower Atmosphere Study“. Sie bündelte ein breites Spektrum von biologischer, chemischer und physikalischer Ozeanographie sowie Atmosphärenchemie und war regional auf den Küstenauftrieb vor Mauretanien fokussiert. Diese Region ist durch wichtige SOLAS-relevante Phänomene und Prozesse gekennzeichnet, zu denen atmosphärischer Staubeintrag aber vor allem Auftriebsphänomene gehören, die für viele Komponenten (Eisen, Nährstoffe, CO_2, flüchtige Halogenkohlenwasserstoffe) und Prozesse (Stickstoff-Fixierung, Ozean-Atmosphäre-Gasaustausch) eine zentrale Rolle spielen. Auftriebsgebiete in Regionen mit starkem Staubeintrag stellen gewissermaßen biogeochemische Reaktoren dar, die gleichzeitig durch vertikale (Makro- und Mikro-) Nährstoffeinträge aus der Atmosphäre und dem Mesopelagial angetrieben werden. Zugleich stellen sie Regionen dar, über die eine rasche Ventilation von unterhalb der Deckschicht produzierten klimarelevanten Spurengasen (CO_2, Lachgas, Bromoform etc.) erfolgt. Die zu beobachtenden Ozean-Atmosphäre-Flussdichten liegen zum Teil um Größenordnungen über den im offenen oligotrophen Ozean vorgefundenen Verhältnissen.

Research Objectives

R/V METEOR cruise No. 68 was divided into three individual legs (see Table I, Fig. I), each of these with its own scientific focus, which are described in detail below.

Table I Legs and chief scientists of R/V METEOR cruise 68

Leg	Period	Ports	Chief Scientists
M68/1	27.04.2006 – 02.06.2006	Bridgetown (Barbados) Recife (Brazil)	Prof. Dr. A. Koschinsky
M68/2	06.06.2006 – 09.07.2006	Recife (Brazil) Mindelo (Cape Verde)	PD Dr. P. Brandt
M68/3	12.07.2006 – 06.08.2006	Mindelo (Cape Verde) Las Palmas (Spain)	Prof. Dr. A. Körtzinger

Master: M. Kull (M68/1 – M68/3)

M68/1: Fluid geochemistry, biology and geological setting of hydrothermal systems at the southern MAR (4°S - 10°S)

Following the investigations performed during and subsequent to cruises M62/5, CD169 and M64/1, the research cruise M68/1 was aimed to continue the detailed interdisciplinary work at

the selected vent sites. This included mapping and exploration for additional hydrothermal vent systems on a regional scale and sampling of hydrothermal vent fluids, associated vent fauna (both macro- and microbiology), host rock and sulphide samples.

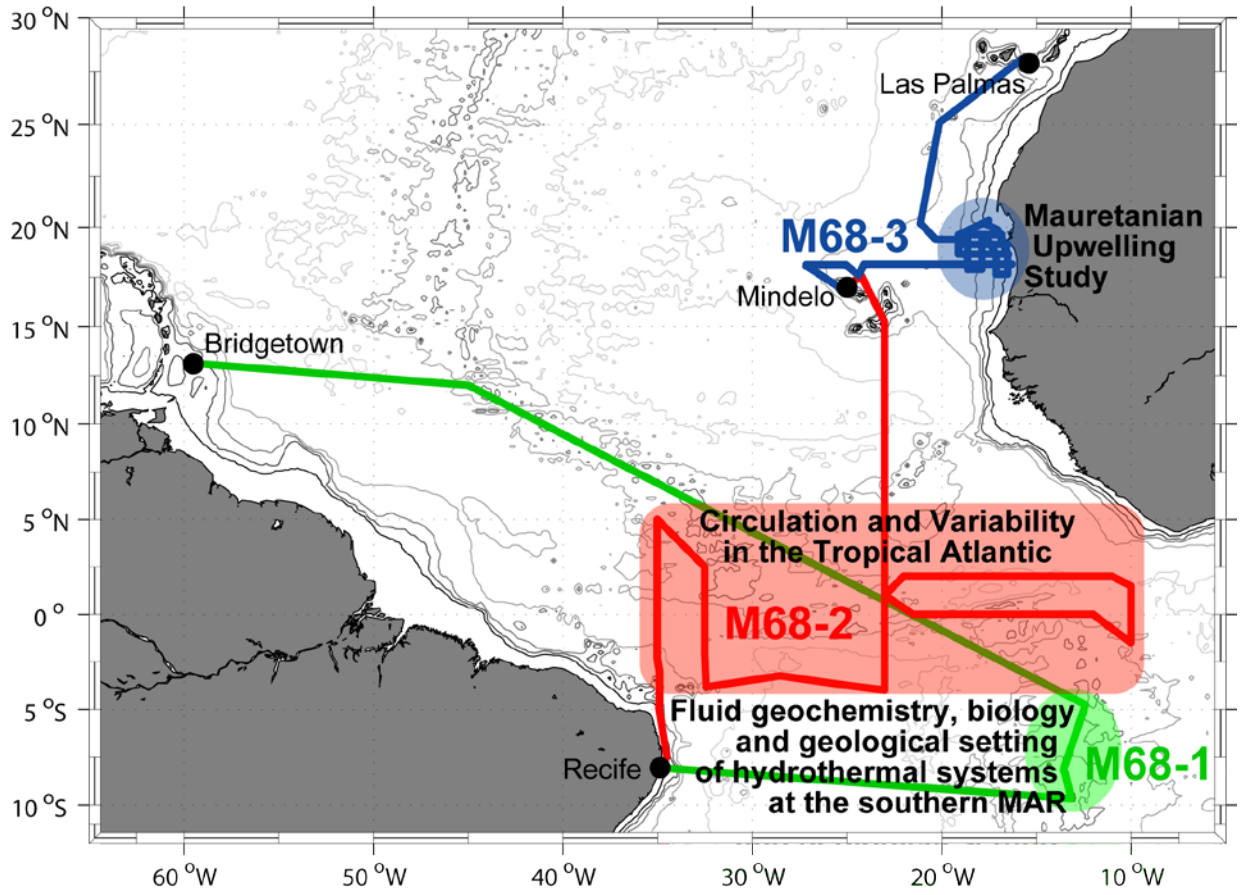

Fig. I Working areas of the individual legs of R/V METEOR cruise 68

Research objectives were:

(1) Locating and characterising the vents for the 4°48'S, 8°10´S, 8°18´S and 9°33´S hydrothermal plumes, where the hot vent sources have not yet been found;

(2) Quantifying the hydrothermal fluxes (heat, gases, metals) and the role of mixing for plume dispersal and distribution of hydrothermal fluids and gases;

(3) Assessing the origin and dispersal of vent fauna and variability of the communities linked to the physico-geochemical environment;

(4) Determining the factors controlling the composition and temporal variability of hydrothermal fluids and the microbial communities they support.

From previous cruises, the locations of several neutrally-buoyant plumes in the water column above the spreading axis were known. M68/1 was aimed to locate the sources of these plumes

where not already known and determine their areal extent, their mass venting rate, their associated fauna and the volcanic and tectonic environment which hosts them.

The 4°48'S and 9°33'S sites are the southernmost hydrothermal vent fields presently known on the MAR. The fauna that occurs at these vents offers the unique opportunity to examine if the large equatorial fracture zones in the Atlantic form a barrier for the spreading of hydrothermal fauna between northern and southern MAR vent fields. Also for the microbial communities it is possible that geographical separation of the habitats, in addition to differences in hydrochemical conditions and physical properties, lead to differences in their compositions.

Our preliminary data indicate that the temperature-depth conditions in a hydrothermal vent system in combination with phase separation processes may be more important for many dissolved components in the fluids than the host rock. The fact that the hydrothermal fields at 4°49'S (and presumably 8°18'S) and at 9°33'S are situated in different water depths (3000m and 1500m, respectively) offer excellent conditions to investigate the effect of water depth (and related phase separation) on the chemical composition of the vent fluids and the biology of the vent fields.

Both the 4°48'S and 9°33´S areas of hydrothermal activity occur in ridge segments with signs of recent volcanic activity rather than in tectonically active regions. Consequently, there appears to be a direct link at these areas between magma production and hydrothermal circulation. This is in apparent contrast to the plumes found around 8°S which are both located off-axis and so presumably more strongly related to tectonic rather than volcanic processes.

One of the major goals of the DFG SPP 1144 is to assess the temporal variability of the hydrothermal flux. The short-term evolution of the vent fluids and related changes in the vent ecosystems will be recorded through repeated sampling (in a frame of several years) of the same vent structures, especially in the young 4°48'S field. The recently settled mussel population in the 9°33'S Lilliput Field offers the rare opportunity to follow the periodicity of shell growth increments and fluid venting. Investigating the mineralogy and geochemistry of massive sulfides and manganese oxide crusts in combination with age dating of hydrothermal precipitates and host rocks will provide a long-term time frame of hydrothermal activity at the various vent sites and document its relation to the volcanic activity.

M68/2: Circulation and Variability in the Tropical Atlantic

The ocean has a major influence on tropical Atlantic climate variability mainly through the influence of tropical Atlantic SST on variations of the Atlantic marine ITCZ complex. The most notable climate impacts involve the variability of rainfall over northeast Brazil and the coastal regions surrounding the Gulf of Guinea, and the fluctuations in rainfall and dustiness in sub-Saharan Africa (Sahel). On interannual time scales the tropical Atlantic climate variability is correlated with tropical SST variability and in particular with SST fluctuations in the cold tongue region. The cold tongue appears in the eastern equatorial Atlantic during June-August and is marked by relatively low temperatures compared to its surroundings. Recent studies have shown that different oceanic processes play an important role in the SST variability in the cold tongue. Among them are zonal advection, zonal and meridional current divergence, and diapycnal

mixing below the equatorial mixed layer. In addition, the heat budget of the equatorial mixed layer and SST is affected by eddy fluxes due to tropical instability waves. However, a better understanding of the different physical processes in the tropical Atlantic is not only important for the understanding of the SST variability, it is a necessary condition for the improvement of climate predictions by ocean-atmosphere models. Up to now, many models show a bias towards higher temperatures in the eastern tropical Atlantic and are thus unable to realistically simulate the equatorial cold tongue temperatures and associated climate variability.

By incorporating results of previous research cruises and model simulations, the second leg of M68 was aimed at addressing the following topics:

- Supply pathways toward to equatorial upwelling region and toward the upwelling within the cyclonic gyres north and south of the equator;
- Role of tropical instability waves for the exchange between east- and westward flowing current as well as for diapycnal mixing processes;
- Role of STC variability, and particularly of EUC fluctuations for the SST variability in the eastern equatorial Atlantic;
- Heat budget of the equatorial mixed layer using microstructure measurements to estimate diapycnal mixing and tracer (helium) observation to estimate equatorial upwelling.
- Supply pathways of oxygen-rich water masses toward the oxygen minimum zone of the tropical North Atlantic.

Goals of biogeochemical observations were a better understanding of the effect of high CO_2 on marine ecosystems and sea-to-air gas fluxes and better estimates of the production and emission of radiatively and chemically active gases in the tropical Atlantic.

M68/3: Mauritanian Upwelling Study

The third leg of METEOR cruise 68 was carried out in the programmatic frame of the international "Surface Ocean Lower Atmosphere Study" (SOLAS) and presents the 2nd major cruise of German SOLAS. It combined a wide spectrum of biological, chemical and physical oceanography as well as atmospheric chemistry under a regional focus on Cape Verdean waters and coastal upwelling off Mauritania. This region is characterized by important SOLAS-relevant phenomena and processes – most importantly atmospheric dust deposition and coastal upwelling – which have major influence on substances (iron, nutrients, CO_2, volatile oxygenated and halogenated organics) and processes (nitrogen fixation, ocean-atmosphere gas exchange). Upwelling regions in major dust deposition areas can be viewed as biogeochemical reactors which are fueled simultaneously by vertical supply of macro and micro nutrients from the mesopelagial below and the atmosphere above. At the same time, these regions provide means of ventilation of radiatively and chemically active trace gases (e.g., CO_2, nitrous oxide, bromoform)

which are produced sub-surface. The resulting flux densities are larger than in the oligotrophic background waters.

More specifically the scientific program of the M 68/3 cruise encompassed the following themes and questions:

- Hydrographic and microstructure measurements (hydrographic survey with regular CTD and ADCP measurements as well as measurements of turbulence and vertical mixing with free sinking micro-structure sensor);
- Carbon, oxygen and nutrients dynamics (air-sea CO_2 and O_2 fluxes in oligotrophic ocean vs. upwelling regimes, surface ocean carbon and nutrient dynamics in organic and inorganic, particulate and dissolved pools of recently upwelled waters);
- Production of organic trace gases using empirical and experimental approaches (role of sub-surface chlorophyll maximum, species- and light-dependence of production, role DOM/POM, bacterial production);
- Production of volatile organoiodine compounds (inorganic precursors, role of DOM/ enzymes, CDOM – Chromophoric Dissolved Organic Matter);
- Production of hydroxylamine, nitrous oxide and methane (formation pathways of hydroxylamine, air-sea fluxes of nitrous oxide and methane);
- Marine boundary layer photochemistry and aerosol formation (air-sea fluxes of oxygenated organic species, chemical/biological precursors/sources, importance for aerosol formation);
- Aerosol iodine chemistry (speciation of iodine in aerosol and rain, source of iodine associated with the Mauritanian upwelling);
- Trace metals (redox speciation, input via dust, iron solubility);
- Nitrogen fixation and nutrient limitations (contribution of the different diazotrophic groups to total community nitrogen fixation, limiting nutrient for nitrogen fixation, response of various diazotrophic groups to nutrient and Saharan dust amendments).

Acknowledgements

We gratefully acknowledge the friendly and professional cooperation and efficient technical assistance of Captain M. Kull, his officers and crew, who substantially contributed to the overall scientific success of R/V METEOR cruise No. 68. We also appreciate the most valuable help of the Leitstelle METEOR in Hamburg. The work done was funded by the Deutsche Forschungsgemeinschaft.

METEOR-Berichte 09-4

Circulation and Variability in the Tropical Atlantic

PART 1

Cruise No. 68, Leg 1

April 27 – June 2, 2006
Bridgetown (Barbados) – Recife (Brazil)

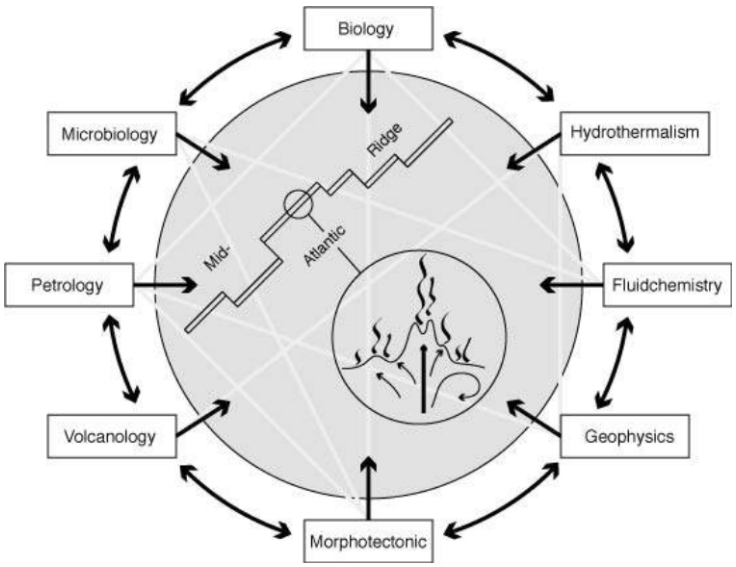

Fluid geochemistry, biology and geological setting of hydrothermal systems at the southern MAR (4°S - 10°S) (MAR-SÜD III)

A. Koschinsky, A. Billings, C. Devey, N. Dubilier, A. Duester, D. Edge, D. Garbe-Schönberg, C. German, O. Giere, R. Keir, K. Lackschewitz, H.A. Mai, H. Marbler, J. Mawick, B. Melchert, C. Mertens, W.-T. Ochsenhirt, M. Peters, S. Sander, O. Schmale, W. Schmidt, R. Seifert, C. Seiter, U. Stöber, I. Suck, M. Walter, S. Weber, D. Yoerger, M. Zarrouk, F. Zielinski

Project Leader: Andrea Koschinsky

Table of Contents Part 1 (M68/1)

1.1 Participants

Name	Function	Institute
Koschinsky, Andrea, Prof. Dr.	Chief Scientist	IUB
Billings, Andrew	AUV	WHOI
Devey, Colin, Prof. Dr.	Geology, Petrology	IFM-GEOMAR
Dubilier, Nicole, Dr.	Hydrothermal Symbioses	MPI Bremen
Duester, Alan	AUV	WHOI
Edge, David	ROV	NOC
Garbe-Schönberg, Dieter, Dr.	Fluid Chemistry	Univ. Kiel
German, Chris, Dr.	AUV, photo mapping	WHOI
Giere, Olav, Prof. Dr.	Zoology	MPI Bremen
Keir, Robin, Dr.	Gases (Methane)	IFM-GEOMAR
Lackschewitz, Klas, Dr.	Documentation ROV	IFM-GEOMAR
Mai Hoang, Anh	ROV	MARUM
Marbler, Herwig, Dr.	ROV	IUB
Mawick, Jule	Fluid Chemistry	IUB
Melchert, Bernd	Bathymetry	IFM-GEOMAR
Mertens, Christian, Dr.	Physical Oceanography	Univ. Bremen
Ochsenhirt, Wolf-Thilo	Weather Technique	DWD
Peters, Marc	Sulfur Isotopes	Univ. Münster
Sander, Sylvia, Dr.	Fluid Chemistry	IUB/Univ. Otago
Schmale, Oliver	Gases (Methane)	IFM-GEOMAR
Schmidt, Werner	ROV	MARUM
Seifert, Richard, Dr.	Gases (Hydrogen)	Univ. Hamburg
Seiter, Christian	ROV	MARUM
Stöber, Uwe	Physical Oceanography	Univ. Bremen
Suck, Inken	ROV	MARUM/Fielax
Walter, Maren, Dr.	Physical Oceanography	Univ. Bremen
Weber, Stefan	Gases (Hydrogern)	Univ. Hamburg
Yoerger, Dana, Dr.	AUV	WHOI
Zarrouk, Marcel	ROV	MARUM
Zielinski, Frank	Hydrothermal Symbioses	MPI Bremen

Participating Institutions

IUB	International University Bremen; now: Jacobs University Bremen GmbH, Campus Ring 8, D-28759 Bremen, Germany, e-mail: a.koschinsky@iu-bremen.de
WHOI	Woods Hole Oceanographic Institution, 93 Water Street, Woods Hole, MA 02543, USA, e-mail: cgerman@whoi.edu
IFM-GEOMAR	Leibniz-Institut für Meereswissenschaften an der Universität Kiel, Düsternbrooker Weg 20, 24105 Kiel - Germany, e-mail: pbrandt@ifm-geomar.de
MPI	Bremen Max-Planck Institut für Marine Mikrobiologie, Celsiusstr. 1, D-28359 Bremen, e-mail: ndubilier@mpi-bremen.de
NOC	National Oceanography Centre, Southampton, UK, European Way, Southampton, SO14 3ZH, UK, e-mail: ade@noc.soton.ac.uk
MARUM	Zentrum für Marine Umweltwisenschaften, Universität Bremen, Leobener Straße, D-28359 Bremen, e-mail: cseiter@marum.de
DWD	Deutscher Wetterdienst, Geschäftsfeld Seeschiffahrt, Bernhard-Nocht-Str. 76, 20359 Hamburg - Germany, e-mail: edmund.knuth@dwd.de
UBU	Universität Bremen, Institut für Umweltphysik, Otto-Hahn-Allee, UW1, Postbox 330440, 28334 Bremen - Germany, e-mail: mrhein@theo.physik.uni-bremen.de
IfBM	Institut für Biogeochemie und Meereschemie, Bundesstraße 55 20146 Hamburg, e-mail: seifert@geowiss.uni-hamburg.de
FIELAX GmbH	Schifferstrasse 10 - 14, 27568 Bremerhaven, Germany, e-mail: inkens@awi-bremerhaven.de or: info@fielax.de
Univ. Münster	Geologisch-Paläontologisches Institut, Corrensstr. 24, D-48149 Münster, e-mail: hstrauss@uni-muenster.de
Univ. of Otago	Department of Chemistry, Otago, New Zealand, PO Box 56, Dunedin, New Zealand, e-mail: sylvias@chemistry.otago.ac.nz
CAU	Christian-Albrechts-Universität Kiel, Institut für Geo-wissenschaften, Abt. Geologie, Olshausenstraße 40, D-24118, Kiel Germany, e-mail: dgs@gpi.uni-kiel.de

1.2 Research Program

Following the investigations performed during and subsequent to cruises M62/5, CD169 and M64/1 it was of prime importance during cruise M68/1 to continue the detailed interdisciplinary work at the selected vent sites on the southern Mid-Atlantic Ridge (MAR). This includes mapping and exploration for additional hydrothermal vent systems on a regional scale and sampling of hydrothermal vent fluids, associated vent fauna (both macro- and microbiology), host rock and sulphide samples.

Our goals were:

(1) Locating and characterising the vents for the 4°48'S, 8°10´S, 8°18´S and 9°33´S hydrothermal plumes (Fig. 1), where the hot vent sources have not yet been found;

(2) Quantifying the hydrothermal fluxes (heat, gases, metals) and the role of mixing for plume dispersal and distribution of hydrothermal fluids and gases;

(3) Assessing the origin and dispersal of vent fauna and variability of the communities linked to the physico-geochemical environment;

(4) Determining the factors controlling the composition and temporal variability of hydrothermal fluids and the microbial communities they support.

The work plan included detection and mapping of the hydrothermal plumes by CTD and turbidity sensors and localization of the hydrothermal emanation sources using the AUV ABE (WHOI). ABE dives consisted of three phases, first looking for the largest hydrothermal signal in the neutrally buoyant plume, then searching for the interception of the rising plume, and in the third phase a detailed sensor and photo mapping of the active area was carried out.

Bathymetric mapping was carried out with the multibeam system of RV Meteor, and high-resolution mapping of the AUV. The ROV Quest (MARUM, Univ. Bremen) was deployed in parallel and subsequent to the AUV discoveries in the known and newly discovered fields to sample rocks, sulfides, fluids and animals. Sample recoveries were complemented by onboard measurements of chemical compounds in the fluids, microbial experiments, and preparation of animal samples.

1.3 Narrative of the Cruise

Cruise M68/1 began at 09:00 a.m. on April 27, sailing from Bridgetown, Barbados. The transit to the first working area at 5°S on the Mid-Atlantic Ridge (MAR) took 12 ½ days, due to strong head-wind and swell. The long transit time was being used by the interdisciplinary scientific team, composed of geologists, oceanographers, geochemists and biologists, supported by the technical teams of the ROV Quest (MARUM, Univ. Bremen) and the AUV ABE (Woods Hole Oceanographic Institution) to equip the labs and coordinate its activities. Besides the preparations for the deployment of the equipment, the transit time was also a much-appreciated

opportunity for a scientific exchange between the different working groups and disciplines. We carried out a little hydrothermalism workshop covering four afternoons, during which scientists presented the background of their work. In addition, the ROV and AUV teams provided us with a detailed insight into how the equipment functions and the possibilities that their devices offer.

On the way to our first working area close to 5°S, 12°W we released so-called ARGO-Floats, which we were asked to deploy by NOAA in Miami, at 45°W, 40°W and 35°W. When the weather improved we tested several pieces of equipment. An ROV test dive to 1000m worked perfectly and a CTD deployment to 100m too. As this was the first time that the Autonomous Underwater Vehicle (AUV) „ABE“ was on board Meteor, the crew practiced deployment with the crane and, after a short manoeuvre on the surface, recovery of the vehicle.

During the night of May 9/10 we finally arrived in our first working area at 5°S, first deploying three transponders as preparation for the first dive of the AUV ABE, which followed immediately after a CTD station. A complete AUV survey for the exploration of hydrothermal vents consists of three phases. During phase 1, the wide head of the hydrothermal plume is mapped on a larger scale (at 200-300 m above the seafloor), using the CTD, redox and turbidity sensor data to locate the center of the hydrothermal plume. In Phase 2, based on the data from phase 1, the seafloor is mapped at high resolution from 50 m above the seafloor with a survey line spacing which should allow the rising stem of the plume to be intercepted. As the rising plume has a limited width, this information already enables a good location of the active vent site. In the 3rd phase, a photo survey of a limited area directly around the rising stem is carried out from 5 m above the seafloor, providing information about the smoker structures and faunal abundances. This information can then be used to prepare a ROV dive in detail. With this combination of the two devices, which can be deployed in parallel, we achieved an optimum use of the ROV and precious ship time.

The first AUV dive covered the vent fields Turtle Pits, Red Lion and Wideawake, known from the cruises CD-169 and M64/1 in 2005, and also included sites southwest and east of these fields, where we had detected hydrothermal signals in the water column last year. In parallel, the first ROV dive in the Wideawake mussel field and the Turtle Pits hot vent field started in the morning of May 10. After a total dive time of 12 hours without technical problems, the ROV brought mussel samples, hot fluids and rock samples on board. The nights were also filled with intense hydrographic investigations of the area to gain more information about how the hydrothermal plumes are spreading in the water column and hence about the regional input of hydrothermal material to the oceans. Numerous plume signals at different sites were recorded. In the morning of May 11 the ROV started its second dive, targeted at the Red Lion field with its four very different smokers.

With the ROV working perfectly, May 12th saw the 3rd dive in a row to finish the program in Wideawake and Turtle Pits. Besides the successful search for the rare Calyptogena clam, the largest success of this dive was the measurement of the hottest vent fluid found so far, with 407°C, at the Turtle Pits vent. Sampling of rocks with the ROV was complemented by three volcanite wax corer stations.

While the ROV was still finishing sampling in the known vent fields at 5°S, the AUV ABE had already found several new locations with indications of hydrothermal input in an area

between the hot vent fields Turtle Pits and Red Lion, and at other sites displaying anomalies in turbidity, temperature and redox potential. Additionally, the photo mapping with ABE had recorded clear indications of hydrothermalism. During the 4th dive of the ROV on May 14 we found a 12 meter-high chimney emanating 399°C hot fluid and black smoke. The site was called "Sisters Peak". The ROV continued its way according to the data of the AUV dive evaluation and in the afternoon it reached a fissure with intense colonization of mussels and other animals, which we named "Golden Valley". In the evening, the ROV reached the 3rd hydrothermally active site, which was characterized by high turbidity of the water ("Foggy Corner") – probably caused by bacteria. This new locations became the starting point for ROV dive no. 5 the following morning. It is also a low-temperature diffuse source, however it differs in its appearance and colonization from the previously discovered mussel valley, which was also revisited to sample mussels and fluids. The remaining time was dedicated to the hot smoker Sister Peaks.

As further work in the 5°S area, a number of CTD stations were carried out. North and south of the 5°S area 2 hydrographic profiles were carried out (CTD/LADCP/130 He samples). For the purpose of long-term observation of the background current and for the precise determination of tidal amplitudes and phases, a current meter mooring was deployed in the area, which will remain there for one year. Deploying the CTD/MAPR combination from a drifting ship (Tow-yo) produced 3 high-resolution transects of temperature anomalies and turbidity both along and across the axis of the valley. Plume anomalies were detected in several density layers and could partly be assigned to the known vent fields. Several weaker signals lie south of the known vents and indicate the presence of further (possibly diffuse) hydrothermal sources.

After 6 very successful working days we had a transit of 25 hours to the next target area at 9°33'S. This site is much shallower (1500 m) than the 3000 m deep sites at 5°S. A diffuse hydrothermal field, which was called Lilliput during its discovery cruise M64/1 in 2005 because of the high abundance of very young mussel populations, was already known. Four dredges and one wax corer station retrieved volcanic rock from this area. While the AUV was searching for signals of active hydrothermal venting around the Lilliput field, the ROV had to stay on deck for a day. A complicated problem in the winch for the A-frame made a deployment of the ROV impossible. After the repair, the ROV descended immediately at 5 p.m. on May 18 for its 6th dive. This dive started in a diffuse site that we had observed during an OFOS track in 2005 and continued over a bizarre underwater landscape consisting of lava pillars, lava domes and wide caves (we called the place "Roman City") and finally led us to a diffuse-flow mussel field just south of Lilliput. The photo mapping and sensor records of the AUV 5 m above the seafloor revealed further strong signals of hydrothermal activity, which were followed on May 19 during the 7th ROV dive. Besides the known Lilliput field, more diffuse active emanation sites north of Lilliput were discovered and sampled. In addition to the common mussels, shrimps and crabs, also dense accumulations of hydrozoans (giving the site the name "Candelabrum Meadow"), gorgonians and some tube-forming worms could be observed. Even though we did not find any high-temperature field in the area at 9°33' S, which had been expected based on a clear anomaly of gases and metals about 300-400 m above the seafloor, we could still consider this leg of the expedition with its diverse occurrences of widespread low-temperature hydrothermal activity very successful.

After 7 hours of transit from the Lilliput area to the Nibelungen field at 8°18'S the first station on May 19 was a CTD station destined to confirm the hydrothermal plume that was found here during cruise M62/5 in December 2004. This area, which had already been investigated during this former cruise with extensive CTD work and ROV deployments, is characterized by very complex current patterns and temporal variability of the location and intensity of the hydrothermal plume. Therefore, it had not been possible to detect the exact location of the vent site and the whole area had been named "Cheating Bay". The CTD station data could immediately confirm the existence of the plume at the expected water depth 300 m above the seafloor, and the coordinates for the first dive of AUV ABE could be set. The third AUV dive finally revealed the source of the plume: a black smoker in a large field of otherwise dead chimneys. Two CTD Tow-yo tracks confirmed the strong temporal variability of plume dispersion in Cheating Bay: during one station, the plume signal was clearly visible east of the now known position of the source, another time west of it.

Now that the location of the Nibelungen field was identified, the increasing winds and strong swell made the deployment of the ROV impossible. Finally on May 24 the weather had improved. After only 20 minutes on the bottom Quest had already found the source of the strong redox, temperature and turbidity anomalies that ABE had located: "Drachenschlund" (Dragon Throat). This vent does not represent a chimney structure, but is a four meter deep crater with a diameter of about half a meter, from which an enormous volume of black smoke emanates at high velocity. This made sampling of the fluids and temperature measurements very difficult, but still shipboard analysis of the fluid samples gained above the crater throat could immediately prove to us that Nibelungen is a vent characterized by serpentinization processes. However, only little serpentized rock could be found during 1 dredge and 5 volcanite wax corer stations.

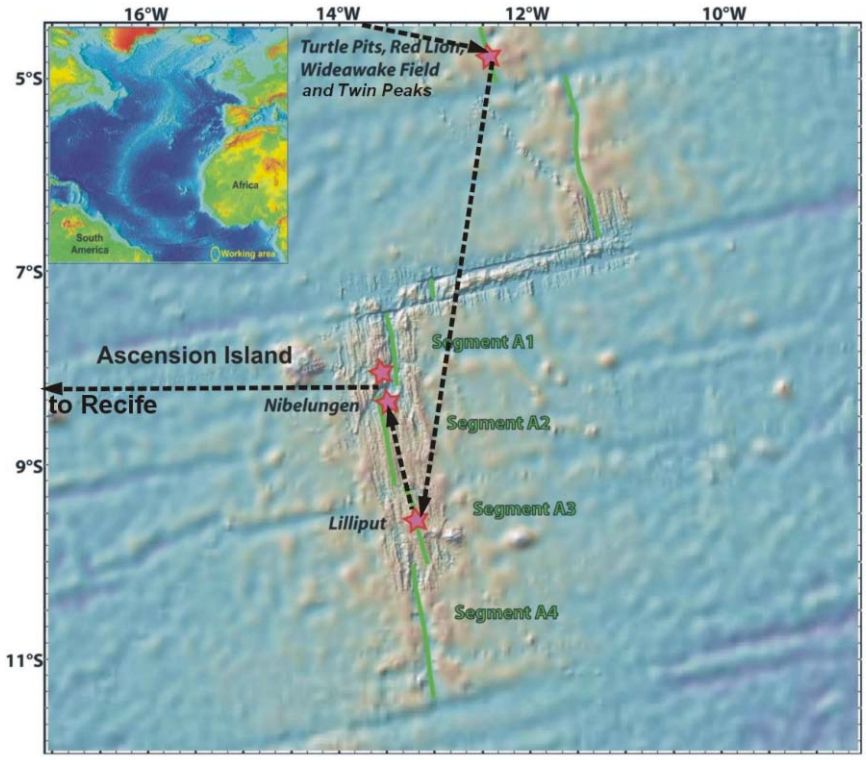

Fig. 1.1 Cruise track and working areas of cruise M68/1

As the ROV was only deployed again after the location of the Nibelungen field was known, the intermediate time was used by a CTD Tow-yo and one dredge for preparing another target area at 7°57'S for AUV dives. This area in the A1 segment close to Ascension had shown turbidity and temperature anomalies during CTD stations and TOBI sidescan sonar deployments of former cruises. These anomalies apparently originated from terrace structures at the western rift valley, close to the center of the segment – a geological situation similar to the Logatchev field at 15°N on the MAR. The Tow-yo data of the oceanography team could indeed identify a distinct plume with its maximum turbidity anomaly lying directly above terraces cut into the valley walls. The AUV dive phase 1 localized the hydrothermal signals, whereas a dredge along the slope recovered hydrothermal breccia, so that the 2nd dive phase of ABE could be prepared. However, as this dive did not result in the clear localization of the hydrothermal source, as we had hoped for, we stopped work in this area for the rest of this cruise, because station work time was coming to its end and a further search did not appear useful. Instead, the station work was finished with a dredge in the Nibelungen field, a CTD station at 8°10'S and an ROV dive in the Lilliput mussel field at 9°33'S, where again mussels were recovered for experiments with the symbiotic bacteria and where fluid and lava samples were taken from the area with the lava columns.

1.4 Preliminary Results

1.4.1 Geology of the Working Area

A general description of the geologic situation of the working areas was given in the cruise reports of the former cruises M62/5 and M64/1. More detailed information on geologic features of the areas at 5°S, 8°S, and 9°S is given in chapter 1.4.3.2 "Description of the ROV dives" of this report.

1.4.2 AUV Dives

1.4.2.1 Technical Description of the AUV

(C. German, D. Yoerger, A. Billings, A. Duester)

The *Autonomous Benthic Explorer* (*ABE*) is a fully autonomous underwater vehicle used for exploring the deep ocean up to depths of 4500 meters. *ABE* produces bathymetric and magnetic maps of the seafloor and has also been used for near-seabed oceanographic investigations, to quantify hydrothermal vent fluxes. Most recently, *ABE* has been used to locate, map, and photograph deep sea vent sites following preliminary work by towed and lowered instruments. *ABE* has taken digital bottom photographs in a variety of deep sea terrains, including the first autonomous surveys of an active hydrothermal vent site. By the end of M68/1, ABE has completed 181 dives in the deep ocean over 16 cruises, covering more than 3000 km of survey tracks at an average survey depth of deeper than 2000 meters.

ABE is a three body, open frame vehicle that utilizes glass balls as flotation in two free-flooded upper pods while the single, lower housing is host to the batteries that power the vehicle and all of its electronics. This separation of buoyancy and payload gives a large righting moment

which simplifies control and allows the five vertical and lateral thrust propellers to be located inside the protected space between the three, faired bodies. For general use, ABE uses long "baseline" transponders, which allow deep seafloor surveys over distances of ca.5 kilometers to be carried out. In addition, ABE also carries an acoustic doppler velocity log (DVL) which provides short-range, high-precision navigation. With these navigation systems, ABE has the ability to follow tracklines with a repeatability of order 10m line-spacing or better.

ABE carries six standard sensors which include:

- a SIMRAD SM2000 200kHz multibeam sonar, rated to 3000m
- an Imagenex 675kHz scanning sonar, rated to ≥4500m
- a 3-component Develco fluxgate magnetometer, rated to ≥4500m
- 2 SeaBird 9/11+ CTD systems, rated to ≥4500m
- SeaPoint optical backscatter sensor (OBS) rated to ≥4500m
- a digital still camera imaging system, rated to ≥4500m

NB: for M68/1 an Eh sensor was also interfaced to the AUV through an on-going collaboration between the *ABE* group and Dr Koichi Nakamura (Japan).

All data are stored on the vehicle and retrieved upon recovery.

ABE operates autonomously from the support research vessel. It has no tether, and is controlled in real-time by onboard computers using its own rechargeable batteries for all power. After reaching the seafloor and performing a series of checks, ABE releases its descent weight to become neutrally buoyant and begins its pre-programmed survey. A dive can consist of any mix of water column investigations (e.g. hydrothermal plume surveys) at constant water depths, seafloor geophysical investigations at fixed heights above the seafloor (anywhere from 50-200 m off depending on the application: e.g. magnetics, high-resolution bathymetric mapping) and digital photography at a height of just 5 meters above the seafloor. ABE usually surveys between a 20-30 km long track and 15-30 hours of survey time, depending on sensor payload, survey type, and terrain). At the end of its dive, ABE releases two ascent weights to become positively buoyant and returns to the surface at 15-20m/minute.

Three different phases of data acquisition can be used for hydrothermal exploration:

Phase I: non-buoyant plume surveys. Using previously collected MAPR and/or CTD tow-yo data, the ABE vehicle is pre-programmed to fly a survey pattern that traverses the seafloor at a fixed depth (order 200m above the seabed) with ca. 300m line spacing, to map out the core and distribution of a non-buoyant hydrothermal plume (key sensors: CTD, E_h, optical backscatter).

Phase II: seafloor mapping and buoyant-plume interception. Using information from Phase I, a ca. 1km^2 area is chosen for more detailed analysis. This comprises high-resolution multibeam

mapping from 50m above the seabed. At this height, 30m-spaced lines also ensure interception of any rising buoyant plumes allowing sources of high-temperature hydrothermal vents to be located (key sensors: Simrad SM2000, CTD, E_h, optical backscatter and vertical displacement of the vehicle by the rising plume).

Phase III: bottom-photography of vents and vent-communities. Once a buoyant plume has been intercepted the source of venting is known to within ±100m. The final phase, therefore, is to conduct systematic photo-mapping of an area order 200m x 200m, at 5m above the seabed, to precisely locate vents and areas of diffuse flow (key sensors: Digital Still Camera, CTD, E_h, optical backscatter and vertical displacement of the vehicle by rising plumes).

1.4.2.2 First Results of AUV Dives

Overview

During cruise M68/1, ABE was deployed on 11 successful dives in 4 research areas. There were 4 dives at 5°S, 2 dives in the Lilliput Area, 3 dives at Nibelungen and 2 in the centre of the A1 segment near 8°S. A final, 12th, scheduled dive – which would have been a Phase III dive in A1 segment was cancelled to allow time for a last ROV dive at Lilliput at the end of the cruise.

5°S Area

Four dives were completed at 5°S, ABE dives 171-173 were dedicated to exploration for, and location of new hydrothermal fields. Dive 174 was a time-series repeat photo-survey of the Turtle Pits and Wideawake areas that had first been photo-mosaiced by ABE in March 2005 and had revealed fresh glassy lavas apparently over-flowing already-established Wideawake diffuse-flow vent communities.

ABE 171 Summary:

Launch: 2006/05/10 07:02	Recovery: 2006/05/11 06:16
Survey start: 2006/05/10 11:14	Survey end: 2006/05/11 03:27
Survey distance: 31.70 km	Ave survey depth: 2793 m

ABE171 was a Phase 1 dive. We obtained Eh and backscatter hits at two potentially new sites as well as over Red Lion and Turtle Pits. The dive was planned with the depth alternating on each trackline between 2750 and 2850 meters. For the first block of lines in the west, the vehicle paused during the depth changes, so each line was run at the desired depth. The lines to the east did not include the appropriate pause during the depth change, so the vehicle changed depth over about the first half of each line. Eh signals showed the locations of the Red Lion, Turtle Pits, and Wideawake fields discovered by ABE in 2005 (CD169) as well additional signals which were

used to target further ABE missions and successful location of new vent sites found during ABE173.

ABE 172 Summary:

Launch: 2006/05/12 09:14	Recovery: 2006/05/13 01:33
Survey start: 2006/05/12 12:38	Survey end: 2006/05/12 22:28
Survey distance: 16.36 km	Ave survey depth: 2926 m

ABE172 was a Phase 2 dive, originally planned in two blocks. We terminated the dive after the first block. The dive was progressing slower than expected and we determined it would not get to the prime search area in the second block before depleting its batteries. The vehicle started in the SW corner, so it was driving with or against the current. When the vehicle timed out on the first two tracks driving to the SE, it was driving into the current. The current then rotated about 90 degrees, and we saw no more timeouts. Plots of Eh sensor data showed that the only substantial hits were in the SW corner at about the same place where the vehicle timed out on SE-bound tracklines. No T or optical backscatter anomalies accompanied this Eh hits: diffuse flow?

ABE 173 Summary:

Launch: 2006/05/13 15:54	Recovery: 2006/05/14 09:27
Survey start: 2006/05/13 18:49	Survey end: 2006/05/14 06:01
Survey distance: 15.68 km	Ave survey depth: 2961 m

ABE173 did a combined Phase 2 and Phase 3 survey. The dive succeeded in locating three vent sites which were visited later the same day by the ROV. These vents were determined from Eh, optical backscatter, and temperature data. By this measure the dive was extremely successful, but a programming error prevented the SM2000 from running and resulted in the camera quitting early, soon after photographing the black smoker site Sisters Peak. Despite this disappointment, the camera did run through the first several vent sites and gave good pictures showing diffuse flow, mussels, shrimp, and an active black smoker. At least as important was the fact that the water column data were sufficient to accomplish the primary goal of the dive – to guide the ROV to the vent sites. Fig 1.2 shows the Phase 3 (T1) temperature measurements that were used to target all three vents visited by the ROV.

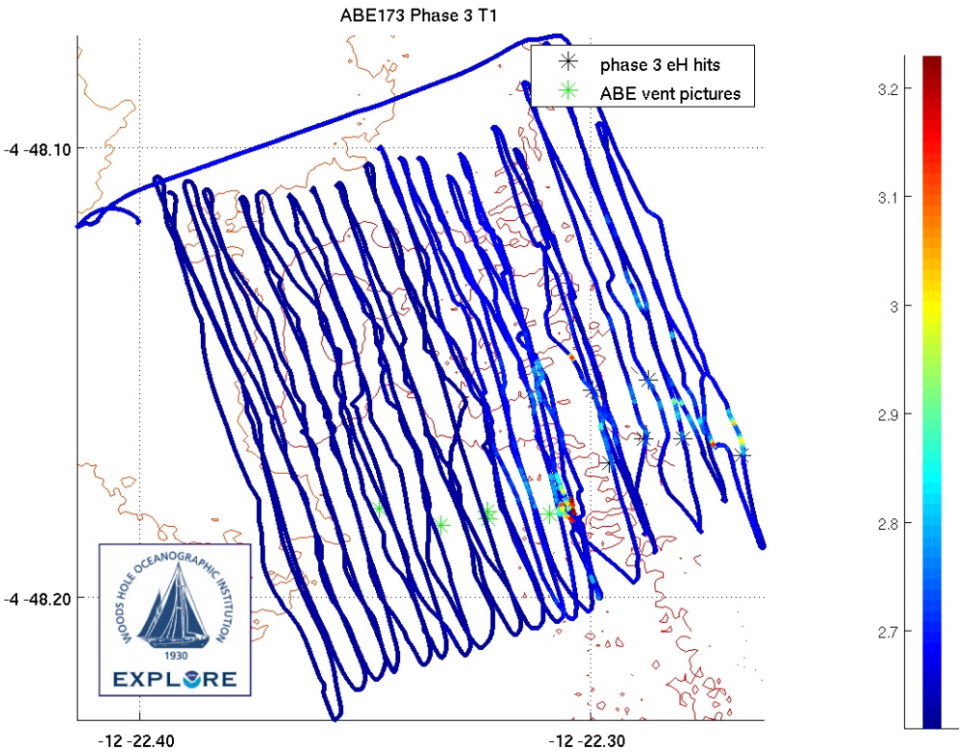

Fig. 1.2 Phase 3 (T1) temperature measurements recorded during the AME173 dive

ABE 174 Summary:

Launch: 2006/05/14 23:21	Recovery: 2006/05/15 10:16
Survey start: 2006/05/15 02:04	Survey end: 2006/05/15 07:12
Survey distance: 6.51 km	Ave survey depth: 2966 m

ABE174 was a phase 3 dive designed to repeat the survey we made on ABE154 at the Turtle Pits and Wideawake sites. The dive went well and all 5740 photos were recorded properly. The vehicle had two collisions with structures in Turtle Pits. In addition to the areas covered in ABE154, we also added a block to the east and a cross track block over the initial Wideawake survey area.

The Turtle Pits block is to the northwest, the main Wideawake block is in the center, and the extension of the Wideawake survey lies to the east. The vehicle held the 5 meter track spacing fairly well except when flying over the big structures in Turtle Pits. The crooked track in the center of the Turtle Pits block is the line over the big spires. The vehicle made it over the large spire without a collision but collided squarely with the next structure even though the downlooking sensors measured ranges that were too short, and the vehicle was backing off as the collision occurred. Happily, the vehicle suffered no apparent damage, just a large black mark on its nose.

Lilliput Area, 9°30'S

Two dives were completed in this area. First, a Phase II dive was conducted to carry out high-resolution bathymetric mapping of the OFOS and Lilliput Sites and to continue exploration and mapping north along the neovolcanic axis. Based on those results a further Phase III dive was chosen which identified a new diffuse flow field "Candelabrum Meadows" and a large extinct hydrothermal deposit in the very NE of our survey.

ABE 175 Summary:

Launch: 2006/05/17 06:55	Recovery: 2006/05/18 02:01
Survey start: 2006/05/17 08:40	Survey end: 2006/05/17 23:49
Survey distance: 28.28 km	Ave survey depth: 1436 m

ABE 175 made a successful phase 2 survey at Lilliput. Fig. 1.3 shows the Eh data for the run superimposed on the new SM2000 bathymetry. At least three solid hits were detected.

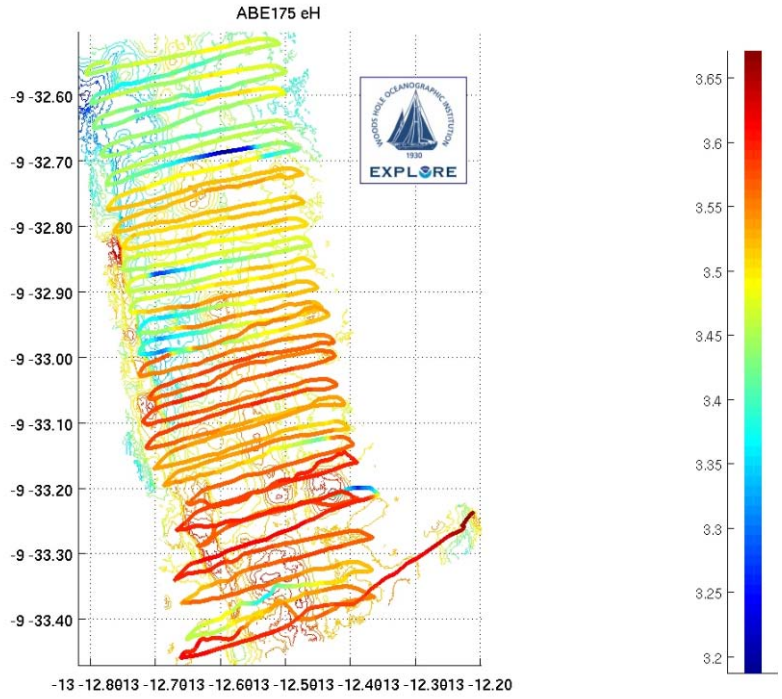

Fig. 1.3 Eh data for the ABE175 run superimposed on the new SM2000 bathymetry

ABE 176 Summary:

Launch: 2006/05/18 19:50	Recovery: 2006/05/19 07:56
Survey start: 2006/05/18 21:44	Survey end: 2006/05/19 06:15
Survey distance: 9.18 km	Ave survey depth: 1487 m

ABE176 was a phase 3 dive at Lilliput. The vehicle located at least three vent sites. One was marked by strong temperature, Eh, and optical backscatter signals, the other two had much lower signatures but were clearly apparent in bottom photographs. The vehicle took 5000 pictures which showed a variety of vent animals and diffuse flow. The area featured a prominent mound about 25 meters high that was heavily fissured. ABE was able to fly over this feature without a problem. Small T-anomalies in the North East coincide with a large "extinct" hydrothermal field.

Nibelungen Area, 8°18'S

Three dives were dedicated to this area to explore for, locate and photograph the new "Drachenschlund" black smoker vent.

ABE 177 Summary:

Launch: 2006/05/20 15:34	Recovery: 2006/05/21 09:52
Survey start: 2006/05/20 20:03	Survey end: 2006/05/21 06:53
Survey distance: 22.34 km	Ave survey depth: 2697 m

ABE177 was the Phase 1 dive at the Nibelungen site. The dive was conducted at a constant depth of 2700 meters centred on previously located CTD plume signals. The dive recorded significant Eh anomalies in mid-water toward the centre of our survey but approximately 400m West of where the Drachenschlund vent was eventually detected. In fact, the vehicle flew directly over the vent site while converging onto its connector line after rising to survey height on ABE 177 but saw little indication of the vent.

ABE 178 Summary:

Launch: 2006/05/21 18:45	Recovery: 2006/05/22 15:04
Survey start: 2006/05/21 21:21	Survey end: 2006/05/22 11:29
Survey distance: 21.74 km	Ave survey depth: 2844 m

ABE178 was a phase 2 dive at Nibelungen. The dive succeeded in locating the vent, but we were a little lucky. The main survey area showed no substantial hits on Eh, backscatter, or temperature. But on the connector line from the landing spot to the start of the first line, the vehicle got solid hits on all sensors. In hindsight, the survey block should have been moved more to the east. Fig. 1.4 shows the Eh data superimposed on the multibeam bathymetry. Eh, backscatter and temperature all showed strong hits at the very beginning of the survey over the Drachenschlund site.

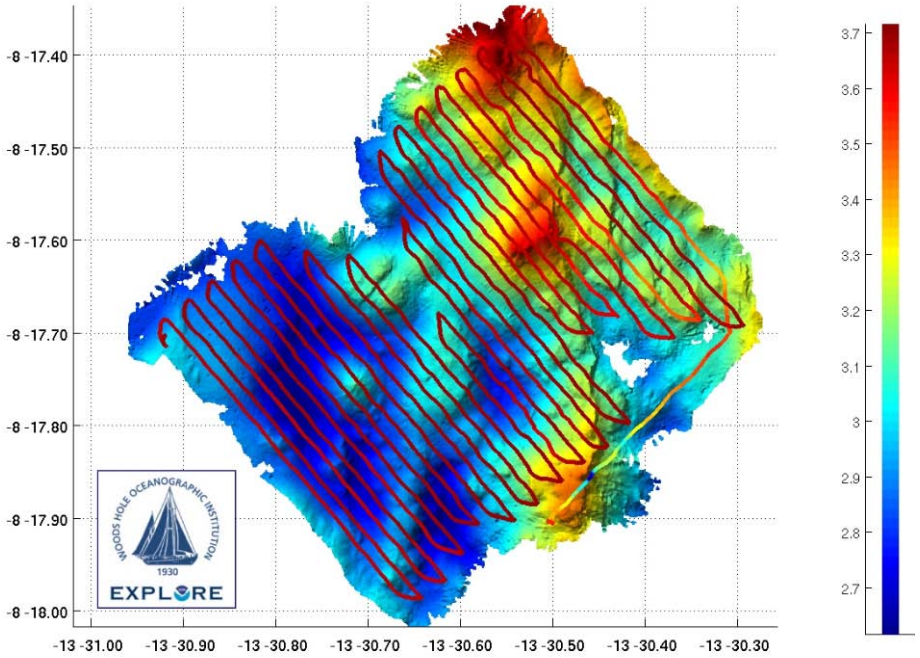

Fig. 1.4 Eh data superimposed on the multibeam bathymetry for the ABE178 dive

ABE 179 Summary:

Launch: 2006/05/22 20:49	Recovery: 2006/05/23 10:23
Survey start: 2006/05/23 00:06	Survey end: 2006/05/23 06:58
Survey distance: 3.18 km	Ave survey depth: 2860 m

ABE179 was a very successful “truncated” phase 3 survey at Nibelungen. The vehicle passed directly over a black smoker that was named Drachenschlund (Dragon's Throat). The site was very rugged: over 200 meter tracklines the vehicle changed depth by 90 meters on one side of the rise and 40 meters on the other side. The vehicle had trouble when attempting to descend the steep slope on the 2nd through 5th eastbound tracklines. When it reached the sharp drop-off, the vehicle would reduce forward thrust to maintain the proper distance from the seafloor, at which point the current would force the vehicle back. So the vehicle would get stuck at the cliff edge, confirmed in ABE’s photographs. The ROV pilots reported similar problems in attempting to fly down to the east from the crest of the hill.

Fortunately, ABE managed to get over the drop-off on the line that really counted. ABE flew over the edge of the smoker field on the eastbound descending line, then flew directly over the smoker on the return ascent. Fig. 1.5 shows the temperature (T2) data for the run.

There is only one significant hit, directly above the Drachenschlund vent even though Eh and backscatter anomalies were also observed along the cliff-top where the vehicle stalled, to the south west. Although ABE photographed additional extinct chimneys – and more were found with the ROV on subsequent dives – it seems likely that there is only one high-temperature fluid flow source at this site – the Drachenschlund vent, itself.

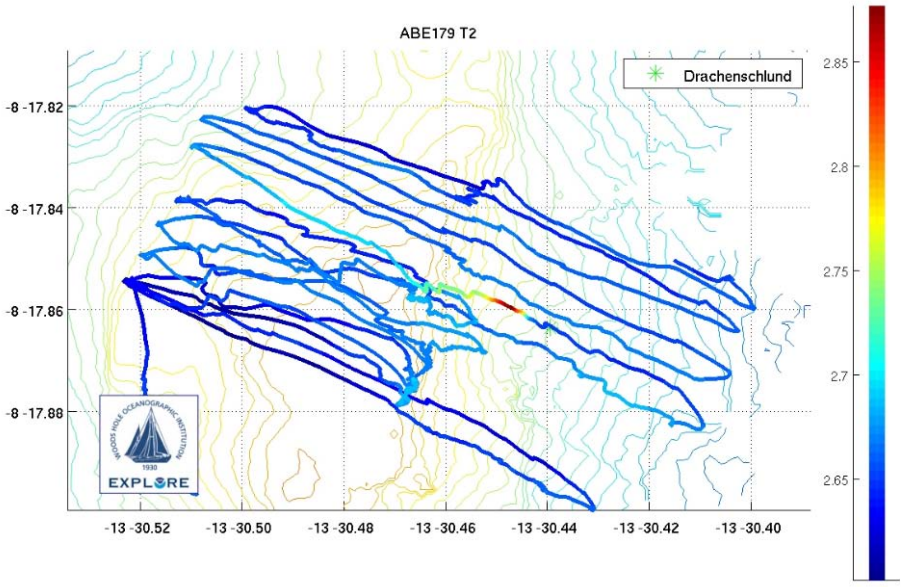

Fig. 1.5 Temperature (T2) data for the ABE 179 run

A1 Segment, 7°57'S

Two final ABE dives were conducted, centered at 7°57'S where previous observations of particle-rich plume anomalies from CTD profiles and TOBI/MAPR data were confirmed by CTD tow-yo during this expedition. Although only minimal water column work had been conducted, it was possible to continue ABE exploration by close coordination with the ROV team who were simultaneously investigating the Drachenschlund vent located by ABE during dives 177-179.

ABE 180 Summary:

Launch: 2006/05/24 07:00	Recovery: 2006/05/25 05:44
Survey start: 2006/05/24 09:28	Survey end: 2006/05/25 02:59
Survey distance: 35.21 km	Ave survey depth: 2601 m

ABE180 was a phase 1 dive at the 8°S site. It provided some weak clues, which we followed up in ABE181 with no conclusive result. The dive took place over a shelf cut into a very steep cliff – the A1 segment's western rift-valley wall. The shelf was split in two parts. The survey lines were conducted at previously reported plume height (2600m) and planned to align at their western end with the 2700 contour. Lines were aligned East-West and designed to span the entire target depth range on the seafloor, 2700-2900m.

From Eh records, the two most significant hits were shortly after leaving the mooring and then when crossing back near the landing spot, but the magnitude of these hits was rather small.

ABE 181 Summary:

Launch: 2006/05/26 05:59	Recovery: 2006/05/27 02:12
Survey start: 2006/05/26 08:30	Survey end: 2006/05/26 23:11
Survey distance: 21.06 km	Ave survey depth: 2787 m

ABE181 was a phase 2 survey at the 8°S site. It did not find any plausible sources for the significant plume anomalies found in the CTD tow-yo.

In the SE corner of our survey the vehicle stalled for long periods. Clearly, driving along a steeply dropping edge should be avoided in the future. Better to drive off the edge, despite the problems encountered in ABE 179, and then approach the cliff at the floor level, climbing the cliff to proceed. We saw little if any significant plume activity on any of the sensors. The SM2000 bathymetry for the area, previously hidden in shadow in TOBI sidescan, reveals an area that is flat with low backscatter. There is a rise toward the drop-off, then the steep drop-off itself. Unfortunately, survey lines timed out when approaching our prime target area from ABE 180 in the SE corner of the plateau.

1.4.3 ROV Deployments

1.4.3.1 Technical Description of the ROV

(C. Seiter, D. Edge, H. A. Mai, H. Marbler, W. Schmidt, I. Suck, M. Zarrouk)

During M68-1, the remotely operated vehicle (ROV) “QUEST4000m" was used aboard R/V METEOR on its 9th cruise mission. "QUEST4000m" is operated by and installed at MARUM, Center for Marine Environmental Sciences at the University of Bremen, Germany and was designed and built by Schilling Robotics, Davis, USA.

The free-flying ROV "QUEST4000m" (Fig. 1.6) is equipped with an RDI 1200 Hz Doppler Velocity Log (DVL), which, in combination with 60 kW electrical propulsion power from seven electric ring thrusters provides a relative positioning accuracy of the vehicle within decimeters. When combined with the ship’s hull-mounted IXSEA Posidonia USBL positioning system an absolute GPS positioning accuracy withing 10-15 m could be obtained during cruise M68-1.

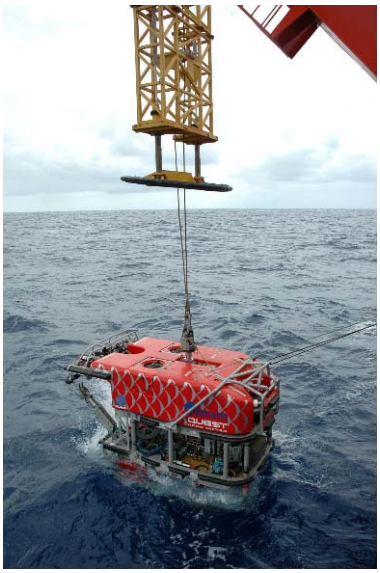

Fig. 1.6
MARUM ROV “QUEST4000m” deployed from the A-frame mounted launch and recovery system (LARS) behind the stern of R/V METEOR

The "QUEST4000m" telemetry and power supply system SeaNet with its two vehicle installed HUBs provides the capacity of using up to 16 video and 60 RS-232 data channels. The data transfer and communication - control data to the vehicle as well as sensor, diagnostics, and video data from the vehicle - is done via one single mode optical fibre and can be observed and controlled during operation.

The basic "QUEST4000m" vehicle set up includes on port side a 5-function manipulator (“Rigmaster”) and on starboard side a 7-function master arm controlled slave manipulator (“Orion”) for task requiring sampling tools and devices. Two hydraulically driven toolskid-mounted drawers with boxes and/or custom built mounting frames provide the accessability and storage of these tools and devices, as well as of samples.

Detailed photo shooting and camera filming is possible with four video cameras and one digital still camera. In addition, the set up contains three small fix-focus colour cameras for tool and device handling observation tasks. Further equipment installed on the vehicle front includes two lasers for dimension measuring, a CTD with additional turbidity and high temperature sensor, an acoustic beacon finder for site marking and/or positioning, and a scanning sonar for mapping and also safety reasons in steep and dangerous environments.

During cruise M68-1, “QUEST4000m” performed 11 dives including one dive for LAR training and system stability testing. All dives were planned in cooperation with the science team and were based on a combination of the results of the Woods Hole Oceanographic Institute (WHOI) autonomous underwater vehicle (AUV) ABE phase 1-3 survey flights, CTD station results (Oceanography Institute, University of Bremen), and on results from previous cruises, i.e. M62-5 and M64-1. A total dive time of 108 hrs 13 min including 67 hrs 32 min bottom time was achieved with highly efficient operational quality.

Table 1.1 gives a short overview of the M68-1 station numbers, Marum ROV “QUEST4000m” dive numbers, sites visited, maximum dive depth and all LAR and bottom start and end times. For detailed descriptions of the single ROV dives see chapter 1.4.3.2.

Table 1.1 Overview about M68-1 station and Marum dive numbers, sites, and all LAR and botom start and end times

M68-1 Station #	Marum Dive #	Date	Site	Depth (m)	Time Launch	Time Start (Bottom)	Time End (Bottom)	Time on Deck	Bottom Time	Total Dive Time
	85	05.05.06	Test Dive	920	15:30			17:30		**02:00**
03ROV	86	10.05.06	Wideawake/ Turtle Pits	3000	12:30	14:21	22:20	00:38	**07:59**	**12:08**
07ROV	87	11.05.06	Red Lion	3000	10:15	12:30	21:00	23:22	**08:30**	**13:07**
12ROV	88	12.05.06	Turtle Pits/ Wideawake	3000	11:10	13:02	21:33	23:53	**08:31**	**12:43**
20ROV	89	14.05.06	Comfortless Cove	3000	11:02	12:58	21:15	00:15	**08:17**	**13:13**
24ROV	90	15.05.06	Comfortless Cove	3000	14:55	17:10	23:11	01:00	**06:01**	**10:05**

Table 1.1 Overview about M68-1 station and Marum dive numbers, sites, and all LAR and botom start and end times (continued)

M68-1 Station #	Marum Dive #	Date	Site	Depth (m)	Time Launch	Time Start (Bottom)	Time End (Bottom)	Time on Deck	Bottom Time	Total Dive Time
39ROV	91	18.05.06	Roman City/ Limtoc	1500	18:15	19:22	23:58	01:11	**04:36**	**06:56**
41ROV	92	19.05.06	Lilliput/Candelabrum Maedow	1495	15:00	16:06	22:44	00:13	**06:38**	**09:13**
63ROV	93	24.05.06	Nibelungen	2900	13:50	15:45	22:28	01:50	**06:43**	**12:00**
69ROV	94	26.05.06	Nibelungen	2900	13:40	15:33	21:45	00:05	**06:12**	**10:25**
70ROV	95	27.05.06	Roman City/ Limtoc	1500	13:42	14:50	19:55	22:05	**04:05**	**08:23**

The following scientific tools and devices were used on "QUEST4000m" during the above - mentioned dives for obtaining biological, geological, sediment, and fluid-geochemical samples. All tools were primarily handled or released with the 7-function "Orion" slave manipulator, if necessary supported by the 5-function "Rigmaster" manipulator:

- fine mashed nets with and without lid for mussels, clams, polychaetes, and sediment samples
- KIPS fluid nozzle and high temperature sensor on a T-handle for fluid samples and in-situ T monitoring He-sample tubes for fluid samples, pressure keeping MicroCat CTD on a spool for measuring oceanographic parameters in and above hot vent plumes
- suction gun with rotary sampler for sediment, glass, gravel, and biological samples
- Niskin bottles for fluid samples
- fine cotton sack for particle sampling above hot vents
- buoyant markers with ground weight for marking new hydrothermal sites
- metal scoops for sediment and biology samples

On two dives, an ADCP from the Oceanography Institute, University of Bremen was mounted on the ROV in place of the rotary sampler. ADCP, rotary sampler/suction pump, and KIPS valve and pump, were topside software controlled.

1.4.3.2 Description of the ROV Dives

(C. Devey, K. Lackschewitz, B. Melchert)

Wideawake and Turtle Pits (Stations 3ROV (Dive 86) and 12ROV (dive 88))

Both dives aimed at sampling fluids, rocks and biology in the Turtle Pits high temperature field and the Wideawake diffuse flow area. During the first dive we were able to take co-located biological and fluid samples (with temperatures around 18°C) at a Wideawake vent (Figure 1.7 a), and sample the fresh lava flow which marks the eastern margin of the field (and apparently overlies a low-temperature vent at Wideawake, see Figure 1.7 b).

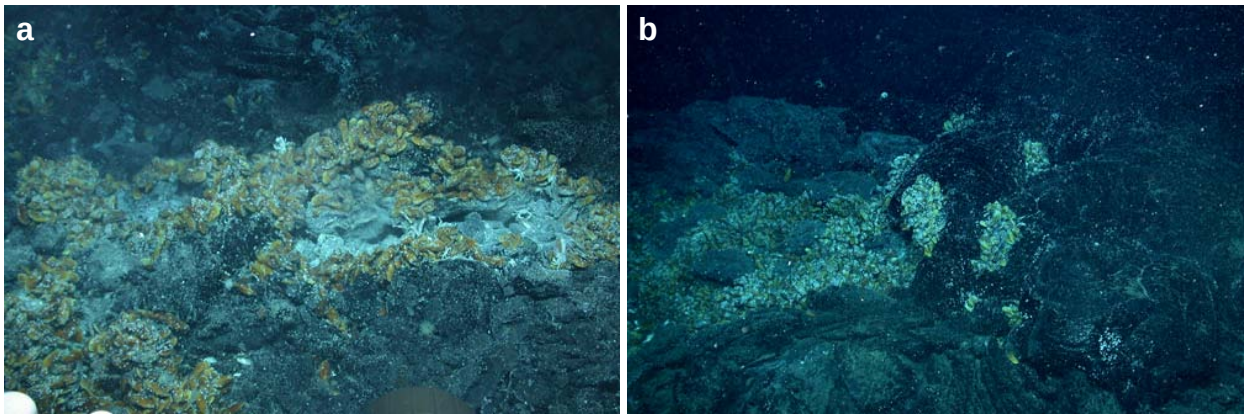

Fig. 1.7 **a**: The Wideawake vent sampled for fluids and biology during 3ROV. **b**: Fresh lava apparently covering part of a Wideawake vent, where mussels have started to settle

This fresh lava appears to have more sediment cover this year than last, based on photo comparisons. The second dive (12ROV) also returned one specimen of Calyptogena clam. The sampling at Turtle Pits consisted of collection of water samples (using both KIPS, Niskin bottles and helium tubes) from the high temperature vents, including one sample during 12ROV which gave the highest temperature yet recorded worldwide on a spreading axis vent of 408.5°C. Collection of sulphide samples at the hot vents was also achieved – no mussel samples could be collected at Turtle Pits, the fresh lava visible on the ABE pictures from 2005 was also no longer accessible, presumably covered with chimney debris in the last year. Photomosaicing of the largest chimney at Turtle Pits, "Southern Tower", shows how quickly these structures grow. Since May 2005 the Tower has risen by 4m!

Red Lion Hydrothermal Field (Station 7ROV (dive87))

The Red Lion hydrothermal field was discovered and sampled in 2005 during the RV Charles Darwin cruise 169 and the RV Meteor cruise M64/1. During M68/1 we visited this field again in order to document any changes in the structure of the chimneys and in the biological activity and to continue our time-series experiments. The Red Lion hydrothermal field is characterized by 4 active chimneys called Shrimp Farm, Zuckerhut (Sugarhead), Mephisto and Tannenbaum. During dive 87 (station 7ROV), we surveyed the relative positions of these structures using USBL (Posidonia) and DVL navigation on the ROV. We determined the Posidonia position of Shrimp Farm (4°47.827 S/12°22.604 W, 3047 m water depth) and measured the position of the other three smokers relative to this (see Figure 1.8, below).

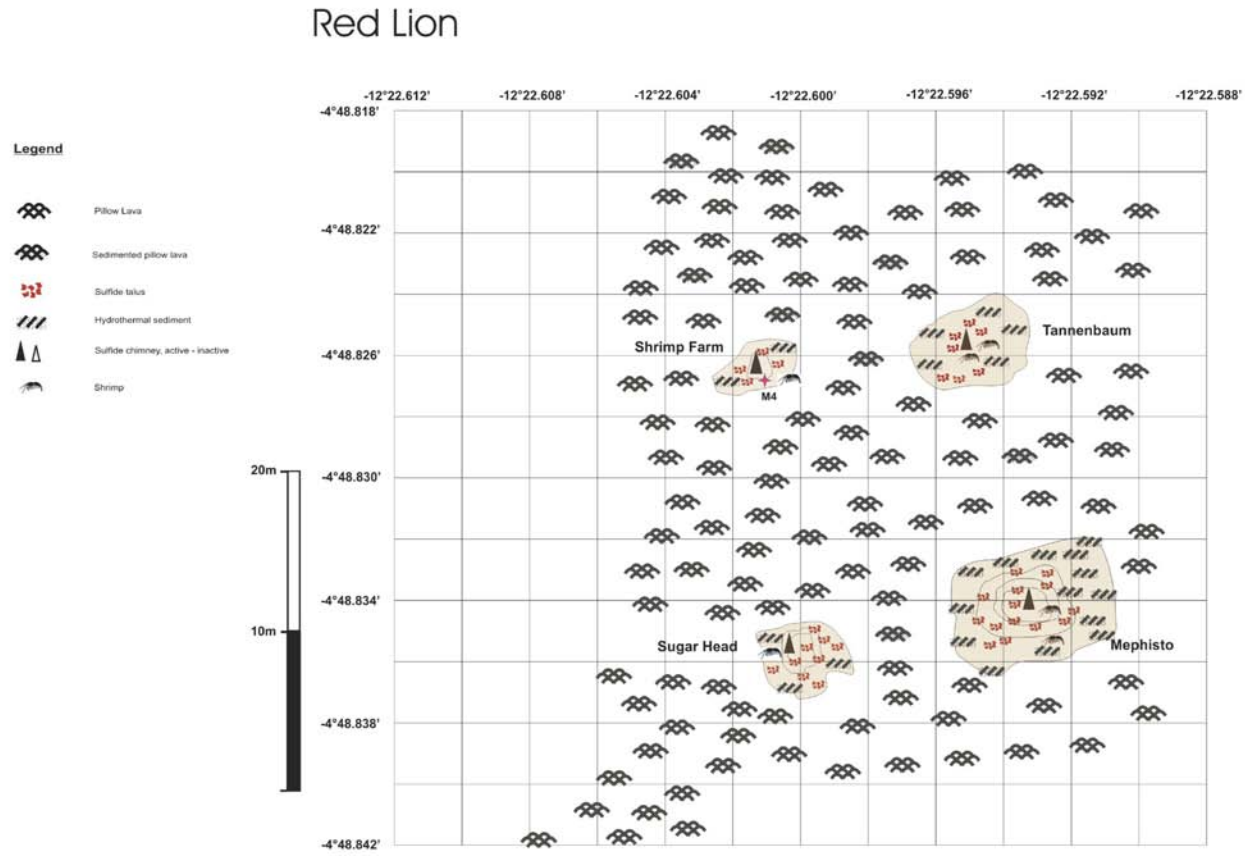

Fig. 1.8 Map of Red Lion field based on measurements made during station 7ROV

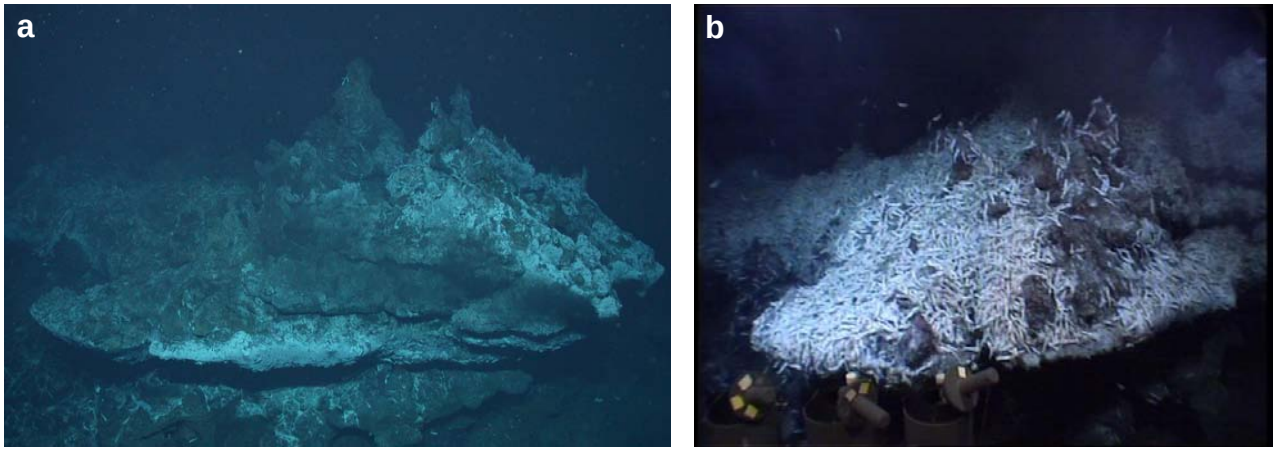

Fig. 1.9 **a**: Showing chimney "Shrimp Farm" with only a few shrimps during M68/1 (2006). **b**: "Shrimp Farm" covered with shrimps during M64/1 (2005)

In comparison to the M64/1 expedition the shrimp coverage has drastically decreased at the Shrimp Farm smoker, whereas Mephisto had more extensive shrimp colonization this year (Figures 1.9 a and b). We sampled a net with shrimps, a sulfide sample and fluid samples from

the high temperature vents at Mephisto. During fluid sampling we recorded a constant temperature of 345°C whereas the maximum temperature measured was 380°C. A second sulfide sample was taken at the base of Tannenbaum.

The New Vent Field "Comfortless Cove" (Stations 20ROV (dive 89) and 24ROV (dive 90))

Based on an ABE survey, the ROV started dive 89 at 4°48.13'S/12°22.35'W where the Eh-sensor of ABE measured 3 distinct anomalies. The area is characterized by a mound consisting of pillows (Fig. 1.10).

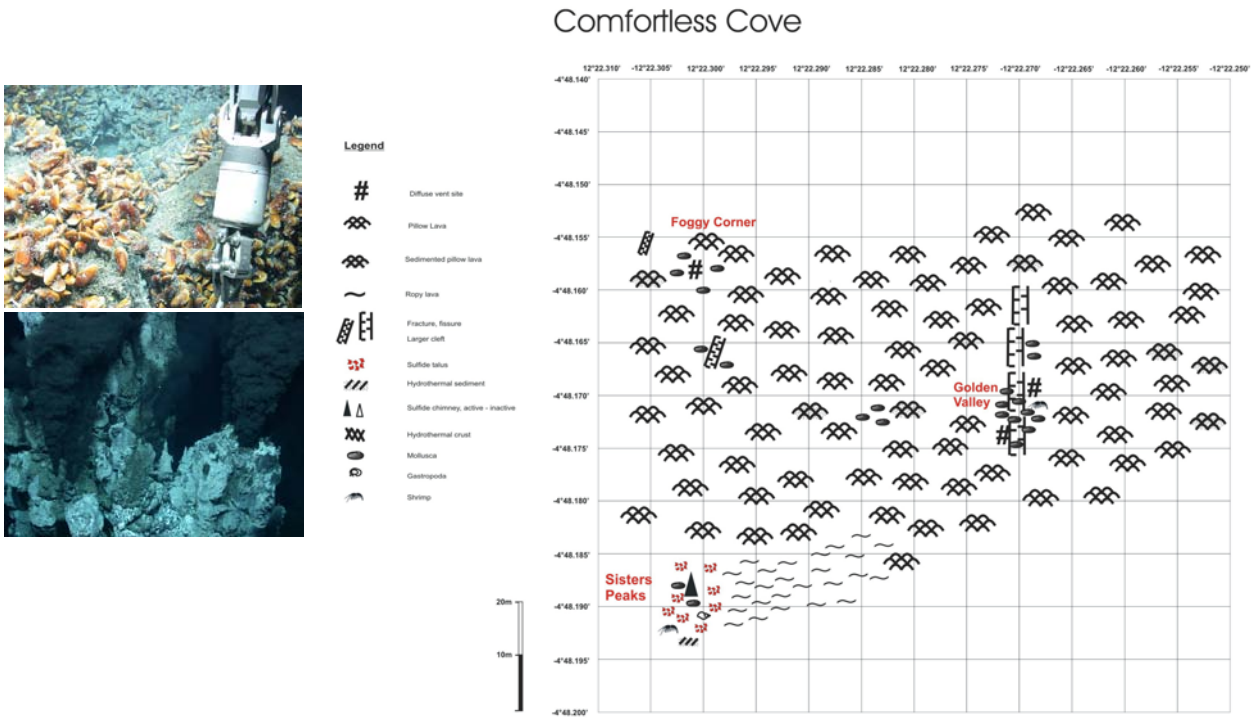

Fig. 1.10 Map of region around Comfortless Cove area compiled on the basis of ROV observations. The pictures showing dense population of *Bathymodiolus* in the Golden Valley (up) and high-temperature chimneys at Sisters Peak (bottom)

The area with the highest Eh-anomaly is related to a 12.8 m high smoker with two spires (named „Sisters Peak") approximately 70 m southeast of the mound (4°48.188'S/12°22.301'W, 2996 m; Fig. 1.15 and 1.16). The east spire of this smoker is inactive, whereas the west spire is venting intensely. Temperature measurements revealed exit temperatures of up to 399°C. The base of the chimney is colonized by mussels, crabs and shrimps which were sampled for taxonomic studies (see chapter „Zoology"). A sulfide pile at the eastern base of the chimney is covered by a very fresh and probably young lava flow.

We found an intensely-colonized mussel field („Golden Valley", see Fig. 1.10) in a N-S oriented fissure somewhat north and east of Sisters Peak. We placed "Marker 6" (4°48.166'S / 12°22.267'W, 2981 m) at this site. On ROV dive 90 we took biological and fluid samples and measured a temperature of 3.6°C between the mussels. Another diffusely venting field lies approximately 50 m to the northwest of Golden Valley, almost along strike from Sisters Peak.

The size of the field is 10 * 20 m and is characterized by lots of mussel patches and a diffuse venting with temperatures of up to 5°C. The cloudy water which characterized this area led us to name it “Foggy Corner”. Here, we placed “Marker 7” (4°48.159’S/12°22.306’W) and sampled diffuse fluids.

Diffuse Vent Fields Around Lilliput (Stations 39ROV (dive 91), 41ROV (dive 92) and 70ROV (dive 95))

Three AUV and two ROV dives were dedicated to the area around Lilliput. The AUV deployments yielded several additional targets located both north and south of Lilliput. The ROV dives then studied these, with station 39ROV (dive 91) going south and 41ROV (dive 92) revisiting Lilliput and exploring the area to the north.

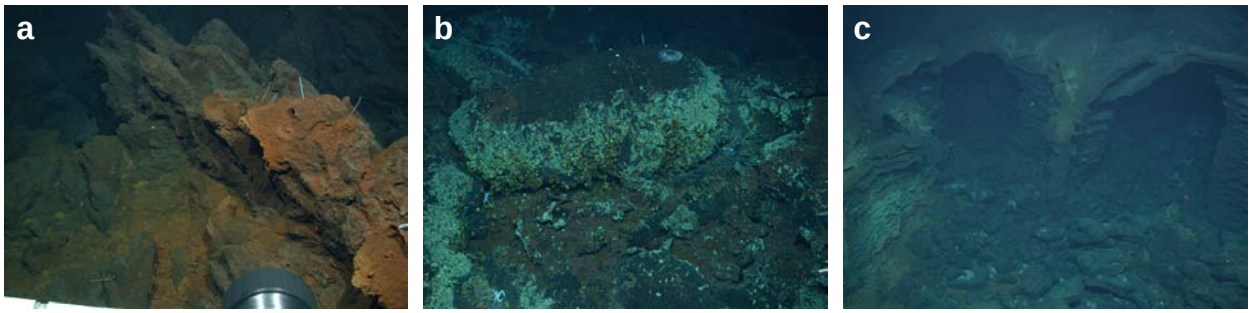

Fig. 1.11 **a**: Extinct hydrothermal mound. **b**: Mussel field south of Lilliput. **c**: Lava drainout roof-and-column structure, columns have hydrothermal flow

The area is characterised by evidence for two distinct types of hydrothermal activity;

(a) large mounds of orange-coloured, presumably Fe-rich hydrothermal sediments at which we found no evidence for present-day venting (Fig. 1.11 a)

(b) diffuse venting (e.g. Fig. 1.11 b) apparently sometimes associated with high-porosity lava-sheet fields showing columns and roof-collapse (Fig 1.11 c).

Lilliput is an example of this type of venting. Figure 1.12 shows a detailed bathymetric map of the area around Lilliput from the ABE SM2000 sonar together with the TOBI sidescan image and the tracks of ROV dives carried out there during M68-1.

The Lilliput vent field itself is characterized by red-orange Fe-oxide-rich hydrothermal deposits which we sampled successfully at the site of the M64/1 “Marker A” (9°32.845’S/13°12.546’W, 1496m). Close to the deposits several mussel patches with mostly juvenile mussels, some crabs and a few shrimps are concentrated.

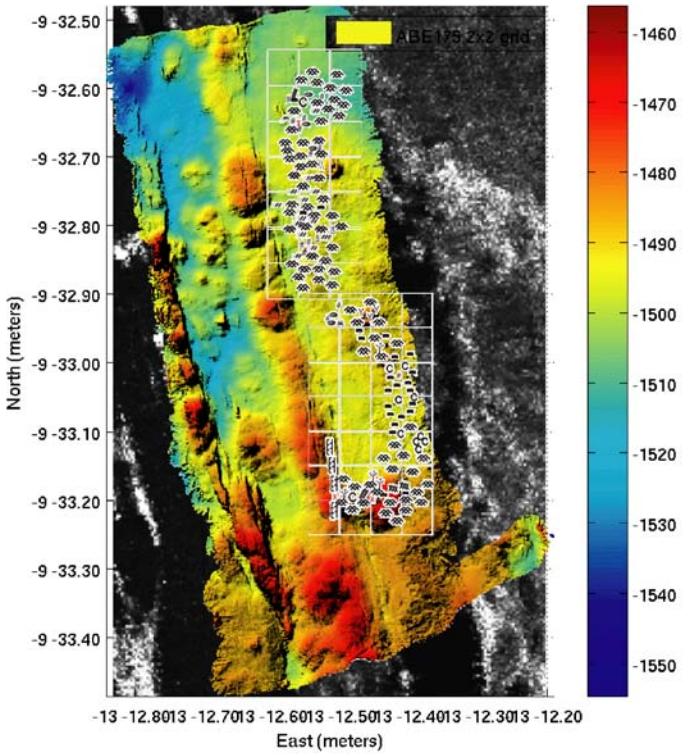

Fig. 1.12 TOBI-side scan imagery, ABE SM2000 bathymetry and ROV-based seafloor observations around the Lilliput field

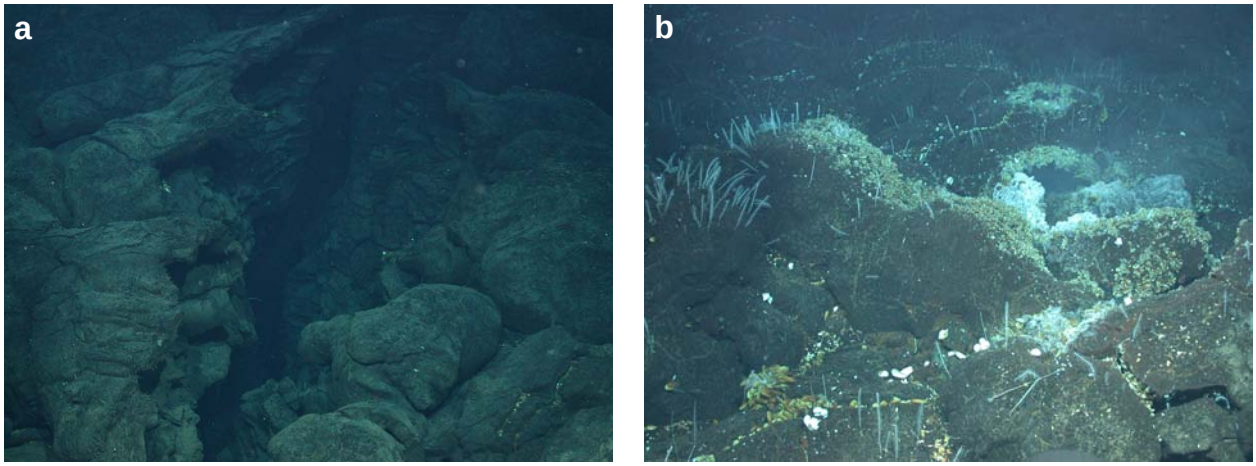

Fig. 1.13 **a**: Fissure with lava tongues flowing downwards. **b**: The diffuse venting field “Candelabrum Meadow”

Shimmering water is visible above some of the mussel patches. During our fluid sampling program at one of these sites we measured temperatures up to 4.8°C (background temperature is 4.0°C). Approximately 200m NNW of Lilliput (at 9°32.675’S/13°12.562’W, 1501m) we found another diffuse venting field based on the results of the AUV deployment. The field is characterized by mussel colonies and some collapsed pillows with venting of milky water in some places. Temperature measurements gave values of up to 6.6°C.

A third diffuse venting field lies approximately 70m ENE of the field described above (9°32.653'S/13°12.552'W). The area between both these fields shows a broad fissure where downward flowing lava tongues indicate this fissure as their eruption source (Fig. 1.13 a). The third diffuse venting field shows abundant hydrozoans of the species *Candelabrum* growing on top of the pillows (Fig. 1.13 b) leading us to call it "Candelabrum Meadow". During the fluid sampling we measured a temperature of up to 7°C.

The Nibelungen Hydrothermal Field (Stations 62ROV (dive93) and 69ROV (dive94))

During the Meteor cruise M62/5 in 2004, we found strong evidence for hydrothermal activity on a topographic high that rises to 2900 m depth from the rift valley floor at 3500 m between 8°17' S and 8°19' S to the East of the tip of ridge segment A2 (named Cheating Bay). High methane concentrations (up to 115 nmol/l) together with layers of increased light scattering peaking at 2700m depth in the vicinity of 8°18'S, 13°31'W indicated the presence of venting in this area, although black smokers were not directly observed (Devey et al., 2005). During cruise M68/1 we discovered the Nibelungen vent site with the AUV "ABE" by eH- and photo-mapping at the eastern side of Cheating Bay (see chapter AUV).

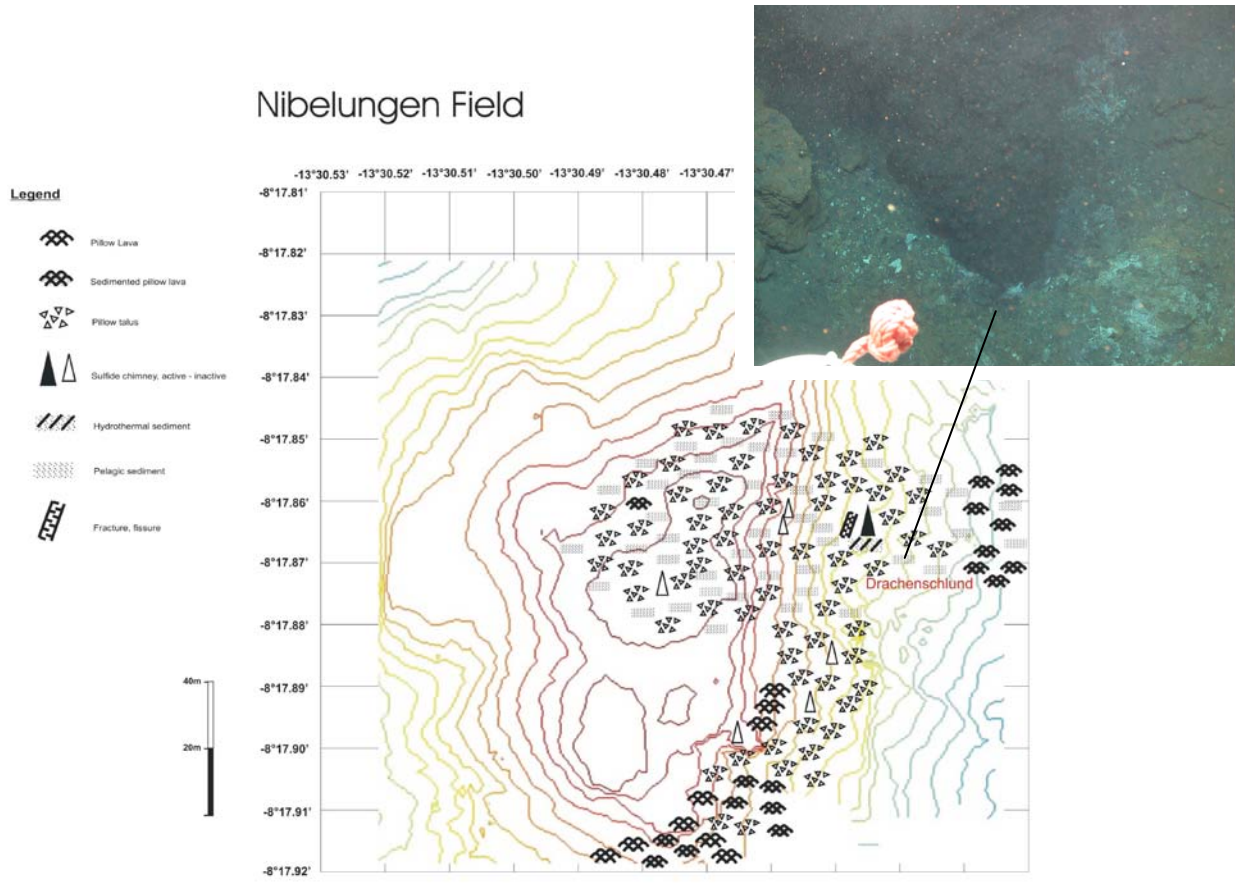

Fig. 1.14 Map of the area of the Nibelungen vent site and the active smoking crater site "Drachenschlund" at the Nibelungen Field

The following dive of the ROV "Quest" (station 62ROV) revealed active and inactive vent sites along a steep slope at 2905 m water depth (see Fig. 1.14). The only active vent site (located at 8°17.853'S, 13°30.443'W) is characterised by a 4-5 m wide crater, where intense flow of hydrothermal fluid produced a black smoker from an estimated 0.5 m wide hole (see picture in fig. 1.14). Although it was difficult to come close to the hole, we sampled hot fluids about 1m above the seafloor at constant temperatures of 90°C. The highest measured temperature was 175°C. The 4 m high crater wall consists of talus of basaltic and serpentinized clasts and breccias. The fauna was sparse, consisting of anemones and polychaetes which we sampled during dives 62 and 69. We named this smoking crater "Drachenschlund". On top of the northern crater rim we placed a marker (#9). At both sides of the crater several extinct groups of chimney spires are located (Fig. 1.15 a).

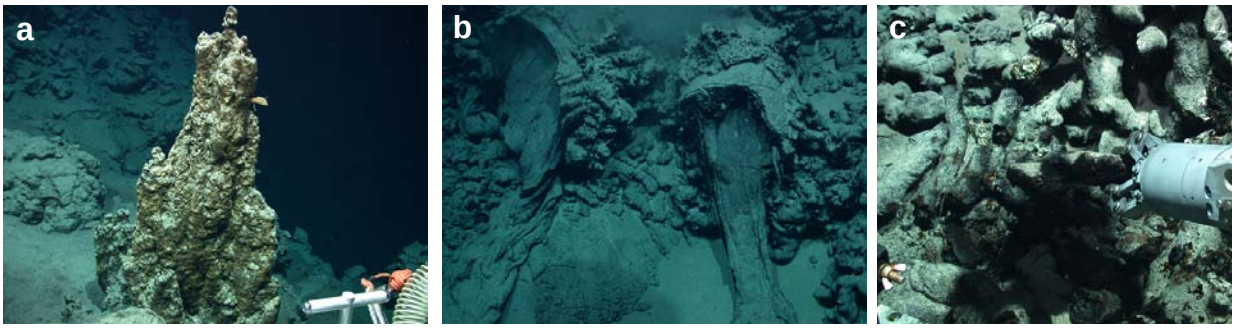

Fig. 1.15 **a**: Inactive chimney spire on a steep slope at the Nibelungen Field. **b**: Broken pillow shells out of which the last lava remnants have drained. **c**: Small lava buds on the southeast corner of the Nibelungen massif

During dive 69ROV we mapped the southern extent of the Nibelungen field. Several extinct chimneys were found along the 2900 m contour line of the slope almost as far south as the southeastern edge of the hill (8°17.898'S, 13°30.468'W). The south-easternmost corner of the hill shows broken pillow shells out of which the last lava remnants have drained (Fig. 1.15 b) and abundant small lava tubes (Fig. 1.15 c). The slope below the 2900 m contour line is characterized by sediment and a lot of talus material. Above this line the slope consists mainly of pillow lavas.

1.4.4 Description of Rocks and Hydrothermal Precipitates

(K.S. Lackschewitz, C.W. Devey, S. Petersen)

During cruise M68/1 a total of 8 ROV dives, 10 wax corers and 3 dredge stations recovered geological samples from hydrothermal fields and the ocean crust between 5°S and 10°S along the slow-spreading Mid-Atlantic Ridge. The samples consist of fresh to altered basalts, sulfides, Fe-oxyhydroxides and serpentinized breccias. More information on all the successful sampling stations is given in Table 1.2.

During the stations 3ROV (dive #86) and 12ROV (dive #88), fresh lava crusts and volcanic glass were recovered from the Wideawake diffuse flow area. The stations were also targeted at the high-temperature chimneys of the Turtle Pits hydrothermal field. One sample is a typical piece from a massive sulfide mound forming the base of the "Two Boat" chimney and is characterized by recrystallized chalcopyrite, pyrite ± haematite, magnetite(?) and anhydrite. Another sample is rubble of a beehive structure from the "Southern Tower" consisting of chalcopyrite, sphalerite and pyrrhotite. 7ROV recovered several sulfide samples from the "Red Lion" hydrothermal field. Sample 7ROV-1 was taken from the base of "Tannenbaum", comprising recrystallized marcasite, pyrite and sphalerite, whereas samples 7ROV-2 to –4 were taken from base of "Mephisto" and are characterized by marcasite, chalcopyrite, sphalerite, wurzite and pyrite.

Table 1.2 Rocks and hydrothermal precipitates

No.	Date / time	Lat / Long	Depth	comment
3ROV-6B	10.05.06/17:28	Wideawake 4°48.640'S/ 12°22.363'W	2980 m	Sparsely plagioclase-phyric lava crust with glass
3ROV-7B	10.05.06/17:37	Wideawake 4°48.640'S/12°22.363'W	2980 m	Sparsely plagioclase-phyric lava crust with glass
3ROV-8	10.05.06/17:28	Wideawake 4°48.620'S/ 12°22.345'W	2984 m	volcanic glass chips
6VSR	11.05.06/08:57	4°47.82'S/ 12°22.62'W	3036 m	Few pieces of fresh volcanic glass
7ROV-1	11.05.06/14:32	Red Lion 4°47.826'S/ 12°22.595'W	3046 m	chimney outer wall fragment from base of Tannenbaum
7ROV-6	11.05.06/18:42	Red Lion 4°47.834'S/ 12°22.593'W	3045 m	Outer thin wall of a high-temp. chimney from base of Mephisto
7ROV-7	11.05.06/18:52	Red Lion 4°47.834'S/ 12°22.593'W	3045 m	Altered sulfide rubble from base of Mephisto
7ROV-8	11.05.06/18:55	Red Lion 4°47.834'S/ 12°22.593'W	3045 m	Altered sulfide rubble from base of Mephisto
12ROV-1	12.05.06/13:49	Turtle Pits 4°48.576'S/ 12°22.418'W	2994 m	massive sulfide from base of Two Boats
12ROV-2	12.05.06/15:28	Turtle Pits 4°48.576'S/ 12°22.414'W	2985 m	beehive rubble from Southern Tower
12ROV-3B	12.05.06/17:43	Wideawake 4°48.6'S/ 12°22.3'W	2980 m	Glassy lava crust
12ROV-9B	12.05.06/21:26	Wideawake 4°48.6S/ 12°22.3'W	2980 m	sheet lava with glass crust
14VSR	13.05.06/15:22	4°48.10'S/12°22.38'W	2989 m	Small volcanic glass chips
20ROV-1A	14.05.06/15:30	Comfortless Cove 4°48.188'S/12°22.301'W	2996 m	Altered chimney fragments from base of Sisters Peak
20ROV-2	14.05.06/17:00	Comfortless Cove 4°48.188'S/12°22.301'W	2996 m	Chimney outer wall fragment from base of Sisters Peak
20ROV-3A, -B	14.05.06/17:05	Comfortless Cove 4°48.188'S/12°22.301'W	2996 m	3A: Massive sulfide with a 0.5 cm Fe-oxide crust from base of Sisters Peak 3B: Lava flow from base of Sisters Peak overflowing sulfides
28DS-1 to -3	17.05.06/12:23	9°32.79'S/13°12.25'W	1441 m	Old pillow segments with mm-thick Mn-crust
30VSR	17.05.06/21:54	9°33.90'S/13°12.30'W	1456 m	A few volcanic glass chips
31VSR	17.05.06/22:45	9°33.70'S/13°12.41'W	1476 m	Fresh volcanic glass chips
33VSR	18.05.06/00:44	9°33.09'S/ 13°12.55'W	1479 m	A few volcanic glass chips
36VSR	18.05.06/9:42	9°31.94'S/13°12.78'W	1477 m	200g volcanic glass chips

Table 1.2 Rocks and hydrothermal precipitates (continued)

No.	Date / time	Lat / Long	Depth	comment
39ROV-1	18.05.06/21:38	Roman City 9°33.148'S/13°12.420'W	1486 m	red FeO(OH) mud
39ROV-2	18.05.06/21:43	Roman City 9°33.148'S/13°12.420'W	1486 m	aphyric basalt
39ROV-6A	18.05.06/23:55	Limtoc 9°32.956'S/ 13°12.524'W	1494 m	volcanic glass crust
39ROV-7B	18.05.06/23:56	Limtoc 9°32.956'S/ 13°12.524'W	1494 m	FeO(OH) crust
41ROV-1	19.05.06/17:11	Lilliput 9°32.845'S/ 13°12.546'W	1495 m	red FeO(OH) mud
41ROV-14	19.05.06/22:40	9°32.639'S/ 13°12.490'W	1496 m	volcanic glass
46VSR	21.05.06/12:45	8°17.31'S/ 13°35.82'W	2904 m	Sheet flow fragment with glass
54VSR	22.05.06/14:36	8°15.80'S/ 13°31.10'W	3211 m	Soft white sediment
57VSR	23.05.06/4:45	8°21.06'S/ 13°35.00'W	2807 m	Some glass above cloth
58VSR	23.05.06/6:40	8°22.48'S/ 13°35.07'W	2774 m	Almost empty, some glass on outside
62ROV-1	24.05.06/17:48	Nibelungen 8°17.884'S/ 13°30.451'W	2906 m	inactive chimney fragment
62ROV-2	24.05.06/18:45	Nibelungen 8°17.858'S/ 13°30.358'W	2906 m	inactive chimney fragment
62ROV-6	24.05.06/20:57	Nibelungen 8°17.853'S/ 13°30.443'W	2903 m	serpentinzed breccia from Drachenschlund crater
62ROV-11	24.05.06/22:15	Nibelungen 8°17.853'S/ 13°30.443'W	2903 m	breccia of altered basalts from Drachenschlund crater
66DS-1 to -8	25.05.06/23:03	7°57.14'S/ 13°27.72'W	3034 m	Several massive basalt and pillow pieces, some with glass
69ROV-1	26.05.06/17:00	Nibelungen 8°17.916'S/ 13°30.482'W	2878 m	Lava tube
69ROV-2A	26.05.06/20:10	Nibelungen 8°17.916'S/ 13°30.438'W	2898 m	strongly altered wall rock
70ROV-4	27.05.06/18:00	Roman City 9°33.094'S/ 13°12.410'W	1495 m	Lava piece from Roman City
71DS-1 to -4	28.05.06/05:40	Nibelungen 8°17.83'S/ 13°30.51'W	2854 m	Pillow buds and a hydrothermal crust with Mn-coating (-2)

During station 20ROV (dive #89) outer chimney wall fragments were sampled from the base of the high-temperature chimney "Sisters Peak" at the newly-discovered Comfortless Cove hydrothermal field (see Fig. 1.16). These chimney fragments consist of an outer pyrite-marcasite crust followed by pyrrhotite-sphalerite and an inner zone of chalcopyrite. In addition, we recovered a piece of a relatively fresh lava flow covering a sulfide pile at the eastern base of the chimney.

During two ROV stations (39ROV, dive #91; 41ROV, dive #92) hydrothermal Fe-oxyhydroxide-rich crusts and mud were sampled from three diffusely venting hydrothermal fields (Roman City, Limtoc, and Lilliput) around 9°33 (see Fig. 1.16). During both dives we also sampled a basalt, a glass crust and volcanic glass chips. At station 70ROV (dive 95) a lava piece from top of the "Roman City" roof was recovered (see Fig. 1.16).

Geological sampling during stations 62ROV (dive #93) and 69ROV (dive #94) at the Nibelungen hydrothermal field recovered sulfide samples from inactive chimneys, lava fragments, as well as serpentinized and basaltic breccias, from the „Drachenschlund" smoking crater.

Three dredges at 7°57'S (station 66DS), 8°18'S (station 71DS), and 9°32'S (station 66DS) recovered old pillow segments with a 1mm Mn-crust, pillow buds with a mm-thick glass crust and basalt fragments with glass crusts, respectively.

At 9 wax core stations we recovered varying amounts of volcanic glass.

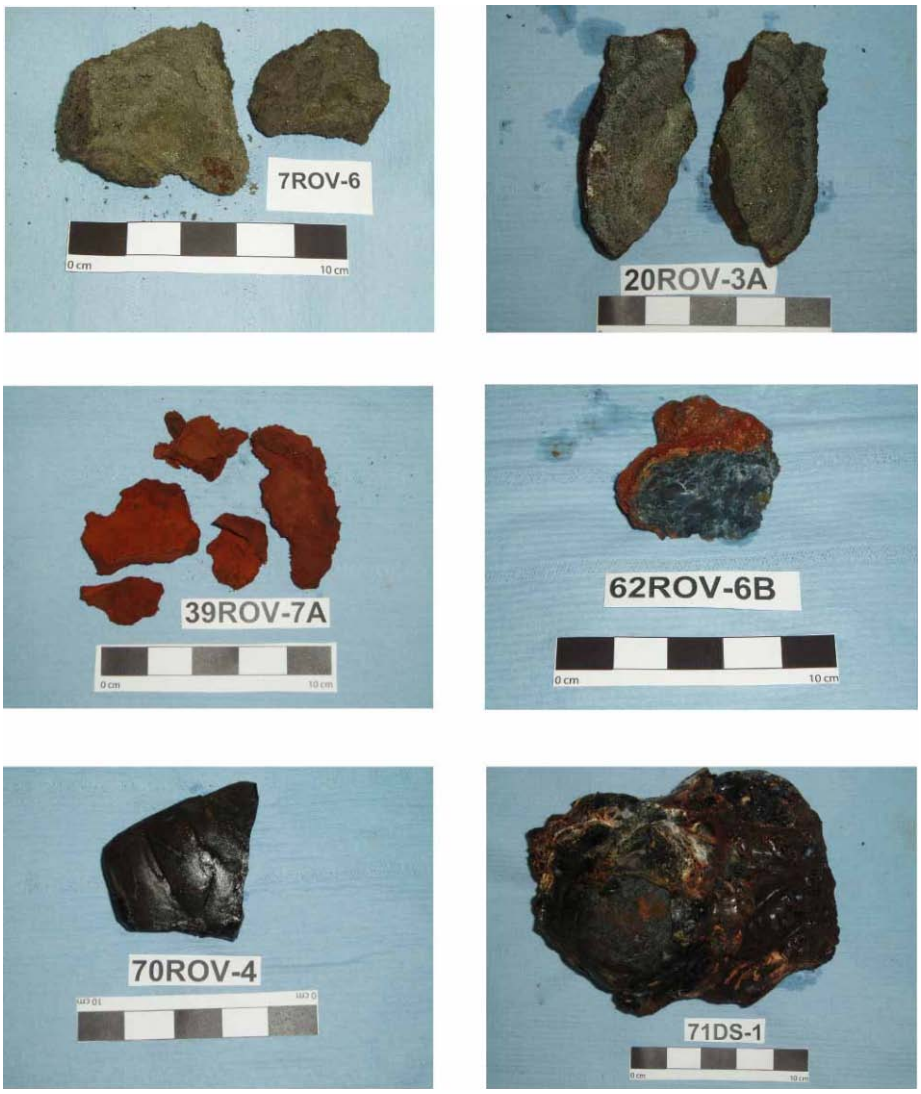

Fig. 1.16 Geological samples recovered during ROV and dredge (DS) stations: 7ROV-6: High-temperature chimney wall fragment from the Red Lion hydrothermal field (base of "Mephisto" chimney); 20ROV-3A: complete chimney wall from the Comfortless Cove hydrothermal field (base of "Sisters Peak" chimney); 39ROV-7A: Fe-oxyhydroxide crust from Limtoc low-temperature hydrothermal field; 62ROV-6B: altered serpentinized breccia from the Nibelungen hydrothermal field (from the rim of the "Drachenschlund" crater): 70ROV-4: Lava piece from top of the "Roman City" roof; 71DS-1: Pillow bud from the eastern flank of the Nibelungen hydrothermal field

1.4.5 Hydrography (CTD, MAPR & Lowered ADCP)

(M. Walter, C. Mertens, U. Stöber)

During the Meteor cruise M68/1, the temperature, salinity, turbidity and velocity field of the near field of several hydrothermal plumes were mapped to describe the general hydrography in the target areas and to study the spreading of the plumes. For the same purpose, water samples were taken for water and gas chemistry analysis (see section on water chemistry/gases). A hydrothermal plume in the local background stratification should be marked by negative anomalies in temperature and salinity as well as by an increase in turbidity. In addition to the plume mapping, the temperature and density field as well as the vertical shear of the horizontal velocity field will be analyzed to determine the strength and distribution of vertical mixing processes in the water column in the rift valley environment.

1.4.5.1 Instrumentation and Methods

CTD

During the M68/1 cruise a total of 27 conductivity-temperature-depth (CTD) casts was carried out using a Sea-Bird Electronics, Inc. SBE 911plus system additionally equipped with a Wet Labs LSS backscatter sensor (E. Baker, NOAA/PMEL) and a redox potential/Eh probe (R. Seifert).

The CTD sensors were calibrated at Sea-Bird Electronics in September 2004. The underwater unit was attached to a SBE 32 carousel water sampler with 22 Niskin bottles. Two bottles were left out for the lowered ADCP system, hence a maximum of 22 bottles was used.

LADCP

All the hydrographic stations were accompanied by current measurements with a lowered acoustic Doppler current profiler (LADCP) system attached to the CTD and water sampling carousel. Two RDI 300 kHz Workhorse Monitor instruments were used in the setup in a synchronized Master-and-Slave mode, with the upward looking (SN 1973) as Slave and the downward looking (SN 2161) as Master. For four of the stations, only a single (downward looking) instrument was used. During three of those stations (64 CTD, 67 CTD & 72 CTD), the second instrument was prepared for or used in an ROV experiment. The instruments were powered by an external battery supply, consisting of 35 commercial quality 1.5V batteries assembled in a pressure resistant Aanderaa housing. The system was set to a ping rate of 1 ping/s and a bin length (= vertical resolution) of 10 m in the Master-and-Slave mode.

MAPR

Four Miniature Autonomous Plume Recorder (MAPR, courtesy of Dr. E. Baker, NOAA/PMEL) were used in addition to the CTD package for plume mapping. MAPR are self-contained instruments, which record data at pre-set time intervals from temperature (resolution 0.001°C), pressure (0 - 6000 psi gauge sensor), and nephelometer (Sea Tech Light Backscatter Sensor,

LBSS) sensors. The instruments were attached to the hydrographic wire at distances between 50 and 200m from the CTD to extend the mapping range of towed yo-yo CTD casts.

Helium

For measurements of the He concentrations and isotopic signature, water samples were taken from Niskin bottles of the rosette (258 samples in total) and the ROV (5 samples) and sealed head space free and gas tight in 40 ml copper tubes. He isotope measurements will be performed at the IUP, section of Oceanography, at the University of Bremen with a fully automated UHV mass spectrometric system. The sample preparation includes gas extraction in a controlled high vacuum system. A split of the sample is analyzed for ^{4}He, ^{20}Ne and ^{22}Ne with a quadrupole mass spectrometer. At 14 K He is separated from Ne and released into the sector field mass spectrometer for analysis of ^{3}He and ^{4}He (for precision details see Sültenfuß et al. 2006).

The primordial components of helium isotopes are ideal tracers for large-scale distribution of vent fluids in the water column also in the South Atlantic (Rüth et al. 2000). Samples of this cruise should provide a picture of a more regional distribution of dispersing vent fluids in the water column leading to an estimate of its volume. $CH_4/^{3}He$ ratios separate CH_4 of hydrothermal fluids from other sources.

ROV Experiment

During two of the ROV dives (24 ROV & 69 ROV), one of the ADCPs was mounted on the frame of the ROV to measure vertical velocities of the rising plume of the Sisters Peak and Drachenschlund smokers, respectively. Additionally, a pumped MicroCat (Sea-Bird Electronics, Conductivity and Temperature Recorder SBE 37-SMP) which measures temperature, salinity and pressure at high precision (absolute precision $\Delta T = 0.002°C$, $\Delta C = 0.0003S/m$, $\Delta p = 0.1\%$ of the max. range) , was lowered into the plume to monitor coinciding temperature fluctuations.

Mooring

A current meter mooring was equipped with 3 Aanderaa Recording Current Meter RCM 11 which measure acoustically current speed ($\Delta V = 0.0015m/s$) and direction ($\Delta° = 5°$). All instruments carry a temperature sensor ($\Delta T = 0.05°C$), two of them are fitted with a pressure gauge ($\Delta p=0.25\%$ of the max. range).

vmADCP

Additionally, shipboard ADCP (75 kHz Ocean Surveyor) data were recorded on the transit across the equator from the rim of the Brazil trading zone at 1°N to the working area at 5°S on request of P. Brand (PI M68/2).

FLOATs

Four ARGO floats (R.J. Roddy, NOAA/AOML) were launched during the transits to and from the working area crossing 45°W, 40°W, 35°W, and 17°W latitude.

1.4.5.2 First Results

5° S area (Turtle Pits, Red Lion and Comfortless Cove fields)

The work in the 5°S area comprised 12 hydrographic stations in total. Two hydrographic sections with 3 profiles each (CTD/LADCP/Water sampling/130 Helium samples) were carried out north (8 CTD, 9 CTD, & 10 CTD) and south (16 CTD, 17 CTD, & 18 CTD) of the 5°S area. The local topography is closed to the sides below a water depth of 2500 m, hence these two sections form a box where measurements of the current field and the stratification allow to calculate fluxes of volume, heat and helium into and out of the vent field area.

The area was dominated by along-valley northward currents with a slight westward component, which were modulated in strength with a tidal frequency. The average current velocity below a depth of 2500 m was 5 cm/s, with maxima of more than 15 cm/s. The strongest currents were orientated northward (Fig. 1.18). The volume transport associated with the flow amounts to 0.25 Sv (10^6 m^3/s) across the section north of the vent sites.

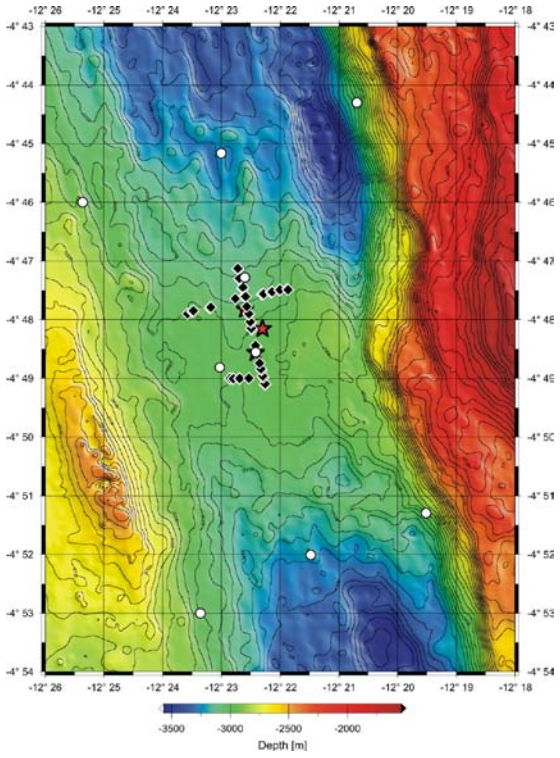

Fig. 1.17 Map of the 5°S working area. Red stars denote the vent sites, white dots classical CTD/LADCP stations and black diamonds water samples during tow-yo casts. Map by O. Schmale

For an accurate determination of the background flow field and for the precise determination of tidal amplitudes and phases, a one-year current meter mooring was deployed at the sill of the valley, in the center of the vent fields at 12°22.5'S, 4°48.2'S.

A detailed mapping of the hydrothermal plumes, both along and across the axis of the valley, was accomplished with 3 towed transects of a CTD/MAPR combination (Tow-yos, 13 CTD, 19 CTD, and 22 CTD), where up to four MAPR were mounted in a distance from 50 to 200 m above the CTD on the cable.

The horizontal and vertical extent of the plumes in the water column could be detected by the observation of several parameters as potential temperature (ΔΘ), backscatter (Δntu), and redox potential (Eh).

The along-valley tow-yo track (13 CTD) crossed the latitudes of the three sites Turtle Pits, Comfortless Cove, and Red Lion (Figs. 1.17, 1.19), and shows clearly the different temperature anomalies in the effluent layers of the plumes of Turtle Pits and Red Lion (Comfortless Cove is located further east of the track than the other two, and not as easily identifiable as the other two), which are shifted to the north from the sources, coinciding with the dominant flow direction. Weaker signals upstream of the known vent sites indicate the possible presence of yet unknown (possibly diffusive) vent sites. The maximum (negative) temperature anomalies exceeded 1/100K on this transect.

The across-valley tow-yos show that the plume is focused in the centre of the valley, and has a lateral extent of less than one kilometer (Fig. 1.20).

The density field in the 5°S area is dominated by the flow over the sill in the axial valley. Downstream of the sill, the isopycnals (and hence the plume anomalies) deepen and the water column stretches as a result.

Further work in this area consisted of one profile at Turtle Pits (4 CTD), Red Lion (5 CTD), and the location of a turbidity anomaly detected by ABE a year before (1 CTD), respectively, to determine the amplitude of the anomalies and the density range of the effluent layer close to the sources.

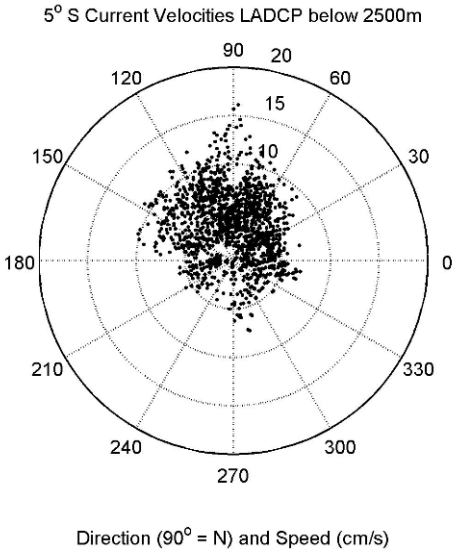

Fig. 1.18
Scatter plot of amplitude and direction of the currents measured below 2500 m water depth in the 5°S area. Most of the data points have a northward component, i.e. fall into the E-N-W segment of the diagram (N=90°). The amplitude of these deep currents (distance from the centre of the plot) ranges from a few centimeters to more than 15 cm/s

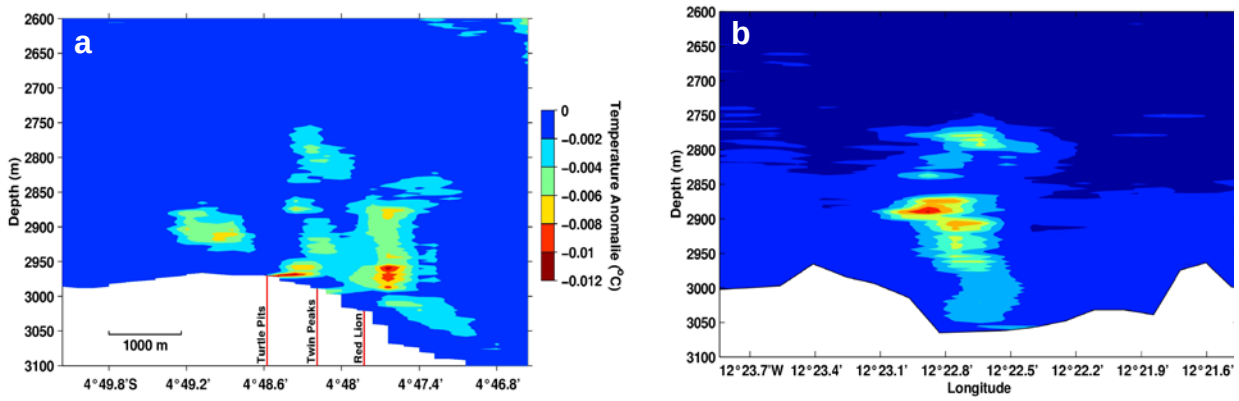

Fig. 1.19 **a**: Anomalies of potential temperature °C along a south-north orientated tow-yo track (13 CTD) across the 5° S vent sites. The positions of the hydrothermal sites Turtle Pits, Comfortless Cove and Red Lion are marked in red. Currents are predominantly northward; the temperature anomaly south of Turtle Pits is thus upstream of the known vents and could not be clearly assigned to a source. **b**: Backscatter signal along a west-to-east orientated tow-yo track north of the 5° S vent sites (22 CTD). The lateral extent of the core plume signal is < 1km. Data from the CTD nephelometer in Δntu relative to background

9° S area (Liliput)

Since the 9°33´S site is quite shallow (1500 m), hydrothermal anomalies in the water column are difficult to observe. Hydrothermal fluids in shallower areas have lower maximum temperatures and lower metal contents and hence often carry no turbidity signal; on the other hand, the background variability of temperature is high in this depth range because it is situated between the shallow Antarctic Intermediate Water and the upper North Atlantic Deep Water.

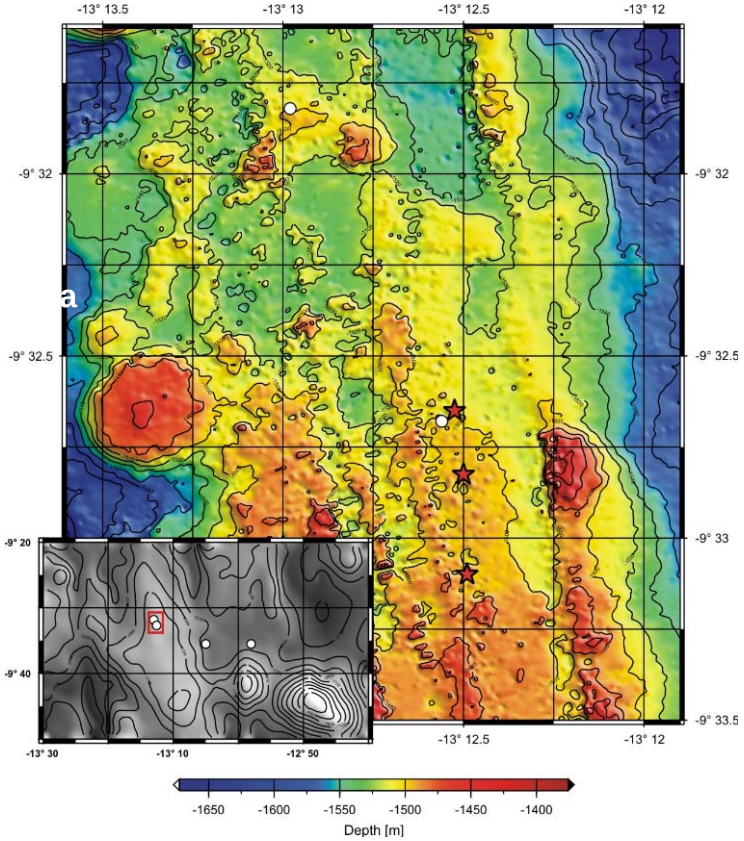

Fig. 1.20
Map of the 9°S working area. Red stars denote the vent sites, white dots classical CTD/LADCP stations. Map by O. Schmale

The hydrographic work at the site was therefore restricted to a profile directly at the Liliput field (27 CTD), which showed only minor anomalies in turbidity and redox potential close to the seafloor.

Additionally, a series of 3 stations (29 CTD, 34 CTD, & 37 CTD) was carried out from the spreading axis out to the east to study the far field plume spreading and dilution away from the valley by means of the primordial Helium signal.

8° S area (Nibelungen field, Cheating Bay)

The part of the working area at 8°S named aptly “Cheating Bay” was subject to thorough hydrographic work during the Meteor cruise M62/5 in December 2004. Because of the complex current patterns and strong tidal variability, it had not been possible to detect the exact location of the vent site causing the observed hydrothermal plume signal.

The work in Cheating Bay started therefore with the reoccupation of the M62/5 station 1230 (43 CTD), which had shown the largest anomalies in turbidity and methane during that cruise. Again, large anomalies of those two parameters were found in the depth range between 2680 and 2750 m, with a second maximum between 2800 and 2900 m. The two cores of the plume signal were already observed during M62/5; they are probably caused by the strong mixing in the region which is modulated in strength by the tidal cycle and affects the stratification at the vent site and hence the density horizon of the effluent layer.

The strong mixing in the form of internal wave breaking (which gives rise to the short-lived occurrence of density inversions and well-mixed layers) is also hampering the detection of temperature anomalies in this area, so plume mapping is restricted to turbidity and methane anomalies.

Directly in the plume, there is a strong signal in the turbidity and only a somewhat heightened variability in T and S. The methane and hydrogen output of the Nibelungen field is rather strong (see Chapter 1.4.6. on Gases in hydrothermal fluids and plumes).

Two tow-yo casts (one -47 CTD- from S to N across the position of the large anomaly, the other -64 CTD- approximately in W-E direction on a line crossing the large anomaly position as well as the now known position of the source) confirmed the already suspected strong temporal variability of the plume spreading in Cheating Bay: During the first track (Fig. 1.22 a), the plume signal was clearly visible west of the now known position of the source (the black smoker ‘Drachenschlund’ at 8°17.865’S, 13°30.440’W). During the second cast, no anomaly could be traced at the location of the former large-anomaly position, but strong turbidity and methane signals were observed to the east of the source. It is not clear yet whether these latter anomalies belong to the same source (Drachenschlund), or whether there is a second vent site located even farther to the east.

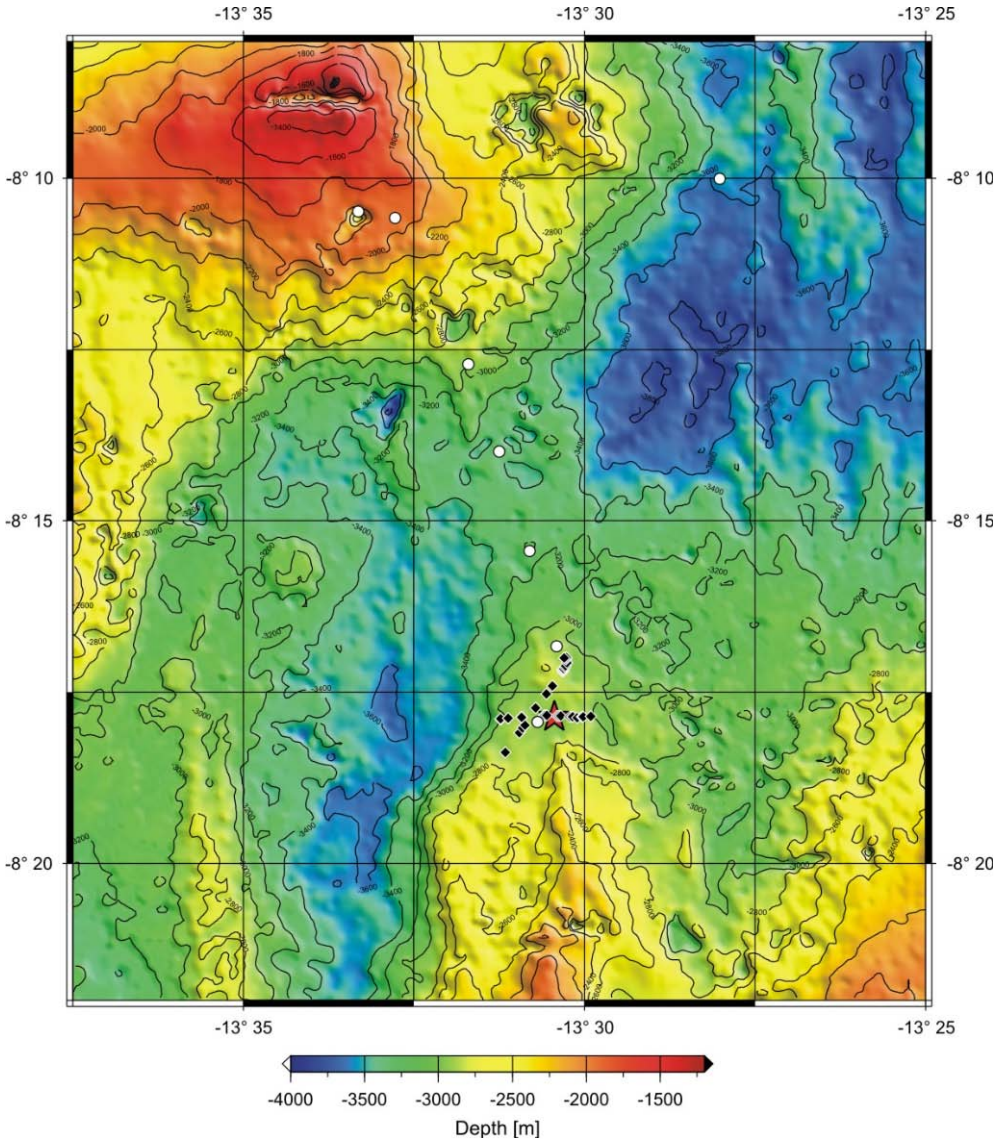

Fig. 1.21 Map of the 8°S working area. Red stars denote the vent sites, white dots classical CTD/LADCP stations and black diamonds water samples during tow-yo casts. Map by O. Schmale

Despite the failure to find the source of the hydrothermal signal in the water column during M62/5, the horizontal spreading of the plume was satisfactory mapped in both along and across rift valley direction. Virtually no traces of elevated turbidity and methane were observed at the outer edges of the station grid, thus the calculation of inventories is possible.

To complete the mapping, and to compare the background flow condition to those in 2004, a transect of 4 CTD/LADCP/water sampling profiles (49-52 CTD) was measured across the rift valley at the shallow sill north of Cheating Bay.

As an attempt to measure the strength of the Drachenschlund vent and to complement the calculation of the output of the source by helium inventories, an ROV experiment was conducted with combined measurements of fluctuations of temperature and vertical velocities in the rising

plume. The magnitude of the vertical velocities w was between 10 and 20 cm/s at heights between 5 to 20 m above the crater; several orders of magnitude larger than the typical w (10^{-7} m/s) in the ocean, and enough to lift the ROV considerably up.

The cause of this anomaly, the black smoker 'Drachenschlund' is situated at 8°17.9'S. Due to the hydrothermal output, the turbidity is enhanced in the whole region below a depth of 2500m. White lines represent isopycnal surfaces, black lines denote positions of the different instruments along the track. Data from MAPR in Δntu relative to background.

During M62/5, a methane maximum was observed at a depth of approximately 1900 m on the western wall of the rift valley at a latitude of 8°10'S. Since this was an isolated measurement and no further information about the (possibly hydrothermal) source of this was available, a repeat of this station was carried out, and two more CTD/water sampling profiles were taken at a submarine hill in the inside corner between segments A1 and A2 to localize the origin of the methane plume (59 CTD, 67 CTD, & 72 CTD). The signals found during the casts were small, but consistent (temperature and backscatter anomalies close to the seafloor at a depth of about 1900 m). However, there were no significant gradients, and the deep currents were variable, so no clear target could be identified.

Another CTD Tow-yo cast (45 CTD) in the 8°S area was done as a preparation for the AUV exploration at 7°57'S. This area was chosen as a potential target because it showed strong turbidity and accompanying temperature anomalies close to a terraced structure at the western rift valley in the TOBI/MAPR deployments of M62/5. This years' tow-yo data could indeed identify a distinct plume with its maximum turbidity anomaly lying directly above the terraces (Fig. 1.22 b). However, the subsequent AUV dives did not result in the clear localization of the hydrothermal source, and no further work was done in that area.

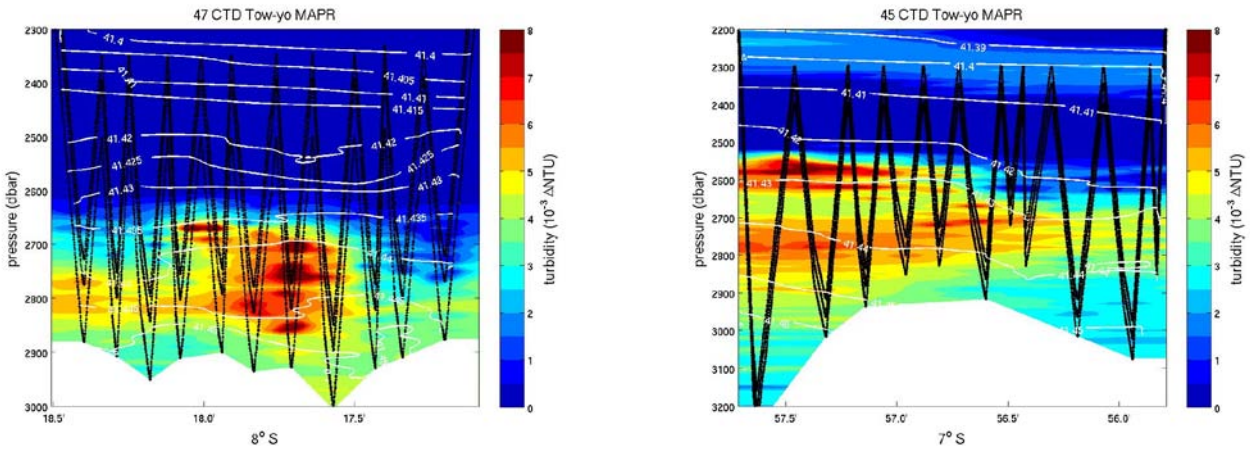

a **b**

Fig. 1.22 **a**: Turbidity anomaly along a Tow-yo track with CTD and MAPR (Miniature Autonomous Plume Recorder) across the plume dispersion in S-N direction in the Nibelungen field. **b**: Backscatter signal from MAPR LSS sensors along tow-yo track at 7°57' S. The turbidity anomaly was accompanied by an -albeit small- temperature anomaly, which indicates the presence of a hydrothermal source somewhere in the area. White lines represent isopycnals, black lines denote positions of the different instruments along the track. Data from MAPR in Δntu relative to background

1.4.6 Gases in Hydrothermal Fluids and Plumes

(R. Keir, O. Schmale, R. Seifert, S. Weber)

Hydrothermal vents produce variable amounts of methane and hydrogen that depend on geological controls and on the temperature of the venting. These gases were measured on board during M68; the measurements were carried out on water column samples and on vent fluids obtained during the ROV dives. In addition, gas samples were conserved for subsequent carbon isotope analysis in the isotope laboratories at IFM-GEOMAR and at the University of Hamburg. Table 1.3 contains a list of the methane and hydrogen measurements carried out on these stations as well as on vent fluids collected during the ROV dives.

Table 1.3 a Sample list for CTD-stations

Station	Profile	Long. W	Lat. S.	CH4	δ^{13}CH4	δDCH4	H2	□D
1CTD	001	12°23.022	4°48.804	20	20		18	
4CTD	002	12°22.414	4°48.554	14	14		11	
5CTD	003	12°22.60	4°47.28	14	14			
8CTD	004	12°19.514	4°51.297	16	16		14	
9CTD	005	12°21.479	4°52.010	16	16			
10CTD	006	12°23.36	4°53.0	16	16			
13CTD	007	Tow-yo		22	22		17	
16CTD	008	12°25.36	4°46.0	16	16			
17CTD	009	12°23.0	4°45.16	17	17			
18CTD	010	12°20.693	4°44.299	17	17			
19CTD	011	Tow-yo		10	10			
22CTD	012	Tow-yo		21	21			
27CTD	013	13°12.98	9°31.82	19	19		17	
29CTD	014	13°05.01	9°35.51	22	22		19	
34CTD	015	12°58.01	9°35.50	21	21			
37CTD	016	13°12.560	9°32.679	18	18		16	
43CTD	017	13°30.69	8°17.94	21	21		15	
45CTD	018	Tow-yo		22	22			
47CTD	019	Tow-yo		19	19		15	
49CTD	020	13°30.41	8°16.50	16	16		15	
50CTD	021	13°30.803	8°15.440	17	17		14	
51CTD	022	13°31.25	8°13.99	16	16		15	
52CTD	023	13°31.70	8°12.71	16	16		15	
59CTD	024	13°28.021	8°10.009	21	21		8	
64CTD	025	Tow-yo		22	22		21	
67CTD	026	13°33.316	8°10.484	15	15		14	
72CTD	027	13°32.78	8°10.58	17	17		8	

Table 1.3 b Sample list for ROV-stations

Station	ROV	Purge Trap CH4	Vacuum Extraction CH4	δ^{13}C CH4	δDC H_4	H2	δD H2	Fluid
3	ROV	4	12	6		6	1	1
7	ROV	2	6	6	2	6		
12	ROV	1	3	3	1	4		
20	ROV	2	4	4	1	5		
24	ROV	2	6	6		5		
39	ROV		4	4		2		
41	ROV		12	6		6		
62	ROV	2	3	3	4	4	3	
69	ROV	2	2	2	2	4		
70	ROV		6	6		6		

1.4.6.1 Methods

In order to analyze methane and hydrogen by gas chromatography, the dissolved gases were extracted from the seawater sample by one of three techniques. The majority of the water samples obtained from the CTD casts were processed by the partial vacuum technique described by Rehder et al. (1999). These gas samples will be analyzed for the $^{13}C/^{12}C$ ratio of methane in laboratories at IFM-GEOMAR and the University of Hamburg. This same procedure was used to analyze fluids obtained by the KIPS sampler on the ROV. In this case the fluid was drawn into evacuated 500 ml bottles, which were half filled. In total, about 800 and 600 individual measurements were performed for hydrogen and methane respectively.

Two additional methods of extracting the gas samples were applied to selected samples. Methane was stripped and concentrated using the purge and trap technique (Seifert et al., 1999). This gas was then released directly into a gas chromatograph equipped with a FID. Dissolved gasses were also extracted by applying high vacuum and ultrasound to the water sample while being heated up to the boiling point. As with the partial vacuum technique, aliquots of the gas were analyzed for hydrogen and methane on separate gas chromatographs.

1.4.6.2 Methane and Hydrogen in the Water Column

Twenty seven CTD stations and tow-yos were carried out during M68/1 (Table 1.3 a). Selected preliminary results are given below.

5°S

At 5°S, a series of stations and tow-yos bracketed vent sites located on the sill in the middle of this rift valley segment (Figs. 1.17 and 1.23). Despite the presence of these sources, methane concentrations in the surrounding water remained relatively low (Fig. 1.24). At depths greater than 1000m, methane concentrations are mostly about 0.5 nmol/L. A few samples exhibited higher concentrations of about 1 nmol/L in the vent plumes. In contrast, hydrogen increased sharply in the vent plumes at about 2800 to 3000m, with concentrations reaching 25 nmol/L. This contrast may be due to the nature of the venting in this area, some of which is characterized by extremely high temperature fluid in volcanic systems that produce high hydrogen to methane ratios. The highest methane (3.5 nmol/L) and hydrogen (25 nmol/L) in the water column were observed in a plume to the east of Red Lion (Fig. 1.24)

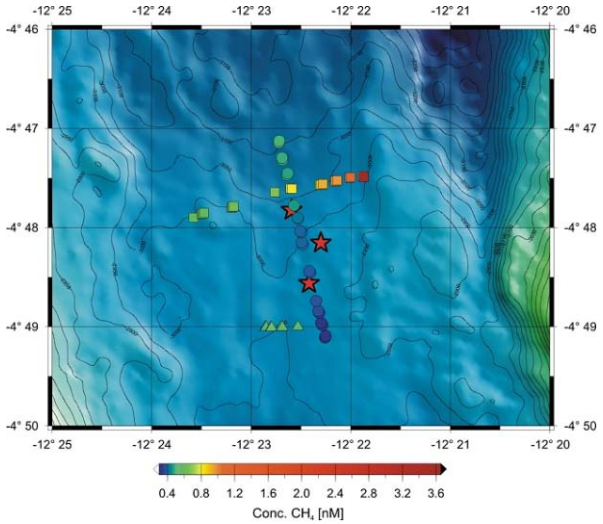

Fig. 1.23
Sampling positions of 5°S tow-yo stations with methane concentrations color coded

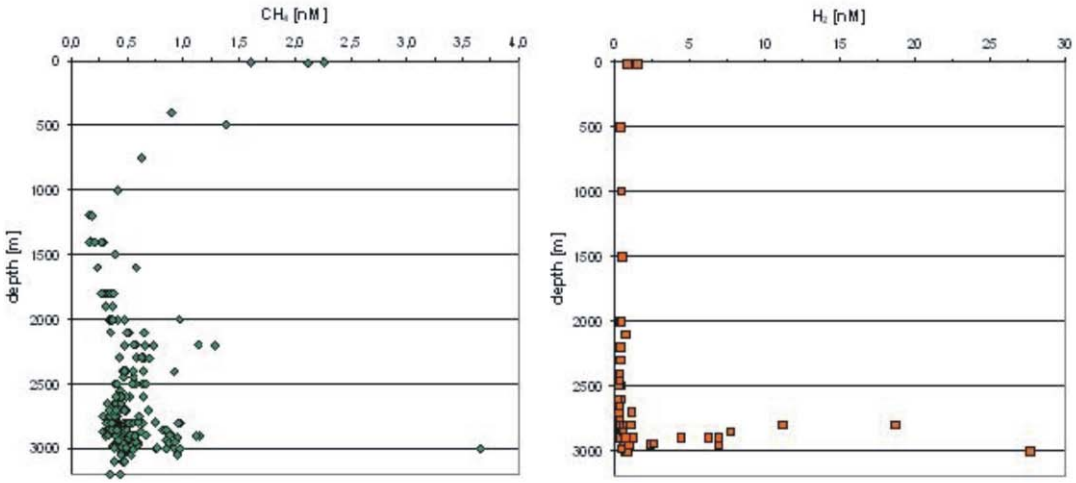

Fig. 1.24 Methane and hydrogen versus depth in 5°S area

9°30'S

In this region, 4 CTD stations were conducted (Fig. 1.20). The two on-axis stations clearly showed an increase of methane and hydrogen in the bottom water. One of these stations was located near the Lilliput vent; the other was taken near an expired mussel bed observed during cruise M64. The presence of bottom methane and hydrogen in this area may indicate that venting may be taking place nearby (Fig. 1.25 a). The profiles at these stations indicate there may also be a weak plume signature at about 1000m depth.

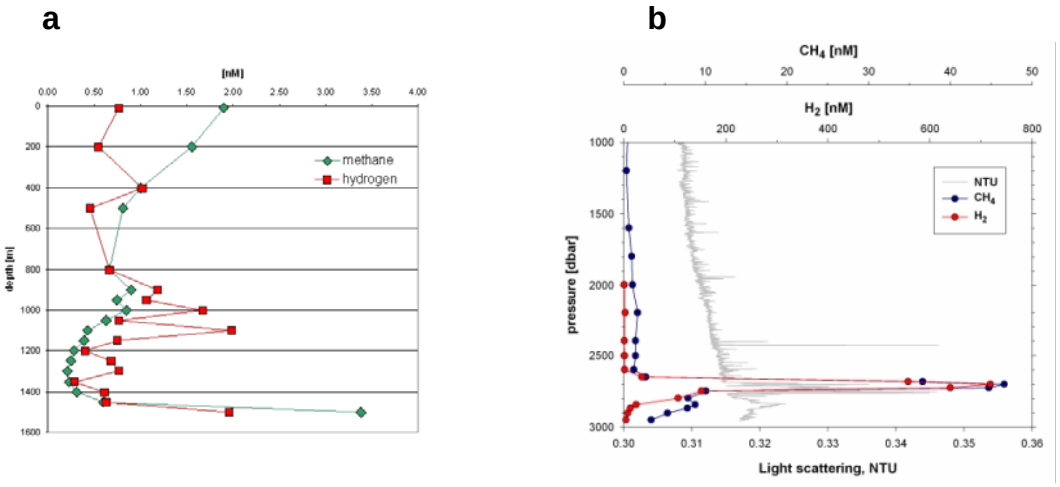

Fig. 1.25 **a**: Methane and hydrogen versus depth at 9°31.8'S, 13°13'W. **b**: Methane, hydrogen and optical backscatter at Station 43CTD (8°17.9'S, 13°30.7'W)

8°S

Several vertical CTD profiles were taken between 8°10'S and 8°20'S along the Mid-Atlantic Ridge, and 2 tow-yos were conducted across Cheating Bay at about 8°18'S (Fig. 1.21). We first re-occupied Station 1230 of M62/5, where a very strong methane anomaly had been observed in December, 2004. Once again, a methane plume containing about 50 nmol/L was observed at this position. Hydrogen concentrations reached 700 nmol/L in this plume (Fig. 1.25 b). A subsequent AUV dive discovered a black smoker about 650 meters to the east of this position ("der Drachenschlund"). It would appear that the very much higher fluxes of methane and hydrogen from this vent are responsible for plumes in the surrounding region that often contain on the order of 10 nmol/L CH_4.

A subsequent tow-yo CTD from east to west over the "Drachenschlund" found a plume sitting to the east of this vent (Fig. 1.26). Whether the plume from the Drachenschlund shifted with the currents or whether it originated from a second vent located farther to the east is not known at this time.

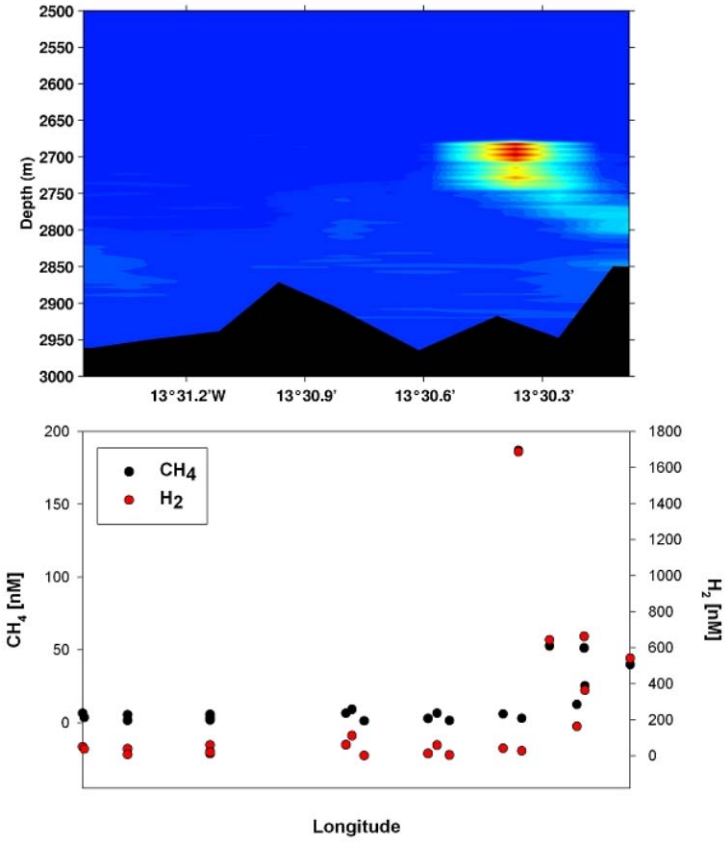

Fig. 1.26
Tow-yo (64CTD) from east to west across the "Drachenschlund" vent at 13°30.4'W. Upper section shows turbidity anomaly. The lower diagram shows methane and hydrogen concentrations of the discrete water samples as a function of position

In Figure 1.27, we show a diagram of hydrogen versus methane concentrations for all paired measurements on the same extracted gas samples. The good correlation between the measurements appears to be because of the trend found in Cheating Bay, which contained almost all of the higher gas concentrations measured in the water column. The ratio of hydrogen to methane increase appears to be about 14:1, which is about twice that observed in the Drachenschlund vent fluid. The reason for this is not known; this rather surprising result is subject to corrections that need to be made for incomplete gas extraction.

Besides Cheating Bay, CTD stations were conducted in the rift valley and adjacent to the promontory located at 8°09'S, 13°34'W (Fig. 1.21). The latter stations were taken because a methane anomaly had been observed to the east, at 8°10'S, 13°28'W on previous cruise M62/5 as well as on the repeat station of this cruise (59CTD). As a first guess, two stations were placed on the ledge at the southeast corner of the promontory. The results of the hydrogen and methane measurements show that methane sharply increases to about 4 nmol/L in a 100 m thick layer above the bottom and that hydrogen increases by a small amount (Fig. 1.28). These results indicate that there is venting from near the top of the promontory at circa 2000m depth but that we were not in the immediate vicinity of the vent with our first attempts.

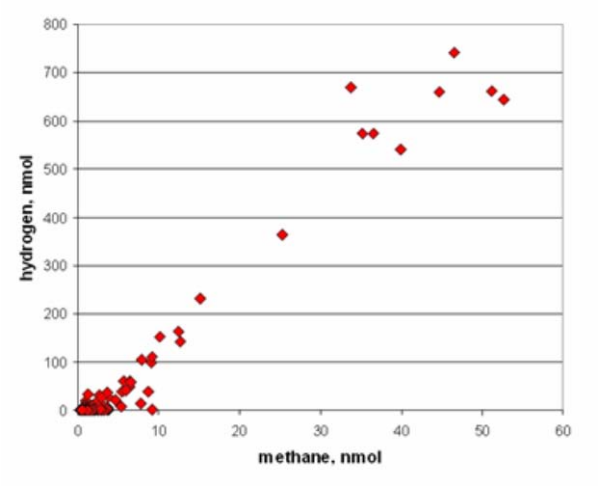

Fig. 1.27
Water column hydrogen versus methane for M68 stations

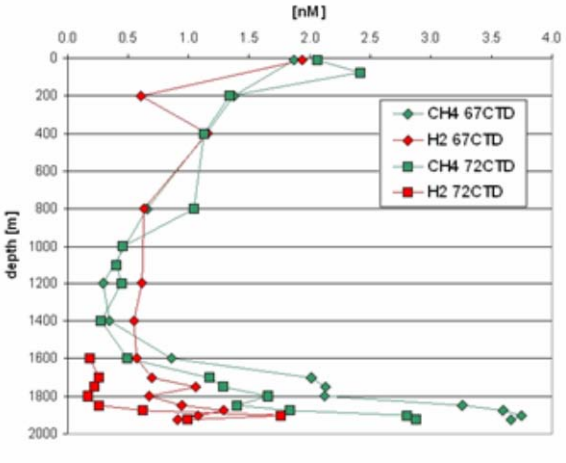

Fig. 1.28
Methane and hydrogen versus depth near 8°10'S, 13°33'W

1.4.7 Metals and Other Compounds in Hydrothermal Fluids and Plumes

(D. Garbe-Schönberg, S. Sander, J. Mawick, M. Peters, A. Koschinsky)

1.4.7.1 Sampling and Analytical Methods

Hydrothermal fluids are characterized by their unique chemical and isotopic composition, which is significantly different from ambient seawater (e.g., von Damm, 2004). Scientific objectives for fluid chemical analyses, both on-board and subsequently in the home laboratories, include the detection of hydrothermal plumes in the water column, and a quantification of the chemical and isotopic composition of hydrothermal fluids discharging from the ocean crust via distinct vent sites - either through black smokers or diffuse venting.

Three different types of samples were collected for chemical and isotopic analyses: (i) vent fluid samples collected with the Kiel Pumping System (KIPS) by inserting a titanium sampling nozzle into the orifice of smoker structures; (ii) samples from discharging vent sites collected with three Niskin flasks (5 l volume), mounted at the front of the MARUM ROV QUEST; (iii) water column samples from the CTD/Rosette, equipped with 24 bottles à 10 l volume.

1.4.7.1.1 Sampling With the KIPS Fluid Sampling System

One pre-requisite for an accurate estimate of the composition of hydrothermal fluids venting at high-temperature Black Smokers or from diffuse mussel-field sites is sampling of the hydrothermal fluids without entrainment of ambient seawater which would cause immediate precipitation of sulphides and barite and, hence, loss of these compounds from solution. One important measure of the purity of the sampled hydrothermal fluid is temperature. Consequently, real-time *in-situ* measurement of the temperature helps to guide the tip of the sampling nozzle to the hottest region within the vent orifice where the purity of the venting fluid is highest and least diluted with seawater. Another pre-requisite is that all materials coming into contact with the sampled fluid are inert and have lowest adsorption coefficients preventing systematic errors introduced by either contamination or losses due to adsorption. Precipitation during cooling of the sampled fluid, however, cannot completely be avoided.

A fully remotely controlled flow-through system – the Kiel Pumping System (KIPS-3) mounted on the ROV's starboard tool sled (Fig. 1.29) was used for this purpose (Garbe-Schönberg et al., 2006). The multiport valve has 9 ports connected to 9 single PFA flasks with 675 ml volume each (Nalgene, USA). Each bottle was equipped with a check valve at the outlet. The flasks are mounted in three racks A-C, with every rack containing three horizontally positioned bottles, allowing an easy transfer of the racks to the laboratory where sub-sampling was done. Flasks were pre-filled with ambient bottom seawater (North Atlantic Deep Water, NADW) obtained from CTD hydrocasts. A 24 V deep sea mechanical gear-pump is mounted downstream to the sample flasks, thus avoiding contamination of the samples. The pumping rate can be adjusted by the voltage applied from the ROV's dimmable port (Hub 2, port # 2); it was set to approx. 800 ml/ min at 26 VDC. The standard pumping time per sample was set to 4-5 min making sure that the flask volume was exchanged at least 4 times. The outlet of the KIPS system is located on the porch at the front-side of the ROV, where video control allows the observation of warm fluids leaving the system. In addition, a flow mobile was attached to the outlet tube.

Fig. 1.29
ROV "QUEST" with KIPS mounted on the starboard side of the tool sled (Foto: D. Garbe-Schönberg)

A high-precision thermistor temperature sensor (manufactured by H.-H. Gennerich, Bremen) inside a stainless steel pressure housing was attached parallel to the nozzle. The sensor is connected to the ROV's modified CTD-60_77 (Sea and Sun, Trappenkamp, Germany) using two channels for data handling: a broadband channel for temperatures < 100 °C, and a dedicated high-temperature channel for the range 100 – 450 °C. The 90% time constant of the sensor in water is better than 12 s. Two individual sensors were used during this cruise: sensor #2 during dives #86 - #89, and sensor #1 for all subsequent dives. A pre-cruise calibration was performed by H.-H.Gennerich with the CTD-60_77 housing equilibrated to 2.4°C water temperature, simulating *in-situ* conditions during the cruise.

First on-board analyses showed that hydrothermal fluids at the Turtle Pits and Sisters Peak high-temperature Black Smoker sites could be sampled with high purity: the chlorinity of 285 mM of fluids from the Turtle Pits *Marker #2 Vent* was very close to the hydrothermal endmember value of 269 mM extrapolated from samples taken during M64/1 in 2005.

Immediately after recovery of the ROV on deck, KIPS sample racks were transferred to the laboratory. Usually, 3-5 flasks were filled at each site. Two ml for the analysis of dissolved Mg as a measure for hydrothermal fluid purity were taken from every flask. For subsequent analyses of dissolved ions the complete volume of one flask was transferred to a N_2-flushed FEP bottle, homogenised, and then sub-sampled for the different analyses. Another flask was dedicated for the analysis of dissolved gases and isotopic composition, the sampling technique is described elsewhere in the respective gas chemistry chapter. An overview scheme of sub-samples taken is given in Table 1.4.

Table 1.4 Overview of sub-samples taken and analytical parameters determined on-board and, later, to be determined in the home laboratories

Analysis on-board	diss. Oxygen (Winkler)	filtered/ not filtered acidified	Filtered/ not filtered not acidified		Ligand titration	Fe, Mn, Zn, Cu (ASV)	Eh, pH, sulphide, Cl, Mg		C1-C4 HC	H2, CH4			Sulphide		
Analysis on-shore		REE, trace metals, major elements (CAU-Kl)	Anions (CAU-Kl)	Mg, Majors (CAU-Kl)	Organic complexation (Uni Otago-NZ)	Trace metals, major and minor elements (IUB-HB)	Anions (IUB-HB)	Amino acids (IUB-HB)		C and H isotopes CH4 (Uni-HH)	H2 isotopes; organic compounds (Uni-HH)	S and O isotopes in dissolved sulfate (Uni-MS)	S isotopes in dissolved sulfide (Uni-MS)	O and H isotopes of water (Uni-MS)	DIC-C isotopes (Uni-MS)
Volume (ml)	10	100	20	2	100	100	50	200	120	250	250	2	600	5	20
	Bottle 1								Bottle 2			Bottle 3			

1.4.7.1.2 Overview on methods

Dissolved oxygen and dissolved Mg*:* by titration**.**

Dissolved sulfate has been fixed as barium sulfate. At the University of Münster, sulfur and oxygen isotope measurements will be carried out by masspectrometer (Finnigan Mat 251).

Dissolved Sulfide: sulfide fixation with a zinc acetate. The concentration of the different sulfur species will be determined by HPLC at the BGR, Hannover.

Dissolved inorganic carbon: determination of the isotopic composition of the inorganic carbon fraction at the University of Münster.

Major, minor, and trace elements: (Na, K, Ca, Mg, Sr, Ba, B, Fe, Mn, Cu, Zn) by ICP-optical emission spectrometry (Ciros SOP; Spectro), and trace elements (e.g., I, Br, B, Li, Al, Ti, Cs, Ba, Sr, Y-REE, Fe, Mn, Cr, V, Cu, Co, Ni, Pb, U, Mo, As, Sb, W) by ICP-MS (Perkin Elmer).

Anions: Aliquots of hot hydrothermal fluids have been stored in LDPE bottles until analysis for Cl, Br, I, SO_4, SiO_2.

Amino acids and other organic compounds: stored in acid-cleaned PE bottles, or poisoned with $HgCl_2$ in 100 ml glass bottles, which were acid-cleaned and pre-combusted at 480°C before use.

Particles from fluid samples: Filters were kept in plastic dishes for later inorganic analysis, or frozen for later organic analysis, in addition to organic analyses of the fluids.

Analytical Procedures On-board:

pH and Eh measurements were carried out with WTW electrodes (Ag/AgCl reference electrode).

Winkler titration of dissolved oxygen: immediately after sample recovery.

Chloride titration: with siver nitrate

Photometric determination of dissolved inorganic silica, iron and sulfide concentrations were performed with a Biochrom Libra S12 spectral photometer (extinction: Si: 810 nm; Fe: 511 nm, and Sulfide at 660 nm).

Chemoluminescence determination of iron(II): Fe(II) was determined by flow injection analysis using a modified Fe-chemilumenescence method described by Croot and Laan (2002).

Titrimetric determination of calcium and magnesium is carried out with 0.01 M EDTA, and from the resulting concentration of titrated ions, the Ca^{2+} value is subtracted to calculate the Mg^{2+} concentration**.**

Voltammetric determination of Fe, Mn, Zn, Cu, Cd, and Pb by CSV/ASV were performed using either a Metrohm system comprising a 757 VA Computrace run with a standard PC, an 813 Compact Autosampler and two 765 Dosimats or a system consisting of an EcoChemie μAutolab II, an IME interface and a Metrohm 663 VA stand. Filtered aliquots were submitted to a digestion process in a UV Digestor (Model 705, Metrohm), which contains a high pressure mercury lamp (500 W), decomposing organic metal complexes. For Fe, the highly

sensitive cathodic stripping voltammetric method of Obata and van den Berg (2001) were used. Mn concentrations were determined using anodic stripping voltammetry in an alkaline ammonia buffer solution (Locatelle and Torsi, 2001). For Cu, Pb, Cd, and Zn analyses samples were buffered at pH 4.6 with 1 M acetate buffer solution and measured by ASV (Application Bulletin Metrohm 231/2).

Ligand titration. Cu^{2+}-binding ligand concentration ($[L_{Cu}]$) and conditional stability constant (K''_{CuL}) were measured using the competing-ligand-equilibration cathodic-stripping-VA technique with salicylaldoxim (SA) as the competing ligand (Sander et al., 2004). The Gerringa (Gerringa et al., 1995) method was used to receive numerical values for $[L_{Cu}]$ and K''_{CuL}.

1.4.7.2 First Results

1.4.7.2.1 *In-Situ* Temperatures and Chemistry of Black Smoker Hydrothermal Fluids

A dedicated high-precision thermistor-based temperature sensor integrated within the KIPS fluid sampling system and mounted parallel to the sampling nozzle was used for our temperature measurements of hydrothermal fluids. It has to be kept in mind that fluids emerging at the top of a 12 m tall chimney may have already cooled or mixed with seawater inside the chimney structure. Moreover, vigorous venting involves turbulent mixing of hydrothermal fluids with seawater leading to a highly chaotic temperature distribution within the orifice. It becomes evident that temperature measurements under these conditions and with a ROV are difficult to hold in position. However, quite constant temperature readings could be obtained for some high-temperature vents including the Marker #2 vent at Turtle Pits, where we measured with T_{max} = 408.3 °C the highest temperature ever obtained for a fluid on the seafloor worldwide. Boiling of the emerging fluids could be observed visually and was video-recorded. This temperature at a depth of 2986 m coincides with the experimentally determined temperature for the critical point of seawater (Bischoff and Rosenbauer, 1988), where vapour phase and fluid cannot be discriminated anymore. This suggests that the phase-separated hydrothermal system at Turtle Pits and Sisters Peak (T_{max} = 400.3°C) might react under supercritical conditions. In contrast, non-phase-separated fluids emerging at the Mephisto and Tannenbaum vents in the Red Lion hydrothermal system - in only 1 nm distance to Sisters Peak - both have temperatures of 347 and 349°C, respectively (Table 1.5). The following Figs. 1.30 to 1.34 illustrate the conditions during our fluid sampling of the high-temperature black smoker chimneys.

Table 1.5 Measured temperatures of venting hydrothermal fluids

Area	*Site*	*Station #*	T_{max} [°C]	*Average* ± *1σ* [°C]	*Sample No.*
MAR 5° S					
Turtle Pits	Marker #2 Vent	12 ROV	408.7	405.7 ± 1.1	3 ROV-10/11 12 ROV-4/ -8
NN	Sisters Peak	24 ROV	400.3	395.4 ± 2.2	20 ROV-4/ -7
Red Lion	Mephisto	7 ROV	346.3	345.6 ± 0.3	7 ROV-3/ -5
Red Lion	Tannenbaum	7 ROV	349.0	348.0 ± 1.5	not sampled
Red Lion	Shrimp Farm	7 ROV	193.0	191.8 ± 1.5	7 ROV-9/ -11
Wideawake	Wideawake mussel field	3 ROV	19.2	17.4 ± 1.9	3 ROV-1/ -4
NN	Marker # 6 mussel field	24 ROV	10.0	9.4 ± 0.4	24 ROV-1/ -3
NN	Golden Valley mussel field	24 ROV	3.6	3.4 ± 0.1	24 ROV-6/ -8
MAR 9° S					
180 m S Liliput	Musselfield 180 m S Liliput	39 ROV	17.3	16.3 ± 0.6	39 ROV-3/ -5
Liliput area	Musselfield between pillows	41 ROV	4.9	4.7 ± 0.1	41 ROV-3/ -5
Liliput area	Musselfield with cloudy water	41 ROV	6.5	6.3 ± 0.2	41 ROV-6/ -8
Liliput area	Northern border of ABE map	41 ROV	6.8	6.6 ± 0.2	41 ROV-10/ -12
MAR 8° S					
Nibelungen	Dragon Troat	62 ROV	192	153 ± 27	62 ROV-5, -9/ -10

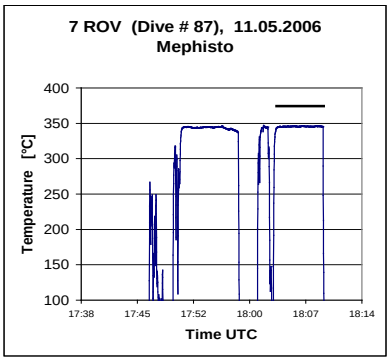

Fig. 1.30
Mephisto Vent, Red Lion. Max. temp. measured at orifice on top of the chimney: **346.3°C**, at 3098 m water depth. Samples 7 ROV-1 to -3 were taken from 7:50 – 18:08 UTC

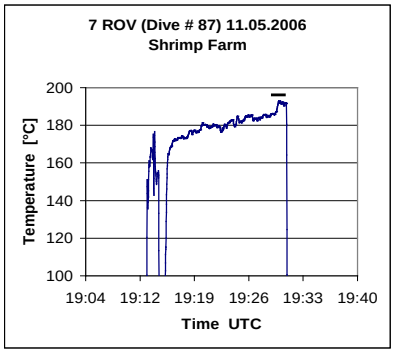

Fig. 1.31
Shrimp Farm Vent, Red Lion. In-situ max. temp. measured at orifice on top: **193.0°C**, at 2986 m water depth. Samples 7 ROV-1 to -3 were taken from 19:16 – 19:30 UTC

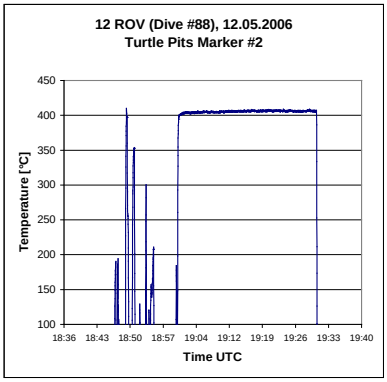

Fig. 1.32
Marker #2 Vent, Turtle Pits in the same orifice, 1m above ground. Max. temp.: **408.7°C**, at 2988 m water depth. Samples 12 ROV-4 to -8 were taken from 19:01 – 19:30 UTC

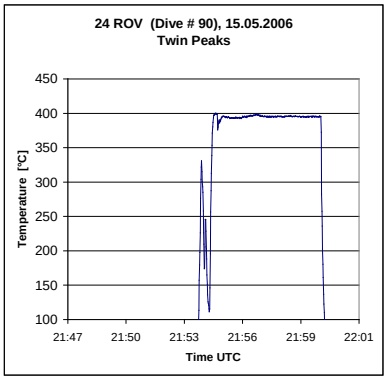

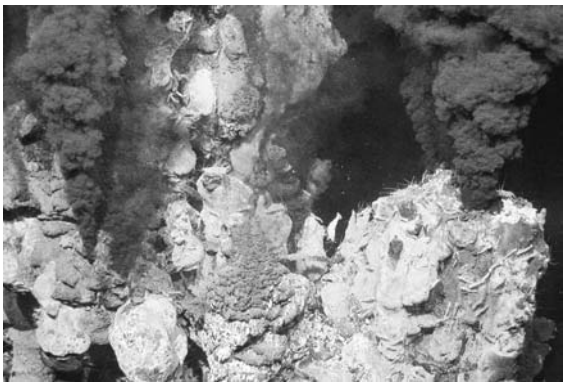

Fig. 1.33
Sisters Peak, at the same orifice on the top as 20 ROV. Maximum temp. measured was **400.3°C**, at a water depth of 2988 m. No samples taken

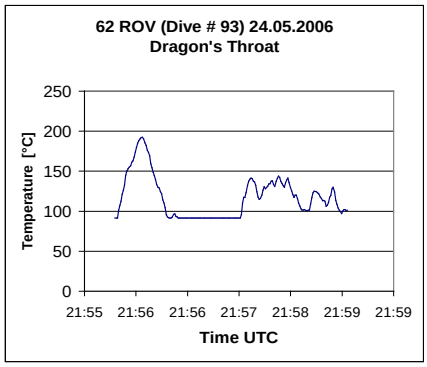

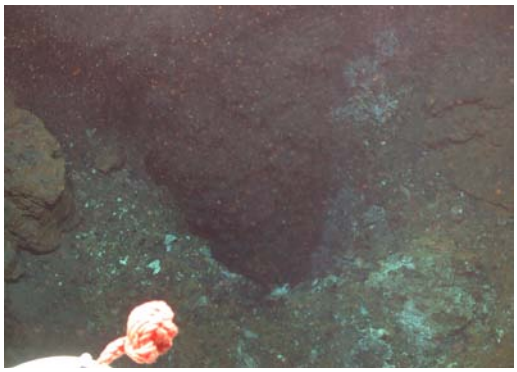

Fig. 1.34
Dragon's Throats, approx 1 m above orifice. Max. temp.: **192°C**, at a water depth of 2910 m. Samples 62 ROV-5 and -9/-10 taken from 20:08 until 20:18 UTC

Onboard analysis of the fluid samples recovered by the ROV revealed a large spectrum of fluid compositions from samples of different fields. The 407°C hot smoker Two Boats at Turtle Pits, which was discovered last year, is still characterized by phase separation und emanation of a salt-depleted vapour phase (Fig. 1.32) with high concentrations of hydrogen, iron, and copper. The pH is as low as 3.1. The hot vent Sisters Peak in the Comfortless Cove field between Turtle Pits and Red Lion shows basically the same chemistry, and although boiling could not directly be observed, depleted chlorinity (the samples are on the same mixing line of fluids and seawater as the Turtle Pits ones, Fig. 1.35) and high metal concentrations indicate a common fluid source of the two vents. In contrast, in the Red Lion field NW of Comfortless Cove the four different smokers display cooler temperature (between 193°C for Shrimp Farm and 349°C for Mephisto and Tannenbaum) and show no phase separation. This indicates that these fluids have never been as hot as the Turtle Pits and Sisters Peak ones and that is probably a separate vent system.

While the fluids at 5°S are clearly a result of water-rock interaction in a basaltic system, the vent crater "Drachenschlund" at Nibelungen indicates fluid reactions with mantle rocks, i.e. serpentinization reactions. Besides the very high gas concentrations (see chapter 1.4.6), high Fe and Cu contents confirm this assumption. The high H_2/CH_4 ratio (see chapter 1.4.6) and the extremely high Cu concentrations indicate an endmember fluid temperature in the range of 360-400°C, because Cu precipitates as chalcopyrite at temperatures <350°C. The fluids are probably not hotter than 400°C, because at the depth of the field the boiling point would be around 400°C and phase separation is not apparent from the chlorinity data (Fig. 1.35).

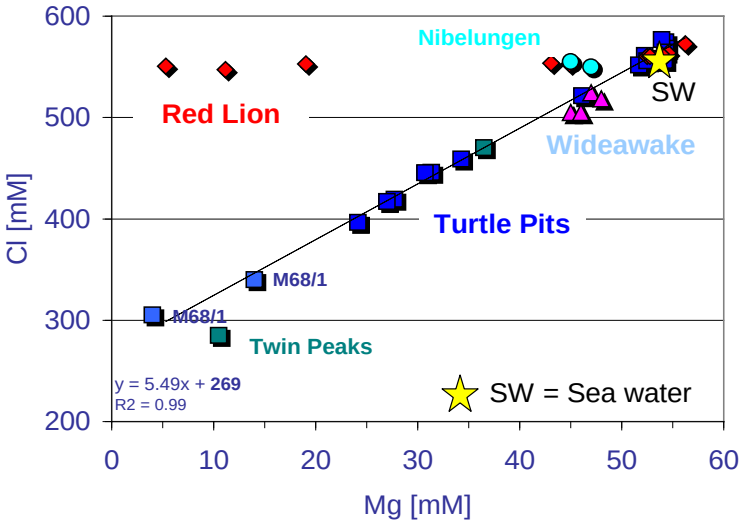

Fig. 1.35 Plot of chlorinity versus Mg concentrations with data from M64/1 and M68/1. Pure seawater has a Mg concentration of 54 mM, while the hydrothermal endmember is assumed to have Mg = 0 mM. Turtle Pits and Sisters Peak fluids area clearly phase-separated, while Red Lion and Nibelungen fluids are not

Table 1.6 Comparison of the geochemistry of high temperature vents and diffuse flow mussel fields

	$T_{in\ situ}$ (°C)	pH	Eh (mV)	O_2 (ml/l)	S^{2-} (µM)	Cl^- (mM)	Si (µM)	Mg^{2+} (mM)	Ca^{2+} (mM)	Fe_{ges} (µM)	Fe^{2+} (µM)	Fe^{2+} (µM)	Cu^{2+} (nM)	Zn^{2+} (nM)	Pb^{2+} (nM)
(A) High Temperature Vents															
5°S															
Turtle Pits & Comfortless Cove															
min	***350***	***3.1***	***-304***		***5.7***	***285***	***231***	***4.0***	***7.5***	***9.4***	***4.0***	***0.3***	***2.8***	***111***	***0***
max	***407***	***7.9***	***70***		***957***	***540***	***5925***	***36.5***	***12.0***	***3675***	***3240***	***6498***	***1622***	***938***	***4.1***
median	***395***	***4.1***	***-212***		***217***	***325***	***840***	***12.3***	***8.3***	***1564***	***1665***	***2096***	***82***	***648***	***0.7***
Red Lion															
min	***186***	***5.5***	***-289***		***37.8***	***555***	***267***	***41.5***	***9.0***	***1.78***	***1.1***	***7.0***			
max	***346***	***7.3***	***-47***		***1027***	***560***	***1416***	***55***	***12.0***	***888***	***26.6***	***130***			
median	***345***	***6.2***	***-182***		***343***	***555***	***767***	***48.5***	***11.0***	***49.3***	***15.9***	***83***	***29.9***		
Nibelungen															
min	***30***	***6.4***	***-357***		***0.6***	***550***	***86***	***45***	***13.0***	***11***	***3.2***	***2.3***	***60.8***	***1158***	
max	***90***	***7.9***	***-90***		***7.0***	***555***	***2263***	***47***	***14.0***	***843***	***796***	***930***	***5693***	***8700***	
median	***90***	***7.1***	***-236***		***3.0***	***553***	***1175***	***46***	***13.5***	***121***	***71***	***50***	***435***	***5446***	
(B) Diffuse Flow Mussel Fields															
5°S															
min	***30***	***6.4***	***-357***		***0.6***	***550***	***86***	***45***	***13.0***	***11***	***3.2***	***2.31***	***60.8***	***1158***	
max	***90***	***7.9***	***-90***		***7***	***555***	***2263***	***47***	***14.0***	***843***	***796***	***930***	***5693***	***8700***	
median	***90***	***7.1***	***-236***		***3***	***553***	***1175***	***46***	***13.5***	***121***	***71***	***50***	***435***	***5446***	
Liliput															
min	***4.8***	***6.0***	***-190***	***< 0.5***	***4***	***550***	***57***	***52.5***	***10.0***	***0***	***0***	***0.15***	***8.04***	***140***	***0***
max	***15.8***	***7.9***	***42***	***5.27***	***341***	***555***	***1082***	***55.5***	***10.0***	***43***	***42***	***25***	***76.5***	***650***	***1.9***
median	***6.8***	***6.7***	***-89.5***	***3.12***	***22.5***	***550***	***114***	***55.0***	***10.0***	***2.7***	***2***	***5.4***	***20.1***	***272***	***0.4***

Note: Mg not corrected for interference by Fe(II)

1.4.7.2.2 Mussel Fields in Areas with Diffuse Hydrothermal Fluid Flow

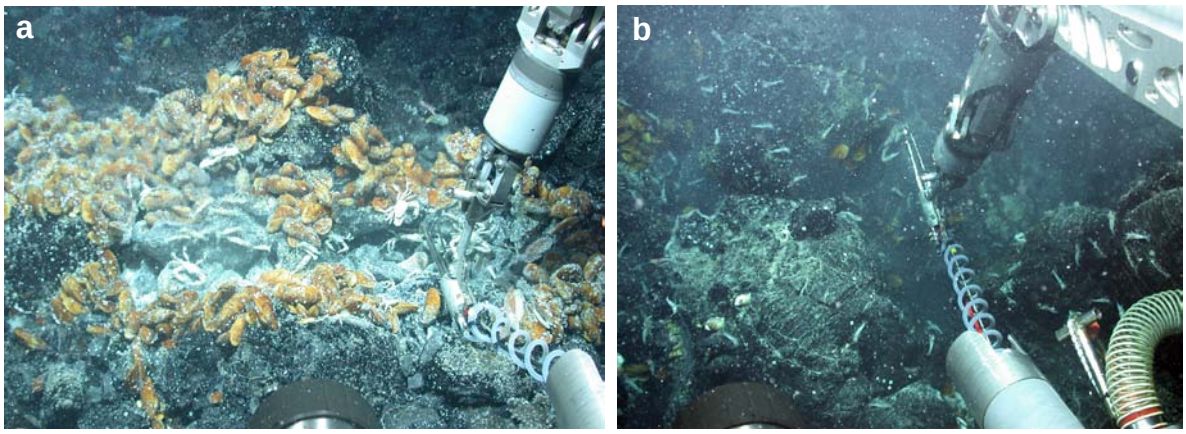

Fig. 1.36 **a**: Area 5° S, Wideawake mussel field, abundant shrimps and crabs in the pond, T = 16.7 °C, KIPS samples 3 ROV-1 to -4. **b**: Area 5° S, Marker #6 site, turbid water from diffuse vents along cracks, abundant shrimps, T = 10 C, KIPS samples 24 ROV-1 to -3

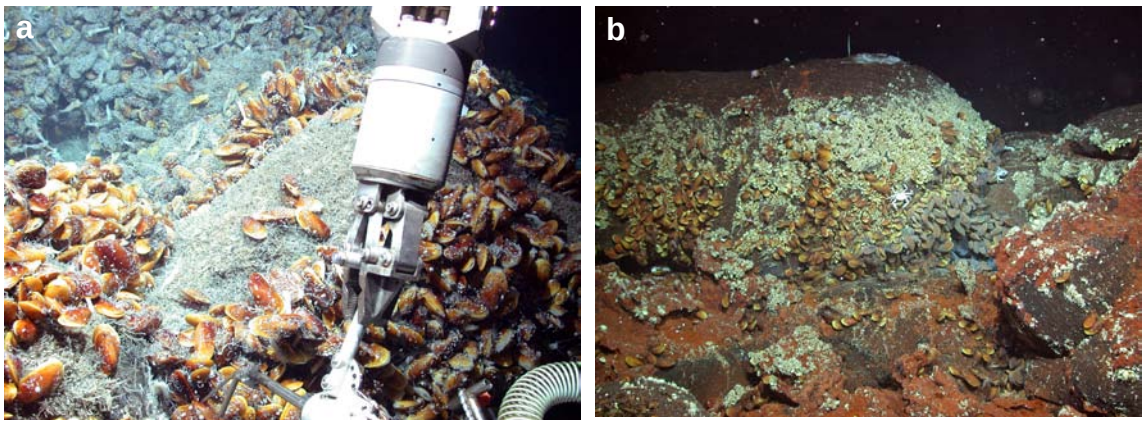

Fig. 1.37 **a**: Area 5° S, Golden Valley mussel field, dense *Bathymodiulus*, filamentous bacteria, shrimps, T = 3.6 °C, KIPS samples 24 ROV-6 to -8. **b**: Liliput area 9° S, 180m S Liliput, small crack w/ abundant mussels, bacterial mats, and shrimps, T = 16.7 °C, KIPS samples 39 ROV-3 to -5

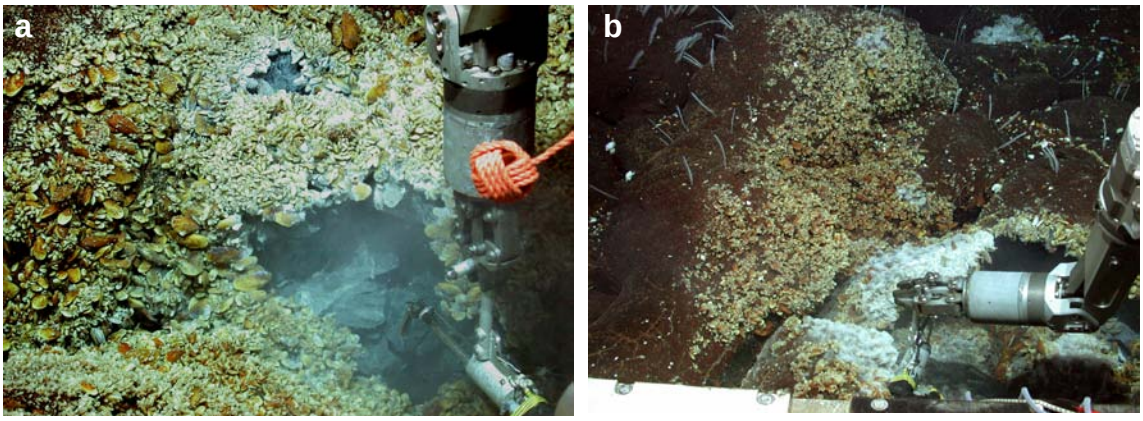

Fig. 1.38 **a**: Liliput area 9° S, w/ dense mussel kindergarten, cloudy water, T = 6.6 C, KIPS samples 41 ROV-6 to -8. **b**: Liliput area 9° S, Northern border of ABE map, small crack w/ abundant mussels, bacterial mats, and shrimps, T = 6.8 C, KIPS samples 41 ROV-10 to -12

All individual on-board fluid chemistry data from the diffuse fluids are listed in Table 1.7 and further parameters will be measured once the samples have returned to the home lab. However, since a large uncertainty is attached to the on-board magnesium values, the extrapolation to calculate endmember: seawater ratios in these samples is not allowing many interpretation of the data yet.

Eh, on the contrary to pH, is a good indicator for the hydrothermal influence of the samples as reducing compounds such as free dissolved sulphide, hydrogen and methane, produced during the hydrothermal process. The correlation shown in Figure 1.39 indicates, that in the diffuse hydrothermal samples the strongly reducing character, mirrored by a negative Eh, is mainly caused by free sulphide, which is present in a much higher concentration than methane and hydrogen.

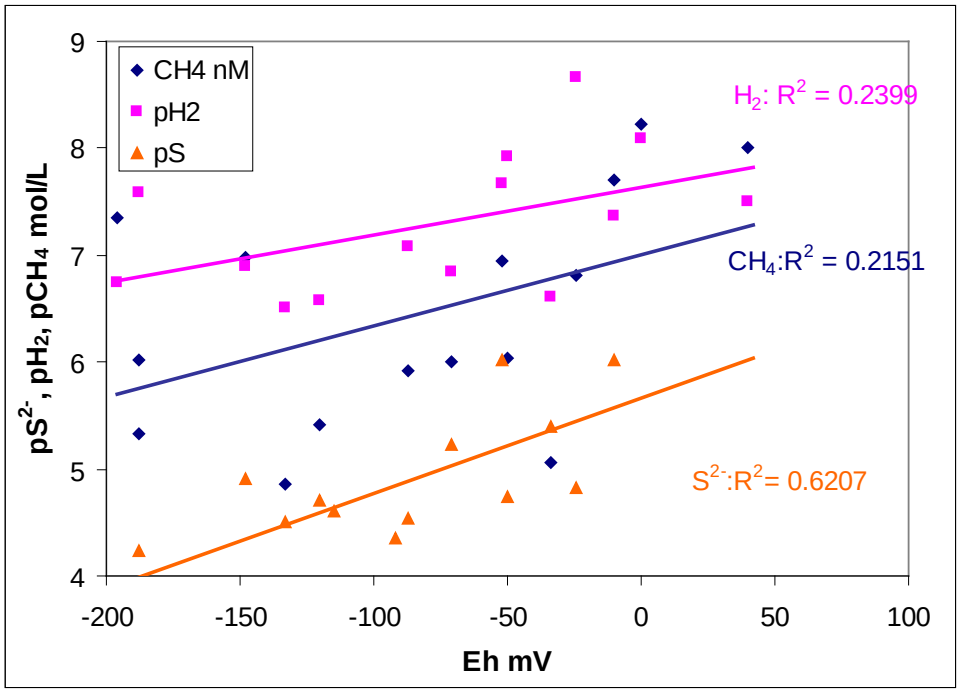

Fig. 1.39 Correlation of the Eh with reducing components in the diffuse hydrothermal fluid samples taken during M68/1. (Note that the concentrations of sulphide, methane and hydrogen have been plotted as the negative logarithm. Methane and hydrogen data from R. Seifert and S. Weber)

Table 1.7 On-board fluid chemistry data from samples taken at diffuse hydrothermal sites

ID	T (°C)	pH	Eh (mV)	O_2 (ml/l)	S^{2-} (µM)	CH_4 nM	H_2 nM	Cl^- (mM)	Si (µM)	Mg^{2+} (mM)	Fe_{ges}*(µM)	Fe^{2+*} (µM)	Fe^{2+**} (µM)	Cu^{2+} (nM)	Zn^{2+} (nM)
5°S Widewawake mussle field															
3 ROV-5 N1		7.8	0			6	8	560			10.3	4.7	0	34.8	128
3 ROV-1/2 b1,	17.5	6.7	-188	1.77	59.1	959		550			12.5	7.8	4.3	218	396
12 ROV-10 N3		7.8	-196		115	44	180						0.43	1.49	379
24 ROV-3 b7	9.6	7	-148	5.16	12.2	104	126	550	338	52.5	1.43	0.71	1.71	10.7	421
24 ROV-4 N1		7.9	40			10	31		39				0	12.1	650
24 ROV-4N2	3.2	7.9	-10		0.94	20	42		32	54	0	0	0	3.28	33.6
24 ROV-8 b4	3.6	7.7	-52	5.1	0.94	113	21	550	25		4.64	1.25	2.25	6.49	365
Lilliput south															
39 ROV-8 N1		7.8	42										1.154	8.04	253
39 ROV-8 N2		7.8						550					0.198		
39 ROV-3 b9	15.8	6.2	-190					550							
39 ROV-4 b8	15.8	6.3	-188	0	341	4600	26	555		52.5	15	15	16	11.4	140
70 ROV-2 b2	8.5	5.9	-34		4	8865	250		256	55			25	22.7	650
70 ROV-5 b4	10	6.5	-133		31	13878	313		285	54.5			16.7	76.5	177
70 ROV-9 N1		7.6	-71		6	1007	143		57	55.5			0.15	37.6	247
70 ROV-10 N2		7.3	-120		20	3918	263		93	55			0.37	28.9	148
Lilliput center and north															
41 ROV-5 b7	4.8	7.2	-24	5.27	15	155	2				3.2	1.4	1.38	17.4	479
41 ROV-6 b6	6.6	6.5	-87	3.12	29	1188	84	550			6.8	7.5	13.8	14	454
41 ROV-8 b1	6.3	6.5	-115		25								6.02		
Cadelabrum Meadow north of Lilliput															
41 ROV-10 b3	7	6.6	-50		18	926	12	555					4.69	32.8	291
41 ROV-12 b4	6.5	6.9	-92		45						3.6	3.4	8.7	9	421

* Fe redox speciation measured photometrically
** Fe^{2+} measured by chemiluminescence
H2 and CH4 data from R. Seifert and S. Weber (see Chapter 1.4.6)

1.4.7.2.3 Organic Complexation of Copper in Hydrothermal Vent Samples

The complexation of copper and other heavy-metals with free inorganic sulphides in hydrothermal waters is considered to dominate their chemical speciation and bioavailability (Edgcomb et al., 2004; Luther III et al., 2001). However, recent studies on the effect of heavy metals on *Bathymodiolus azoricus*, a deep-sea Mytilid bivalve very common in the Mid Atlantic Ridge (MAR) hydrothermal vent fields, showed that these organisms in combination with their methanotroph and thiotroph symbiotic bacteria have mechanisms to protect themselves from heavy metal toxification including the production of metallothioneines and antioxidants (Bebianno et al., 2005; Company et al., 2004; Cosson and Vivier, 1997).

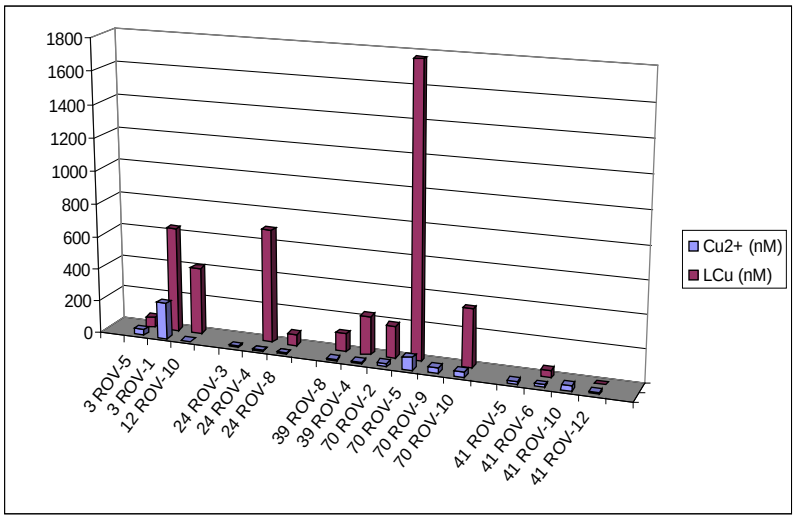

Fig. 1.40
Total dissolved copper concentrations [Cu_T] and Cu-binding ligand concentrations [L_{Cu}] in diffuse hydrothermal fluid samples taken during M68/1 cruise

It is now also well established that in the ocean at large, the biological availability of all essential or toxic metal ions are controlled by the formation of strong complexes with natural organic matter ligands of which many are presumed to be of biological origin, produced either to acquire metal-ions (e.g. Fe^{3+} (Van den Berg, 1995)) or to reduce their toxicity (e.g. Cu^{2+} (Dupont et al., 2004; Moffett and Brand, 1996)). However, the link between these detoxification mechanisms and possible metal binding ligands released into the hydrothermal vent environment as conditioning reagents for the local hydrothermal bio-community has not been made yet (by other researchers) and a first study in samples from the Logatchev field and the Kermadec Arc had shown that organic copper binding ligands can be found in hydrothermal vent fluids.

The goal of the present study was:

A. To confirm that the presence of organic copper binding ligands in samples from deep-sea hydrothermal vent systems can be generalised. Therefore a large number of samples has been measured to obtain the ligand concentration [L_{Cu}].

B. To determine the conditional stability constant $K''_{CuL,Cu2+}$ (salinity 35, pH 7.8) and compare them with values of ambient seawater.

C. To gain information about the selectivity of L_{Cu} (i.e. in competition with other heavy metals such as Zn, Pb, Cd, and Fe).

D. To collect sample material for structural and stable isotope analysis with the focus to find out if L_{Cu} is produced biotically and abiotically.

Pictures of sampling sites are shown in 1.4.7.2.1 and 1.4.7.2.2.

1.4.8 Hydrothermal Symbioses

(N. Dubilier, F. Zielinski)

Our main goal for this cruise was to investigate the transfer of energy from vent fluids to the dominant members of the faunal community at many of the Southern MAR vent sites, the mussels *Bathymodiolus* sp. These mussels have greatly reduced guts, and their main source of nutrition is symbiotic bacteria that live in their gills. Two types of symbionts coexist in the gill cells: thiotrophic bacteria that use reduced sulfur compounds such as sulfide as an energy source and fix CO_2 as a carbon source, and methanotrophic bacteria that use methane as both an energy and a carbon source. The energy sources for the mussel symbioses are delivered by the hydrothermal fluids that carry high concentrations of sulfide, methane, hydrogen, and other reduced compounds. The concentrations of these energy sources vary over time and space and play a major role in determining the biomass, activity and productivity of the vent community. We have defined these interactions between hydrothermal and biological processes as the geobiological coupling between vent fluids and symbiotic primary producers.

During this cruise, we contributed to our ongoing studies of geobiological coupling at MAR vents by:

1) Identifying the energy sources used by the mussel symbionts
2) Comparing the rates at which different energy sources are used by the symbionts
3) Comparing how consumption rates of different energy sources are related to their concentrations at vent sites

To collect geochemical data at a scale relevant to the mussel community, we worked in close collaboration with the fluid and gas chemistry groups, and on-board analyses of hydrogen and methane uptake were in collaboration with Richard Seifert and Stefan Weber.

Mussels were collected using the ROV manipulator arm in nets (40 cm length with a 20 cm diameter opening, mesh size 1000 µm) at different sites in the Wideawake, Comfortless Cove (Sisters Peak and Golden Valley), and Lilliput vent fields (Table 1.8).

Table 1.8 Mussel collection sites at Southern MAR vent sites

Sample	Station Number	Site	Coordinates
1	3 ROV-6	Wideawake (Marker 1)	4° 48,6404 S 12° 22,3634 W
2	12 ROV-9	Wideawake (Marker 1)	4° 48,6404 S 12° 22,3634 W
3	20 ROV-1	Sisters Peak (Marker 5)	4° 48,188 S 12° 22,301 W
4	24 ROV-5	Golden Valley (no marker?)	4° 48,166 S 12° 22,271 W
5	39 ROV-6	S of Lilliput “Limtoc” (no marker?)	9° 32,955 S 13° 12,531 W
6	70 ROV-8	S of Lilliput “Limtoc” (no marker?)	9° 32,9606 S 13° 12,5339 W

On board, the mussels were dissected and prepared for morphological and molecular analyses in the home laboratory. For on board analyses of uptake rates of energy sources, gill tissues (that contain the bacterial symbionts) were incubated in methane, sulfide, and hydrogen and the decrease of these energy sources over time was measured in the head space or fluid of the incubation vial. Carbon fixation rates were determined radioactively, using $^{14}CO_2$ for sulfide and hydrogen, and $^{14}CH_4$ for methane. Vials with mussel foot tissue (that is symbiont free) or with only sea water were used as controls.

Although not all results from our on-board experiments were available at the time of writing this report, some first results can be summarized at this point. No uptake of methane was measured, neither in the labeled nor the unlabled experiments. This result was unexpected because at least one mussel specimen collected from the Wideawake vent site in the previous year, contained methane-oxidizing symbionts. Possibly, methane concentrations were too low in the incubation (< 30 µM), as other authors were only able to show significant $^{14}CH_4$ uptake at methane concentrations above 50 µM.

Sulfide is clearly used as an energy source by the mussel symbionts, based on experiments showing a much greater decrease of sulfide in vials containing mussel gill tissues than in the controls with foot tissue or seawater (Fig. 1.43). In correspondence to the linear decrease in sulfide, $^{14}CO_2$ fixation rates increased linearly until sulfide concentrations apparently became too low for further $^{14}CO_2$ fixation (Fig. 1.41).

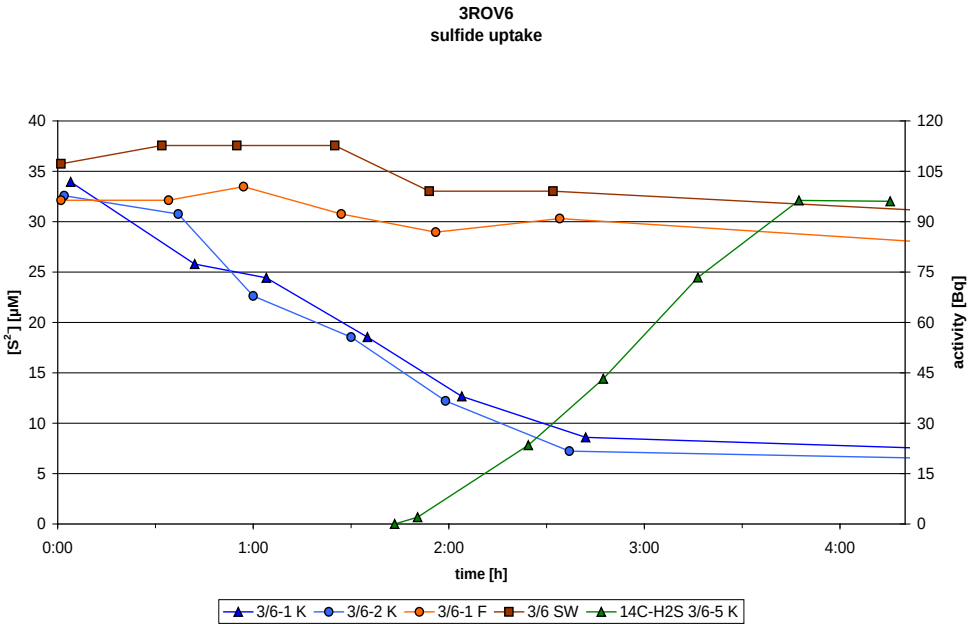

Fig. 1.41 Decrease of sulfide in symbiont-containing gill tissues from 2 mussel individuals (blue lines) is linear until approx. 8 µM sulfide, while almost no decrease of sulfide was observed in seawater (orange line) and symbiont-free foot tissue (burgundy line). Fixation of $^{14}CO_2$ (green line) increased linearly, but leveled off at the end of the experiment, in correspondence to the leveling off of sulfide uptake rates

Sulfide consumption rates were significantly higher in mussels collected from Wideawake than in those collected from Lilliput. Intriguingly, sulfide concentrations in Wideawake diffuse fluids were higher at 80 – 750 µM than those in Lilliput at 31 – 36 µM, indicating a possible correlation between sulfide concentrations in the mussel environment and symbiotic activity.

Hydrogen was also used as an energy source, although at much lower rates than sulfide. Fixation rates of $^{14}CO_2$ were correspondingly lower for hydrogen than for sulfide. This corresponds well with the concentrations of these two energy sources at the collection sites on Southern MAR vent fields, where hydrogen concentrations were at least 100-fold lower than those of sulfide.

In summary, our first results indicate that both sulfide and hydrogen can be used as energy sources by mussel symbionts, and that the rates at which these energy sources are used are dependent on their concentrations in the mussel environment. This result is surprising given that the oxidation of hydrogen provides the bacteria with more energy than the oxidation of sulfide and needs to be confirmed in further experiments and during the following cruises.

1.4.9 The Hydrothermal Vent Fauna in SMAR – a Characterization of Three Communities

(O. Giere)

Summary: The faunistic communities encountered during M68/1 are characterized and related to their specific environment. The mussel (*Bathymodiolus*) populations, dominating at several vent sites, are diverging in their size-frequency distribution and the potential reasons are discussed. The striking absence of the typical vent macro- and even meiofauna in the surroundings of the smoker "Drachenschlund" are outlined.

Faunistic sampling was performed for several scientific goals:

a) Sampling for a taxonomical characterization as a comparison to the vent sites north of the equator (various museum specialists),

b) Fixing for revealing the population genetics of species at various sites (T. Shank, USA),

c) Freezing material for isotopic analyses as a contribution to food web analyses

d) Fixing for ultrastructural investigations, especially in symbiotic animals.

On the basis of the numerous samples taken, a picture of three different communities can be drawn:

Mussel beds at diffuse venting sites (Wideawake, 5° S, and Liliput, 9° S):

The diffuse vent sites sampled (Wideawake, 5° S, and Liliput, 9° S) are dominated by dense thickets of *Bathymodiolus* of quite differing size distributions. While at Wideawake larger mussels dominated (80% >8 cm), the Liliput were fields dominated by smaller specimens (only 1.5 % >6.5 cm, post-settlement stages prevailing). Size-frequency plots illustrate this discrepancy (Fig. 1.42 a, b).

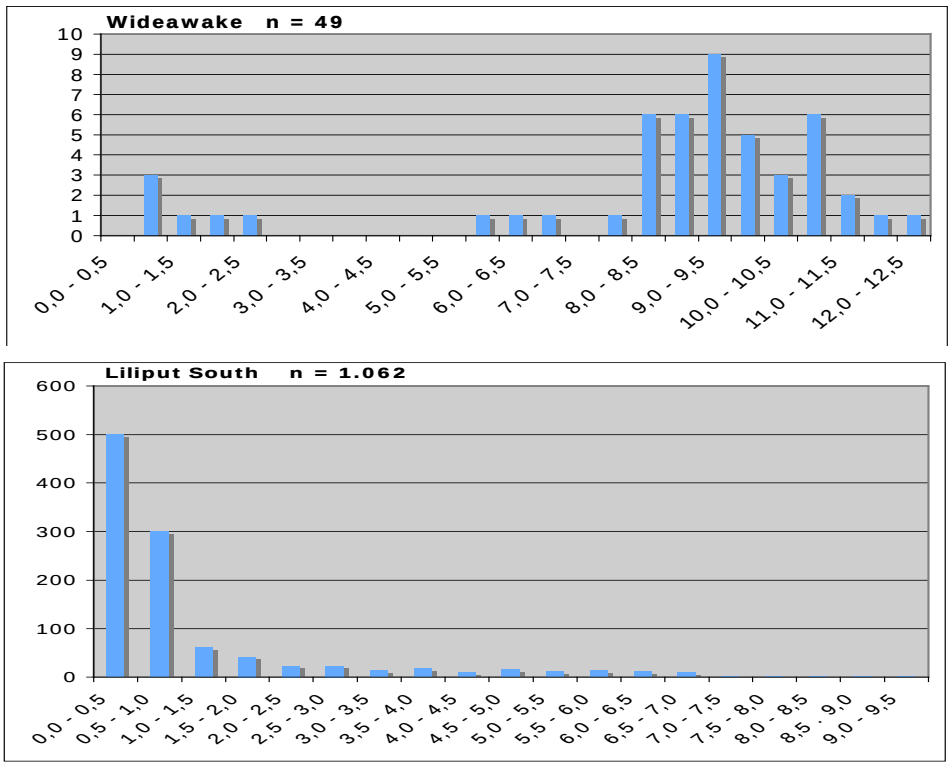

Fig. 1.42 a, b
Comparison of size-frequency distributions of *Bathymodiolus* at 5° S (Wideawake) and 9° S (Lilliput)

It was observed that most of the mussels at 9° S were more elongate and thinner-shelled than those at 5° S. However, these differences occurred also within the Liliput populations (Fig. 1.43 a), ruling out the possibility that they might relate to different age groups.

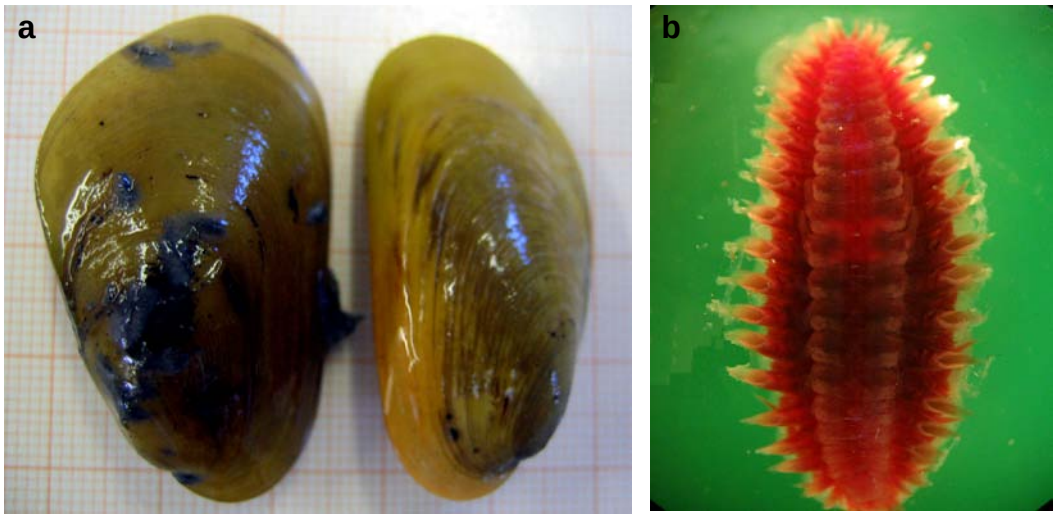

Fig. 1.43 **a**: Different shell shapes of *Bathymodiolus* sp. from the Liliput South mussel field. **b**: Commensalic polychaete *Branchipolynoe*, living in *Bathymodiolus* sp., length 1.5 cm

The species identity of this key taxon needs to be clarified by the few specialists, since external shape is subject to much variation. Muscle and shell scar preparations have been already made to support the taxonomist's work. We will perform age determinations on the basis of micro-increments in the shell structure which can yield a picture of the settlement history of the respective vents. The wide distribution of this genus can be explained by its planktotrophic and widely dispersing larvae and its ecological flexibility: As a bacteria-symbiotic specialist, the mussel can also switch (for a while?) to filter feeding sustaining itself on bacterial flocks suspended in the inhaled water current.

At the vertical walls of hot smokers, *Bathymodiolus* is represented at selected sites in smaller patches only. At the Wideawake mussel sites, usually somewhat apart from the mussel thickets, one could occasionally find a rarity in the Atlantic, the white clam *Calyptogena* sp. Only one specimen could be retrieved at M68/1, and will be studied ultrastructurally and genetically. In contrast to the Pacific vents, Calyptogena from the MAR lacks detailed description and investigation.

The notorious commensal of these mussels, the polychaete *Branchipolynoe* sp. (Fig. 1.43 b) was to be found in the northern fields in almost each specimen, while the southern mussel populations were only little infested. Also here, the species affiliation needs to be identified.

In order to efficiently evaluate the fauna in the mussel thickets, the sample has been washed out and the remainder sieved. By far most frequent were the molluscs: small gastropods (probably *Lirapex*) dominated in the southern fields, two kinds of limpets (Lepetodrilids and Fissurellids, cf. Pseudorimula) at the northern sites. The limpets preferably attach themselves to the shells of live mussels. These molluscs are typical grazers feeding on the bacterial films on all

substrates around vents. In the richly structured mussel beds they have an effective shelter against predators.

Predators are represented by various polychaete worm groups (Aphroditidae, see Fig. 1.44 a, Polynoidae, Phyllodocidae).

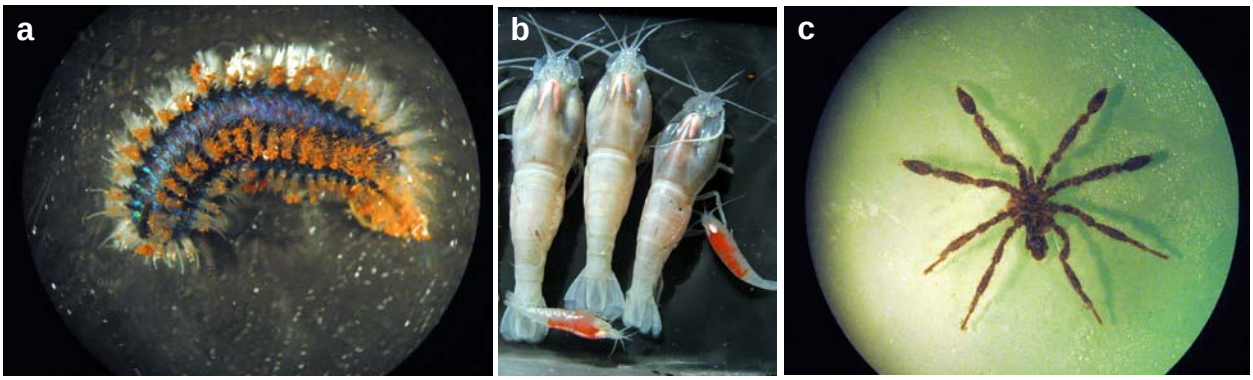

Fig. 1.44 **a**: Representative of the predacious polychaete family Aphroditidae. **b**: Typical shrimps (white: *Rimicaris exoculata*, red: *Mirocaris fortunata*) from the chimneys of black smokers (length of Rimicaris: 7 cm). **c**: A pantopod (Pycnogonida, Ammotheidae) from mussel beds, size: 1 cm

Other, more frequently occurring polychaetes belong to the feeding guild of deposit feeders/detritivores. A terebellid (cf. *Amathys*) is particularly frequent. It builds its small tubes of fine particles, often fluffy precipitates and debris, probing the sediment in its environment with its numerous head tentacles. The spionid polychaetes found have the same feeding strategy. In a community with abundant life, the consumers of dead or moribund animals have an important ecological role. Among the larger of these scavengers is the crab (cf. *Segonzacia*) which occurs frequently both in mussel fields and at hot smokers. Another conspicuous scavenger occurring in singular specimens among the mussels is the large conid snail *Phymorhynchus*. It is necrophagous, taking up freshly dead or moribund animals.

Especially near the “hot spots” with outflows of shimmering water, some shrimps can be observed climbing over the surface of the mussels: *Rimicaris* sp. (white shrimp, Fig. 1.44 b) and occasionally also the smaller, reddish *Mirocaris fortunata* (Liliput area).

The nutritive basis of *Rimicaris* is disputed; the species probably combines bacterial food cultivated on especially formed mouth parts and inner carapace surfaces with bacterial films scraped off the surfaces in the environment using its mouth parts. *Mirocaris* is necrophagus, living on dead or moribund *Rimicaris*.

The bizarre looking and regularly occurring Pantopoda (sea spiders, Pycnogonida, Ammotheidae (Fig. 1.44 c) have piercing and sucking mouth parts.

Their food basis in mussel fields is not clear, probably small sea anemones, soft corals or hydroid colonies. Frequent members of the meiofauna are the representatives of cyclopoid copepods of a reddish colour. Living on the surface of the thicket of byssus threads and mussel shells, they also make short excursions into the water, only to return immediately to their substrate. Cyclopoids are known to be micro-predators. Their food basis in the vent mussel

community is unknown. Some suspension feeders can usually be found in direct vicinity of the mussel fields, filtering the flow of venting water: soft corals (gorgonians), hydrozoan colonies (e.g. *Candelabrum*), small actiniarians attach themselves preferably to exposed sites (top of lava blocks) where they filter the vent fluids rich in particle suspensions.

Comparable to blue mussel beds in shallow waters, the thickets of vent mussel shells and byssus threads are populated by a well definable community of invertebrates of various size and trophic groups. They differ in their food basis, at the vents the chemosynthetic free-living or symbiotic bacteria, in shallow waters the photosynthetically driven phytoplankton. As for their production, the deep-sea communities are comparable to their shallow-water counterparts (Giere et al., 2003), and thus truly represent oases of life in the sparsely populated deep-sea.

The fauna at the Black Smoker situated at 5° S:

The hydrothermal fauna in the vicinity or on the walls of black smokers is less clearly definable and more varying than that of the mussel beds at diffuse venting fields. Amazingly close to the vent outlets with their hot fluids aggregate rich populations of the key species, the white vent shrimp *Rimicaris exoculata* (see Fig. 1.44 b). The often thick clumps of their bodies remind of a "swarming" behaviour in insects. In contrast, on the cooler surfaces the shrimps are regularly dispersed, keeping a certain distance and actively moving their mouthparts in a sweeping mode over the rock surfaces. A relation to the activity of the smoker was indicated at the smoker "Shrimp Farm" whose flanges were densely covered by huge populations of shrimps in 2005, while in 2006 this smoker was less active and the shrimp populations were much reduced, concentrated in small patches only. In contrast, at the neighbouring "Mephisto", a reversed process could be observed; it now had a white appearance due to its dense cover with shrimps. Whether this switch in the population centre is due to increased settlement of young recruits due to more attractive vent conditions, remains open since the settlement cues and the growth curves of these shrimps are as yet, undetermined.

The mussel *Bathymodiolus* sp. is regularly, but patchily, found attached to crevices and even vertical walls of the smokers. But the small size classes seem to be absent here. This species has its centre of occurrence certainly at the diffuse vent sites. On a smaller scale, the mussel thickets are populated by essentially the same community of small fauna as in the mussel beds. Among the numerous shrimps, many crabs climb (*Segonzacia mesatlantica*) searching for suitable moribund animals. In the surroundings and at the base of the smokers suspension feeders occur such as actiniarians or gorgonians. In the sheltered crevices of rocks, terebellid detritus feeders (cf. *Amathys*) extend their tentacles out of their small tubes. Occasional gastropods (cf. *Lirapex*) can also be encountered. Summarizing, the fauna at the hot smokers, although spectacular in their close contact to the hot effluents, has a lower diversity than that of the vent mussel fields and is clearly dominated by the white shrimps.

The fauna around the crater vent "Dragon's Throat, 8° S:

The surroundings of the powerful smoker were devoid of the typical vent fauna except for numerous parchment-like, flexible tubes of chaetopterid polychaetes of unknown identity (Fig.

1.45) which were attached to the loose alterated rocks and sand of the crater walls. Some 15 specimens have been removed from their tubes and fixed for genetic and taxonomical studies. The absence of all vent-related macrofauna might reflect difficulties for larvae to settle on fairly loose sediment, but the complete absence of meiofauna in the voids of the sand points to other hostile environmental conditions, such as high concentrations of toxic heavy metals bound as sulfides.

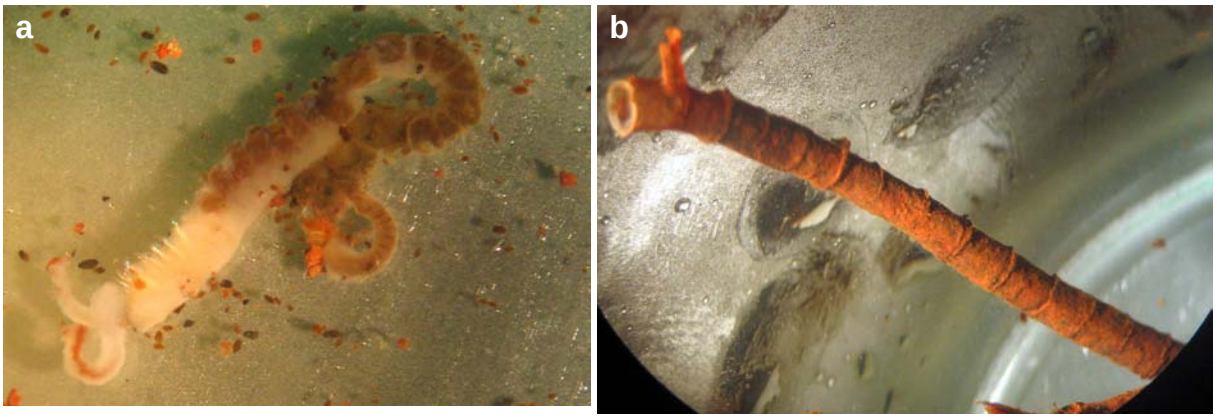

Fig. 1.45 **a, b**: A chaetopterid polychaete and its annulated tube from the crater walls of the smoker "Drachenschlund"

In comparison, the M68/1 - studies of fauna communities in the MAR hydrothermal fields south of the equator show essentially the same taxonomic composition and ecological structure as those in the North (Gebruk et al., 1997). Despite some taxonomic differences, this overall correspondence could not be anticipated considering the huge Romanche Fracture Zone which might have been a barrier restricting or at least filtering dispersal of vent animals. The data of M68/1 so far underline the conclusion drawn from the results of M 64/1 that delineation of a separate zoogeographical province (see Van Dover et al., 2002) for the South Atlantic vent sites near the equator is not required.

1.5 Ship's Meteorological Station

(W.-T. Ochsenhirt)

METEOR left the port of Bridgetown in the forenoon of April 27. The weather situation was characterized by an easterly to northeasterly trade wind of Bft 4 to 5, a broken sky and short shower activity associated with head easterly swell up to 2.5 m.

On May 02 the northern limit of the Intertropical Convergence Zone (ITCZ) was met near 05° North 38° West with easterly to northeasterly winds of 5 to 6 Bft and shower squalls of Bft 7. The wind decreased not before May 05 and became easterly force 3 to 4.

On the following day, shortly before crossing the equator near 25° West, METEOR left the ITCZ. The cruise to the first area of investigation near 04,8°S 12,3°West, arriving there on May 09 in the evening, was affected by southeasterly trade winds caused by a South Atlantic high

between 40° and 45° South. METEOR remained in this region during the whole time of research. The range of wind speed was 2 to 4 Bft with a sea of 1.5m and mostly scattered clouds. This situation continued from May 17 in the second area of investigation near 09,5°S 13,5° W.

The third area, reached on May 20, was situated more northwesterly near 08,3° S 13,5° W. One day later in the evening an intensive shower activity began with easterly gusts up to Bft 7.

Since the ridge of the subtropical high expanded northerly the wind from east to southeast increased to Bft 5 or 6, with gusts up to 7. The height of the sea and swell increased to 2,5 and 3 m, in some cases of converging swell more than 3m. On May 05 the wind and sea decreased slowly. The wind became southeasterly of 4 to 5 Bft.

1.6 Station List M68/1

Table 1.9 Station list of M68/1 cruise

RV METEOR cruise M68/1												
							Begin / on seafloor		End / off seafloor			
Date	St. No.			Start Sci.	End Sci.	Latitude	Longitude	Water	Latitude	Longitude	Water	Recovery
		Instruments	Location	Program	Program	S°	W°	depth (m)	S°	W°	depth (m)	Remarks
		M68/1										
10.05.06	1 CTD	CTD/Ro	Turtle Pits area	02:56	05:06	4°48.80'	12°23.01'	2955				
10.05.06	2 AUV	AUV phase 1	Turtle Pits area	08:12	06:38*	4°48.80'	12°22.55'		4°48.94'	12°22.89'		*11/05/06
10.05.06	3 ROV	ROV	T. Pits/Wideawake	14:24	22:28	4°48.63'	12°22.33'	2982	4°48.57'	12°22.41'	2981	12 samples (bio-fluid-rock)
11.05.06	4 CTD	CTD/Ro	Turtle Pits area	00:48	15:47	4°48.55'	12°22.41'					no depth signal
11.05.06	5 CTD	CTD/Ro	Turtle Pits area	04:14	06:22	4°47.28'	12°22.62'					no depth signal
11.05.06	6 VSR	VSR	Turtle Pits area	08:17	09:41	4°47.82'	12°22.62'	3036				fresh glass
11.05.06	7 ROV	ROV	Red Lion	10:32	23:25	4°47.49'	12°22.61'	3051	4°47.83'	12°22.57'	3046	
12.05.06	8 CTD	CTD/Ro	Turtle Pits area	00:18	02:20	4°51.30'	12°19.51'	2936				
12.05.06	9 CTD	CTD/Ro	Turtle Pits area	03:47	06:03	4°52.01'	12°21.48'	3185				
12.05.06	10 CTD	CTD/Ro	Turtle Pits area	07:12	09:22	4°53.00'	12°23.36'	2988				
12.05.06	11 AUV	AUV phase 2	Turtle Pits area	10:24	02:40*	4°48.63'	12°23.19'		4°48.20'	12°23.18'		*13/05/06
12.05.06	12 ROV	ROV	T. Pits/Wideawake	11:09	23:35	4°48.56'	12°22.43'	2991	4°48.64'	12°22.37'	2976	
12.05.06	13 CTD	tow-yo	Turtle Pits area	03:19	13:30	4°50.12'	12°22.10'	3009	4°46.32'	12°22.85'	3174	
13.05.06	14 VSR	VSR	Turtle Pits area	14:20	16:05	4°48.10'	12°22.38'	2992				glass chips
13.05.06	16 CTD	CTD/Ro	Turtle Pits area	18:14	20:10	4°46.00'	12°25.36'					
13.05.06	17 CTD	CTD/Ro	Turtle Pits area	21:11	23:27	4°45.16'	12°23.00'	3246				
14.05.06	18 CTD	CTD/Ro	Turtle Pits area	00:35	02:44	4°44.30'	12°20.69'	3048				
14.05.06	19 CTD	tow-yo / MAPR	Turtle Pits area	03:44	08:23	4°49.01'	12°23.23'	2988				
14.05.06	20 ROV	ROV	Twin Peaks	11:06	23:58	4°48.17'	12°22.35'	2993	4°48.17'	12°22.29'		
15.05.06	21 AUV	AUV phase 3	Turtle Pits area	03:30	11:20	4°48.64'	12°22.35'		4°49.10'	12°22.12'		
15.05.06	22 CTD	tow-yo / MAPR	Turtle Pits area	01:35	09:08	4°48.05	12°23.94	3012	4°47.32'	12°21.17'	3057	
15.05.06	23 SM	mooring	Turtle Pits area	13:30	13:30	4°.48.46'	12°22.63'	3001	4°48.20	12°22.50'	2990	
15.05.06	24 ROV	ROV	Turtle Pits area	15:06	01:32*	4°48.14'	12°22.92	2993	4°48.18'	12°22.29'	2991	*16/05/06
17.05.06	25 EM	EM120	Liliput area	02:39	03:44	9°30.40'	13°13.25'		9°34.61'	13°12.39'		
17.05.06	26 AUV	AUV phase 2	Liliput area	08:18	03:07*	9°33.24'	13°12.16'		9°32.15'	13°12.67'		*18/05/06
17.05.06	27 CTD	CTD/Ro	Liliput area	09:50	10:57	9°31.82'	13°12.98'	1501				
17.05.06	28 DS	dredge	Liliput area	11:53	12:23	9°32.80'	13°12.25'	1441	9°32.63'	13°11.91'	1590	old volc.+corals
17.05.06	29 CTD	CTD/Ro	Liliput area	18:48	20:26	9°35.51'	13°05.01'	2302				
17.05.06	30 VSR	VSR	Liliput area	21:30	22:16	9°33.90'	13°12.41'	1439				glass particles
18.05.06	31 VSR	VSR	Liliput area	22:25	23:08	9°33.70'	13°12.41'	1475				fresh glass
18.05.06	32 VSR	VSR	Liliput area	22:18	00:13	9°33.42'	13°12.50'	1473				empty
18.05.06	33 VSR	VSR	Liliput area	00:24	01:09	9°33.09'	13°12.65'	1479				empty
18.05.06	34 CTD	CTD/Ro	Liliput area	04:40	06:18	9°35.50'	12°58.01'	2357				empty
18.05.06	35 VSR	VSR	Liliput area	07:52	08:40	9°32.90'	13°12.60'	1487				empty
18.05.06	36 VSR	VSR	Liliput area	08:21	10:06	9°31.94'	13°12.78'	1477				glass chips
18.05.06	37 CTD	CTD/Ro	Liliput area	10:27	11:41	9°32.67'	13°12.56'	1500				
18.05.06	38 EM	EM120	Liliput area	12:34	17:52	9°33.12'	13°12.58'		9°35.00'	13°11.90'		one track
18.05.06	39 ROV	ROV	Liliput area	18:20	01:13	9°33.20'	13°12.51'	1475	9°32.92	13°12.55'	1494	
18.05.06	40 AUV	AUV phase 3	Liliput area	21:25	09:02*	9°33.12'	13°12.41'		9°32.54'	13°12.71'		*19/05/06
19.05.06	41 ROV	ROV	Liliput area	15:12	00:18	9°32.87'	13°12.54'	1496	9°32.67'	13°12.52'		
20.05.06	42 EM	EM120	transit	00:40	10:07	9°30.00'	13°13.00'		8°18.50'	13°29.54'		mapping of ridge axis
20.05.06	43 CTD	CTD/Ro	Nibelungen	10:34	12:37	8°17.94'	13°30.69'	2938				
20.05.06	44 AUV	AUV phase 1	Nibelungen	18:12	11:00*	8°17.85'	13°30.49'		8°18.00'	13°.12.49'		*21/05/06
21.05.06	45 CTD	tow-yo	Nibelungen	00:10	06:22	7°57.63'	13°28.22'	3273	7°55.83'	13°27.31'	2866	
21.05.06	46 VSR	VSR	Nibelungen	12:05	13:24	8°17.31'	13°35.82'	2935				glass, sheet flow
21.05.06	47 CTD	tow-yo	Nibelungen	14:10	19:15	8°18.40'	13°31.17'	2916				
21.05.06	48 AUV	AUV phase 2	Nibelungen	19:53	15:55*	8°17.89'	13°30.55'		8°15.86'	13°31.06'		*22/05/06
22.05.06	49 CTD	CTD/Ro	Nibelungen	21:05	23:10	8°16.50'	13°30.41'	2981				
22.05.06	50 CTD	CTD/Ro	Nibelungen	00:18	02:36	8°15.42'	13°30.79'	3179				
22.05.06	51 CTD	CTD/Ro	Nibelungen	03:52	06:19	8°14.00'	13°31.25'	3404				
22.05.06	52 CTD	CTD/Ro	Nibelungen	07:20	09:25	8°12.71'	13°31.70'	2949				
22.05.06	53 VSR	VSR	Nibelungen	10:43	12:29	8°11.01'	13°26.61'	3491				empty
22.05.06	54 VSR	VSR	Nibelungen	13:57	15:23	8°15.80'	13°31.10'	3211				soft white sediment
22.05.06	55 AUV	AUV phase 3	Nibelungen	22:40	11:36*	8°17.90'	13°30.52'		8°21.03'	13°33.69'		*23/05/06

Table 1.9 Station list of M68/1 cruise (continued)

RV METEOR cruise M68/1												
							Begin / on seafloor			End / off seafloor		
Date	St. No.			Start Sci.	End Sci.	Latitude	Longitude	Water	Latitude	Longitude	Water	Recovery
		Instruments	Location	Program	Program	S°	W°	depth (m)	S°	W°	depth (m)	Remarks
		M68/1										
23.05.06	56VSR	VSR	Nibelungen	02:19	03:40	8°19.02'	13°35.29'	2885				empty
23.05.06	57 VSR	VSR	Nibelungen	04:11	05:33	8°21.06'	13°35.00'	2807				some glass
23.05.06	58 VSR	VSR	Nibelungen	06:03	07:26	8°22.48'	13°35.07'	2774				some glass on outside
23.05.06	59 CTD	CTD/Ro	Nibelungen	12:50	15:20	8°10.00'	13°28.02'	3610				
23.05.06	60 EM	EM120	7.58-area	18:49	00:40	8°18.00'	13°27.50'		7°53.00'	13°27.52'		
24.05.06	61 AUV	AUV phase 1	7.58-area	08:05	06:50*	7°57.08'	13°27.99'		7°54.73'	13°28.61'		*25/05/06
24.05.06	62 ROV	ROV	Nibelungen	13:59	01:53	8°17.88'	13°30.40'	2949	8°17.85'	13°30.42'	2904	
25.05.06	63 EM	EM120	transit	07:00	09:53	7°55.02'	13°28.10'		8°17.90'	13°31.30'		
25.05.06	64 CTD	CTD/Ro	Nibelungen	10:03	14:58	8°17.91'	13°31.24'	2963				
25.05.06	65 EM	EM120	transit	15:08	17:58	8°17.86'	13°29.94'		7°56.00'	13°32.00'		
25.05.06	66 DS	dredge	Nibelungen	22:03	01:15	7°57.14'	13°27.72'	3044	7°56.77'	13°27.86'	3250	
26.05.06	67 CTD	CTD/Ro	Nibelungen	02:52	04:17	8°10.48'	13°33.32'	1921				
26.05.06	68 AUV	AUVphase 2	7.58-area	07:07	03:13*	7°57.02'	13°27.94'		7°56.54'	13°27.82'		*26/05/06
26.05.06	69 ROV	ROV	Nibelungen	13:40	00:10	8°17.92'	13°30.45'	2915	8°17.87'	13°30.41'		
27.05.06	70 ROV	ROV	Liliput area	13:45	20:56	9°33.01'	13°.12.38'	1495	9°32.97'	13°12.52'		
28.05.06	71 DS	dredge	Nibelungen	04:45	07:39	8°17.89'	13°30.36'	2951	8°17.83'	13°30.49'	2854	
28.05.06	72 CTD	CTD/Ro	Nibelungen	08:35	09:58	8°10.58'	13°32.76'	1916				

Abbreviations: VSR: Vulkanit-Stossrohr (volcanite wax corer); **DS**: dredge; **CTD/Ro**: CTD and rosette; **MB**: Multibeam-Sonar; **AUV**: Autonomous underwater vehicle ABE; **ROV**: Remotely operated vehicle QUEST

1.7 Acknowledgements

We would like to thank Captain Kull and his crew on R/V Meteor for their professionalism and excellent cooperation during cruise M68/1, which was a major contribution to the success of the expedition. Furthermore, we acknowledge the professional patronage of the German Ministry of Foreign Affairs as well as of Captain Berkenheger at the "Leitstelle Meteor".

We wish to thank the German Science Foundation (DFG) for funding the cruise and the subsequent scientific work in the framework of the priority program SPP 1144 “From Mantle to Ocean: Energy-, Material-, and Life Cycles at Spreading Axes”.

1.8 References

Bebianno, M.J. et al., 2005. Antioxidant systems and lipid peroxidation in *Bathymodiolus azoricus* from Mid-Atlantic Ridge hydrothermal vent fields. Aquatic Toxicology, 75(4): 354.

Bischoff, J.L., Rosenbauer, R.J., 1988. Liquid-vapor relations in the critical region of the system NaCl-H2O from 380 to 414°C: A refined determination of the critical point and two-phase boundary of seawater. Geochim. Cosmochim. Acta, 52: 2121-2126.

Company, R. et al., 2004. Effect of cadmium, copper and mercury on antioxidant enzyme activities and lipid peroxidation in the gills of the hydrothermal vent mussel Bathymodiolus azoricus. Marine Environ. Res., 58(2-5): 377.

Cosson, R., Vivier, J.-P., 1997. Interactions of metallic elements and organisms within hydrothermal vents. Cah. Biol. Mar., 38: 43-50.

Croot, P.L., Laan, P., 2002. Continuous shipboard determination of Fe(II) in polar waters using flow injection analysis with chemiluminescence detection. Analytica Chim. Acta 466: 261-273.

Dupont, C.L., Nelson, R.K., Bashir, S., Moffett, J.W., Ahner, B.A., 2004. Novel copper-binding and nitrogen-rich thiols produced and exuded by *Emiliania huxleyi*. Limnol. Oceanogr., 49(5): 1754-1762.

Edgcomb, V.P. et al., 2004. Sulfide Ameliorates Metal Toxisity for Deep-Sea Hydrothermal vent Archea. Applied Environ. Microbiol. (April): 2551-2555.

Garbe-Schönberg, D., Koschinsky, A., Ratmeyer, V., Jähmlich, H., Westernströer, U., 2006. KIPS – A new Multiport Valve-based all-Teflon Fluid Sampling System for ROVs. EGU General Assembly, Vienna, April 2006

Gebruk, A.V., Galkin, S.V., Vereshchaka, A.L., Moskalev, L.I., Southward, A.J., 1997. Ecology and biogeography of the hydrothermal vent fauna of the Mid-Atlantic Ridge. Adv. Mar. Biol., 32: 93-144.

Gerringa, L.J.A., Herman, P.M.J., Poortvliet, T.C.W., 1995. Comparison of the linear Van den Berg/Ruzic transformation and a non-linear fit of the Langmuir isotherm applied to Cu speciation data in the estuarine environment. Mar. Chem., 48: 131-142.

Giere, O., Borowski, C., Prieur, D., 2003. Biological Productivity in Hydrothermal Systems. In: Halbach, P.E., Tunnicliffe, V., Hein, J.R. (eds.), Energy and Mass Transfer in Marine Hydrothermal Systems. Dahlem Workshop, Berlin, October 14-19, 2001, Dahlem Univ. Press, Berlin, 211-233.

Grasshoff, K., Ehrhardt, M., Kremling, K., 1983. Methods of Seawater Analysis. Verlag Chemie, Weinheim.

Luther III, G.W. et al., 2001. Chemical speciation drives hydrothermal vent ecology. Nature (London), 410(12 April): 813-816.

Moffett, J.W., Brand, L., 1996. Production of strong, extracellular Cu chelators by marine cyanobacteria in response to Cu stress. Limnol. Oceanogr., 41: 388-395.

Rüth, C., Well, R., Roether, W., 2000. Primordial 3He in South Atlantic deep waters from sources on the Mid-Atlantic Ridge. Deep-Sea Res. I 47: 1059-1075.

Sander, S., Kim, J.P., Anderson, B., Hunter, K.A., 2004. Effect of UVB irradiation on Cu2+-binding organic ligands and Cu2+ speciation in alpine lake waters of New Zealand. Environ. Chem., submitted.

Sander, S.G., Koschinsky, A., Massoth, G., Stott, M., Hunter, K.A., 2006. Organic complexation of copper in deep-sea hydrothermal vent systems. In preparation for submission to Geophys. Res. Let.

Sültenfuß, J., Roether W., Rhein M., 2006. The Bremen Mass Spectrometric Facility for the Measurement of Helium Isotopes, Neon, and Tritium in Water. International Symposium on Quality Assurance for Analytical Methods in Isotope Hydrology, IAEA CN 119/7, in press.

Van den Berg, C.M.G. (1995). Evidence for organic complexation of iron in seawater. Mar. Chem., 50: 139-157.

Van Dover, C.L., German, C.R., Speer, K.G., Parson, L.M., 2002. Evolution and biogeography of deep-sea vent and seep invertebrates. Science, 295: 1253-1257.

Van Dover, C.L., 2000. The ecology of hydrothermal vents. Princeton University Press, Princeton New Jersey.

METEOR-Berichte 09-4

Circulation and Variability in the Tropical Atlantic

PART 2

Cruise No. 68, Leg 2

June 6 – July 9, 2006
Recife (Brazil) – Mindelo (Cape Verde)

Peter Brandt, Uwe Beckmann, Jürgen Fischer, Natalie Fischer, Tim Fischer, Andreas Funk, Susann Grobe, Niels Gülzow, Verena Hormann, Frank Malien, Uwe Koy, Mario Müller, Gerd Niehus, Wolf-Thilo Ochsenhirt, Uwe Papenburg, Benjamin Rabe, Jens Schafstall, Anke Schneider, Martina Schütt, Lothar Stramma, Toste Tanhua, Doris Veleda, Peter Wiebe, Claudia Winkelmann, Rainer Zantopp

Table of Contents Part 2 (M68/2)

2.1 Participants

Name	Function	Institute
Brandt, Peter, PD Dr.	Chief Scientist	IFM-GEOMAR
Beckmann, Uwe	CTD, technology	IFM-GEOMAR
Cavalcante, Marcelo	Brazilian observer	
Fischer, Jürgen, Dr.	LADCP, moorings	IFM-GEOMAR
Fischer, Natalie	Helium	UBU
Fischer, Tim	ADCP, shipboard sampling	IFM-GEOMAR
Funk, Andreas, Dr.	CTD, ADCP, radiosondes	IFM-GEOMAR
Grobe, Susann	CO_2, alkalinity	IFM-GEOMAR
Gülzow, Niels	H_2O_2	IFM-GEOMAR
Hormann, Verena	Salinometry, radiosondes	IFM-GEOMAR
Koy, Uwe	Microstructure	IFM-GEOMAR
Malien, Frank	O_2, nutrients	IFM-GEOMAR
Müller, Mario	LADCP, computers	IFM-GEOMAR
Niehus, Gerd	Moorings, CTD	IFM-GEOMAR
Ochsenhirt, Wolf-Thilo	Meteorological technology	DWD
Papenburg, Uwe	Moorings, technology	IFM-GEOMAR
Rabe, Benjamin, Dr.	APEX, CTD, shipboard sampling	IFM-GEOMAR
Schafstall, Jens	Microstructure	IFM-GEOMAR
Schneider, Anke	CFC, SF6	IFM-GEOMAR
Schütt, Martina	CFC, SF6	IFM-GEOMAR
Stramma, Lothar, Dr.	Salinometry, CTD	IFM-GEOMAR
Tanhua, Toste, Dr.	CFC, SF6	IFM-GEOMAR
Veleda, Doris	CTD	UFPE
Wiebe, Peter	CO_2, alkalinity	IFM-GEOMAR
Winkelmann, Claudia	Helium	UBU
Zantopp, Rainer	Moorings, CTD	IFM-GEOMAR

Participating Institutions

IFM-GEOMAR Leibniz-Institut für Meereswissenschaften an der Universität Kiel, Düsternbrooker Weg 20, 24105 Kiel - Germany, e-mail:pbrandt@ifm-geomar.de

DWD Deutscher Wetterdienst, Geschäftsfeld Seeschiffahrt, Bernhard-Nocht-Str. 76, 20359 Hamburg - Germany, e-mail: edmund.knuth@dwd.de

UBU Universität Bremen, Institut für Umweltphysik, Otto-Hahn-Allee, UW1, Postbox 330440, 28334 Bremen - Germany, e-mail: mrhein@theo.physik.uni-bremen.de

UFPE Universidade Federal de Pernambuco, Av. Arquitetura, s/n 50740-550 - Cidade Universitária, Recife - PE, Brasil, e-mail: moa@ufpe.br

2.2 Research Program

The measurement program of M68/2 consisted of station hydrographic observations with a CTD/O_2 rosette including water sampling for tracer, oxygen and nutrient probing. Of particular importance were underway current measurements with both shipboard ADCPs (Ocean Surveyor, 38 kHz und 75 kHz). In addition to horizontal advection by different zonal current bands, diapycnal mixing plays an important role for the heat budget of the mixed layer. In the region between 23°W and 10°W specifically, diapycnal mixing processes were measured on station using a loosely tethered, free-falling microstructure probe and a high-frequency (1200 kHz) LADCP, lowered with the CTD/O_2 rosette at the same station.

During M68/2 an intensive mooring program was carried out. This program particulary consisted of the recovery of two equatorial current meter moorings at 35°W and 23°W. To record changes in the equatorial currents on intraseasonal to interannual time scales, a mooring array was installed at 23°W. This array consists of four current meter moorings and is aimed at quantifying the variability of the thermocline water supply toward the equatorial cold tongue. Another equatorial current meter mooring was installed at 10°W in cooperation with the multi-national PIRATA program. In preparation of a planned new Sonderforschungsbereich [German Special Research Program], a profiling CTD/O_2 was moored at 5°N, 23°W. The goal of this mooring is to observe the transport of oxygen-rich waters toward the oxygen minimum zone in the tropical North Atlantic. The final mooring of M68/2 was deployed near the Cape Verde Islands shortly before arrival at the port of Mindelo.

Helium probes were taken along the meridional sections (23°W and 10°W) and zonal sections (equator and 2°N) in the upper 500m of the water column. Biogeochemical water sampling, including O_2, nutrients, CO_2, CFC, and SF_6 measurements, was carried out during regular CTD/O_2 stations.

In support of the international AMMA program, twice daily radio soundings were taken during M68/2.

2.3 Narrative of the Cruise

R/V METEOR departed from Recife on June 6, 2006 at 10:00L. At that time, some of the instruments (two moored CTD profilers) shipped from Woods Hole, Massachusetts, to Recife should have been delivered to METEOR. Unfortunately, the customs strike in Brazil put a severe damper on these plans, and on-time delivery did not take place. It was decided to ask for permission to take delivery of the instruments upon the ship's arrival at the island of Fernando de Noronha, where the Brazilian observer was scheduled to disembark from METEOR.

R/V METEOR headed north toward the Brazilian shelf along 35°W where scientific work started with the first CTD/O_2 station early in the morning of June 7. The measurements along this section concentrated on the upper ocean so that the CTD/O_2 profiles were taken to a depth of 1300m only, or near bottom in the shallower waters near the shelf. The CTD/O_2 measurements were accompanied by current measurements with two Workhorse ADCPs attached to the CTD/O_2 rosette, as well as by two shipboard ADCPs, so-called Ocean Surveyors of 38 kHz and 75 kHz, respectively. Both instruments obtain their heading input from the 3D-Ashtech GPS receiver as well as from METEOR's Fiber Optic Compass (FOG).

Water samples were taken using the water bottles of the CTD/O_2 rosette as part of the intense biogeochemical program during M68/2. During most of the stations, water samples were analyzed with respect to their contents of chlorofluorocarbons (CFC), sulfur hexafluoride (SF_6), helium, oxygen, nutrients (nitrate, nitrite, phosphate, silicate), dissolved inorganic carbon (DIC), total alkalinity (Alk), and hydrogen peroxide (H_2O_2).

Along the northward cruise track, CTD stations were spaced apart by about 20' – 30' of latitude, somewhat denser near the shelf and near the equator. On June 9, 09:00L, METEOR approached the position of our current meter mooring. The mooring had been deployed in August 2004 and contained four current meters, three CTD sensors, two ADCPs, and one RAFOS sound source. The releases were contacted using the hydrophone board unit, and the release command was sent at 09:10L, with the top element surfacing only a few minutes later. The mooring was then recovered without any problems. A first view of the obtained data showed that all instruments worked well, yielding an instrument and data recovery rate of 100%.

At the mooring position, a first test station with our microstructure profiler (MSS) was carried out with the profiler winch attached at the port side stern rail. The ship's course and speed (max of 1 to 1.5 kn suggested) were adjusted in accordance with wind and surface current to ensure that the microstructure profiler would fall free and clear astern on the port side. After adjusting the profiler sink velocity by changing the weights of the MSS, the first data set was obtained. At this position, the strong eastward velocity of the Equatorial Undercurrent advected the profiler eastward, away from the ship steaming with 1 kn through the water while drifting southwestward. Thus there was no risk of losing the profiler by cutting the cable with the ship's propeller.

After the MSS test station, the first APEX float was deployed successfully, and the CTD/O_2 section along 35°W was continued. Water samples were taken at every other station for the full set of biogeochemical analyses. The stations in between were used instead for the calibration of Microcats to be deployed within the mooring array along 23°W.

On June 10, we received information from Mr. Marcos Fonseca (Windrose Serv. Mar.), the ship's agent in Brazil, that the moored profilers were onboard the 53ft sail boat AUSSTEIGER, arriving at Fernando de Noronha in the morning of June 13. The same day, Mr. Fonseca and two customs officers would take an airplane to Fernando de Noronha to facilitate customs clearance and delivery of the moored profilers to METEOR on June 14 at 08:00L.

On June 11, the CTD/O_2 section along 35°W was completed with the last station at 5°N. At this position a sound source mooring had been deployed during METEOR cruise M62/2, however, from the received RAFOS float data we knew that the sound source did not work from the very

beginning. After approaching the mooring position at 09:20L, the release responded to the signal from the board unit via hydrophone, and about 10 min after sending the release command, the top element was observed at the sea surface. Recovery went smoothly and was completed at 10:00L. Following the mooring recovery another MSS test station was taken. Due to weak winds and currents, there was no problem in obtaining almost constant sink velocities of 0.6 or 0.7 m/s down to 350m depending on the number of ballasting rings attached to the profiler. The last activity at the 35°W section was a CTD/O_2 test station. During the previous CTD/O_2 casts we observed too strong a tilt of the ADCPs attached to the CTD rosette. We changed the ballast at the CTD rosette, which significantly improved the tilt with smaller pitch and roll angles throughout the CTD test cast. At 13:00L, METEOR began an ADCP section from 35°W, 5°N to 32°30'W, 2°30'N and further to 32°30'W, 3°50'S, the location of the island of Fernando de Noronha. One ARGO float each was deployed at two degrees north and south of the equator, and two CTD stations were carried out to test the performance of our releases to be used for the mooring deployments later during the cruise.

On June 14 at 07:30L we arrived at the island of Fernado de Noronha. After disembarking the Brazilian observer, we contacted the sailboat AUSSTEIGER. They had already arrived one day earlier as did the two customs officer and the ship's agent, Mr. Marcos Fonseca. There were no further complications with customs clearance at the island, and all-in-all we experienced only a minor time delay. All of the shipped equipment was found in good condition, and we felt fortunate to have the profiler available for our two moorings in the central tropical Atlantic. At 11:00L the ship headed toward the position of our next mooring recovery.

On June 15 at 10:00L we arrived at the mooring position. After lowering the hydrophone, we were not able to obtain a clear contact with the single release on the mooring. The release code was submitted nonetheless but without success. It appeared that some noise from the ship interfered with the signal of the hydrophone board unit, and after switching off the Kongsberg EM120 multi-beam echo sounder transmitting at 12kHz, we were able to receive clear signals from the release. The release code was submitted again and we received the message "Release executed". However, the mooring did not come to the surface. Though repeatedly submitting the release code numerous times, nothing happened. As there was no additional time available because of the very tight mooring program, we decided to depart from the mooring position without recovering the sound source mooring. Another ARGO float was deployed at the mooring position, and METEOR headed toward the southern end of the 23°W section beginning at 4°S. Along the cruise track another two ARGO floats were deployed at 27°W and 25°W, respectively.

During the late evening of June 16, the hydrographic section along the 23°W section commenced with a first CTD/O_2 cast at 4°S. Several CTD/O_2 casts and the first set of regular microstructure stations were carried out during the following day. The depth reached by the microstructure profiler strongly depends on the strength of the vertical shear of the horizontal velocity. Near the equator in particular, only very shallow profiles could be obtained because of the very strong Equatorial Undercurrent (EUC) with core velocities above 1m/s at about 70m depth. During the night station on June 17, the acquisition computer of the microstructure profiler did not receive data from the profiler and it soon became evident that the cable was broken. We switched to a different cable, and microstructure measurements commenced after the mooring deployment on June 18.

The deployment of the first mooring of our equatorial array at 23°W began at 1015L with a drift test. The ship headed against the southeasterly winds with a velocity of about 1kn through water. A drift velocity of about 2.5kn to the south resulted due to prevailing wind and currents. After the drift test the bathymetry of the deployment area was surveyed with the multi-beam echo sounder which, during the last METEOR leg, has proven to be a highly accurate instrument. The obtained topographic data showed that the initially chosen mooring position was situated in an almost flat region of about 3680m water depth. The mooring deployment ran very smoothly, and after merely 2h 20min all instruments were in the water. We had to steam an additional hour to reach the anchor drop position. The final mooring position was determined to be at 0°44.95'S, 22°59.60'W. During the night following the mooring deployment, CTD/O_2 and microstructure measurements were continued.

Two mooring operations had been scheduled for the following day, June 19. Recovery of the French mooring located at 0°00.01'N, 23°07.51'W was started early in the morning. This mooring included a PIRATA Workhorse ADCP, an IFM-GEOMAR Longranger ADCP and several Aanderaa current meters (LOCEAN, C. Provost). The release responded accurately, and the first flotation elements surfaced after just a short while. The ship's Zodiac was used to first recover the release and its flotation package, followed by all other instruments in short order. A first inspection of the ADCP records indicated complete data sets, although located shallower than originally planned, with the upward looking ADCP located right in the core of the EUC which resulted in strong mooring motion and vertical excursions of the top elements. The Aanderaa current meter tapes were not scheduled to be read during this cruise but to be sent to LOCEAN, Paris, to be read and analyzed there. Following the successful mooring recovery, we commenced with a multi-beam echo sounder survey and found the former mooring position was located amidst smooth topography. Water depths within half a mile around the chosen mooring position varied only between 3680m and 3690m. The drift test with 1.5kn through water against the southeasterly wind again yielded a southward drift because of the strong westward flowing SEC. The mooring deployment started very smoothly, all instruments including the moored profiler moved from the aftdeck into the water without any problems. At the end of the long 2.5km long wire segment for the moored profiler, the wire shifted from its straight position behind the ship and moved strongly to the port side of the ship. Severe tension was building on the mooring wire, and the captain decided to turn the ship to the port side to reduce tension on the mooring wire. However, the mooring wire shaved against the ships hull, resulting in some scuffs to its plastic jacket. As the mooring was at risk for being lost, the ship had to turn quickly to the starboard side, thereby leaving the drift track toward the planned anchor drop position.

After submerging the releases into the water and after attaching the mooring wire to the anchor still firmly attached to the ship's aft deck, the ship made a wide turn for about 2.5h with about 2kn through water to reach the planned mooring position. The anchor was dropped at the proper and intended position. We believe that this very unusual mooring deployment resulted from the fact that the long mooring line segment of the moored profiler dropped into the depth range of the very strong EUC and was advected eastward. For future applications, one must consider alternative strategies to deploy similar moorings in the equatorial region. The submerging of the mooring top was concluded from the disappearance of the ARGO signal from

the transmitter at the moorings top element. The mooring position was determined as 0°00.0S and 23°06.8'W.

During the following night, we completed two CTD casts, with the second one already at the next mooring position. After the topographic survey of the mooring area in the morning of June 20, we chose a mooring position at a water depth of 4310m, about 110m deeper than suggested by the 2' Sandwell topography. The mooring deployment proceeded without any problems, and the anchor was dropped exactly at the planned position. The final mooring position was determined as 0°45.0'N, 22°59.5'W.

Two more CTD casts were taken during the following night. A drift test at the next mooring position showed rather weak surface currents, contrary to the previous deployments. The survey using the multi-beam echo sounder revealed a depth of about 4950m at the planned mooring position, with a variation of only a few meters nearby. The mooring deployments started right after lunch on June 21. The ship drifted along the planned track, and after about 3h, all instruments had been launched from the aftdeck into the water. METEOR had to steam another 45min to reach the anchor drop position, and the final mooring position was determined as 0°00.0'N, 21°29.6'W. This was the last mooring of our equatorial mooring array aimed at studying the role of the equatorial circulation for tropical Atlantic climate variability in the frame of the BMBF Verbundvorhaben "Nordatlantik".

After the successful installation of the mooring array, the zonal section along the equator commenced with combined microstructure und CTD/O_2 observations at 21°W. The distance between successive stations was chosen as 1° in longitude. We completed this section at 12°W during the night of June 24, and METEOR headed toward the southernmost point of the meridional section along 10°W.

Along the 10°W section, nine CTD casts were taken between 1°30'S and 1°30'N. In between, on June 26 at 11:00L, deployment of the French mooring as part of the PIRATA program was started. Following the drift test and topographic survey, the top element, including the PIRATA Workhorse ADCP, was launched smoothly into the water. At the second 2000m length of the parafil rope, the parafil slipped out of the fitting when leaving the capstan. The loose end was captured just before it went into the water (stopped by hand by the bosun and a crew member). We had to cut off about 30m of the parafil rope that were damaged during the rescue action. The 30m of parafil were replaced by 30m of 1/4'' wire. At 16:00L the anchor was dropped, and the final mooring position was estimated as 0°01.28'N, 09°51.23'W. As we were not completely sure that the other fittings would withstand the launch tension, we steamed in the direction of likely drift of the top elements in case of any broken rope, but no sightings were obtained. Thus, we concluded that the mooring had been successfully deployed.

On June 27 at 17:30L the zonal section along 2°N commenced with the first CTD/O_2 cast at 12°W. It was completed on June 30 at 19:30L with the last cast at 22°W. Along this westward cruise track, CTD stations were spaced apart by about 1° of longitude. METEOR headed toward 23°W, 1°N to continue the 23°W section that was interrupted for the eastern box limited by the section along the equator, 10°W, and 2°N. Near the equator, CTD stations were spaced apart by 20' of latitude, and by 30' of latitude starting at 3°N.

The mooring deployment at 5°N started early in the morning of July 1. This mooring contains one of the moored profilers that were delivered to Fernado de Noronha. Equipped with an oxygen sensor, it is aimed at studying the oxygen supply to the oxygen minimum zones in the eastern Tropical Atlantic. After a drift test and a survey with the multi-beam echo sounder, the top element including a Longranger ADCP was deployed at 06:30L. At about 09:30L the anchor was dropped exactly at the planned position, and submergence of the top element was observed about 20 min later. Following the mooring deployment, the section along 23°W was continued with CTD casts spaced apart by 30' of latitude. On July 7, 13:30L the 23°W section was completed at 15°15'N, only a few miles west of the island of Maio, Cape Verde. At this location, a calibration cast for the fluorometer to be moored north of Cape Verde was taken down to 200m with water samples about every 10m.

Early in the morning of June 8, we arrived at the location of our last mooring. After performing microstructure measurements and a CTD cast down to near bottom, the area was surveyed with the multi-beam echo sounder revealing a flat topography at almost exactly the target depth. The mooring operations ran very smoothly, and the anchor was dropped at the planned location. As we had attached a POSIDONIA release at the top element of the mooring, we were able to exactly track the final position of the mooring. It is: 17°35.39N, 24°15.12W. After tracking the top element, the release was activated and it was recovered together with the two Benthos flotation elements. The scientific work of METEOR cruise M68/2 ended at 16:30L and the ship headed toward Mindelo where the cruise ended on July 9, 09:00L (Fig. 2.1).

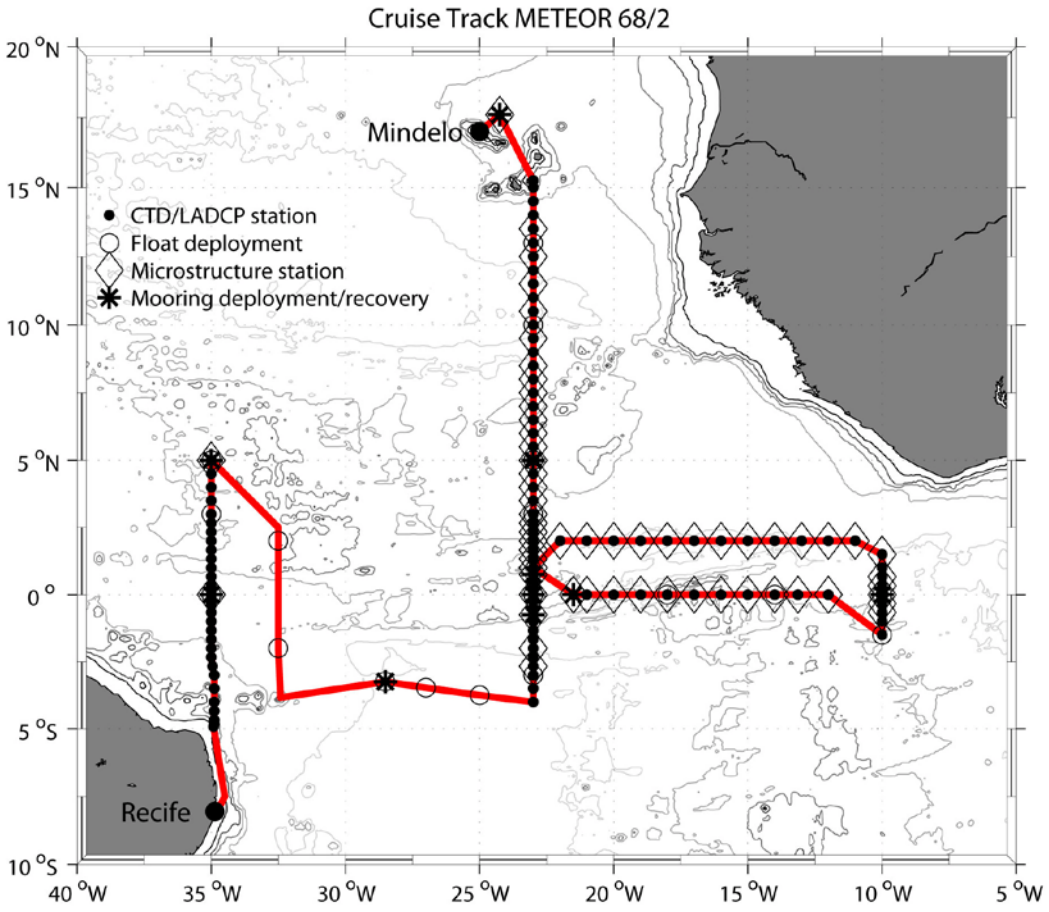

Fig. 2.1 Cruise track of METEOR cruise 68/2

2.4 Preliminary Results

2.4.1 CTD Measurements in the Tropical Atlantic

(L. Stramma, A. Funk, V. Hormann)

2.4.1.1 Calibration and Data Quality of CTD and Oxygen Measurements

In total 115 CTD profiles were sampled during cruise M68/2 (Table 2.8). The CTD-system used during the METEOR cruise 68/2 was a Seabird Electronics Inc. of Bellevue, Washington, USA (SBE) 9 plus. The IFM-GEOMAR Kiel SBE-2 with serial number 09p24785-0612 was used. Connected was a pressure sensor (s/n 80024). Two independent sets of temperature, conductivity and oxygen sensors were used. The sensors of the primary set were a temperature sensor (s/n 2826), a conductivity sensor (s/n 2512) and an oxygen sensor, a Seabird SBE-43 sensor (s/n 0194) recording oxygen voltage but no oxygen temperature, as was the case in the former Beckman oxygen sensors. The secondary set of sensors was a temperature sensor (s/n 4547), a conductivity sensor (s/n 2859) and an oxygen sensor (s/n 0992). Starting from profile 51 also a fluorescence (Chlorophyll a) sensor was attached to the CTD but was not calibrated. A second Seabird CTD, IFM-GEOMAR SBE-4, was available as backup system, but was not used.

Routinely, CTD casts were made from surface to about 1300 m depth. Only stations located at a mooring position and two at the Brazilian shelf reached down to the bottom. Sound speed profiles derived from the deep casts were used as input for precise depth sounding at the mooring locations with the multi-beam echo sounder.

The monitor of the pinger used on earlier METEOR cruises to determine the bottom approach of the CTD was removed from the recording lab at the last stay at the shipyard. The only other monitor for the pinger had a broken power supply and was also not usable. The bottom alarm by a ground weight was not working reliably and on all three profiles of the 35°W section reaching to the bottom the CTD touched the bottom. Therefore, the missing monitor of the pinger is a strong limitation for the deep use of our CTD system. At the beginning the primary sensor system was used. At Profile 3 some unstable density layer appeared in the upper ocean. At Profile 16 the primary temperature and conductivity sensors showed large variability below about 2000 dbar while the secondary sensors stayed stable. Therefore, for processing the data only the sensors of the secondary sensor set were used. The pump of the primary sensor set was exchanged after Profile 16, and also the primary sensors worked well afterwards. Problems appeared at the beginning of the stations, as it took up to several minutes until the pump of the seabird system started. Flashing the sensors with salt water just before the start of the CTD solved this problem.

At Profile 24, the pump turned on but went off again during descent in the upper ocean and the upper 90 m of this profile can not be used. However, the upcast profile could be calibrated to replace the downcast CTD Profile 24. On Profile 45 a deep CTD profile was planned as this profile was close to a mooring which was recovered afterwards. Due to a problem with the winch cable the connection broke down at 1940 dbar, and the CTD cast was aborted.

The setup with two independent sensors was ideal to check the sensor behavior. While the older primary thermometer had a recent IFM-GEOMAR lab calibration, the new secondary thermometer had the original Seabird calibration. After applying the two independent

calibrations to the sensors the temperature readings differed by less than 0.001°C. In addition recordings with electronic reversing pressure meters and reversing thermometers were made during the first part of the cruise to make sure that no jumps or drifts appeared.

The Seabird bottle release unit used with the rosette connected to the Seabird instrument worked properly and reliable except for 2 or 3 times, when one bottle did not close.

For calibration purposes several water samples were taken from the rosette bottles at most stations. Bottle salinities were determined with a Guildline Autosal salinometer (Guildline Instruments Inc, Smith Falls, Canada). A Guildline Autosal salinometer (Kiel AS7) was installed already at the beginning of leg M68/1. During M68/1 no reliable measurements could be made even after the installation of an additional stabilizer for the power supply. During M68/2 the same salinometer worked very well, although nothing was changed. Presently the only explanation is that during M68/1 electric equipment was used by one of the participating groups that disturbed the salinometer.

The CTD values to be calibrated were chosen from the downcast profiles to avoid hysteresis problems. Calibration of the SBE-2 secondary CTD conductivity sensor was carried out for the 115 profiles using a total of 214 dual samples. First some obviously bad values were tagged and removed. In addition, bad or erroneous data were rejected when exceeding 2.8 times the standard deviation of the conductivity difference. This criterion still includes 98% of the calibration data. After correcting the conductivity with respect to temperature, pressure and conductivity itself as well as for a time trend, the rms difference between the bottle and CTD conductivity samples was 0.0022 mS/cm, corresponding to 0.0020 in salinity.

Oxygen from the bottle samples was determined using the Winkler titration method. The calibration of the secondary oxygen sensor was done with a stronger limitation than for conductivity with a 1.8 rms criterion to place more emphasis on the reliable values. The calibration of oxygen was carried out with 569 samples used which met the 1.8 rms criterion. After correcting with respect to pressure and temperature as well as with respect to a time trend and pressure dependence and a relation to the oxygen values themselves and the oxygen value itself, the rms difference was 0.03 ml/l. As only a few stations reached to depth deeper than 1300 m, the oxygen calibration for the deep profiles was slightly less accurate (but better than 0.04 ml/l). With regard to the investigation of the oxygen minimum zones the CTD oxygen data turned out to be a high quality data set.

2.4.1.2 Oxygen Minima Distribution in the Equatorial Atlantic

In the eastern tropical Atlantic, oxygen minimum zones (OMZs) exist in the depth range 200 to 800 m. The OMZs are a consequence of a combination of ocean ventilation, which supplies oxygen, and respiration, which consumes oxygen (e.g. Karstensen et al. 2007). Although the extrema of the oxygen minimum appear in the Guinea and Angola Dome regions at about 10°N and 10°S, the oxygen minimum at intermediate depth is clearly present near the equator. As the equatorial currents transport either oxygen-rich water to the OMZ or export oxygen-poor water from the OMZs, the circulation of the equatorial Atlantic is of large interest for the observed differences in oxygen distribution.

Cruise M68/2 covered a hydrographic box in the central equatorial Atlantic, with an eastward leg along the equator from 23°W to 10°W, and a westward leg at 2°N, closed by meridional sections at 23°W and 10°W. The meridional CTD-oxygen distributions clearly show a connection between equatorial oxygen minima and the off-equatorial OMZs. The oxygen distribution along the equator (Fig. 2.2) shows two well-separated cores of the oxygen minimum at about 260 m and 450 m depth. The cores stretch along the entire section of more than 1000 km, from 10°W to 23°W. The depth of these oxygen minimum cores corresponds well with the mean current field of the westward oriented Equatorial Intermediate Current (EIC) in Fig. 2.2. The current field derived from a mooring deployed at the equator at 23°W since 2004 shows a stable mean of the EIC, with two cores, however with a strong annual signal at these depths (Brandt et al., 2006). These observations highlight the role of the EIC in the oxygen budget of the OMZs arises from.

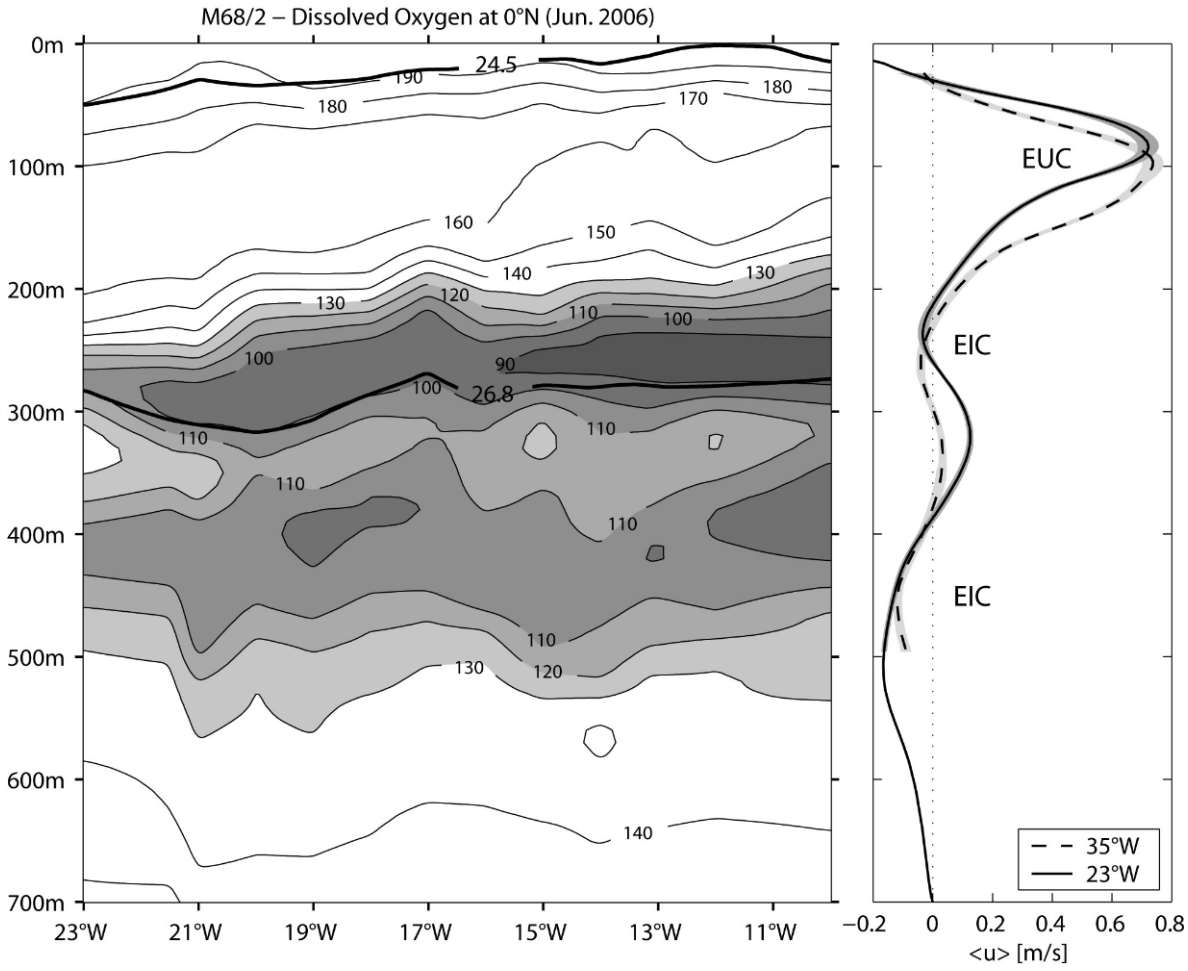

Fig. 2.2 Dissolved oxygen [µmol/kg] along the equator in June 2006. The thick black isolines (left panel) mark potential density surfaces, showing decreasing depth towards the east. The zonal velocity profiles (right panel) at 0°N, 23°W (solid) and 35°W (dashed) with standard error (shaded) were derived from moored instruments for the period March 2004 to February 2005

In detail there are of course deviations from this mean scenario, for example the velocity distribution derived during June 2006 along the equator from the shipboard ADCP showed the EIC at depths of 450 to 600 m, while at 250 m depth eastward as well as westward currents were observed. The annual cycle calculated from 2 years of data shows a minimum strength of the EIC near June, explaining the difference between the velocity field and the oxygen distribution in June 2006. This further indicates that the water mass characteristics represent an integral part of the annual mean, even when the currents weaken or reverse for a short time period.

The EUC is known to shift from larger depth in the west to shallower depth in the eastern Atlantic. The signature of the upward movement is also visible in the oxygen distribution along the equator. The high oxygen water carried with the EUC eastward becomes slowly less oxygenated to the east as well as the vertical extent of the high oxygen water is reduced. A shallow isopycnal marked in Fig. 2.2 shows also well the upward shift toward east.

2.4.2 Current Observation

(T. Fischer, V. Hormann, A. Funk)

2.4.2.1 Ocean Surveyor: Technical Aspects

The cruise saw two vessel-mounted RDI Ocean Surveyor ADCPs in use from June 7th to July 9th. One unit (75 kHz, OS75) is permanently fixed to the ship's hull, the second unit (38 kHz, OS38) was lowered into the well located in mid-ship and fixed hydraulically. Both units worked in narrowband mode, delivering current velocity to depths of up to 750m (OS75) and 1500m (OS38). There were no interferences with the various acoustic devices on board, except the Doppler-Log (78 kHz) drastically reducing the depth range of Ocean Surveyor 75 to about 200 meters. The Doppler-Log's use was confined to the absolutely necessary minimum during mooring activities.

Both ADCP units were controlled by computers using VMDAS software version 1.40 under MS Windows NT. Pinging was as fast as possible (2.4 seconds for OS75; 2.85 seconds for OS38), single pings recorded in partitions of 100 bins @ 8m (OS75) resp. 50 bins @ 32m (OS38). Navigation information available to ADCP units and control computers were:

Heading from FibreOpticGyro (FOG) via synchro interface, binarily recorded with pings;

Position from ASHTECH GPS via synchro interface, binarily recorded with pings;

Position from ASHTECH GPS and heading, pitch and roll from ASHTECH array,

seperately recorded as NMEA textstrings via serial interface.

For best results, ASHTECH heading and position were used to calculate current velocities from ADCP output. As short gaps of 2 to 5 minutes occurred in ASHTECH navigation data about twice or thrice a day, the slightly less accurate FOG heading and TRIMBLE GPS position

(recorded by the ship's DVS-system) were used to fill the gaps. Position data from both GPS-sources are sufficiently accurate to recognize the distance between the antennas as well as the swell-induced antenna movement. During post processing, misalignment angle and amplitude factor for both transducers were obtained from water track calibration when the ship accelerated/decelerated. Standard deviations for misalignment angle were 0.46° (OS75) and 0.37° (OS38), for amplitude factor 0.01 (OS75) and 0.006 (OS38). These values match the data quality of previous cruises.

Beginning about June 17th, current velocities calculated from OS38 data exhibited increasingly steplike deviations without any pattern and not related to navigation, reaching their highest level about June 30th during the 2°N-section. These deviations could not be observed with OS75, and were presumably caused by slight movements of the OS38-transducer by less than 1°. After fixing the transducer to the well once more, the problem seemed to be solved.

2.4.2.2 Current Sections

The Ocean Surveyor data were mapped on a regular grid, using a Gaussian weighted interpolation scheme, and a best estimate of the currents at 35°W, 32.5°W, 23°W, 10°W, 0°N and 2°N was obtained. The flow across these meridional and zonal sections is described briefly.

a) Meridional Sections

The 35°W section runs from 5°S to 5°N and shows clearly the banded structure of the near-surface zonal flow (Fig. 2.3). The EUC is centered at the equator, with its core at about 80 m depth and a velocity of about 100 cm/s. Below the EUC, there is an indication for the westward EIC. The South Equatorial Undercurrent (SEUC) is found between about 4.5°S and 3°S, with its core at about 200 m depth, and the North Equatorial Undercurrent (NEUC) is present at the northern boundary of the section. In the intermediate depth range, both the Southern and Northern Intermediate Countercurrents (SICC and NICC) are observed between about 1.5° and 3° S and N, respectively. The North Brazil Undercurrent (NBUC), here directed north-westward, shows up near the coast.

Due to time constraints, the first part of the 23°W section, running to 1°N, was limited to 4°S and the SEUC, which seems to have turned more southward compared to 35°W, was missed almost completely. After finishing the eastern equatorial box, the 23°W section was continued up to about 15°N 15’ (Fig. 2.4). Both equatorial currents, the EUC and EIC, are still well developed at 23°W and there are clear indications for the SICC and NICC as well. To the north of about 3°N, two bands of the North Equatorial Countercurrent (NECC) are observed. While the first band extends up to about 7°N, the core of the second one is located at about 8°N.

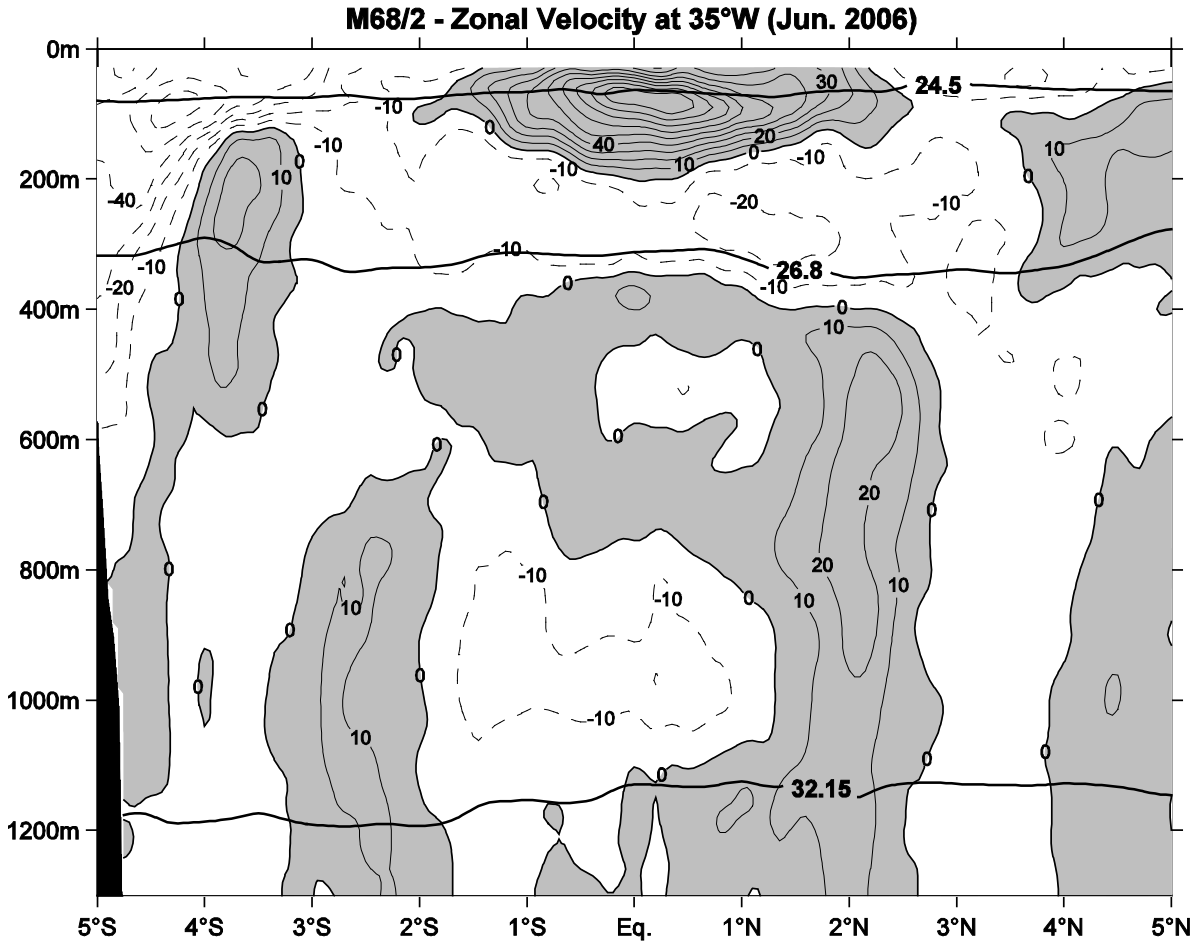

Fig. 2.3 Zonal velocity [cm/s] at 35°W from Ocean Surveyor; eastward currents in grey. Marked are isopycnals σ_θ = 24.5, σ_θ = 26.8 and σ_1 =32.15 [kg/m³] (thick solid lines)

b) Zonal Sections

The meridional sections at 23°W and 10°W show the EUC core shifted to the south of the equator, but nevertheless strong eastward velocities dominate the depth range of the EUC (upper 200 m; Fig. 2.5, upper panel). Underneath the EUC, a band of weak eastward velocities is observed down to about 400 m depth, but there are also indications for westward velocities at about 250 m depth. The prevailing westward velocities between about 400 and 700 m are attributable to the EIC. However, Brandt et al. (2006) showed the existence of two mean westward cores of the EIC below the EUC at 23°W, with a strong annual signal superimposed at these intermediate depths. Near June, the annual cycle reveals a minimum strength of the EIC, explaining the nearly missing upper core of this current at 0°N during June 2006. The alternating eastward and westward current bands below 400m are characterized by small vertical wavelengths typical for equatorial deep jets. These jets show a large zonal coherence along the equator.

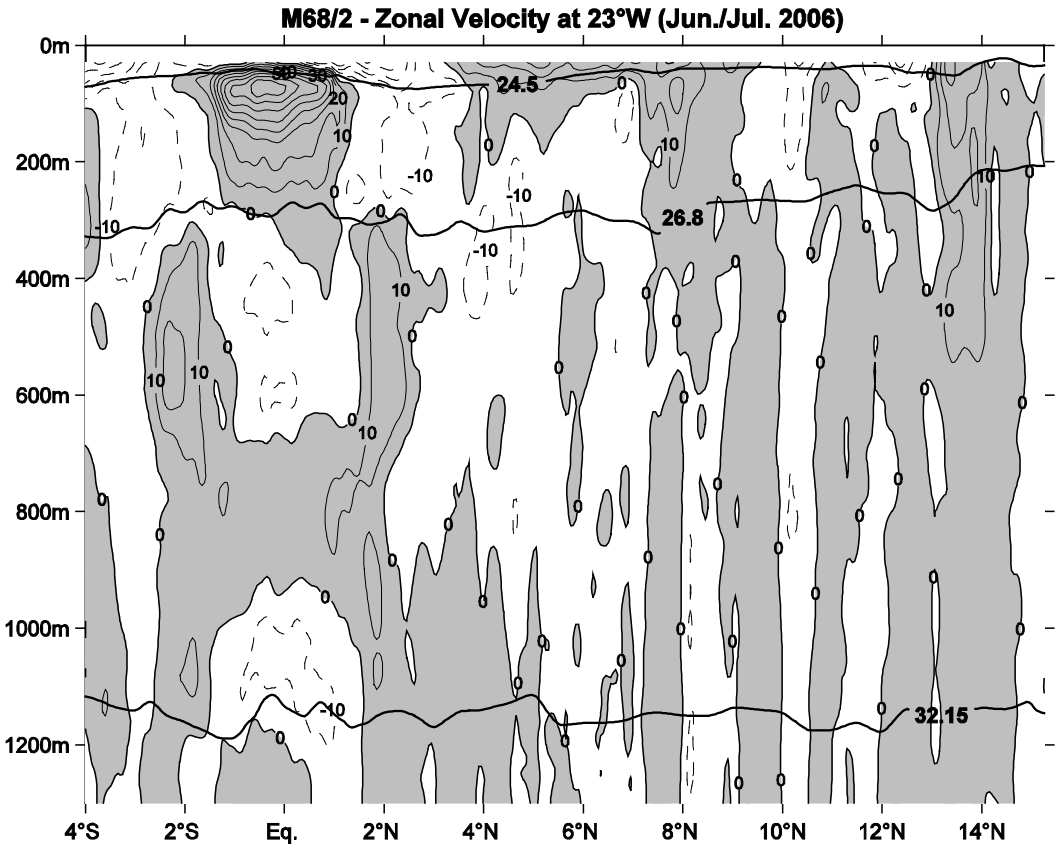

Fig. 2.4 Zonal velocity [cm/s] at 23°W from Ocean Surveyor; eastward currents in grey. Marked are isopycnals σ_θ = 24.5, σ_θ = 26.8 and σ_1 =32.15 [kg/m³] (thick solid lines)

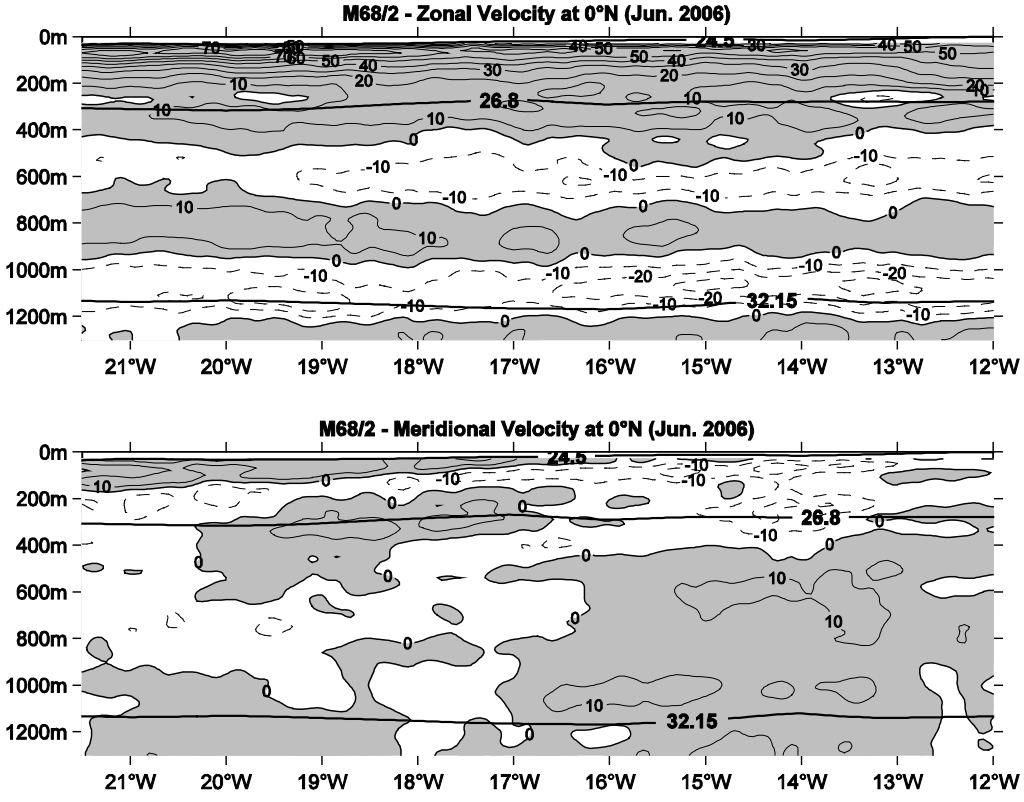

Fig. 2.5 Zonal (upper panel) and meridional (lower panel) velocity [cm/s] at 0°N from Ocean Surveyor; eastward and northward currents in grey. Marked are isopycnals σ_θ = 24.5, σ_θ = 26.8 and σ_1 =32.15 [kg/m³] (thick solid lines)

2.4.2.3 Lowered ADCPs

(J. Schafstall, J. Fischer)

Different from the usual LADCP work the focus during M68/2 was to evaluate whether high frequency ADCPs may be used for turbulent mixing studies. For this purpose a 1200 kHz Workhorse ADCP was attached to the CTD-Rosette working in a downward looking mode. The first trials were with different vertical resolution and with beam velocities.

The first result was that the velocity variances increased in relation to the vertical resolution; short 25cm bins with high variance, and long 100cm bins with significantly lower variance. This is due to longer pulses and higher accuracy of individual pings at large depth cells.

After this first test we decided to use 50cm cells and 0.5s intervals as a compromise between range (larger at large depth cells) and storage required. This setting was used throughout the rest of the cruise at every CTD station except 3, where we used the classic LADCP procedure (2 * 300kHz ADCPs) and instrument tracking with METEOR'S Posidonia. This should enable a comparison of the LADCP estimate of Rosette motion with its measured path.

Inspection of the profiles revealed large tilt angles and consequently we tried to reduce these by appropriate ballasting. However, we got the impression that beside symmetrical ballasting total weight is also important (could not be tested). Remaining tilts were still relatively large (up to 10°).

First data inspection was performed by comparing down- and up-casts with the expectation that the up-cast should show much higher variance, as the ADCP measures within the turbulence field generated by the CTD package. In fact this was observed.

Treating the 4 beams as individual measurements of the turbulent flow field, we performed a statistical analysis of the variance in depth coordinates for comparison with the microstructure measurements. Vertical resolution was 5m depth cells. We inspected many profiles and found no reliable variance enhancement where one would expect these (e.g. in the shear layers of the EUC). There should be some additional analysis with focus on the turbulent layers detected in the microstructure data.

On three stations we tried to track the underwater package by Posidonia. Although undisturbed tracking was not possible, we think it might be feasible to extract valuable data. Remember, the LADCP processing aims at separating ocean currents from package motion in an inverse routine. Inclusion of a first guess of the latter could help to improve the inversion. This might be a step forward in LADCP processing.

2.4.3 Mooring Operations

(R. Zantopp, J. Fischer)

2.4.3.1 Recoveries

Mooring work during M68/2 consisted of the recovery of 4 moorings, and the deployment of seven moorings (Table 2.1). The mooring work began in the morning of June 9 with the recovery of mooring KR4 located just north of the equator at 35°W.

This mooring contained a RAFOS sound source and several current meters, ADCPs and Microcats to study the variability of the equatorial current system (EUC and EIC). After arrival at the mooring position, KR4 was released after successful acoustic ranging. The new digital MORS deck unit worked well, but is extremely uncomfortable to use. All instruments came aboard in good shape, and all instruments contained full records.

During the morning of June 11 we recovered the sound source at 5°N, 35°W, which had not worked due to some unknown failure. Mooring work was rather routine and uncomplicated.

Several days later on June 15, we had scheduled the recovery of mooring KR2. At the mooring site the response from the Mors release unit was interfered with by another sound source (METEOR's multi-beam echo sounder), but after this was switched off we received a clear response from the single release in that mooring. However, after many release commands with a "receipt and execute" from the release we found the release still locked at its depth. We concluded that the release might be tangled in a wire loop preventing its ascent to the surface. As time did not permit any dredging operation we stopped the procedure and headed to the next CTD station. Hopefully, there will be another opportunity to recover this mooring.

Table 2.1 Mooring and Instrument Recovery during METEOR Cruise 68/2

Mooring KR4				**Notes**
Latitude	0	5.76	N	Combined current meter and sound source
Longitude	35	1.19	W	mooring north of 35W PIRATA mooring.
Water depth	4540			
Mag. Var.	-19.5			100% data recovery!
Deployment	8/13/2004	15:10		
Recovery	6/9/2006	13:10		
Item	Depth	Instr.	s/n	
KR4_01	146	Mini TD	41	good data
	146	RDI-SC	267	
KR4_02		150		good data
KR4_03	149	MicroCat	2249	good data
	151	RDI-SC	393	
KR4_04		150		good data
KR4_05	294	MicroCat	2251	good data
KR4_06	499	Argonaut	D294	good data
KR4_07	650	Mini TD	42	good data
KR4_08	652	Argonaut	D299	good data
	750	RAFOS	22	
KR4_09	809	Argonaut	D304	good data
KR4_10	962	MicroCat	3144	good data
KR4_11	1107	Argonaut	D329	good data

Table 2.1 Mooring and Instrument Recovery during METEOR Cruise 68/2 (continued)

Mooring KR3				**Notes**
Latitude	5	0.00	N	Sound source mooring
Longitude	35	0.00	W	
Water depth	3753			
Mag. Var.	-19			
Deployment	8/11/2004	16:58		
Recovery	6/11/2006	13:20		
Item	Depth	Instr.	s/n	
	804	RAFOS	23	did not work

Mooring KR2				**Notes**
Latitude	3	14.03	S	Sound source mooring
Longitude	28	31.42	W	
Water depth	5100			
Mag. Var.	-19			
Deployment	5/17/2003	19:02		
Recovery	6/11/2006	13:20		Recovery failed
Item	Depth	Instr.	s/n	
	795	RAFOS	13	

French Mooring 23W Equ.				**Notes**
Latitude	0	0.01	S	
Longitude	23	7.51	W	
Water depth	3930			
Mag. Var.	-19.5			
Deployment	5/29/2005	16:55		
Recovery	6/19/2006	8:09		
Item	Depth	Instr.	s/n	
	49	ADCP	509	
F2_01		WH 300		
F2_02	60	Mini TD	68	good data
	60	ADCP	2290	
F2_03		LR 75		good data
F2_04	605	RCM-4	5486	data not read
F2_05	755	RCM-4	4445	data not read
F2_06	905	RCM-4	4587	data not read
F2_07	1055	RCM-4	5891	data not read
F2_08	1205	RCM-4	4588	data not read
F2_09	1355	RCM-4	5897	data not read
F2_10	1505	RCM-4	5899	data not read

2.4.3.2 Deployments

All deployments had a deep CTD cast (for obtaining a precise estimate of the sound speed profile), followed by a bathymetric survey with METEOR's multi-beam echo sounder and a mooring deployment simulation (drift test).

Deployments began with mooring AO_03 during the afternoon of June 18 after a deployment simulation (drift test) and a detailed survey of the topography. We found a well suited area of flat bottom and determined the target location. Mooring work was planned for 3 hours at a deployment speed of about 2.5 kn SOG while METEOR headed against south-easterly winds. Currents appeared to be mainly southwest, and the resulting deployment track was to the south. The actual deployment took a little less than three hours, and we had to tow the mooring to the anchor drop position.

Mooring AO_01, on June 19, was the second and most densely equipped mooring (2 ADCPs, McLane Profiler, current meters and Microcats). During the deployment, which began similar to the previous deployment, some unexpected difficulties arose from a combination of the mooring design and the current field. Apparently the 2500m long wire segment along which the profiler should move, hung down so deep that it was pulled sideways by the EUC. The wire on the stern of the ship moved sharply to the port side and was in danger of being cut by the microstructure winch. It took some time and extreme maneuvering to straighten out the wire behind the ship. However, after a rather long towing operation, we were able to drop the anchor almost as planned. Submergence was determined from the cessation of the ARGOS watchdog data stream.

AO_02 is the second (northern) off-equatorial mooring and was deployed at 0° 45.00'N, 22° 59.50'W on June 20. The deployment followed the usual drift test and a detailed bathymetric survey. The whole deployment procedure took 4.7 h, including an observation of the top element submerging. AO_04 was the second (eastern) equatorial mooring deployed on June 21 at 0° 00.00'N, 21° 29.60'W. The anchor drop position was as planned, and the top element was observed as it went under.

Mooring FR_10W was deployed for our French colleagues in the PIRATA framework. It contained only one WH-ADCP and a MORS rotor current meter. However, during deployment we experienced some accidental shortcomings. Firstly, the ARGOS beacon was apparently not transmitting (either defect, or batteries not connected). Secondly, one wire shot of 25m was put into wrong place (not affecting instrument depth). However, a dramatic event occurred at the last Kevlar termination when the wire separated from the termination, and the deck crew just managed to secure the end before it went into the sea. We had to cut 30m of Kevlar and made a new termination which was tension tested prior to deployment. To compensate for the 30m end we put in a 30m ¼'' wire shot. However, there was some anxiety when the anchor was dropped. We were not able to observe the descent of the mooring top after the anchor drop, and we surveyed the area along the likely surface drift. Nothing was detected and we concluded that the mooring was deployed successfully. An attempt to talk to the release was also non-conclusive, as we received only two acoustic signals within the correct range.

Mooring AO_05 was deployed in the early morning of July 03, 2006. The deployment proceeded extremely well, and after three hours the anchor was dropped as planned (see Table 2.2). We were able to observe the descent of the top element from near by, with the radio signal ceasing at that moment.

Cape Verde Mooring V440 was deployed on the last day of the scientific work during M68/2. Topographic survey and deployment simulation were as during the other deployments. We began to deploy the mooring at 10:00L (11:00 UTC), and the duration was scheduled for 4.5 hours.

Already after 3.5h of very smooth operation the anchor was on stand-by, but we had to tow quite a while before anchor drop 17° 35.66'N, 24° 14.98'W at 15:56 UTC. On top of the mooring we mounted a Mors Release with transponder mode for tracking the mooring with METEOR's Posidonia system. Final depth of mooring top was 30 m (designed for 40 m), and its final position was 17° 35.39'N, 24° 15.12'W. After tracking the mooring we released the monitoring element and recovered it a few minutes later. At about 17:30 UTC mooring work was completed.

Table 2.2 Deployment Tables

Mooring Deployment Equatorial Atlantic AO_01					**Notes:**		
Vessel:	METEOR						
Deployed:	19-Jun	2006	19:53				
Vessel:							
Recovered:							
Latitude:	0	0.001	S				
Longitude:	23	6.800	W				
Water depth:	3931	Mag Var:	-16.3				
ID	**Depth**	**Instr. type**	**s/n**	**Startup log**			
		Argos WD	11278				
		ADCP WH					
	126	up	508	**x**			
	126	Mini-TD	24				
	130	Microcat	52	**x**			
	234	Microcat	55	**x**			
	399	Microcat	278	**x**			
	621	ADCP LR up	2395	**x**			
	687	RCM-8	9930	**x**			
	842	Argonaut	D182	**x**			
	998	RCM-8	9964	**x**			
		M-CTD					
	2264	MMP	120	**x**			
	3573	Release	174	Code:	9337	**9339**	**A**
	3573	Release	110	Code:	E972	**E974**	**A**
					Interrogate	Release	Mode

Mooring Deployment Equatorial Atlantic AO_02				**Notes:**
Vessel:	METEOR			
Deployed:	20-Jun	2006	15:25	
Vessel:				
Recovered:				
Latitude:	0	45.000	N	
Longitude:	22	59.500	W	
Water depth:	4310	Mag Var:	-16.0	

Table 2.2 Deployment Tables (continued)

ID	Depth	Instr. type	s/n	Startup log			
		Argos WD	15172				
	51	Mini-TD	24				
	87	Microcat	381	**x**			
	138	Microcat	780	**x**			
	200	Microcat	921	**x**			
		ADCP 150					
	301	up	589	**x**			
	301	Mini-TD	11				
	397	RCM-8	9346	**x**			
	552	RCM-8	9932	**x**			
	697	RCM-8	5881	**x**			
	851	Argonaut	D143	**x**			
	1007	RCM-8	8412	**x**			
	3632	Release	188	Code:	8181	**8182**	**B**
	3632	Release	189	Code:	8183	**8184**	**B**
					Interrogate	Release	Mode

Mooring Deployment Equatorial Atlantic AO_03 **Notes:**

Vessel:	METEOR		
Deployed:	18-Jun	2006	18:21
Vessel:			
Recovered:			
Latitude:	0	44.950	S
Longitude:	22	59.710	W
Water depth:	3700	Mag Var:	-16.5

ID	Depth	Instr. type	s/n	Startup log			
		Argos WD	15173				
	47	Mini-TD	22				
	83	Microcat	922	**x**			
	144	Microcat	925	**x**			
	205	Microcat	936	**x**			
		ADCP 150					
	307	up	267	**x**			
	307	Mini-TD	27				
	403	RCM-8	9816	**x**			
	558	RCM-8	9349	**x**			
	702	RCM-8	9819	**x**			
	857	Argonaut	D145	**x**			
	1013	RCM-8	9820	**x**			
	3132	Release	190	Code:	8185	**8186**	**B**
	3132	Release	220	Code:	9151	**9152**	**B**
					Interrogate	Release	Mode

Table 2.2 Deployment Tables (continued)

Mooring Deployment Equatorial Atlantic AO_04					**Notes:**		
Vessel:	METEOR						
Deployed:	21-Jun	2006	18:00				
Vessel:							
Recovered:							
Latitude:	0	0.000	S				
Longitude:	21	29.600	W				
Water depth:	4950	Mag Var:	-15.8				
ID	**Depth**	**Instr. type**	**s/n**	**Startup log**			
		Argos WD	2254				
	48	Mini-TD	73				
	81	Microcat	1281	**x**			
	142	Microcat	1282	**x**			
	204	Microcat	1583	**x**			
	455	ADCP LR up	2627	**x**			
	455	Mini-TD	61				
	459	Microcat	1599	**x**			
	553	RCM-8	10501	**x**			
	708	RCM-8	11621	**x**			
	852	RCM-8	9818	**x**			
	1007	Argonaut	D184	**x**			
	4291	Release	428	Code:	2457	**2459**	**B**
	4291	Release	635	Code:	3A95	**3A96**	**A**
					Interrogate	Release	Mode

Mooring Deployment Equatorial Atlantic AO_05					**Notes:**		
Vessel:	METEOR						
Deployed:	3-Jul	2006	11:36				
Vessel:							
Recovered:							
Latitude:	5	0.900	N				
Longitude:	23	0.000	W				
Water depth:	4210	Mag Var:	-14.5				
ID	**Depth**	**Instr. type**	**s/n**	**Startup log**			
		Argos WD	5461				
	57	ADCP LR dn	3173	**x**			
	57	Mini-TD	62				
	103	Microcat M-CTD	1682	**x**			
	616	MMP	11617	**x**			
	1044	Microcat	2478	**x**			
	1045	RCM-8	10779	**x**			
	3513	Release	441	Code:	8A03	**8A04**	**B**
	3513	Release	633	Code:	3A91	**3A92**	**A**
					Interrogate	Release	Mode

Table 2.2 Deployment Tables (continued)

Mooring Deployment Equatorial Atlantic FR_10W					**Notes:**
Vessel:	METEOR				
Deployed:	26-Jun	2006	1:57		
Vessel:					
Recovered:					
Latitude:	0	1.280	S		
Longitude:	9	51.230	W		
Water depth:	5205	Mag Var:	-10.2		
ID	**Depth**	**Instr. type**	**s/n**	**Startup log**	
		Argos WD	66366		
	140	ADCP WH up	509	**x**	
	200	Mors MC3X0	129/92	**x**	
	5150	Release	113		

Mooring Deployment Cape Verde V440-01					**Notes:**
Vessel:	METEOR				
Deployed:	8-Jul	2006	15:56		
Vessel:					
Recovered:					
Latitude:	17	35.390	N		
Longitude:	24	15.120	W		
Water depth:	3601	Mag Var:	-11.2		
ID	**Depth**	**Instr. type**	**s/n**	**Startup log**	
		Argos WD	5510		
	40	Microcat	3753		
	40	Fluorometer	269		
	62	Microcat	3752		
	81	Microcat	1162		
	103	ADCP WH up	1522	**x**	
	103	Microcat	3755		
	127	RCM-11	325	**x**	
	127	Optode	349		
	129	Microcat	2252		
	200	RCM-8	10810	**x**	
	202	Microcat	2255		
	302	Microcat	3754		
	400	Microcat	2256		
	500	Microcat	2254		
	602	RCM-8	11622	**x**	
	603	Microcat	3415		
	753	Microcat	2257		
	899	Watchdog	2265		

Table 2.2 Deployment Tables (continued)

	899	Watchdog	11307				
	900	RCM-8	11265	**x**			
	902	Microcat	2279				
		Sediment					
	999	Trap	97150				
	1002	Microcat	3757				
	1151	Microcat	1550				
	1299	RCM-8	11267	**x**			
	1301	Microcat	1269				
	1498	Microcat	2717				
	1749	Mini-TD	63				
	2001	RCM-8	10818	**x**			
	2003	Microcat	1268				
	2249	Mini-TD	64				
	2500	Microcat	2933				
	2748	Mini-TD	65				
	3003	RCM-8	10776	**x**			
	3005	Microcat	2617				
	3250	Mini-TD	72				
	3511	Microcat	2618				
	3563	Microcat	2472				
	3565	Release	108	Code:	E962	**E964**	**A**
	3565	Release	821	Code:	4AA7	**4AA8**	**A**
					Interrogate	Release	Mode

Microcat / CTD calibration:

Six sets of calibrations were performed for Microcats in order to check their factory settings. The instruments were set to a faster sampling rate (10 sec vs. the normal 15 or 30 min) and mounted on the CTD rosette which was lowered to the ocean bottom during a regular CTD cast. Five to six stops of 4 minutes each (2 minutes during first two stations) were made during the upcast to allow for a stabilized equilibrium. A linear fit was performed for temperature, conductivity and pressure data (where available) from the Microcat and CTD instruments, and resulting rms differences are indicated (see Table 2.3). Some Microcats were equipped with pressure sensors. Three instruments (s/n 2249, 2251, 3144) were done post deployment, all others were done in preparation prior to deployment.

Table 2.3 Results of linear fits

CTD	S/N	Temperature			Conductivity			Pressure		
No.		Bias	Slope	RMS	Bias	Slope	RMS	Bias	Slope	RMS
24	52	-0.0004	0.9993	0.0083	0.0939	0.9972	0.0169			
24	55	-0.0048	1.0001	0.0075	0.0838	0.9976	0.0142			
24	925	-0.0044	0.9998	0.0086	0.1485	0.9946	0.0316			
24	936	-0.0025	0.9996	0.0080	0.1789	0.9937	0.0265			
24	1583	0.0004	0.9991	0.0113	0.0527	0.9980	0.0164			
24	1599	-0.0023	0.9995	0.0102	0.0496	0.9985	0.0142			
24	1682	0.0009	0.9988	0.0124	0.0723	0.9978	0.0193			
24	2478	0.0016	0.9992	0.0118	0.0594	0.9982	0.0176			
24	2614	0.0039	0.9988	0.0137	0.0828	0.9976	0.0215			
26	278	-0.0053	0.9997	0.0062	0.0626	0.9972	0.0415			
26	381	0.0046	0.9998	0.0054	0.0095	0.9981	0.0463			
26	780	-0.0054	1.0004	0.0051	0.1164	0.9951	0.0388			
26	921	-0.0031	0.9998	0.0042	0.0392	0.9979	0.0311			
26	922	-0.0065	1.0003	0.0054	0.0494	0.9971	0.0393			
26	1281	-0.0009	0.9994	0.0040	0.0775	0.9963	0.0361			
26	1282	-0.0065	1.0004	0.0053	0.0142	0.9984	0.0368			
26	2249	0.0015	0.9994	0.0034	0.0332	0.9981	0.0110			
26	2251	-0.0039	1.0000	0.0048	-0.0199	1.0000	0.0175			
26	3144	-0.0008	0.9996	0.0039	0.0426	0.9984	0.0128			
53	3754	-0.0010	0.9998	0.0043	-0.0110	1.0000	0.0041	0.4081	0.9992	1.4083
53	3757	-0.0004	0.9997	0.0037	0.0018	0.9995	0.0039	-0.6978	1.0017	1.1569
73	2252	0.0030	0.9992	0.0080	-0.0596	1.0014	0.0197			
73	2255	0.0019	0.9994	0.0076	-0.0639	1.0015	0.0237			
73	3752	0.0029	0.9991	0.0086	-0.0801	1.0019	0.0255	1.5894	0.9999	0.4151
73	3753	0.0042	0.9991	0.0099	-0.0750	1.0018	0.0237	1.7997	0.9996	0.3944
73	3755	0.0034	0.9993	0.0077	-0.0784	0.1002	0.0240	0.5217	0.9976	0.4270
74	1162	0.0091	0.9970	0.0143	0.0599	0.9977	0.0137			
74	2254	0.0086	0.9971	0.0150	0.0804	0.9971	0.0141			
74	2256	0.0089	0.9969	0.0158	0.1081	0.9963	0.0140			
74	2257	0.0085	0.9969	0.0151	0.0943	0.9961	0.0140			
74	2279	0.0060	0.9974	0.0151	0.0769	0.9975	0.0136			
74	3415	0.0062	0.9974	0.0148	0.0456	0.9981	0.0134	0.4664	1.0015	0.7170
91	1268	-0.0015	0.9996	0.0021	0.0845	0.9973	0.0039			
91	1269	-0.0006	0.9997	0.0022	0.0579	0.9982	0.0045			
91	1550	0.0004	0.9995	0.0020	0.2055	0.9936	0.0025			
91	2472	0.0033	0.9996	0.0025	0.2140	0.9933	0.0029			
91	2617	0.0019	0.9997	0.0021	0.2176	0.9932	0.0029			
91	2618	0.0038	0.9995	0.0022	0.2250	0.9930	0.0028			
91	2933	0.0009	0.9993	0.0020	0.2242	0.9929	0.0026			
91	2717	0.0008	1.0002	0.0020	-0.0260	1.0004	0.0020	3.7863	1.0006	0.2834

It is evident that some batches (casts 26 and 73 for conductivity in particular) are worse than others. However, no reason was evident for this abnormal result. As no time was available to perform another set of calibrations prior to the instrument deployment during this cruise, we suggest that a careful post-deployment calibration be done after the instruments are retrieved.

Wetlabs Fluorometer

(N. Gülzow, J. Fischer)

A Wetlabs Fluorometer is installed in the top element of mooring V440. This had to be calibrated versus filtered water samples. These were taken during our approach to the Cape Verde Islands on a separate 200m CTD cast (Station 114). We took twelve water samples centered on the subsurface chlorophyll maximum that was determined during the downward cast – this covers the depth range at which the Fluorometer will be located in the mooring. The Fluorometer was attached to the CTD rosette with a clear downward view of its optics. By this procedure we also get a rough calibration of the SBE fluorescence sensor of the CTD.

By relative scaling (Fig. 2.6) a comparable profile structure is evident and it should be possible to get a good pre-deployment calibration. However, temperature is way off and needs calibration too.

ADCP data treatment

ADCP data from both instruments from the equatorial station at 23°W (continued by AO_01) have been combined to a continuous data set with all gaps eliminated by interpolation. This processing is described as follows:

Horizontal velocities from both ADCP's are corrected for their compass deviation (location and time correction by mag_dev.m). Data ensembles with less than 20% good pings are eliminated prior to further processing routines. Then data are projected from bins (distance relative to transducer heads) to depth cells by using the pressure sensor information of the ADCPs and an attached Mini-TD-probe. Vertical resolution is 4m for both ADCPs; this corresponds to the original distribution of 4m for up-looking Workhorse ADCP and an oversampling of the 16m bins of the down-looking LongRanger ADCPs.

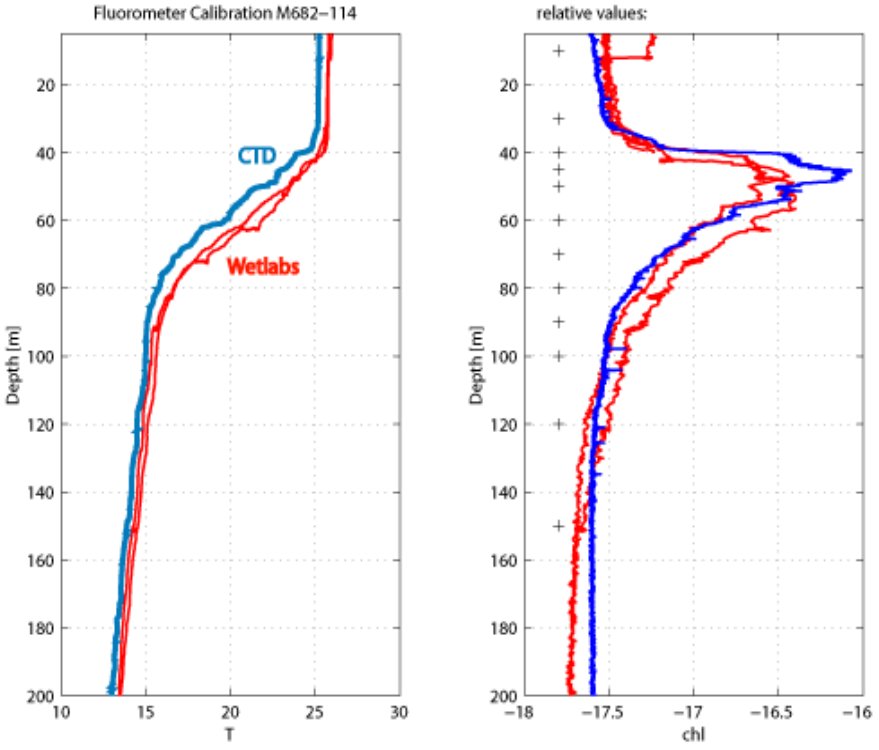

Fig. 2.6
Calibration cast of Wetlabs Fluorometer compared to CTD Station 114. Left: temperature [°C] (sensors close together); right: fluorometer outputs scaled for comparison. Units are relative and need to be calibrated versus filtered water samples. Depths of water samples are marked by plus signs

The data sets are interpolated to an equal time base (necessary due to incorrect times in the Workhorse ADCP), and merged into a combined data set. The combined data set has variable limits due to mooring motion and a gap of some 20m (distance between transducers of 11m plus blanking distance). These gaps were closed by a an advanced Lagrangian interpolation algorithm called **fillmiss.m** available in the Matlab SAGA toolbox. An attempt was made to estimate the accuracy of this procedure by using the end product (interpolated data set as a reference) and introducing a similar gap but with different temporal distribution. This gap was then filled by **fillmiss.m** and the result was compared to the reference. Statistics showed a negligible mean difference (<1cm/s) and a standard deviation of about 3-5cm/s, which appears small relative to the mean speed of the EUC. Another comparison was done with the shipboard ADCP data at times of the mooring recovery. In the next step the gridded data (4m resolution, 1h Intervals) are detided, as there is evidence of substantial tidal flow. Data were low passed at 40h and sub sampled to 12h resolution. Combining the data from the 2004 and 2005 deployments we found the transition from one year to the other suspicious – especially in the meridional component – presumably due to non-perfect compass calibrations of the shallow ADCPs. Several tests were performed with the most stable result from a comparison of the VM-ADCP data and the mooring data. This comparison led to misalignment angles of -6° for the 2004-2005 WH-ADCP and of +6° for the 2005-2006 WH-ADCP. Data from the deeper LongRanger ADCPs seemed to be unaffected (may be masked by the much smaller zonal component), thus no correction was applied to these. – The effect of misalignment is large only when the current speed is large as in the EUC. The effect of this rotation to the mean zonal speed (EUC) is relatively small, of the order of 1cm/s compared to a mean of 70cm/s. WH-ADCP data were corrected accordingly and the whole procedure repeated, yielding the cleaned and sub-sampled final data set suitable for further processing. NB-ADCPs at 35°W also gave the impression of a misalignment angle of -8° compared to OS75 data. However, this appears to be only valid for the relatively short period of the comparison. This leads to unrealistic mean meridional flow structure, and we therefore decided not to rotate the moored ADCP data.

MMP – McLane Moored Profiler

The MMP is a modern observing platform for physical and chemical in-situ measurements over long time intervals. Powered by lithium batteries an electric motor drives a friction wheel for climbing the mooring wire up and down at slow speeds. One million meters is the total range, e.g. 200 profile pairs of 5000m total length (2500m up and down, respectively) can be performed.

During M68/2 we had two of these instruments aboard – we finally got them at Fernando de Noronha – one of them from John Toole (WHOI) and the second one with an additional oxygen sensor (our own). The Toole instrument is used to study equatorial deep jets and is incorporated in our equatorial mooring AO_01 for profiling between 1000m and 3500m on a 4 day profile pair schedule. The position of this mooring is estimated at 0° 00.00’S, 23° 06.80’W. Our own profiler is the core element in mooring AO_05 at 05° 00.90’N, 23° 00.00’W (Fig. 2.7).

The schedule of this instrument calls for paired profiles every 1.6 d. This schedule obtains a full daily cycle every 5 profile pairs or 8 days, and an inertial period of 5.7 days is sampled by 3 to 4 profile pairs. Up- and down profiles follow each other with just a short break in between, and the instrument parks itself in between profile pairs at about 1000m, the lower stop of the profiling range. The LongRanger ADCP serves two purposes, first it will provide an excellent reference for the current measurements of the profiler including tides, and secondly it will give detailed measurements of the NEUC/NECC flow at that location. The Seabird Microcats above and below the profile range as well as the Aanderaa Rotor Current Meter will also be used as references for the CTD and current measurements of the moored profiler.

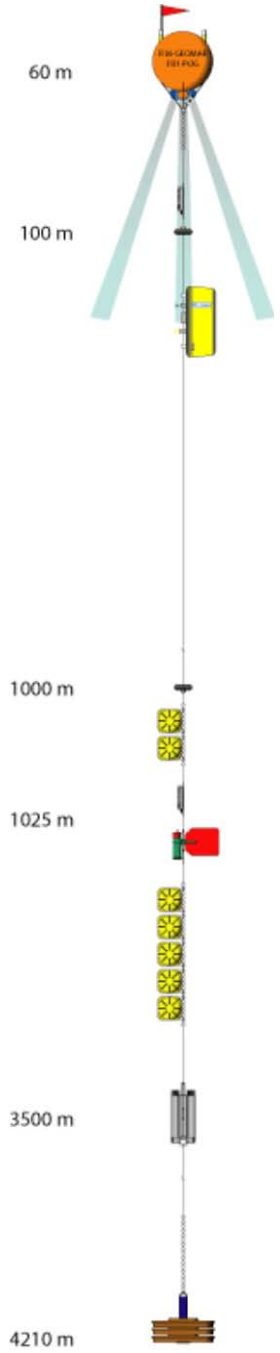

Fig. 2.7
Mooring AO_05 with full instrumentation, MMP, LongRanger ADCP, Aanderaa Rotor Current Meter, and two Seabird Microcats

2.4.3.3 Selected Results

The Equatorial Mooring at 35°W had two ADCPs, one up-, and one downward-looking. Both had full, almost two year long data sets that were processed and merged as described under Section “ADCP data treatment”.

At both locations the flow in zonal direction is dominated by the intense EUC, reaching about 0.7m/s as a deployment long mean (Fig. 2.8). The most obvious time scale of the zonal variability is the annual cycle, which has maximum flow and is nearest to the surface in northern spring. Beside the intensity of the flow, the EUC core shows significant annual depth variability with its deepest expression around September/October. Below the EUC, the EIC has two stable mean cores at both longitudes – here we expect a clue on the existence of a mean EIC and its seasonal cycle.

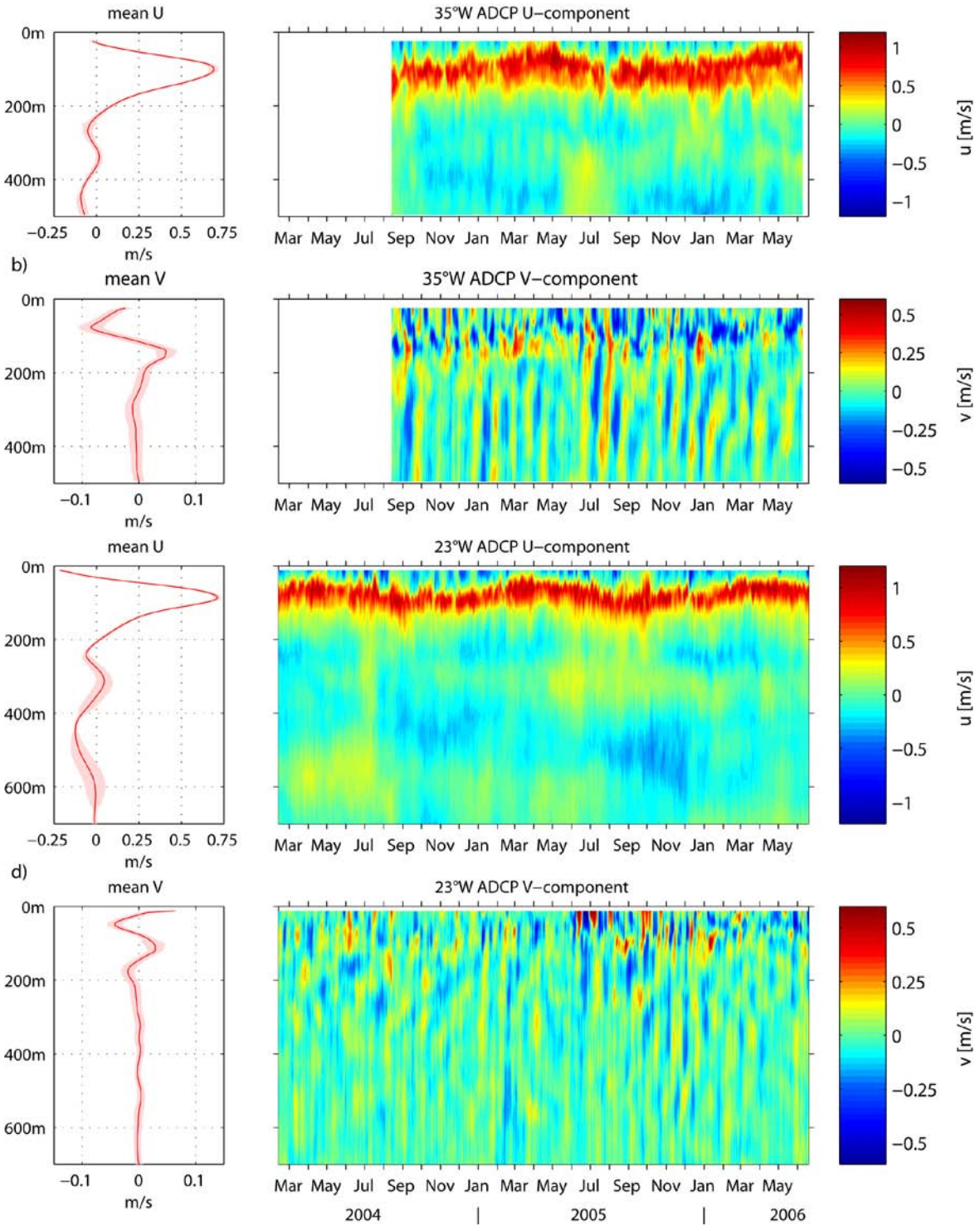

Fig. 2.8 Zonal (a) and meridional (b) velocity at the equator, 35°W from two Narrow-Band 150kHz ADCPs, and zonal (c) and meridional (d) flow at the equator, 23°W from 300kHz WH-ADCP and 75kHz LongRanger ADCP. Data are detided, data gaps in between the instruments were interpolated. The mean flow is calculated by subtracting the annual and semiannual harmonics (solid red line, left panels) with standard error (shaded)

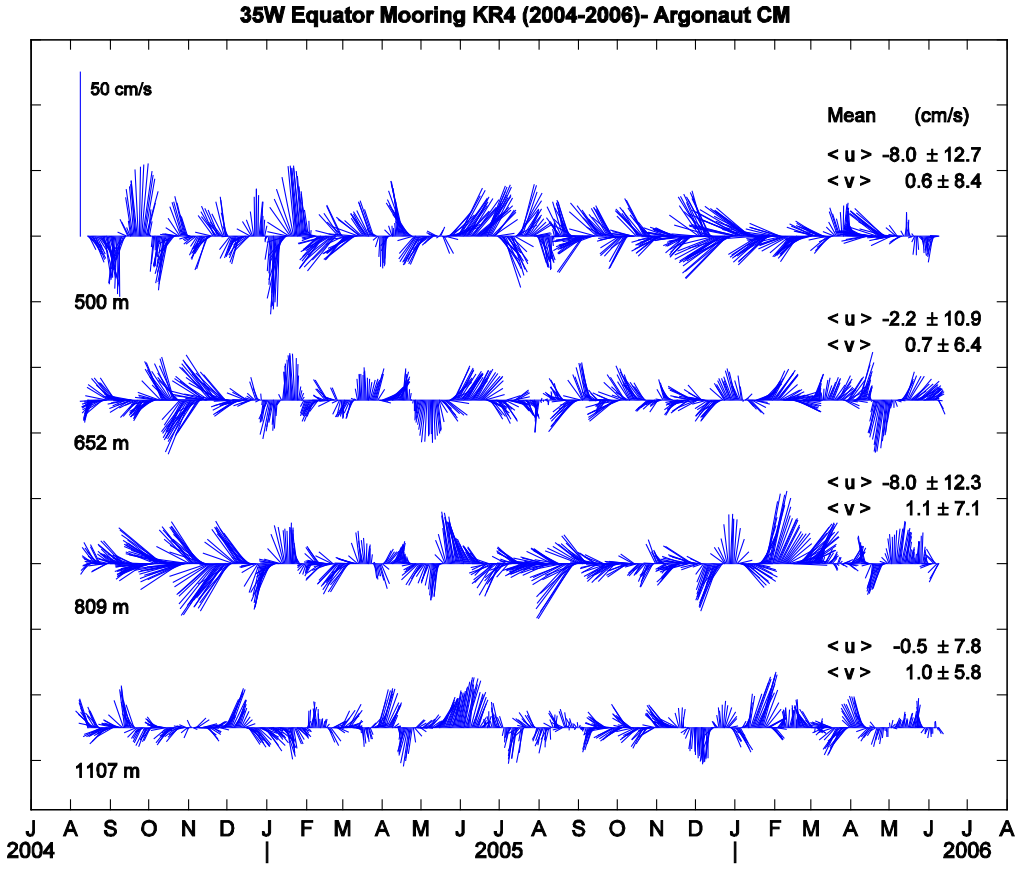

Fig. 2.9 Current vector time series from 4 Argonaut current meters at 35°W. Deployment long means and standard deviations are displayed in graph

The meridional components look totally different and are dominated by high frequency equatorial wave activity. This extends throughout the measurement range (at 35°W these can be clearly seen in the records of the deep (up to 1000m) current meter records (Fig. 2.9). The wave activity also exhibits seasonality (maximum in northern summer) and interannual variability (much stronger in 2005 than in the year before).

In terms of data quality we were able to compare the downward looking ADCP with data from one of the Argonaut current meters. Both instruments show good agreement in the overlapping range. The zonal and meridional components show no significant differences, indication that current amplitudes and direction are of good quality in both instruments. Especially the compasses of the ADCPs have to be treated with great care when performing a quantitative analysis of the meridional flow of the upper layers (see ADCP data treatment).

2.4.4 ARGO Float Deployments

(B. Rabe)

During M68/2 a total of 18 isobaric profiling drifters (floats) were deployed, as shown in Table 2.4. 15 of these of type APEX are part of the sub-project TROPAT within the German ARGO program. These were placed in order to fill gaps in the existing ARGO profiling array and maintain the almost 2700 floats deployed to date, placing floats a minimum of 3° longitude and latitude apart. The APEX are manufactured by Webb Research, Inc. and are all set to profile 2000m, while the drift depth is set to 1500m or 200m. The shallow floats are meant to give further insight into the shallow tropical-subtropical circulation. In addition to sensors for measuring in-situ temperature, salinity (conductivity) and pressure, using a SeaBird CTD sensor, some also carry an Aandera Optode to measure oxygen concentration in the water.

Further floats were deployed on behalf of other research groups: Two 1000m drifting SOLO floats for Woods Hole Oceanographic Institution and one PROVOR for the chemistry group at IFM-GEOMAR. The latter, equipped with a CTD and an oxygen sensor was deployed around 10°N and 23°W, close to a mooring location, and is meant to capture the supply of oxygen-rich water to the oxygen minimum zones closer to the African coast.

Table 2.4 Profiling float deployment positions during M68/2

Float S/N	*WMO*	*ID (DEC)*	*Date*	*Time*	*Longitude*	*Latitude*	*Sensors*	*Depth*	
								Park	*Profile*
2472	1900653	60444	09.06.06	15:56 UTC	35 ° 01.24 ' W	0 ° 03.44 ' N	T/S/P	200	2000
579	WHOI SOLO		10.06.06	20:30 UTC	34 ° 59.38 ' W	3 ° 01.19 ' N	T/S/P	1000	1100
2484	1900650	56452	11.06.06	14:09 UTC	35 ° 00.26 ' W	4 ° 59.24 ' N	T/S/P/O2	200	2000
2477	1900658	60449	12.06.06	17:24 UTC	32 ° 30.03 ' W	1 ° 59.99 ' N	T/S/P	1500	2000
2478	1900659	60450	13.06.06	22:25 UTC	32 ° 29.96 ' W	2 ° 00.06 ' S	T/S/P	1500	2000
2479	1900660	60451	15.06.06	13:22 UTC	28 ° 30.88 ' W	3 ° 14.73 ' S	T/S/P	1500	2000
2473	1900654	60445	15.06.06	22:42 UTC	27 ° 00.15 ' W	3 ° 27.80 ' S	T/S/P	200	2000
599	WHOI SOLO		16.06.06	09:07 UTC	24 ° 59.52 ' W	3 ° 44.53 ' S	T/S/P	1000	1100
2480	1900661	60452	17.06.06	08:20 UTC	22 ° 59.97 ' W	3 ° 00.09 ' S	T/S/P	1500	2000
2485	1900651	56453	19.06.06	11:15 UTC	23 ° 10.94 ' W	0 ° 01.42 ' S	T/S/P/O2	200	2000
2483	1900664	60455	23.06.06	00:18 UTC	18 ° 00.78 ' W	0 ° 00.53 ' S	T/S/P	1500	2000
2481	1900662	60453	24.06.06	11:34 UTC	14 ° 00.52 ' W	0 ° 00.21 ' N	T/S/P	1500	2000
2475	1900656	60447	25.06.06	19:25 UTC	10 ° 00.00 ' W	1 ° 30.00 ' S	T/S/P	200	2000
2482	1900663	60454	26.06.06	22:32 UTC	9 ° 58.57 ' W	0 ° 01.53 ' N	T/S/P	1500	2000
2476	1900657	60448	02.07.06	05:45 UTC	22 ° 59.55 ' W	2 ° 59.38 ' N	T/S/P	1500	2000
2486	1900652	60443	03.07.06	12:05 UTC	22 ° 59.60 ' W	5 ° 02.20 ' N	T/S/P/O2	200	2000
PROVOR	1900120	52551	05.07.06	14:06 UTC	23 ° 00.85 ' W	9 ° 59.09 ' N	T/S/P/O2	500	2000
2474	1900655	60446	06.07.06	16:00 UTC	23 ° 00.49 ' W	13 ° 00.07 ' N	T/S/P	200	2000

2.4.5 Microstructure Mesurements

(U. Koy, J. Schafstall)

In total 202 MSS profiles were sampled during METEOR cruise 68/2 at 60 stations, normally 3 profiles per station (Table 2.5). The microstructure profiling system (MSS) used during the cruise was manufactured by ISW-Messtechnik in collaboration with SEA and Sun Technology (Trappenkamp, Germany) and consists of a profiler, a winch and a data interface. The profiler can operate 16 channels with a very high data transmission rate (1024 Hz) that is sufficient to resolve the small vertical scales of turbulent dissipation in the ocean. It is equipped with two shear sensors (airfoil, 4ms response time), a fast-responding temperature sensor (microthermistor FP07, 12 ms response time), an acceleration sensor, a fast conductivity sensor and typical conductivity, temperature, depths sensors that sample at a lower frequency (24 Hz), in addition we used an oxygen sensor (for details see Table 2.5).

Table 2.5 Microstructure Station overview

MSS Station	METEOR Station	CTD Cast	Date (UTC)	Time (UTC)	Latitude [°N]		Longitude [°W]		Profiles	max. pressure	shear 1	shear 2
Test 1	146	16	6/9/2006	14:57	0	5.04	35	0.59	1-4	175	6052	6054
Test 2	161	30	6/11/2006	13:41	4	59.61	35	0.25	5-8	412	6052	6054
1	173	36	6/17/2006	10:28	-2	40.56	23	0.24	9-11	248	6052	6064
2	175	38	6/17/2006	17:40	-1	59.68	23	0.06	12-14	227	6052	6064
3	177	40	6/18/2006	1:08	-1	20.13	22	59.98	15-17	126	6052	6064
4	178	41	6/18/2006	5:12	-1	0.20	23	0.1	18	10	6052	6064
5	180	42	6/18/2006	18:59	-0	45.40	23	0.15	19-21	58	6052	6064
6	183	45	6/19/2006	2:41	-0	2.40	23	7.5	22-24	66	6052	6064
7	183	45	6/19/2006	5:11	-0	3.17	23	8.92	25-39	76	6052	6064
8	187	48	6/20/2006	7:40	0	45.04	22	59.69	40-42	65	6052	6064
9	189	49	6/20/2006	18:55	1	0.10	23	0.17	43-45	85	6052	6064
10	192	51	6/21/2006	22:06	-0	0.14	21	0.17	46-48	94	6052	6064
11	193	52	6/22/2006	6:28	0	0.09	20	0.07	49-51	202	6052	6064
12	194	53	6/22/2006	14:41	-0	0.00	19	0	52-54	195	6052	6064
13	195	54	6/22/2006	23:25	-0	0.07	17	59.65	55-57	156	6052	6064
14	196	55	6/23/2006	7:58	-0	0.01	17	0.13	58-60	142	6052	6064
15	197	56	6/23/2006	16:30	-0	0.10	16	0.14	61-63	122	6052	6064
16	198	57	6/24/2006	1:08	-0	0.06	14	59.68	64-66	163	6052	6064
17	199	58	6/24/2006	9:25	0	0.01	14	0.01	67-69	223	6052	6064
18	200	59	6/24/2006	18:10	0	7.00	13	7.64	70-72	242	6052	6064
19	201	60	6/25/2006	1:44	-0	0.05	11	59.57	73-75	222	6052	6064
20	204	63	6/25/2006	2:45	-0	0.10	12	0.1	76-78	193	6052	6064
21	205	64	6/26/2006	1:16	-0	39.96	9	59.59	79-81	230	6061	6064
22	206	65	6/26/2006	5:28	0	20.00	10	0	82-84	192	6061	6064
23	207	66	6/27/2006	0:32	0	20.75	9	59.41	85-87	162	6061	6064
24	208	67	6/27/2006	4:37	0	39.87	10	0.36	88-90	153	6061	6064
25	210	69	6/27/2006	12:44	1	30.39	9	59.46	91-93	240	6061	6064
26	211	70	6/27/2006	19:34	2	0.12	11	0.39	94-96	181	6061	6064
27	212	71	6/28/2006	2:06	2	0.40	12	0.1	97-99	177	6061	6064
28	213	72	6/28/2006	8:48	1	59.82	13	0.98	100-102	251	6061	6064
29	214	73	6/28/2006	15:33	1	59.90	14	0.1	103-105	214	6061	6064

Table 2.5 Microstructure Station overview (continued)

MSS Station	METEOR Station	CTD Cast	Date (UTC)	Time (UTC)	Latitude [°N]		Longitude [°W]		Profiles	max. pressure	shear 1	shear 2
30	215	74	6/28/2006	22:22	2	0.13	14	59.74	106-108	216	6061	6064
31	216	75	6/28/2006	5:12	1	59.90	16	0.1	109-111	216	6054	6064
32	217	76	6/29/2006	11:33	2	0.50	16	59.16	112-114	181	6054	6064
33	218	77	6/29/2006	17:47	1	59.90	18	0.2	115-117	162	6054	6064
34	219	78	6/30/2006	0:00	2	0.53	18	58.81	118-120	197	6054	6064
35	220	79	6/30/2006	6:25	2	0.09	20	0.27	121-124	103	6054	6064
36	221	80	6/30/2006	12:53	1	59.92	20	59.67	125-127	273	6054	6064
37	222	81	6/30/2006	19:38	2	0.05	21	59.71	128-130	248	6054	6064
38	223	82	7/1/2006	4:37	0	59.70	23	0.3	131-133	154	6054	6064
39	224	83	7/1/2006	8:35	1	19.98	23	0.1	134-136	243	6054	6064
40	225	84	7/1/2006	12:30	1	39.86	22	59.64	137-139	211	6054	6064
41	226	85	7/1/2006	16:13	1	59.80	23	0.1	140-142	260	6054	6064
42	227	86	7/1/2006	20:12	2	19.93	23	0.04	143-145	280	6054	6064
43	228	87	7/2/2006	0:00	2	39.78	22	59.91	146-148	225	6054	6064
44	229	88	7/2/2006	3:50	2	59.90	22	59.9	149-151	224	6054	6064
45	230	89	7/2/2006	8:24	3	30.01	23	0.05	152-154	283	6054	6064
46	231	90	7/2/2006	12:50	3	57.73	22	59.78	155-157	278	6054	6064
47	232	91	7/2/2006	21:38	4	30.02	22	59.98	158-160	296	6054	6064
48	233	92	7/3/2006	4:37	5	0.80	23	0.5	161-163	265	6054	6064
49	234	93	7/3/2006	16:00	5	29.90	22	59.7	164-166	277	6054	6064
50	235	94	7/3/2006	19:20	6	0.05	22	59.98	167-169	230	6054	6064
51	236	95	7/3/2006	23:53	6	29.88	22	59.86	170-172	249	6054	6064
52	237	96	7/4/2006	4:21	6	59.90	23	0	173-175	244	6052	6064
53	238	97	7/4/2006	8:56	7	29.98	22	5.98	176-178	274	6052	6064
54	239	98	7/4/2006	13:36	7	59.80	23	0.1	179-181	234	6052	6064
55	240	99	7/4/2006	18:30	8	29.92	23	0	182-184	205	6052	6064
56	242	101	6/5/2007	5:20	9	29.95	23	0.04	185-187	236	6052	6064
57	244	103	7/5/2006	16:50	10	29.90	22	59.8	188-190	214	6052	6064
58	246	105	7/6/2006	1:24	11	29.94	22	59.9	191-193	222	6052	6064
59	248	107	7/6/2006	9:54	12	29.83	23	0.04	194-196	273	6052	6064
60	250	109	7/6/2006	18:58	13	29.94	22	59.87	195-199	272	6052	6064
61	255	115	7/8/2006	4:54	17	35.86	24	14.92	200-202	243	6052	6064

The free-falling profiler is optimized to sink at a rate of about 0.6 m/s and is capable of measuring microstructure up to a depth of 500 m. Shear and temperature fluctuations recorded due to vibration of the profiler while sinking can be diagnosed from the spectra of the acceleration sensor time series.

In total, four shear probes (s/n 6052, 6054, 6061, 6064, marked in Table 2.6) were used. A second FP07 fast thermistor was available as backup, but was not used. Routinely, MSS casts were made from the surface to about a depth of 220-260 m. Only stations with excessive vertical velocity shear were stopped when the fall rate of the probe dropped below about 0.3 m/s (see shorter profile in Table 2.5). That was mainly the case at the equator, especially in the western part. First we tried to mount more ballast rings at the probe to increase the depth range, but by using more weight we enhanced mainly the fall rate in the top 30-40 m but did not sufficiently

increase the depth. So we decided to use a combination of ballast and buoyancy rings which is optimized for a fall rate of 0.6 m/s above the EUC, or in low shear zones.

Just after putting the probe in the water at Station 234 we experienced a problem with data transmission and got excessive error messages. We decided to cut off the first 20 m of the sea cable, but after fixing the cable the problem was still there. So we switched to our backup cable, which was only 570 m long (instead of the original 800 m), but for most of our measurements the replacement cable was long enough. All other parts of our equipment worked well until the end of the cruise.

Table 2.6 Sensors of MSS system used during METEOR cruise 68/2

Sensor	Type	Response time	Serial No.
Temperature	PT100	40 ms	
Conductivity	ADM	40 ms	
Pressure	PA-50 Progress	40 ms	
Oxygen	Oxyguard	??	DO522M18
Acceleration	ACC	4 ms	8023
Shear	Airfoil	4 ms	6052
Shear	Airfoil	4 ms	6054
Shear	Airfoil	4 ms	6061
Shear	Airfoil	4 ms	6064
Temperature	NTC; FP07	12 ms	38
Conductivity	Microstructure C-sensor	4 ms	13

2.4.6 Chemical Measurements

(T.Tanhua, M. Schütt, A. Schneider, F. Malien, S. Grobe, P. Wiebe, N. Gülzow)

SF_6

Samples for SF_6 measurements were taken on selected CTD stations during the cruise. Due to analytical difficulties, no samples could be analyzed onboard. However, during the cruise samples from a total of 8 profiles were flame-sealed in ampoules and brought back to the laboratory in Kiel for later analysis of CFC-12 and SF_6. The samples were collected in 350 ml glass ampoules with a headspace of about 40 ml of pure nitrogen gas air.

CFC-11 and CFC-12

Samples for CFC measurements were drawn in syringes (first sample to be collected from the Niskin, followed by the SF_6 sampling) and transferred in amounts of 20 ml to a purge and trap gas-chromatographic unit similar to the one described by Bullister and Weiss (1988). Separation of the dissolved gases was performed using a packed column, and detection was done with an Electron Capture Detector (ECD). The CFCs were calibrated against a standard gas, which was

re-calibrated against a new gas standard provided by CMDL/NOAA in Boulder, CO. The temporal drift of the ECD was corrected for by applying calibration runs made before and after each station. In total, 1380 water samples (of which 190 were double samples) from 69 stations and 13 air samples were successfully analyzed. The reproducibility was determined by analyzing 190 samples twice and the standard deviation was found to be 1.4 % for CFC-12 and 1.0% for CFC-11. An analytical blank of 0.003 pmol/kg was removed from CFC-12; CFC-11 was free of analytical blank.

Nutrients

Nutrients (nitrate, nitrite, phosphate, silicate) were determined from 1320 water samples at 68 CTD-Stations. The nutrient analysis was made with a Continuous-Flow-Autoanalyzer-(CFA) System developed and built at IFM-GEOMAR according to Grashoff et al. (1999). For the determination of phosphate, the method by Bran and Luebbe (Method No. G-175-96 Rev 8) was used.

The precision for nutrient analysis as determined from 134 double samples from 67 stations was determined as (95 % confidence interval): Nitrite 0.008 μmol kg^{-1}; Nitrate 0.18 μmol kg^{-1}; phosphate 0.016 μmol kg^{-1}, silicate 0.19 μmol kg^{-1}, which was approximately 1 % of the nutrient standards. For precision estimates, two duplicate samples were taken and analyzed at 67 stations. Calibration curves were made with nutrients standards from Ocean Scientific International.

Oxygen

Oxygen was analyzed from 1321 Niskin bottles at 68 CTD-Stations according to a standard titration after Winkler (Grashoff, 1999). Two duplicate samples were taken and analyzed at 67 of the stations, and the precision of the measurement was determined as 0.5 μmol kg^{-1} (95 % confidence interval).

Total Dissolved Inorganic Carbon (DIC) and Total Alkalinity

Direct measurements of DIC were made using a coulometric method according to *Johnson et al.* (1993). The measurements were calibrated independently by regular injections of known amounts of pure CO_2. The accuracy was assessed by regular measurement of Certified Reference Materials (CRM, supplied by Dr. Andrew Dickson, Scripps Institution of Oceanography (SIO), La Jolla, CA.

# Stations:	67
# Samples analyzed:	1189
# Duplicates analyzed:	88

Total alkalinity were determined with a potentiometric titration method according to *Mintrop et al.* (2000). The accuracy was assessed by regular measurement of Certified Reference Materials (CRM, supplied by Dr. Andrew Dickson, Scripps Institution of Oceanography (SIO),

La Jolla, CA). During the cruise we found a linear temporal trend in the measurements of CRMs, ranging from +1.93 to 1.42 µmol kg^{-1}, and this was applied to the data set.

# Stations:	67
# Samples analyzed:	1189
# Duplicates analyzed:	88

Table 2.7 Table of analytical precision and information regarding certified reference materials used

		DIC	A_T
CRM:	analyzed bottles	87	79
	batches used	68 & 74	68 & 74
	Mean deviation from certified CRM-value	-1.42 to 1.93	- 0.65 µmol/kg
	standard deviation	1.85 µmol/kg	± 1.90 µmol/kg
Duplicates:	analyzed pairs	88	88
	mean deviation from duplicate value	0.84 µmol/kg	1.49 µmol/kg
	standard deviation	± 0.94 µmol/kg	± 1.29 µmol/kg

Filtration

Samples for biological filtration were taken with the aim of sampling in, above and below the chlorophyll maximum. The depths, however, varied randomly throughout the cruise. Samples were taken with polycarbonate bottles and a volume of 2L was filtered with a low vacuum pressure onto a 0.22 micron 47 mm filter. After that the filters were removed with clean forceps from the filtration rack, packed in a screw cap cryo-vials and stored in the -80°C freezer.

The collection of filtered seawater samples is important for the detection of nifH genes and serves to get an impression which bacteria can be found in the different depths. To get some information about the size and abundances of bacteria in the seawater, some samples were also taken for Flow Cytometry in the lab in Kiel. A volume of 1.9ml seawater from the same bottles was taken and convicted into a screw cap cryo vials. After that a solution of 20% Glutaraldehyde stock was added to the screw cap cryo vials and stored in a -20°C freezer.

H_2O_2

Samples for H_2O_2 measurements were taken with brown polyethylene bottles at six different depths, typically 10, 20, 40, 60, 80 and 100m. Standard water was taken from the deepest Niskin closed, mostly 1300m. A known concentration of a secondary stock standard was added to the standard (deep) water sampler, after which the standard and samples were immediately measured. The samples were kept as cold as possible and direct sunshine was avoided. The samples were mixed with Luminol in a FIA analytical system were the H_2O_2 concentration could be detected photometrically.

Hydrogen peroxide is one of the strongest oxidants that occurs in natural waters and can be used as a tracer. H_2O_2 is principally produced in the water column by photochemical reactions involving dissolved organic matter O_2. During M68/2, we found more H_2O_2 in the surface and declining concentrations with depth, consistent with the photochemical flux.

2.4.7 DVS Meteorological and Surface Underway Data

(B. Rabe)

The central data distributor (DVS) system continuously records a large set of oceanographic and atmospheric parameters from several sensors throughout the cruise. In order to complete the data set obtained from CTD/LADCP measurements and the two vessel-mounted ADCPs, several parameters were post-processed and calibrated. These variables were sea surface temperature (SST) and salinity (SSS) from the thermosalinograph, meteorological parameters including wind speed, wind direction, air temperature, air pressure and humidity as well as bathymetry. The post-processed dataset will be made available to the public by submitting the data to appropriate international data centers.

The METEOR just recently acquired a new database application by Werum Software & Systems. This provides both an “online” database for immediate display as well as web form to download data from an “archive” database by selecting variable names, units and precision. Although the old database was still running during the cruise, previous changes to the ship's hardware during shipyard time meant that some of the data streams were no longer available in the old database while the new one was still in the implementation stage. This concerns the thermosalinograph data and the bathymetric depth from the EM120 multi-beam echosounder. All thermosalinograph data gaps due to outages in the Werum database were filled as best as possible with direct recordings of data from the thermosalinograph.

2.4.7.1 Thermosalinograph Data

a) Post-processing and sensor calibration

Sea-surface temperature and salinity were measured by a thermosalinograph with an intake at the ship's hull at 4m depth. The device was a SeaCat SBE 120 manufactured by Sea-Bird Electronics, Inc. The thermosalinograph worked well throughout the cruise. However, there were problems with the data stream into the DVS and the recording via the SeaSave software on a PC directly connected to the thermosalinograph. These two data streams showed inconsistencies in the time offset of salinity and temperature values. Therefore, the DVS thermosalinograph temperature was compared to the ship's surface temperature sensors on both port and starboard. While the DVS data showed very good agreement, the directly recorded data did not. During times where the DVS database was operating, but did not have thermosalinograph data, the available separately recorded data was manually matched to the surface temperature by adjusting the time of the recorded data. The same time adjustment was used for the salinity data.

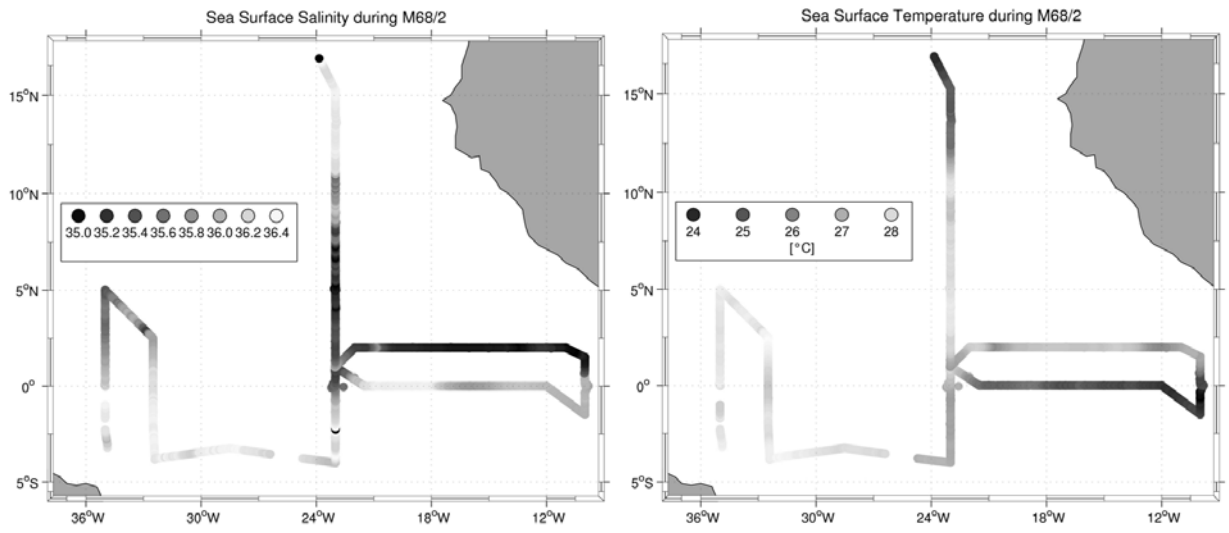

Fig. 2.10 M68/2 thermosalinograph SSS (left) and SST (right), calibrated against CTD data

In post-processing, the temperature and salinity records were calibrated against CTD temperature and salinity data from 4m depth collected during the cruise. A constant offset in thermosalinograph temperature and salinity was found to be most adequate for calibration, being -0.004 °C for thermosalinograph temperature and -0.075 psu for salinity. The standard deviation of the temperature differences between the CTD and thermosalinograph was 0.014 °C. This value can be viewed as the statistical measurement error of the thermosalinograph SST measurements due to the much higher accuracy of the temperature measurements by the CTD sensors. The standard deviation of the salinity differences was somewhat larger, being 0.023 psu, which again reflects the measurement error of the thermosalinograph salinity. For archiving, the constant offsets in temperature and salinity were removed and the data were averaged to five-minute ensembles. The dataset was submitted to the GOSUD/SISMER project, hosted at IFREMER in Brest, France (http://www.ifremer.fr/sismer/program/gosud/).

b) Observations

During the cruise, sea surface temperatures were higher west of about 24°W, where values are generally above 28°C (Fig. 2.10). East of this, down to 4°C lower temperatures are found along the equator, representing the seasonal cold tongue. Small temperature variations of the order of 1°C, visible for example in the 2°N section, are currently compared to the Vessel Mounted ADCP current velocity data and may be linked to Tropical Instability Waves. The SSS shows the expected large-scale pattern, with a salinity minimum near the African coast, north of the equator. Further south, close to the equator the seasonal cold tongue also brings high salinity water to the surface. In addition, small scale variability can be seen, as in the SST (Fig. 2.10).

2.4.7.2 Meteorological Data

a) Data acquisition and post-processing

On R/V METEOR, meteorological parameters are recorded by a weather station from Theodor Friedrichs & Co. The sensors for air temperature, humidity, pressure, wind speed and wind direction are attached to the top platform of the main mast at 40.2 m above sea level. There are wind sensors on both the port and starboard side. The weather station automatically calculates true wind speed and direction from relative wind by using the ship's Doppler log. However, the latter had to be switched off during most of the cruise as it was found to interfere with the vessel mounted ADCPs. Instead, geographical positions from the differential GPS system were used to calculate true wind speed and direction. However, this still did not seem to yield satisfying results when the ship was moving at slow speed, e.g. on-station, so that any wind data collected when the ship had less than 5 kn speed over ground was discarded.

Thus, after removing outliers, the meteorological parameters true wind speed and direction, air temperature, humidity and pressure were averaged into 5-minute ensembles. The meteorological data set will be submitted to the Research Vessel Surface Meteorology Data Center at the Center for Ocean- Atmospheric Prediction Studies, Florida State University (http://www.coaps.fsu.edu/RVSMDC/html/data.shtml).

Radiosoundings were performed twice a day, with real-time data transmission via GTS for ingestion into various mid-range forecast models and to complement the improved African upper air network installed as part of AMMA. After the cruise 64 high-resolution profiles from radiosoundings were delivered to the AMMA database (http://amma-international.org/database/).

b) Observations

Strong northwestward winds were observed in the southeastern part of the cruise (Fig. 2.11). Between 5°N to 10°N, a band of weaker, mainly northward, winds denotes the region of the ITCZ during boreal summer. North of this, winds were dominated by strong southwestward trades. In the west, deviations from the generally expected westward wind are evident. This is likely due to mesoscale variability.

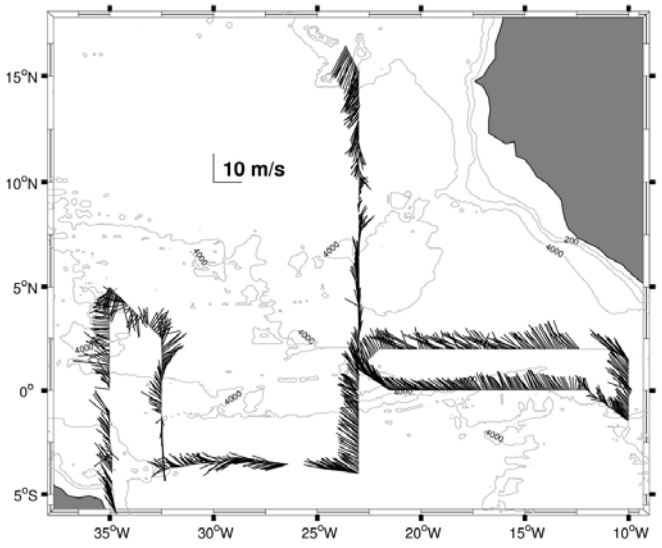

Fig. 2.11
True wind speed at 40m from the METEOR weather station

2.5 Ship's Meteorological Station

METEOR left the port of Recife on June 06 with south-easterly winds about 4 Bft and isolated showers. Along its northerly course, METEOR encountered the edge of the ITCZ (Intertropical Convergence Zone) near 2°S. At this point a period of heavy shower activity began, associated with squalls up to Bft 8. Outside of the shower area, the mean wind speed range was 3 to 5 Bft. From June 08 until June 10, a swell from SE reached the vessel, with additional smaller swell from S to SE.

METEOR remained in the ITCZ for the next days with different intensity of the convective clouds. After passing the most northern waypoint near 5°N 35°W on June 11, the cruise continued heading southeast and south en route to Fernando de Noronha. After a short stop an easterly track began until the 23rd degree of longitude. There for the first time the shower activity ceased, and the weather became fair in the region of the SE trades at about 4 Bft. Then METEOR sailed northerly until 1°N. The weather remained fair until METEOR approached the ITCZ on June 20. The clouds became lower and taller, and the wind increased to 4 and 5 Bft from east to southeast. Further along the equator, the ITCZ remained to the north and the weather was mostly sunny with south-easterly winds about 4Bft. The height of the sea (1.5-2m) resulted mainly from the swell from SE to S, sometimes from N.

During the track to the west near 02° N 23° W no significant weather was observed. Along its northerly course, METEOR encountered the ITCZ again near 4°N 23°W. The intensity of the ITCZ was weak at that time. The weather was characterized by southerly winds of Bft 4 and a broken to overcast cloud intensity. Both ITCZ and METEOR moved northward, and the first showers occurred not until July 04. One day later the ITCZ was already crossed, and the clouds became scattered. The light wind veered south-westerly, later northerly. On July 06, METEOR had left the ITCZ far behind and showers were rare. The northerly wind was in a range of 4 to 5 Bft. The voyage ended in the morning of July 09 in the harbour of Mindelo.

2.6 Station List M68/2

Table 2.8 M68/2 CTD/LADCP stations
Code: BE = begin, BO = bottom, EN = end
Parameters (Par.): 1= CFC, 2=SF_6, 3=He, 4=Oxy, 5=DIC, 6=Alk, 7=Nuts, 8=Sal, 9=H_2O_2, 10=Filtr, 11=Microbiology, 12=PFOS

R/V METEOR cruise M68/2 CTD-stations

SHIP	Station	e	DATE	UTC		POSITION						Uncorr.	MAX	NO. OF	
EXPOCODE	No.	No.	Mmddyy	TIME	CODE	LATITUDE			LONGITUDE			DEPTH	PRESS	BOTTLES	PAR.
06ME68/2	130	1	060706	0722	BE	04	54.96	S	34	55.11	W	828	CTD		
06ME68/2	130	1	060706	0745	BO	04	54.65	S	34	55.17	W		832	21	Bottle test. 8
06ME68/2	130	1	060706	0805	EN	04	54.11	S	34	55.30	W				
06ME68/2	131	2	060706	0924	BE	04	48.47	S	34	52.84	W	983			
06ME68/2	131	2	060706	0953	BO	04	47.85	S	34	53.01	W	1015	1011	21	1.4.5.6.7.8.10
06ME68/2	131	2	060706	1023	EN	04	47.16	S	34	53.15	W				
06ME68/2	132	3	060706	1120	BE	04	40.35	S	34	52.81	W	2426			
06ME68/2	132	3	060706	1159	BO	04	39.69	S	34	52.92	W		1316	2	8
06ME68/2	132	3	060706	1231	EN	04	38.98	S	34	53.00	W				

06ME68/2	133	4	060706	1415	BE	04	20.65	S	34	53.16	W	3520			
06ME68/2	133	4	060706	1450	BO	04	19.95	S	34	53.32	W		1325	2	8
06ME68/2	133	4	060706	1527	EN	04	19.37	S	34	53.62	W				
06ME68/2	134	5	060706	1722	BE	04	00.17	S	34	53.03	W	3460			
06ME68/2	134	5	060706	1755	BO	03	59.78	S	34	53.13	W		1354	21	1.4.5.6.7.8
06ME68/2	134	5	060706	1830	EN	03	59.43	S	34	53.19	W				
06ME68/2	135	6	060706	2104	BE	03	30.57	S	34	52.99	W	2360			
06ME68/2	135	6	060706	2141	BO	03	30.38	S	34	53.08	W		1323	21	--
06ME68/2	135	6	060706	2209	EN	03	30.34	S	34	53.08	W				
06ME68/2	136	7	060806	0113	BE	03	00.35	S	34	53.12	W	3837			
06ME68/2	136	7	060806	0152	BO	02	59.98	S	34	53.46	W		1311	21	1.4.5.6.7.8.10
06ME68/2	136	7	060806	0229	EN	02	59.53	S	34	53.54	W				
06ME68/2	137	8	060806	0429	BE	02	40.00	S	34	56.93	W	3889			
06ME68/2	137	8	060806	0501	BO	02	39.98	S	34	56.98	W		1302	--	--
06ME68/2	137	8	060806	0527	EN	02	40.05	S	34	56.92	W				
06ME68/2	138	9	060806	0735	BE	02	19.95	S	34	59.99	W	3947			
06ME68/2	138	9	060806	0814	BO	02	19.94	S	35	00.02	W		1314	21	1.4.5.7.8
06ME68/2	138	9	060806	0847	EN	02	20.09	S	35	00.03	W				
06ME68/2	139	10	060806	1049	BE	02	00.04	S	35	00.01	W	4053			
06ME68/2	139	10	060806	1128	BO	02	00.39	S	35	00.02	W		1311	Test 2 bottles	
06ME68/2	139	10	060806	1156	EN	02	00.31	S	35	00.03	W				
06ME68/2	140	11	060806	1402	BE	01	40.05	S	34	59.88	W	4080			
06ME68/2	140	11	060806	1439	BO	01	40.06	S	34	59.90	W		1319	21	1.4.5.6.7.8.10
06ME68/2	140	11	060806	1516	EN	01	40.07	S	34	59.88	W				
06ME68/2	141	12	060806	1903	BE	01	20.11	S	34	59.92	W	4345			
06ME68/2	141	12	060806	1943	BO	01	20.25	S	35	00.00	W		1316	Test 3 bottles	
06ME68/2	141	12	060806	2012	EN	01	20.35	S	34	59.98	W				
06ME68/2	142	13	060806	2219	BE	00	59.97	S	34	59.95	W	4373			
06ME68/2	142	13	060806	2251	BO	01	00.00	S	34	59.74	W		1315	21	1.4.5.6.7.8.9
06ME68/2	142	13	060806	2328	EN	01	00.00	S	34	59.72	W				
06ME68/2	143	14	060906	0132	BE	00	39.98	S	34	59:99	W	4460			
06ME68/2	143	14	060906	0204	BO	00	39:97	S	34	59:93	W		1315	--	--
06ME68/2	143	14	060906	0230	EN	00	39:98	S	34	59.83	W				
06ME68/2	144	15	060906	0435	BE	00	19:98	S	34	59:92	W	4515			
06ME68/2	144	15	060906	0508	BO	00	19:96	S	34	59.74	W		1302	--	--
06ME68/2	144	15	060906	0535	EN	00	19.90	S	34	59.45	W				
06ME68/2	145	16	060906	0741	BE	00	00.06	S	34	59.95	W	4543			
06ME68/2	145	16	060906	0919	BO	00	00.43	S	34	59.35	W		4608	20	1.3.4.5.6.7.8.9.12
06ME68/2	145	16	060906	1106	EN	00	00.42	S	34	58.77	W	4543			
06ME68/2	147	17	060906	1804	BE	00	19:95	N	35	00.00	W	4541			
06ME68/2	147	17	060906	1842	BO	00	19.86	N	34	59.61	W		1302	20	1.4.5.6.7.8.9.10
06ME68/2	147	17	060906	1917	EN	00	20.06	N	34	59.224	W				
06ME68/2	148	18	060906	2120	BE	00	39.91	N	34	59.93	W	4544			
06ME68/2	148	18	060906	2156	BO	00	40.00	N	34	59.73	W		1314	4	3
06ME68/2	148	18	060906	2224	EN	00	40.26	N	34	59.70	W				
06ME68/2	149	19	061006	0013	BE	00	59.71	N	34	59.80	W	3620			
06ME68/2	149	19	061006	0102	BO	00	59.70	N	34	59.65	W		1315	20	1.3.4.5.6.7.8.9
06ME68/2	149	19	061006	0138	EN	00	59.63	N	34	59.58	W				
06ME68/2	150	20	061006	0346	BE	01	20.07	N	35	00.00	W	4062			
06ME68/2	150	20	061006	0420	BO	01	20.29	N	34	59.62	W		1303	--	--
06ME68/2	150	20	061006	0448	EN	01	20.44	N	34	59.45	W				
06ME68/2	151	21	061006	0651	BE	01	40.11	N	34	59.97	W	4043			
06ME68/2	151	21	061006	0722	BO	01	40.38	N	34	59.75	W		1320	20	1.4.7.8
06ME68/2	151	21	061006	0759	EN	01	40.61	N	34	59.42	W				
06ME68/2	152	22	061006	0952	BE	02	00.02	N	34	59.99	W	4781			
06ME68/2	152	22	061006	1027	BO	02	00.44	N	34	59.74	W		1314	8	8

06ME68/2	152	22	061006	1127	EN	02	00.63	N	34	59.49	W				
06ME68/2	153	23	061006	1247	BE	02	19.94	N	34	59.91	W				
06ME68/2	153	23	061006	1321	BO	02	20.11	N	34	59.91	W	4140	1337	21	1.4.5.6.7.8.9.10
06ME68/2	153	23	061006	1358	EN	02	20.25	N	34	59.94	W				
06ME68/2	154	24	061006	1600	BE	02	40.20	N	35	00.07	W	3391			
06ME68/2	154	24	061006	1644	BO	02	40.71	N	34	59.91	W		1312	8	--
06ME68/2	154	24	061006	1715	EN	02	40.99	N	34	59.77	W				
06ME68/2	155	25	061006	1909	BE	03	00.11	N	34	59.93	W	3816			
06ME68/2	155	25	061006	1949	BO	03	00.67	N	34	59.92	W		1314	21	1.4.5.6.7.8.9
06ME68/2	155	25	061006	2024	EN	03	00.99	N	34	59.87	W				
06ME68/2	156	26	061006	2303	BE	03	29.99	N	35	00.07	W	3958			
06ME68/2	156	26	061006	2348	BO	03	30.47	N	35	00.09	W		1313	2	calibration
06ME68/2	156	26	061106	0015	EN	03	30.64	N	35	00.14	W				
06ME68/2	157	27	061106	0254	BE	03	59.90	N	34	59.92	W	3487			
06ME68/2	157	27	061106	0325	BO	04	00.08	N	34	59.85	W		1307	21	1.4.5.6.7.8.9.10
06ME68/2	157	27	061106	0403	EN	04	00.29	N	34	59.62	W				
06ME68/2	158	28	061106	0655	BE	04	29.99	N	35	00.07	W	3882			
06ME68/2	158	28	061106	0729	BO	04	30.47	N	34	59.99	W	3896	1318	7	8
06ME68/2	158	28	061106	0758	EN	04	30.75	N	34	59.81	W				
06ME68/2	159	29	061106	1028	BE	04	57.12	N	35	00.02	W	4054			
06ME68/2	159	29	061106	1100	BO	04	57.32	N	34	59.99	W	3997	1315	21	1.4.5.6.7.8.9
06ME68/2	159	29	061106	1140	EN	04	57.68	N	35	00.06	W	3955			
06ME68/2	160	30	061106	1458	BE	04	58.94	N	35	00.13	W	3774			
06ME68/2	160	30	061106	1529	BO	04	59.07	N	35	00.15	W		1308	--	Test
06ME68/2	160	30	061106	1557	EN	04	59.11	N	35	00.09	W				
06ME68/2	163	31	061306	0914	BE	00	39.87	S	32	29.87	W	4559			
06ME68/2	163	31	061306	0947	BO	00	39.48	S	32	29.71	W	4496	1316	21	1.3.4.5.6.7.8
06ME68/2	163	31	061306	1043	EN	00	39.38	S	32	29.26	W				
06ME68/2	164	32	061306	1526	BE	01	19.98	S	32	30.00	W	4360			
06ME68/2	164	32	061306	1555	BO	01	19.97	S	32	29.64	W		1303	21	Test. 9
06ME68/2	164	32	061306	1637	EN	01	15.80	S	32	29.22	W				
06ME68/2	170	33	061606	2255	BE	04	00.01	S	23	00.23	W	5930			
06ME68/2	170	33	061606	2327	BO	03	59.99	S	23	00.30	W	5945	1320	21	1.4.5.6.7.8.9
06ME68/2	170	33	061706	0004	EN	03	59.87	S	23	00.30	W				
06ME68/2	171	34	061706	0256	BE	03	30.14	S	23	00.05	W	5493			
06ME68/2	171	34	061706	0325	BO	03	30.20	S	23	00.06	W		1312	7	9
06ME68/2	171	34	061706	0359	EN	03	30.19	S	23	00.01	W				
06ME68/2	172	35	061706	0706	BE	03	00.02	S	23	00.04	W	5491			
06ME68/2	172	35	061706	0738	BO	03	00.02	S	23	00.07	W		1313	21	1.4.5.6.7.8
06ME68/2	172	35	061706	0815	EN	03	00.09	S	23	00.08	W				
06ME68/2	173	36	061706	1109	BE	02	41.20	S	23	01.00	W				
06ME68/2	173	36	061706	1138	BO	02	41.34	S	23	00.93	W	5577	1316	--	--
06ME68/2	173	36	061706	1209	EN	02	41.31	S	23	00.91	W	5575			
06ME68/2	174	37	061706	1425	BE	02	19.99	S	23	00.03	W	5138			
06ME68/2	174	37	061706	1454	BO	02	00.97	S	23	00.02	W		1303	21	1.4.5.6.7.8.9.10
06ME68/2	174	37	061706	1528	EN	02	19.87	S	22	59.92	W				
06ME68/2	175	38	061706	1836	BE	02	00.64	S	23	01.64	W	5205			
06ME68/2	175	38	061706	1905	BO	02	00.67	S	23	01.60	W	5219	1313	5	8.3
06ME68/2	175	38	061706	1935	EN	02	00.57	S	23	01.52	W	5228			
06ME68/2	176	39	061706	2150	BE	01	40.08	S	23	00.52	W	4949			
06ME68/2	176	39	061706	2219	BO	01	40.11	S	23	00.07	W	4936	1314	21	1.3.4.5.6.7.8.10
06ME68/2	176	39	061706	2257	EN	01	40.07	S	23	00.11	W	4939			
06ME68/2	177	40	061806	0149	BE	01	20.83	S	23	01.21	W	4963			
06ME68/2	177	40	061806	0220	BO	01	20.92	S	23	01.16	W	4966	1312	5	3
06ME68/2	177	40	061806	0248	EN	01	20.80	S	23	01.03	W	4960			
06ME68/2	178	41	061806	0529	BE	01	00.39	S	23	00.60	W	4179			

06ME68/2	178	41	061806	0600	BO	01	00.47	S	23	00.62	W	4186	1315	21	1.3.4.5.6.7.8
06ME68/2	178	41	061806	0637	EN	01	00.57	S	23	00.34	W	4156			
06ME68/2	179	42	061806	0822	BE	00	45.03	S	23	00.00	W	3669			
06ME68/2	179	42	061806	0942	BO	00	44.98	S	22	59.70	W	3680	3654	21	1.3.4.5.6.7.8
06ME68/2	179	42	061806	1106	EN	00	44.99	S	22	59.56	W	3685			
06ME68/2	181	43	061806	2119	BE	00	30.07	S	23	00.06	W	4624			
06ME68/2	181	43	061806	2148	BO	00	30.19	S	22	59.95	W	4622	1313	21	1.3.4.5.6.7.8.9
06ME68/2	181	43	061806	2224	EN	00	30.13	S	22	59.72	W	4628			
06ME68/2	182	44	061906	0004	BE	00	15.22	S	23	00.01	W	4153			
06ME68/2	182	44	061906	0035	BO	00	15.32	S	23	00.00	W	4196	1313	5	3
06ME68/2	182	44	061906	0105	EN	00	15.14	S	22	59.95	W	4147			
06ME68/2	183	45	061906	0330	BE	00	03.33	S	23	09.13	W	3735			
06ME68/2	183	45	061906		BO								1959	--	--
06ME68/2	183	45	061906	0501	EN	00	03.08	S	23	08.72	W	3785			
06ME68/2	185	46	061906	1348	BE	00	07.27	N	23	06.97	W	3792			
06ME68/2	185	46	061906	1411	BO	00	07.30	N	23	06.93	W	3792	701	21	1.3.4.5.6.7.8.9.10
06ME68/2	185	46	061906	1432	EN	00	07.43	N	23	06.75	W	3734			
06ME68/2	186	47	062006	0101	BE	00	24.96	N	23	00.06	W	3868			
06ME68/2	186	47	062006	0133	BO	00	25.06	N	23	00.11	W	3862	1314	21	1.3.4.5.6.7.8.9.10
06ME68/2	186	47	062006	0210	EN	00	25.11	N	23	00.10	W				
06ME68/2	187	48	062006	0418	BE	00	45.07	N	22	59.64	W	4309			
06ME68/2	187	48	062006	0544	BO	00	45.03	N	22	59.50	W	4311	4266	21	1.3.4.5.6.7.8.9
06ME68/2	187	48	062006	0719	EN	00	45.04	N	22	59.49	W	4311			
06ME68/2	189	49	062006	1742	BE	01	00.00	N	23	00.08	W	3239			
06ME68/2	189	49	062006	1812	BO	01	00.06	N	23	00.09	W	3227	1314	21	1.2.3.4.5.6.7.8.9
06ME68/2	189	49	062006	1848	EN	01	00.09	N	23	00.08	W	3227			
06ME68/2	190	50	062106	0756	BE	00	00.01	N	21	30.09	W	4950			
06ME68/2	190	50	062106	0939	BO	00	00.11	N	21	29.44	W	4949	4931	21	1.3.4.5.6.7.8
06ME68/2	190	50	062106	1130	EN	00	00.24	N	21	29.11	W	4950			
06ME68/2	192	51	062106	2239	BE	00	00.45	N	21	00.71	W	5124			
06ME68/2	192	51	062106	2318	BO	00	00.51	N	21	00.62	W	5125	1313	21	1.3.4.5.6.7.8.9.10
06ME68/2	192	51	062106	2356	EN	00	00.69	N	21	00.29	W	5128			
06ME68/2	193	52	062206	0719	BE	00	00.00	N	19	59.98	W	2585			
06ME68/2	193	52	062206	0751	BO	00	00.20	N	19	59.66	W	2543	1314	21	1.3.4.5.6.7
06ME68/2	193	52	062206	0832	EN	00	00.32	N	19	59.20	W	2594			
06ME68/2	194	53	062206	1537	BE	00	00.64	S	19	00.62	W	4163			
06ME68/2	194	53	062206	1608	BO	00	00.36	S	19	00.29	W	4163	1308	21	1.3.4.5.6.7.8.10
06ME68/2	194	53	062206	1715	EN	00	00.18	N	18	59.55	W	4163			
06ME68/2	195	54	062306	0023	BE	00	00.55	S	18	00.78	W	6475			
06ME68/2	195	54	062306	0056	BO	00	00.55	S	18	00.69	W	6467	1312	21	1.3.4.5.6.7.8.10
06ME68/2	195	54	062306	0131	EN	00	00.51	S	18	00.64	W	6468			
06ME68/2	196	55	062306	0853	BE	00	00.21	S	17	01.30	W	4956			
06ME68/2	196	55	062306	0924	BO	00	00.16	S	17	01.16	W	4972	1314	21	1.3.4.5.6.7.8
06ME68/2	196	55	062306	1001	EN	00	00.16	S	17	00.87	W	5041			
06ME68/2	197	56	062306	1725	BE	00	00.11	S	16	01.84	W	3176			
06ME68/2	197	56	062306	1757	BO	00	00.01	S	16	01.91	W	3170	1314	21	1.3.4.5.6.7.8
06ME68/2	197	56	062306	1835	EN	00	00.10	S	16	01.51	W	3217			
06ME68/2	198	57	062406	0159	BE	00	00.03	S	15	01.16	W	3602			
06ME68/2	198	57	062406	0230	BO	00	00.17	N	15	00.85	W	3752	1313	21	1.3.4.5.6.7.8
06ME68/2	198	57	062406	0307	EN	00	00.31	N	15	00.49	W	3775			
06ME68/2	199	58	062406	1018	BE	00	00.03	N	14	00.77	W	3906			
06ME68/2	199	58	062406	1051	BO	00	00.19	N	14	00.68	W	3971	1312	21	1.3.4.5.6.7.8
06ME68/2	199	58	062406		EN										
06ME68/2	200	59	062406	1655	BE	00	00.06	S	13	08.20	W	4457			
06ME68/2	200	59	062406	1726	BO	00	00.02	N	13	07.97	W	4457	1301	21	1.2.3.4.5.6.7.8.10
06ME68/2	200	59	062406	1802	EN	00	00.07	N	13	07.69	W	4423			

06ME68/2	201	60	062506	0240	BE	00	00.18	S	12	00.09	W	3828			
06ME68/2	201	60	062506	0312	BO	00	00.01	N	11	59.72	W	4069	1304	21	1.3.4.5.6.7.8.10
06ME68/2	201	60	062506	0351	EN	00	00.02	N	11	59.45	W	4371			
06ME68/2	202	61	062506	1818	BE	01	29.93	S	10	00.08	W	4808			
06ME68/2	202	61	062506	1848	BO	01	29.92	S	10	00.01	W	4799	1313	21	1.3.4.5.6.7.8.9
06ME68/2	202	61	062506	1923	EN	01	29.99	S	09	59.87	W	4800			
06ME68/2	203	62	062506	2213	BE	01	00.01	S	10	00.00	W	4272			
06ME68/2	203	62	062506	2244	BO	00	59.99	S	09	59.90	W	4275	1314	5	3
06ME68/2	203	62	062506	2315	EN	00	59.99	S	09	59.71	W	4268			
06ME68/2	204	63	062606	0220	BE	00	40.33	S	10	00.44	W	4060			
06ME68/2	204	63	062606	0254	BO	00	40.23	S	10	00.01	W	4031	1307	21	1.3.4.5.6.7.8.9
06ME68/2	204	63	062606	0331	EN	00	40.07	S	09	59.53	W	4042			
06ME68/2	205	64	062606	0630	BE	00	21.18	S	10	00.75	W	4337			
06ME68/2	205	64	062606	0701	BO	00	21.27	S	10	00.64	W	4369	1314	5	3.8
06ME68/2	205	64	062606	0732	EN	00	21.40	S	10	00.38	W	4303			
06ME68/2	206	65	062606	0958	BE	00	00.97	N	09	50.04	W	5203			
06ME68/2	206	65	062606	1120	BO	00	00.89	N	09	49.84	W	5206	4026	21	1.2.3.4.5.6.7.8.9.12
06ME68/2	206	65	062606	1248	EN	00	01.00	N	09	49.53	W	5202			
06ME68/2	207	66	062706	0125	BE	00	20.08	N	10	00.90	W	4745			
06ME68/2	207	66	062706	0157	BO	00	20.13	N	10	00.96	W	4749	1313	21	1.2.3.4.5.6.7.8.9
06ME68/2	207	66	062706	0233	EN	00	20.15	N	10	00.82	W	4750			
06ME68/2	208	67	062706	0533	BE	00	38.76	N	10	02.36	W	4569			
06ME68/2	208	67	062706	0605	BO	00	38.82	N	10	02.29	W	4570	1315	21	3.8
06ME68/2	208	67	062706	0643	EN	00	39.00	N	10	02.18	W	4552			
06ME68/2	209	68	062706	0850	BE	01	00.03	N	10	00.13	W	4667			
06ME68/2	209	68	062706	0922	BO	00	59.98	N	10	00.29	W	4665	1315	21	1.2.3.4.5.6.7.8
06ME68/2	209	68	062706	0958	EN	00	59.98	N	10	00.15	W	4664			
06ME68/2	210	69	062706	1323	BE	01	30.04	N	10	00.22	W	5242			
06ME68/2	210	69	062706	1357	BO	01	30.14	N	10	00.25	W	5241	1301	21	1.3.4.5.6.7.8.9.11
06ME68/2	210	69	062706	1430	EN	01	30.16	N	10	00.33	W	5234			
06ME68/2	211	70	062706	2019	BE	01	59.63	N	11	01.70	W	4420			
06ME68/2	211	70	062706	2059	BO	01	59.61	N	11	02.03	W	4420	1314	21	1.3.4.5.6.7.8.9
06ME68/2	211	70	062706	2133	EN	01	59.51	N	11	02.00	W	4420			
06ME68/2	212	71	062806	0253	BE	02	00.01	N	12	01.54	W	4838			
06ME68/2	212	71	062806	0324	BO	02	00.25	N	12	01.49	W	4841	1307	21	1.3.4.7.8.9.11
06ME68/2	212	71	062806	0404	EN	02	00.44	N	12	01.42	W	4840			
06ME68/2	213	72	062806	0929	BE	01	59.78	N	13	01.04	W	4981			
06ME68/2	213	72	062806	1006	BO	01	59.92	N	13	00.95	W	4984	1312	21	1.2.3.4.5.6.7.8
06ME68/2	213	72	062806	1041	EN	02	00.06	N	13	00.87	W	4991			
06ME68/2	214	73	062806	1615	BE	01	59.26	N	14	01.26	W	5140			
06ME68/2	214	73	062806	1648	BO	01	59.38	N	14	01.16	W	5149	1301	18	1.3.4.5.6.7.8
06ME68/2	214	73	062806	1741	EN	01	59.41	N	14	00.87	W	5149			
06ME68/2	215	74	062806	2308	BE	01	58.92	N	15	00.82	W	5340			
06ME68/2	215	74	062806	2340	BO	01	58.82	N	15	00.89	W	5347	1314	18	1.3.4.5.6.7.8.9.11
06ME68/2	215	74	062906	0036	EN	01	58.82	N	15	00.90	W	5347			
06ME68/2	216	75	062906	0600	BE	01	59.19	N	16	01.82	W	5137			
06ME68/2	216	75	062906	0632	BO	01	59.14	N	16	02.10	W	5159	1313	21	1.3.4.5.6.7.8
06ME68/2	216	75	062906	0709	EN	01	59.14	N	16	02.14	W	5153			
06ME68/2	217	76	062906	1214	BE	02	00.13	N	17	00.51	W	5276			
06ME68/2	217	76	062906	1248	BO	02	00.18	N	17	00.63	W	5284	1314	21	2.3.5.6.8.9.10
06ME68/2	217	76	062906	1325	EN	02	00.23	N	17	00.69	W	5294			
06ME68/2	218	77	062906	1832	BE	01	59.83	N	18	02.04	W	5090			
06ME68/2	218	77	062906	1902	BO	01	59.73	N	18	02.43	W	5162	1314	21	1.3.4.5.6.7.8.9
06ME68/2	218	77	062906	1939	EN	01	59.59	N	18	02.65	W	5179			
06ME68/2	219	78	063006	0048	BE	01	59.91	N	19	00.31	W	5112			
06ME68/2	219	78	063006	0118	BO	01	59.97	N	19	00.44	W	5112	1313	8	3.8.9

06ME68/2	219	78	063006	0152	EN	02	00.00	N	19	00.49	W	5117			
06ME68/2	220	79	063006	0716	BE	01	59.59	N	20	02.43	W	4909			
06ME68/2	220	79	063006	0749	BO	01	59.61	N	20	02.75	W	4947	1314	21	1.2.3.4.5.6.7.8
06ME68/2	220	79	063006	0825	EN	01	59.66	N	20	02.73	W	4934			
06ME68/2	221	80	063006	1333	BE	01	59.94	N	21	00.31	W	4934			
06ME68/2	221	80	063006	1412	BO	02	00.03	N	21	00.00	W	4934	1301	21	3.8.9
06ME68/2	221	80	063006	1441	EN	01	59.93	N	20	59.83	W	4934			
06ME68/2	222	81	063006	2022	BE	01	59.23	N	22	00.82	W	4013			
06ME68/2	222	81	063006	2052	BO	01	59.09	N	22	00.76	W	4024	1313	20	1.3.4.5.6.7.8.9
06ME68/2	222	81	063006	2119	EN	01	59.07	N	22	00.51	W	4055			
06ME68/2	223	82	070106	0520	BE	00	59.02	N	23	01.38	W	3472			
06ME68/2	223	82	070106	0552	BO	00	58.95	N	23	01.33	W	3493	1312	21	1.2.3.4.5.6.7.8
06ME68/2	223	82	070106	0633	EN	00	58.87	N	23	01.05	W	3529			
06ME68/2	224	83	070106	0920	BE	01	19.56	N	23	01.06	W	4571			
06ME68/2	224	83	070106	0952	BO	01	19.46	N	23	01.06	W	4534	1313	21	3.8.11
06ME68/2	224	83	070106	1033	EN	01	19.43	N	23	00.80	W	4600			
06ME68/2	225	84	070106	1314	BE	01	38.80	N	23	00.50	W	4134			
06ME68/2	225	84	070106	1346	BO	01	38.86	N	23	00.39	W	4132	1304	5	3.11
06ME68/2	225	84	070106	1415	EN	01	39.00	N	23	00.25	W	4132			
06ME68/2	226	85	070106	1707	BE	01	59.18	N	23	01.01	W	4324			
06ME68/2	226	85	070106	1739	BO	01	59.29	N	23	00.80	W	4323	1301	21	1.3.4.5.6.7.8
06ME68/2	226	85	070106	1817	EN	01	59.53	N	23	00.66	W	4323			
06ME68/2	227	86	070106	2059	BE	02	19.65	N	23	00.97	W	4270			
06ME68/2	227	86	070106	2130	BO	02	19.52	N	23	01.00	W	4258	1315	8	3.10
06ME68/2	227	86	070106	2204	EN	02	19.54	N	23	00.82	W	4237			
06ME68/2	228	87	070206	0048	BE	02	38.92	N	23	00.75	W	4823			
06ME68/2	228	87	070206	0120	BO	02	38.96	N	23	00.47	W	4819	1315	5	3
06ME68/2	228	87	070206	0152	EN	02	39.04	N	23	00.14	W	4798			
06ME68/2	229	88	070206	0425	BE	02	59.61	N	23	00.06	W	4642			
06ME68/2	229	88	070206	0500	BO	02	59.53	N	22	59.75	W	4642	1312	21	1.3.4.5.6.7.8.9
06ME68/2	229	88	070206	0540	EN	02	59.38	N	22	59.55	W	4647			
06ME68/2	230	89	070206	0906	BE	03	29.85	N	23	00.26	W	4379			
06ME68/2	230	89	070206	0938	BO	03	29.61	N	23	00.02	W	4371	1316	10	3.8
06ME68/2	230	89	070206	1012	EN	03	29.40	N	22	59.82	W	4369			
06ME68/2	231	90	070206	1335	BE	03	57.49	N	22	59.93	W	4217			
06ME68/2	231	90	070206	1404	BO	03	57.35	N	22	59.77	W	4217	1302	21	1.3.4.5.6.7.8
06ME68/2	231	90	070206	1438	EN	03	57.26	N	22	59.59	W	4219			
06ME68/2	232	91	070206	2234	BE	04	30.38	N	22	59.97	W	4115			
06ME68/2	232	91	070306	0000	BO	04	30.22	N	22	59.43	W	4105	4063	18	1.4.5.6.7.8.9.10
06ME68/2	232	91	070306	0151	EN	04	29.60	N	22	59.60	W	4134			
06ME68/2	233	92	070306	0517	BE	05	00.59	N	23	00.34	W	4214			
06ME68/2	233	92	070306	0549	BO	05	00.79	N	22	59.95	W	4208	1313	21	3.8.9
06ME68/2	233	92	070306	0628	EN	05	01.26	N	22	59.34	W	4210			
06ME68/2	234	93	070306	1455	BE	05	29.95	N	23	00.02	W	4231			
06ME68/2	234	93	070306	1525	BO	05	29.94	N	22	59.70	W	4231	1303	7	9.11
06ME68/2	234	93	070306	1556	EN	05	29.86	N	22	59.62	W	4231			
06ME68/2	235	94	070306	2002	BE	06	00.06	N	23	00.01	W	4092			
06ME68/2	235	94	070306	2033	BO	05	59.92	N	22	59.78	W	4099	1315	21	1.4.5.6.7.8.9
06ME68/2	235	94	070306	2110	EN	05	59.74	N	22	59.57	W	4101			
06ME68/2	236	95	070406	0035	BE	06	30.07	N	23	00.12	W	2935			
06ME68/2	236	95	070406	0106	BO	06	29.96	N	22	59.90	W	3119	1314	7	9
06ME68/2	236	95	070406	0138	EN	06	29.71	N	22	59.63	W	2940			
06ME68/2	237	96	070406	0458	BE	06	59.77	N	23	00.08	W	1516			
06ME68/2	237	96	070406	0530	BO	06	59.62	N	22	59.86	W	1452	1316	21	1.4.5.6.7.8
06ME68/2	237	96	070406	0609	EN	06	59.45	N	22	59.94	W	1497			
06ME68/2	238	97	070406	0945	BE	07	29.60	N	23	00.11	W	4390			

06ME68/2	238	97	070406	1017	BO	07	29.41	N	22	59.97	W	4385	1315	6	--
06ME68/2	238	97	070406	1045	EN	07	29.33	N	22	59.68	W	4367			
06ME68/2	239	98	070406	1420	BE	07	59.12	N	23	00.40	W	4422			
06ME68/2	239	98	070406	1450	BO	07	58.91	N	23	00.15	W	4417	1303	21	1.4.5.6.7.8.9.10
06ME68/2	239	98	070406	1527	EN	07	58.59	N	22	59.99	W	4407			
06ME68/2	240	99	070406	2135	BE	08	30.91	N	22	58.98	W	4776			
06ME68/2	240	99	070406	2208	BO	08	30.81	N	22	58.58	W	4777	1314	13	9
06ME68/2	240	99	070406	2238	EN	08	30.82	N	22	58.27	W	4778			
06ME68/2	241	100	070506	0123	BE	09	00.07	N	22	59.74	W	4898			
06ME68/2	241	100	070506	0154	BO	09	00.12	N	22	59.31	W	4894	1313	21	1.2.4.5.6.7.8.9
06ME68/2	241	100	070506	0234	EN	09	00.32	N	22	58.90	W	4898			
06ME68/2	242	101	070506	0601	BE	09	29.65	N	23	00.51	W	4623			
06ME68/2	242	101	070506	0632	BO	09	29.51	N	23	00.07	W	4658	1314	4	8
06ME68/2	242	101	070506	0700	EN	09	29.50	N	22	59.83	W	4673			
06ME68/2	243	102	070506	0958	BE	09	59.95	N	23	00.30	W	5069			
06ME68/2	243	102	070506	1141	BO	09	59.28	N	22	59.73	W	5113	5007	21	1.4.5.6.7.8.9.10
06ME68/2	243	102	070506	1355	EN	09	58.88	N	23	00.80	W	5145			
06ME68/2	244	103	070506	1736	BE	10	29.78	N	22	58.92	W	5186			
06ME68/2	244	103	070506	1807	BO	10	29.98	N	22	59.34	W	5187	1313	7	9
06ME68/2	244	103	070506	1837	EN	10	30.26	N	22	59.47	W	5187			
06ME68/2	245	104	070506	2125	BE	10	59.88	N	22	59.89	W	5146			
06ME68/2	245	104	070506	2157	BO	10	59.96	N	22	59.85	W	5149	1314	21	1.4.5.6.7.8.9.10.11
06ME68/2	245	104	070506	2235	EN	11	00.14	N	23	00.38	W	5149			
06ME68/2	246	105	070606	0205	BE	11	30.08	N	22	59.56	W	5114			
06ME68/2	246	105	070606	0237	BO	11	29.87	N	23	00.02	W	5114	1313	7	9
06ME68/2	246	105	070606	0312	EN	11	29.47	N	23	00.18	W	5115			
06ME68/2	247	106	070606	0603	BE	12	00.08	N	23	00.08	W	5046			
06ME68/2	247	106	070606	0635	BO	12	00.34	N	23	00.23	W	5047	1314	21	1.4.5.6.7.8
06ME68/2	247	106	070606	0711	EN	12	00.56	N	23	00.19	W	5044			
06ME68/2	248	107	070606	1040	BE	12	29.47	N	22	59.86	W	4920			
06ME68/2	248	107	070606	1112	BO	12	29.71	N	23	00.04	W	4917	1312	8	--
06ME68/2	248	107	070606	1145	EN	12	29.98	N	23	00.24	W	4916			
06ME68/2	249	108	070606	1442	BE	12	59.96	N	23	00.05	W	4741			
06ME68/2	249	108	070606	1515	BO	12	59.91	N	23	00.29	W	4739	1302	21	1.4.5.6.7.8.9.11
06ME68/2	249	108	070606	1555	EN	13	00.00	N	23	00.50	W	4737			
06ME68/2	250	109	070606	1941	BE	13	29.21	N	22	59.27	W	4541			
06ME68/2	250	109	070606	2011	BO	13	29.10	N	22	59.27	W	4539	1316	7	9.11
06ME68/2	250	109	070606	2041	EN	13	29.16	N	22	59.16	W	4539			
06ME68/2	251	110	070706	0103	BE	14	00.02	N	22	59.88	W	4322			
06ME68/2	251	110	070706	0135	BO	14	00.08	N	22	59.79	W	4322	1317	21	1.4.5.6.7.9.11
06ME68/2	251	110	070706	0216	EN	14	00.04	N	22	59.75	W	4317			
06ME68/2	252	111	070706	0513	BE	14	29.98	N	23	00.56	W	4088			
06ME68/2	252	111	070706	0545	BO	14	30.09	N	23	00.19	W	4087	1315	--	--
06ME68/2	252	111	070706	0611	EN	14	30.27	N	23	00.25	W	4085			
06ME68/2	253	112	070706	0915	BE	14	59.88	N	23	00.03	W	2672			
06ME68/2	253	112	070706	0948	BO	15	00.09	N	23	00.18	W	2709	1314	21	1.4.5.6.7
06ME68/2	253	112	070706	1027	EN	15	00.43	N	23	00.28	W	2759			
06ME68/2	254	113	070706	1215	BE	15	14.95	N	22	59.59	W	1334			
06ME68/2	254	113	070706	1241	BO	15	15.13	N	22	59.69	W	1315	1013	--	--
06ME68/2	254	113	070706	1302	EN	15	15.20	N	22	59.92	W	1209			
06ME68/2	254	114	070706	1308	BE	15	15.20	N	22	59.92	W	1172			
06ME68/2	254	114	070706	1328	BO	15	15.19	N	23	00.12	W		202	12	Fluorometer
06ME68/2	254	114	070706	1343	EN	15	15.22	N	23	00.19	W				calibration
06ME68/2	255	115	070806	0542	BE	17	35.45	N	24	14.63	W	3592			
06ME68/2	255	115	070806	0655	BO	17	35.97	N	24	14.92	W	3597	3553	21	1.2.4.5.6.7
06ME68/2	255	115	070806	0818	EN	17	36.74	N	24	15.10	W				

2.7 Acknowledgements

We very much appreciated the professionalism and seamanship of crew, officers and Captain of F.S. METEOR which made this work a success. Financial support came from the German Bundesministerium für Bildung, Wissenschaft und Forschung (BMBF) as part of the Verbundvorhaben Nordatlantik (Der Nordatlantik als Teil des Erdsystems: Vom System-Verständnis zur Analyse regionaler Auswirkungen, 03F0443B) and the Verbundvorhaben ARGO (Untersuchungen zu Zirkulation und Wassermassen-Anomalien mit profilierenden Floats im Tropischen Atlantik, ARGO-TROPAT, 03F0367A), and from the German Science Foundation (DFG) as part of the TROPAT (RAFOS) project (Circulation of the shallow subtropical-tropical cell of the Atlantic, SCHO 168/30-1) and the EMMY NOETHER project (Diapycnal mixing processes in the upwelling regions of the tropical Atlantic, DE 13691-1).

2.8 References

Brandt, P., Schott, F.A., Provost, C., Kartavtseff, A., Hormann, V., Bourles B., Fischer, J., 2006. Circulation in the central equatorial Atlantic: Mean and intraseasonal to seasonal variability. Geophys. Res. Lett., 33, L07609, doi:10.1029/2005GL025498.

Bullister, J.L., Weiss, R.F., 1988. Determination of CCl3F and CCl2F2 in seawater and air. Deep-Sea Res., Part I, 35(5): 839-853.

Grasshoff, K., 1999. Methods of Seawater Analysis. In: Grasshoff, K., Kremling, K., Ehrhardt, M. (eds.), Methods of Seawater Analysis. Wiley-VCH, pp 501-519.

Johnson, K., Willis, K.D., Butler, D.B., Johnson, W.K., Wong, C.S., 1993. Coulometric carbon dioxide analysis for marine studies: Maximizing the performance of an automated gas extraction system and coulometric detector. Mar. Chem., 44(2-4): 167-188.

Karstensen, J., Stramma, L., Visbeck, M., 2007. Oxygen minimum zones in the eastern tropical Atlantic and Pacific Oceans. Progr. Oceanogr. (in press).

Mintrop, L., Perez, F.F., Gonzalez-Davila, M., Santana-Casiano, J.M., Körtzinger, A., 2000. Alkalintiy determination by potentiometri: intercalibration using three different methods, Sci. Mar., 26(1): 23-37.

METEOR-Berichte 09-4

Circulation and Variability in the Tropical Atlantic

PART 3

Cruise No. 68, Leg 3

July 10 – August 6, 2006
Mindelo (Cape Verde) – Las Palmas de Gran Canaria (Spain)

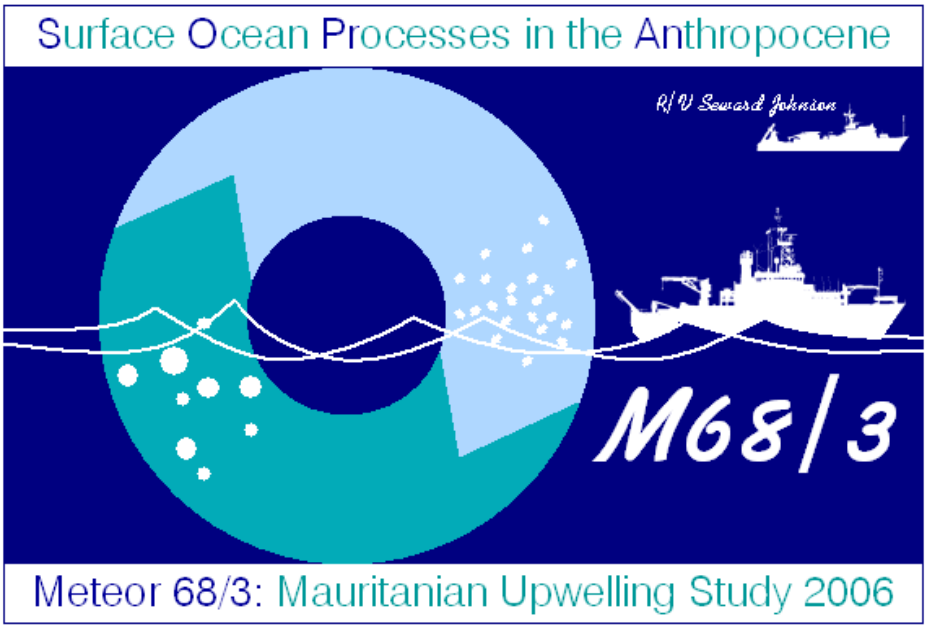

Arne Körtzinger, Christian Albers, Jan Aschmann, Alex Baker, Hermann Bange, Ilana Berman-Frank, Katrin Bluhm, Peter Croot, Thomas Custer, Daniel Franklin, Alina Freing, Sarah Gebhardt, Susann Grobe, Valerie Gros, Rebecca Langlois, Julie LaRoche, Orly Levitan, Gareth Lee, Rudi Link, Frank Malien, Manuela Martino, Kerstin Nachtigall, Gert Petrick, Stefanie Pröbst, Monika Rhein, Jens Schafstall, Christian Schlosser, Rob Sherrell, Tobias Steinhoff, Peter Streu, Stefano Taddei, Douglas Wallace, Eckart Zöllner

Table of Contents Part 3 (M68/3)

3.1 Participants

Name	Function	Institute
Körtzinger, Arne, Prof. Dr.	Chief Scientist	IFM-GEOMAR
Abed, Jemal Ould	Mauritanian Observer	IMROP
Albers, Christian	Halocarbon production	IFM-GEOMAR
Aschmann, Jan	Helium, CTD	UBU
Bange, Hermann, Dr.	N_2O, NH_2OH, CH_4	IFM-GEOMAR
Bluhm, Katrin	Biogenic trace gas production	IFM-GEOMAR
Croot, Peter, Dr.	Trace metals	IFM-GEOMAR
Custer, Thomas, Dr.	Atmospheric chemistry	MPI-CH
Franklin, Dan, Dr.	DMS	UEA
Freing, Alina	N_2O, NH_2OH, CH_4	IFM-GEOMAR
Gebhardt, Sarah	Atmospheric chemistry	MPI-CH
Grobe, Susann	Carbon cycle	IFM-GEOMAR
Gros, Valérie, Dr.	Atmospheric chemistry	LSCE
Langlois, Rebecca	Bioassay, nitrogen fixation	IFM-GEOMAR
Lee, Gareth	DMS	UEA
Levitan, Orly	Bioassay, nitrogen fixation	BIU
Link, Rudolf	CTD, microstructure	IFM-GEOMAR
Malien, Frank	Nutrients, O_2	IFM-GEOMAR
Martino, Manuela, Dr.	Iodinated compounds	UEA
Nachtigall, Kerstin	Nutrients, O_2	IFM-GEOMAR
Ochsenhirt, Werner	Meteorological technology	DWD
Peeken, Ilka, Dr.	Biogenic trace gas production	IFM-GEOMAR
Petrick, Gert	Halocarbons	IFM-GEOMAR
Pröbst, Stefanie	Bioassay, nitrogen fixation	IFM-GEOMAR
Schafstall, Jens	CTD, microstructure	IFM-GEOMAR
Schlosser, Christian	Trace metals	IFM-GEOMAR
Steinhoff, Tobias	Carbon cycle	IFM-GEOMAR
Streu, Peter	Trace metals	IFM-GEOMAR
Taddei, Stefano, Dr.	Micrometeorology	IBIMET-CNR
Zöllner, Eckart, Dr.	Biogenic trace gas production	IFM-GEOMAR

Participating Institutions

BIU	Bar Ilan University, The Mina & Everard Goodman Faculty of Life Sciences, Ramat Gan, 52900, Israel, e-mail: irfrank@mail.biu.ac.il
DWD	Deutscher Wetterdienst, Geschäftsfeld Seeschiffahrt, Bernhard-Nocht-Str. 76, 20359 Hamburg - Germany, e-mail: edmund.knuth@dwd.de
IBIMET-CNR	Istituto di Biometeorologia, Consiglio Nazionale delle Ricerche, Via Giovanni Caproni 8, 50145 Firenze, Italy, e-mail: s.taddei@lammamed.rete.toscana.it
IFM-GEOMAR	Leibniz-Institut für Meereswissenschaften, Düsternbrooker Weg 20, 24105 Kiel, Germany, e-mail: akoertzinger@ifm-geomar.de
IMROP	Institut Mauritanie des Recherches Océanographiques et de Pêches, B.P. 22, Nouadhibou, Mauritania, email: abderahmane05@yahoo.fr
LSCE	Laboratoire des Sciences du Climat et de l'Environnement, CNRS/CEA, Orme des Merisiers, 91191 Gif-sur-Yvette, France, e-mail: Valerie.Gros@cea.fr
MPI-CH	Max-Planck-Institut für Chemie, Abteilung Luftchemie, J.J.-Becher-Weg 27, 55128 Mainz, Germany, e-mail: williams@mpch-mainz.mpg.de
UBU	Universität Bremen, Institut für Umweltphysik, Otto-Hahn-Allee, NW1, 28334 Bremen, Germany, e-mail: mrhein@physik.uni-bremen.de
UEA	School of Environmental Sciences, University of East Anglia, Norwich NR4 7TJ, United Kingdom, e-mail: M.Martino@uea.ac.uk

3.2 Research Program

The third leg of METEOR cruise 68 was carried out in the programmatic frame of the international "Surface Ocean Lower Atmosphere Study" (SOLAS) and presents the 2nd major cruise of German SOLAS. It combined a wide spectrum of biological, chemical and physical oceanography as well as atmospheric chemistry under a regional focus on Cape Verdean waters and coastal upwelling off Mauritania. This region is characterized by important SOLAS-relevant phenomena and processes – most importantly atmospheric dust deposition and coastal upwelling – which have major influence on substances (iron, nutrients, CO_2, volatile oxygenated and halogenated organics) and processes (nitrogen fixation, ocean-atmosphere gas exchange). Upwelling regions in major dust deposition areas can be viewed as biogeochemical reactors which are fueled simultaneously by vertical supply of macro and micro nutrients from the mesopelagial below and the atmosphere above. At the same time, these regions provide means of ventilation of radiatively and chemically active trace gases (e.g., CO_2, nitrous oxide, bromoform) which are produced sub-surface. The resulting flux densities are larger than in the oligotrophic background waters.

More specifically the scientific program of the METEOR 68/3 cruise encompassed the following themes and questions:

- Hydrographic and microstructure measurements (hydrographic survey with regular CTD and ADCP measurements as well as measurements of turbulence and vertical mixing with free sinking micro-structure sensor);
- Carbon, oxygen and nutrients dynamics (air-sea CO_2 and O_2 fluxes in oligotrophic ocean vs. upwelling regimes, surface ocean carbon and nutrient dynamics in organic and inorganic, particulate and dissolved pools of recently upwelled waters);
- Production of organic trace gases using empirical and experimental approaches (role of sub-surface chlorophyll maximum, species- and light-dependence of production, role DOM/POM, bacterial production);
- Production of volatile organoiodine compounds (inorganic precursors, role of DOM/ enzymes, CDOM – Chromophoric Dissolved Organic Matter);
- Production of hydroxylamine, nitrous oxide and methane (formation pathways of hydroxylamine, air-sea fluxes of nitrous oxide and methane);
- Marine boundary layer photochemistry and aerosol formation (air-sea fluxes of oxygenated organic species, chemical/biological precursors/sources, importance for aerosol formation);
- Aerosol iodine chemistry (speciation of iodine in aerosol and rain, source of iodine associated with the Mauritanian upwelling);
- Trace metals (redox speciation, input via dust, iron solubility);
- Nitrogen fixation and nutrient limitations (contribution of the different diazotrophic groups to total community nitrogen fixation, limiting nutrient for nitrogen fixation, response of various diazotrophic groups to nutrient and Saharan dust amendments).

3.3 Narrative of the Cruise

The scientific party for cruise 68/3 embarked the RV METEOR in the port of Mindelo on São Vicente in the morning of July 10. That day a total of six 20' containers had to be loaded to the ship. These included three containers packed with equipment as well as three laboratory containers (one air chemistry container from the MPI in Mainz and two cleanlab containers from Germany and UK) which had to be placed at their planned positions on the main working deck and the forecastle, respectively. The placement of the heavy (12 t) air chemistry container of the Max-Planck Institute for Chemistry by a floating harbor crane to its desired position turned out unsafe due to adverse wind conditions and had to be cancelled. Therefore a second approach had to be made on the following day by a shore-based mobile crane. For this reason, however, the RV METEOR had to change position and berth with its portside.

RV METEOR left the pier on July 12 at 9:00L and anchored in the bay of Mindelo to provide the atmospheric working group with some more time for installation of their large amount of equipment in a seaworthy manner. The one-day delay in loading of the group's laboratory container had made this decision necessary. At 17:00L RV METEOR finally "set sails" and

steamed towards to westernmost station of a hydrographic transect at 18°N which continued until July 21 (see cruise track in Fig. 3.1).

The 18°N hydrographic section extended from 27°W eastwards and concluded at 16°16.4'W in shallow waters of about 39 m depth off Mauritania. Stations were carried out at 1/2°-spacing (with the omission of 26.5°W) and included a short southward excursion to the newly established Cape Verdean Time Series site at 17°35.4'N/24°15.1'W. Station were spaced more densely at about 5' distances above the shelf break. Normal CTD/LADCP profiles extended down to 1000 m depth (or just above seafloor if shallower than 1000 m), with water sampling performed only in the upper 600 m of the water column. At six stations (stations 257, 261, 264, 268, 272, 276) full water depth hydrocasts were carried out.

Station programs varied slightly during the cruise depending on the various groups' working loads but typically started with a 1000 m CTD cast with water samples taken in the upper 600 m only. Often a second CTD cast of the upper 200 m was carried out to provide higher vertical resolution as well as larger water volumes required for biological analyses. Microstructure profiles were made frequently with a strong focus on the shelf and shelf break region. A typical microstructure station consisted of three profiles taken consecutively at the same station. Roughly every second to third station phytoplankton and/or zooplankton net hauls were done. At nine stations additional GoFlo casts (4 samplers at standard depths of 20, 40, 60, and 80 m) were carried out for trace-metal clean seawater sampling (dissolved and particulate trace metals, iron solubility and dissolution experiments).

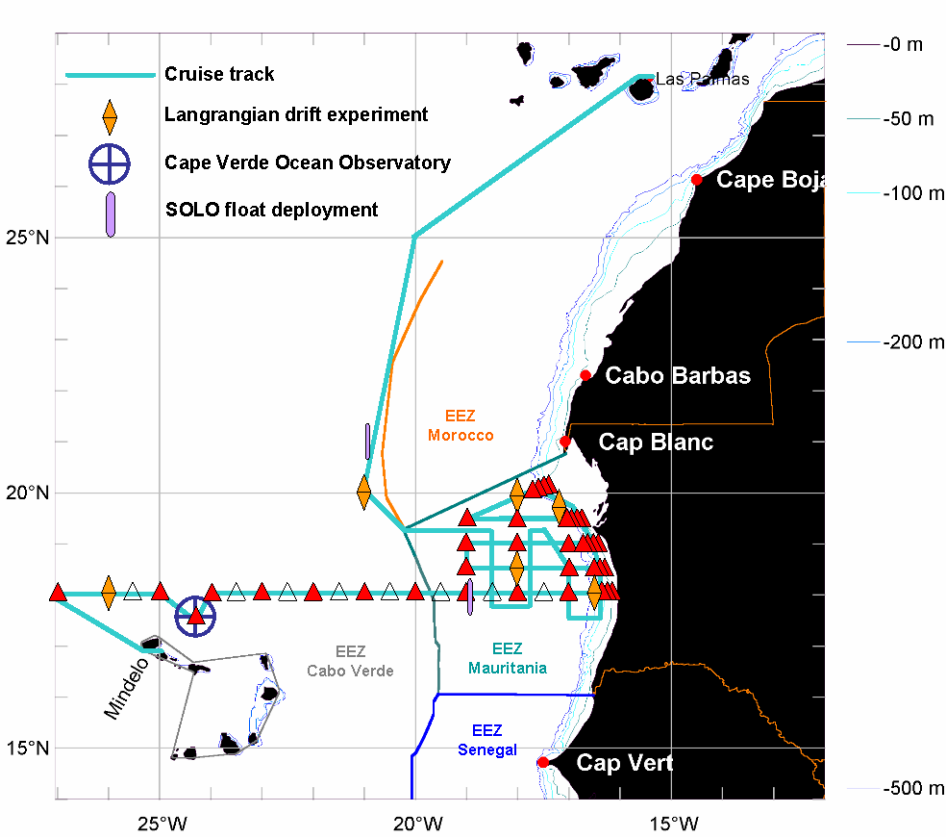

Fig. 3.1 Cruise track of the RV METEOR cruise 68/3 from Mindelo/Cape Verde to Las Palmas de Gran Canaria/Spain (July 10 – August 6, 2006). Shown are locations of hydrographic stations incl. 24h Lagrangian drift stations, the site of the Cape Verde Ocean Observatory, and the deployment sites of two profiling drifters from NOAA/AOML, Physical Oceanography Department in Miami, Florida, USA

After completion of the long 18°N section, four shorter zonal sections (~2° in longitude) were carried out at 18.5°N, 19°N, 19.5°N, and ~20°N. The station program on these sections was similar to the one described above.

Measurements performed on water samples drawn from CTD Niskin bottles generally included the following parameters (list not exhaustive):

- Salinity
- Helium
- SF_6
- Nutrients (Nitrate, nitrite, phosphate, silicate)
- Dissolved oxygen
- Dissolved inorganic carbon (DIC)
- Total alkalinity
- Dissolved organic carbon and nitrogen (DOC/DON)
- Particulate organic carbon and nitrogen (POC/PON)
- δ^{13}C-POC, δ^{15}N-PON
- Chromophoric dissolved organic matter (CDOM)
- Nitrous oxide (N_2O)
- Hydroxylamine (NH_2OH)
- Dimethylsulphide (DMS), Dimethylsulphoniopropionate ($DMSP_{p/d}$)
- Hydrogenperoxide (H_2O_2)
- Trace metals
- Iodide, iodate
- Coccolithophorid species abundance
- Diazotroph abundance and activity
- Photosynthetic kinetic parameters (FRRF - Fast repletion rate fluorometry)
- Photosynthetic efficiency (PhytoPAM)
- Phytoplankton pigments
- Flow cytometry (bacteria, pico- and nanoplankton)
- Utermöhl (microphyto- and zooplankton)
- Bacterial community composition (CARD-FISH)
- Bacterial activity (^{3}H-leucine uptake)
- Primary production (^{14}C uptake)

In order to better resolve enhanced turbulence and mixing on the shelf and near the shelf break, two dedicated microstructure transects were carried out (Transect I: 20°15'N/17°44'W–20°23'N/17°32'W; Transect II: 18°11'N/16°34'W–18°11'N/ 16°24'W). Along these two transects microstructure profiles were acquired continuously at low ship speed (approx. 1.5 kn) for about 7 h each.

A special focus of this cruise was to study diel cycles of biological, chemical and physical properties in surface waters of various biogeochemical settings. For this purpose six 24 h drift stations (258, 277, 286, 299, 304, 311) were performed. At the beginning of each station a patch of surface water was marked by co-located deployment of two Lagrangian drifters: (1) a surface buoy with radar reflector, radio beacon, flash light and flag that carried one or two sample bottle wheels for in situ incubation of quartz bottles at depths of 5 m and/or 20 m, and (2) a surface drifter of the Surface Velocity Program (SVP) with Argos transmitter, thermistor, and holy sock drogue (Table 3.7, section 3.5). RV METEOR followed the surface drifter (1) by optical, radar and radio means for 24 h. Tracking of the SVP drifter by means of a Gonio Argos receiver turned out to be impractical. The estimated directions and intensities of the intercepted Argos messages (90 s interval) were by far not precise enough for tracking purposes. A post-experiment comparison of the drifter trajectories revealed that the two drifters showed rather similar drift behavior during the course of the experiment. It can therefore be assumed that drifter (1) at which all station work was carried out showed near-Lagrangian drift characteristic. The distances covered during the 24 h drift experiment varied from 7 to 27 nm which corresponds to average drifter speeds of 0.3 to 1.1 kts. The two drifters stayed within a distance of 1 to 8 nm whereby the Argos positions of SVP drifter are associated with significantly larger error of sometimes up to 1 nm or more.

A typical sampling schedule of CTD casts (e.g. at 0:00, 6:00, 12:00, 18:00, 24:00 LT), underway sampling and microstructure profiles (e.g. every 3 h) was carried out as close as possible to the drifter (typically 2-4 cables). At the end of each 24 h drift station the surface-tethered incubation drifter was recovered. The SVP drifters were not recovered since they are an official component of the Surface Velocity Program provided by the Physical Oceanography Division of the NOAA/AOML in Miami/FL, USA (Fig. 3.2).

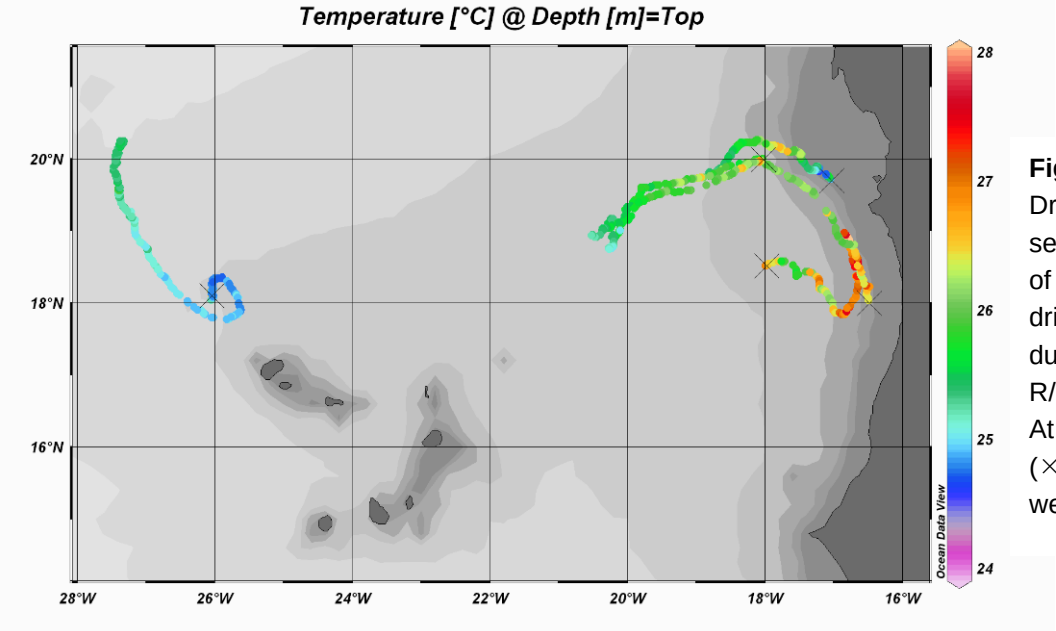

Fig. 3.2
Drift track and measured sea surface temperature of five SVP surface drifters as observed during the course of the R/V METEOR cruise 68/3. At the deployment sites (×) 24 h drift experiments were carried out

During the entire cruise surface seawater was sampled by means of a submersible pump installed in the ship's moon pool. A small CTD probe installed next to the intake provided measurements of surface seawater salinity and temperature. The pumped seawater was used for:

- Continuous pCO_2 measurements using a classical flow-through headspace equilibrator system with NDIR CO_2 detection;
- Continuous pCO_2 measurements using a novel submersible sensor with membrane equilibrator and NDIR CO_2 detection (by Pro-Oceanus Inc., Halifax/Canada);
- Continuous O_2 measurements using a novel oxygen optode (by Aanderaa Instruments, Bergen/Norway);
- Continuous total gas tension measurements using a GTD pro gas tension sensor (by Pro-Oceanus Inc., Halifax/Canada);
- Continuous chlorophyll measurements using a submersible MiniTracka fluorescence sensor (Chelsea Instruments, UK);
- Continuous N_2O measurements using a headspace equilibrator with subsequent GC-ECD detection;
- Discrete sampling for other parameters (e.g. nutrients, DIC, total alkalinity, CDOM, chlorophyll, various biological parameters etc.).

Trace-metal clean surface water sampling was accomplished with a tow fish that was lowered into the water by the auxiliary crane on starboard side aft. Seawater was sampled with an all-teflon membrane pump while the ship was steaming. The pumped seawater was used for trace metal analysis (particularly iron) and for the bioassay work.

A major work component of the biological working groups were a number of dedicated incubation experiments. For this purpose several types of incubators were installed on the working deck and on the forecastle. All incubation devices were fed with large flow rates of surface seawater (through fire extinguishing pumps) to ensure thermostating to near SST and provided with shades for simulation of different light levels. Incubation experiments were performed on the following aspects:

- Long-term (10-day) dark experiments to investigate impact of heterotrophic communities on biogenic trace gas production (jointly with atmospheric working group);
- Possible pathways of biogenic production of iodine and iodinated compounds;
- Impact of variable plankton communities and light intensities on production of inorganic and organic trace gases (jointly with atmospheric working group);
- Bioassays to assess the limitation of nutrients (ammonia, nitrate, phosphate, iron, dust, DOC) under ambient and elevated pCO_2 levels.

In situ light incubations for production of halogenated organic compounds were executed with free-drifting, surface-tethered incubation wheels deployed at 24 h drift stations (see description of 24 h drift stations above).

The RV METEOR Cruise 68/3 also carried a significant atmospheric program which included the following major components:

- Daily size-segregated aerosol sampling for analysis of major ions, soluble nutrient species (Fe, N, P, Si), and iodine species;
- Analysis of headspace samples from various incubation experiments for CO, non-methane hydrocarbons, volatile oxygenated organics, and volatile halocarbons (together with biological group);
- Micrometeorological measurements of air-sea fluxes (DEC – Disjunct Eddy Covariance, VDEC – Virtual Disjunct Eddy Covariance, REA – Relaxed Eddy Accumulation) with online PTR-MS detection (Proton Transfer Reaction Mass Spectrometry) or cartridge sampling;
- GC-MS measurements of mixing ratios of halogenated compounds in air (CH_3Cl, CH_3Br, CH_3I);
- Aethelometer measurements of black carbon;
- Radon measurements with thorium-daughter detection system;
- GC-FIC measurements of methane.

During the RV METEOR Cruise 68/3 two SOLO profiling floats were deployed on behalf of Robert J. Roddy from NOAA/AOML, Physical Oceanography Department in Miami, FL 33149 (Table 3.8, section 3.5).

Due to perfect performance of the CTD-rosette system and the winches, the planned station program of RV METEOR Cruise 68/3 was overachieved. No down-time due to technical problems or bad weather had to be accommodated in the work program. Groups brought home a rich data harvest and mostly achieved their work plans. Only a few technical problems with instrumentation caused significant and in one case fatal damage (see section 3.4.5.1) to scientific components of the M68/3 undertaking. Overall the mission has been very successful and extremely pleasant.

RV METEOR reached Las Palmas de Gran Canaria in the early morning of August 6 (08:00L) and the usual container packing chaos quickly unfolded. The scientific party disembarked in the afternoon.

3.4 Group Reports with Preliminary Results

3.4.1 Hydrographic Measurements

(Jens Schafstall, Rudi Link, Jan Aschmann)

3.4.1.1 CTD/O_2 Measurements

In total, 96 CTD profiles were sampled during cruise M68/3 (Table 3.3, section 3.5). The CTD-system used during the cruise was a Seabird SBE 9plus (Seabird Electronics Inc., Bellevue, Washington, USA). The IFM-GEOMAR Kiel SBE-2 with the serial number 09p24785-0612 was

used (same as during the previous cruise). Connected was a pressure sensor (s/n 80024). Two independent sets of temperature, conductivity and oxygen sensors were used. The sensors of the primary set were a temperature sensor (s/n 2826), a conductivity sensor (s/n 2512) and an oxygen sensor, a Seabird SBE-43 sensor (s/n 0194) recording oxygen voltage but no oxygen temperature, as was the case with the former Beckman oxygen sensors. The secondary set of sensors was a temperature sensor (s/n 4547), a conductivity sensor (s/n 2859) and an oxygen sensor (s/n 0992). Also a fluorescence (chlorophyll a) sensor and a light sensor were attached to the CTD but both are not yet calibrated. A second Seabird CTD, IFM-GEOMAR SBE-4, was available as backup system but did not need to be not used.

Routinely CTD casts were made during our section along 18°N from Cape Verde to the Mauritanian coast every 0.5° from surface to about 1300 m depth with the exception of five deep stations, where the CTD went down to the seafloor. During our work in the Mauritanian coastal area usual CTD casts reached down to about 1000 m depth or to the bottom in shallower waters. At all six 24 h drift stations CTD profiles were taken every 4-6 h to a depth of 200 m.

The Seabird bottle release unit used with the rosette connected to the Seabird instrument worked properly and reliable except for about 5 times, when a bottle was not closed or obviously closed at a wrong depth. For conductivity calibration purposes about 100 water samples were taken from the rosette bottles manly at our deep stations. Bottle salinities were determined with a Guildline (Guildline Instruments Inc, Smith Falls, Canada) Autosal salinometer. But until now we only used the calibration coefficients from the previous cruise M68/2 and checked these values with our samples, which showed no drift.

3.4.1.2 Microstructure Measurements

In total, 210 microstructure profiles were sampled during cruise M68/3 at 37 stations, normally 3 profiles per station (Table 3.4, section 3.5). In addition to the regular microstructure profiles at CTD stations we sampled two dedicated microstructure transects onto the shelf. The microstructure profiling system (MSS) used during the cruise was manufactured by ISW-Messtechnik in collaboration with Sea and Sun Technology (Trappenkamp, Germany) and consists of a profiler, a winch and a data interface. The profiler can operate 16 channels at a very high data transmission rate (1024 Hz) that is sufficient to resolve the small vertical scales of turbulent dissipation in the ocean. It is equipped with two shear sensors (airfoil, 4 ms response time), a fast-responding temperature sensor (microthermistor FP07, 12 ms response time), an acceleration sensor, a fast conductivity sensor and typical conductivity, temperature, depths sensors that sample at a lower frequency (24 Hz). In addition we used an oxygen sensor. For details about the sensor instrumentation see Table 3.1.

Table 3.1 Sensors used with the MSS system during R/V METEOR cruise M68/3

Sensor	Type	Response time	Serial number
Temperature	PT100	40 ms	
Conductivity	ADM	40 ms	
Pressure	PA-50 Progress	40 ms	
Oxygen	Oxyguard	??	DO522M18
Acceleration	ACC	4 ms	8023
Shear	Airfoil	4 ms	6052
Shear	Airfoil	4 ms	6054
Shear	Airfoil	4 ms	6061
Shear	Airfoil	4 ms	6064
Temperature	NTC; FP07	12 ms	38
Conductivity	Microstructure C-sensor	4 ms	13

The free-falling profiler is optimized to sink at a rate of about 0.6 m s^{-1} and is capable of measuring microstructure up to a depth of 500 m. Routinely MSS casts were made form surface to about a depth of 250-300 m (or to the ground if shallower). Shear and temperature fluctuations recorded due to vibration of the profiler while sinking can be diagnosed from the spectra of the acceleration sensor time series. In total four shear probes (s/n 6052, 6054, 6061, 6064 marked in table 3.3, section 3.5) were used, but only shear probes 6052 and 6064 worked well, so after station 258 they were used for the rest of the cruise. A second FP07 fast thermistor was available as backup, but was not used. During our second MSS-transect between station 305 and 306 data transmission broke down and we had to repair the transmission cable. Overall all parts off our equipment worked well throughout the cruise.

3.4.1.3 ADCP Current Measurements

During the cruise we used two vessel-mounted Acoustic Doppler Current Profilers (VM-ADCP, RDI Ocean Surveyor). Data collection was started on July 13 and ended on August 4 upon entering the Spanish EEZ. One unit (75 kHz, OS75) is permanently installed in the METEOR's hull, the second unit (38 kHz, OS38) was lowered into the moon pool located in mid-ship and fixed hydraulically. Both units worked in narrowband mode, delivering current velocity to depths of up to 750 m (OS75) and 1500 m (OS38). We detected no interferences with the various acoustic devices on board with the exception of the Doppler-Log (78 kHz) which drastically reduced the depth range of Ocean Surveyor 75 to about 200 meters. The Doppler-Log's use was therefore confined to the situations when its use was required for safety reasons during activities near the coast of Mauritania. For more details about data collection and navigation informations as well as post processing see the report of the cruise M68/2. Water track calibration for OS75 led to a standard deviation for misalignment angle of 0.62° and for amplitude factor of 0.015 calculated for 5 min ensembles.

Until now, we only used data from the Ocean Surveyor 75 which had adequate depth range and the higher vertical resolution with 8 m bin size compared to the 38 kHz ADCP which worked with a bin size of 16 m.

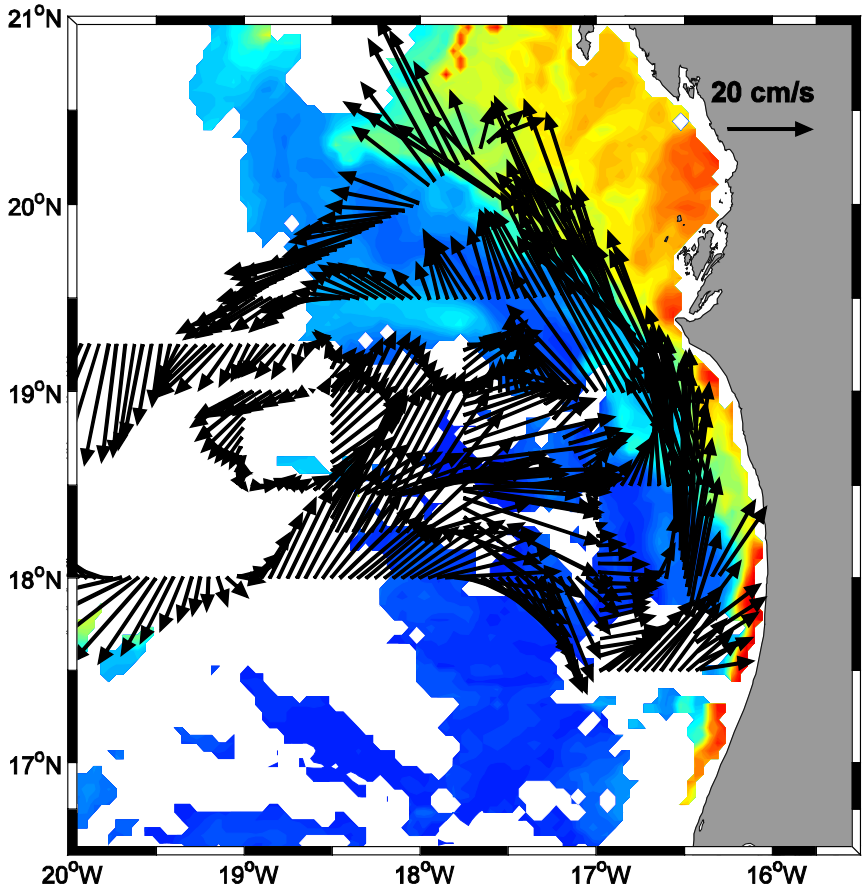

Fig. 3.3
Vectors of vertical mean velocity derived from ADCP bins 2 to 7 (around 20-70 m) of Ocean Surveyor 75. Color code indicates primary production by unscaled surface chlorophyll concentration as observed by the MODIS satellite between July 12 and August 12, 2006

Preliminary Results

The ocean surveyor data were mapped on a regular grid, using a Gaussian weighted interpolation scheme. Two preliminary results are described below:

(1) The near surface flow field is shown by vectors representing vertical mean velocities over a depth range from 20 to 70 m superimposed on a composite of four one-week chlorophyll satellite images taken by the MODIS satellite[1] (Fig. 3.3). The velocity field shows a cyclonic rotation tendency with a strong northward flow near and on the shelf with maximum velocity up to 50 cm s^{-1}. Chlorophyll concentrations associated with primary production driven by upwelling in general are small in the coastal area off Mauritania during this season. Highest values are observed north of 19.5°N and within a rather narrow band along the coast.

(2) Along the 18°N section (27°W to 16.25°W) 23 CTD-stations (marked by ticks at top of Fig. 3.4) were taken at a spacing of 0.5° with a higher resolution closer to the coast. The velocity observed by OS75 shows some eddy like structure within the upper 600 m which are manly in geostrophic balance. These eddies are related to velocity fluctuations with amplitudes up to 30 cm s^{-1} close to the surface. In total the velocity field results in a northward transport of around 4.5 Sv across this section between 27°W and the coast above the σ_θ = 27.2 kg m^{-3} isopycnal.

[1] http://www.marine.csiro.au/dods-data/ocean_colour/modis/global/8_day/

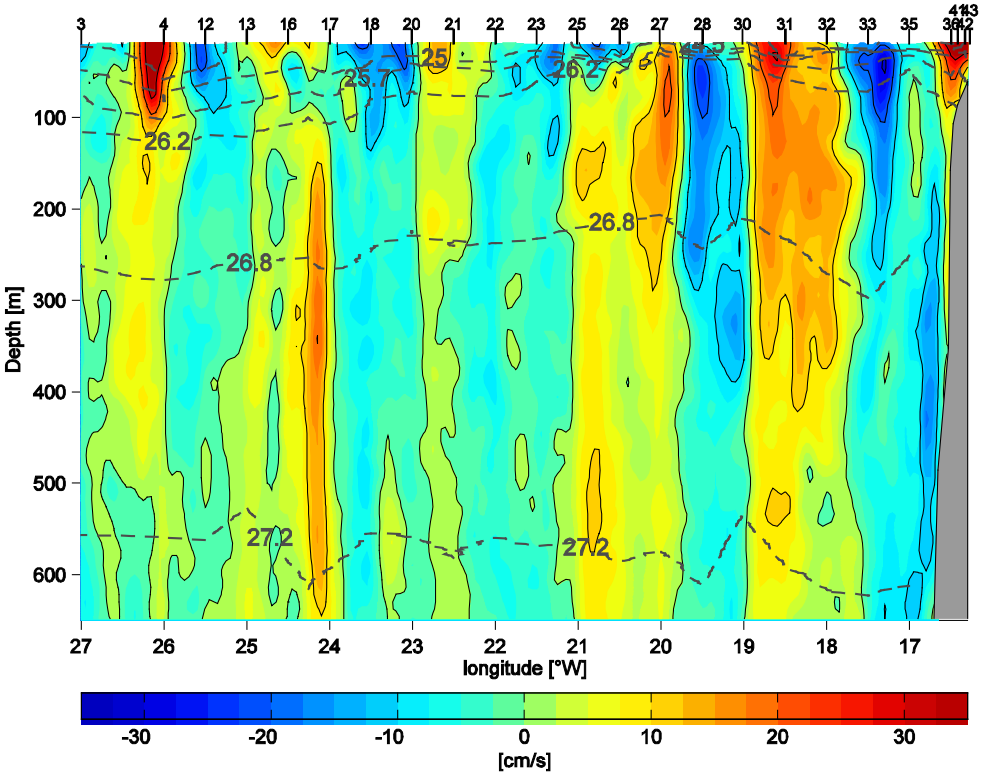

Fig. 3.4
Meridional velocity (cm s^{-1})] along 18°N from Ocean Surveyor 75 (contour interval 10 cm s^{-1}). Marked are isopycnals σ_θ = 24.5, σ_θ = 25, σ_θ = 25.7, σ_θ = 26.8 and σ_θ = 27.2 kg m^{-3} (gray dashed lines). Also shown are the locations of the related CTD casts

3.4.2 Carbon and Nutrients Dynamics

(Tobias Steinhoff, Susann Grobe, Frank Malien, Kerstin Nachtigall, Arne Körtzinger)

Upwelling areas are known to be biochemical reactors and the special emphasis of this project was to investigate the dynamics of inorganic and organic carbon, oxygen and nutrients in the Mauritanian upwelling in contrast to the oligotrophic parts. During cruise M68/3 we performed discrete shipboard analyses of nutrients (nitrate, nitrite, phosphate and silicate), dissolved oxygen, and the inorganic carbon parameters DIC (dissolved organic carbon) and A_T (total alkalinity). Furthermore we sampled TOC/TN (total organic carbon/total nitrogen) for shore-based analysis after the cruise. In addition we operated a number of continuous measurement systems that were run on a constant seawater supply from a submersible pump that was installed in the ships moon pool (~5 m depth). The parameters measured continuously in surface waters are dissolved oxygen (optode), chlorophyll (fluorescence), total gas tension (i.e. sum of partial pressures of all dissolved gases) and partial pressure of CO_2 (pCO_2, two independent methods).

Sampling

Oxygen: Samples were taken in 100 mL glass bottles with glass stoppers. After the bottles were carefully rinsed they were filled to the top and 1 mL $MgCl_2$ and 1 mL KI/KOH solution were added. The bottles were closed and then shaken for approximately one minute and immediately measured once all the samples were taken. Oxygen was analyzed on 941 Niskin bottles from 84 CTD casts.

Nutrient samples: The water for the nutrient analyses was sampled in PE bottles with screw caps. The bottles were rinsed twice and then filled. Nutrients (nitrate, nitrite, phosphate, silicate) were determined in 1002 samples from 84 CTD casts. Also 160 samples were analyzed from several experiments on board (89 samples for the Bioassay-Group, 40 samples for Katrin Bluhm, 18 samples for Eckart Zöllner and 13 underway samples).

DIC/A_T: Samples for the measurements of CO_2 parameters were collected in 500 mL glass bottles with glass stoppers. A short drawing tube was used to fill the bottles from the bottom to the top. The bottles were rinsed with approximately 100 mL and were filled up and overflown by approximately 250 mL. A headspace of about 1 % of sampling volume was achieved by clamping and removing the tube. After closing the bottle the stopper was held down firmly with a rubber band. All samples were analyzed within 24 h of collection. A total of 696 DIC samples and 689 alkalinity samples from 58 casts were analyzed. In addition 40 samples from the underway line were analyzed.

TOC/TN: 24 mL quartz vials were used to take the TOC/TN samples. The vials were carefully cleaned and ashed (450°C, at least 8 h) and the screw caps were cleaned with 2 % DECON® solution, 10 % HCl solution and carefully rinsed with MilliQ water. After drying the caps were screwed on the vials and stored in plastic bags for sampling. The samples were drawn from the Niskin bottles by freefall into the vial without rinsing. After sampling, the vials were immediately stored around -20°C for shorebased analysis.

Discrete Measurements

Oxygen and Nutrients: Oxygen samples were analyzed by standard Winkler-titration. Nutrient analyses were made with a Continuous-Flow-Autoanalyzer-(CFA). The system was developed and built at IfM-GEOMAR Kiel according to standard wet-chemical protocols. For the determination of phosphate the method from the manufacturer Bran + Luebbe was used.

DIC: The DIC analyses were made using a CO_2 extraction with coulometric titration employing the SOMMA system (single operator multi-parameter metabolic analyzer) according to Johnson et al. (1993). The SOMMA collects and dispenses an accurately known volume of seawater to a stripping chamber, acidifies it, sparges the CO_2 from the solution, dries the gas, and delivers it to a coulometer cell, where the CO_2 reacts with the solution and builds an acid that is titrated with OH ions produced in situ electrochemically.

Total Alkalinity: A_T was determined by titration of seawater with a strong acid, following the EMF of a proton sensitive electrode. The titration curve shows two inflection points, characterizing the protonation of carbonate and bicarbonate, respectively. The acid consumption up to the second point is equal to the A_T. Measurements were made with a semi-automatic analyzer, the VINDTA instrument (Versatile Instrument for the Determination of Titration Alkalinity, Mintrop et al., 2000). It consists of two parts: the titration cell with its manifold for filling, draining and acid delivery and the data acquisition and system control unit.

TOC/TN: TOC is determined by shorebased analysis with the High Temperature Catalytic Oxygen method (HTCO) using a Shimadzu TOC-VCSN instrument. After acidification of the sample for removal of inorganic carbon, 150 µL are injected on a heated column (720°C) filled with a catalyst (2 % Pt on Al_2O_3). All organic carbon is converted to CO_2 which is measured

with a non-dispersive infrared gas detector (NDIR). Whilst inside the catalyst column all nitrogen is converted to NO-radicals. After the sample gas has passed the NDIR cell it is transferred in the TN unit, where the NO-radicals react with ozone to excited NO_2. Falling back to their initial state, the excited NO_2 molecules emit light that can be measured. The measurements are currently underway.

Underway Measurements

CO_2 partial pressure: An automated underway pCO_2 system with an NDIR CO_2 detector was operated continuously during the cruise. A continuous flow of seawater was drawn at ~5 m depth from the ship's moon pool which was equipped with a CTD. Every minute a pCO_2 data point together with temperature and salinity from the CTD was logged along with the position data from an independent GPS system.

Furthermore we used a newly developed sub-surface pCO_2 sensor (PSI CO_2 Pro, Pro-Oceanus Systems Inc., Halifax, Canada) which features an NDIR detector and a pump-driven fast interface (patent pending), that provides an equilibrated gas sample to the detector. The sensor was installed inside a cooling box that was flushed with seawater from the pump installed in the ship's moon pool.

Oxygen: Dissolved Oxygen was determined via an optode sensor (Aanderaa Instruments AS, Bergen, Norway). This technique is based on dynamic luminescence quenching. The optode was also installed inside the water bath. Underway oxygen data were calibrated against oxygen values determined from the Niskin bottles by Winkler titration.

Total Gas Tension: The PSI GTD Pro sensor (Pro-Oceanus Systems Inc., Halifax, Canada) was used to measure the sum of the partial pressure of all dissolved gases. A small sample volume of air is equilibrated to all dissolved gases in the water through a special membrane. The GTD was also installed in the water bath.

Chlorophyll: We also installed a chlorophyll fluorescence sensor (MiniTracka, Chelsea Instruments, UK) in the surface water pumping system. Chlorophyll data are not yet calibrated.

Nearly 30,000 concurrent measurements of seawater and atmospheric pCO_2, oxygen, gas tension, SST and SSS were made during the cruise. The pCO_2 data were processed following the recommendations of a data reduction workshop in 2005. Atmospheric pCO_2 data were interpolated to calculate the sea-air pCO_2 difference (here given as ΔfCO_2).

Preliminary Results

Duplicate oxygen samples, that were taken and analyzed at 15 stations, yielded a precision ($\pm\sigma$) of 0.18 ± 0.18 µmol kg^{-1}. For DIC/A_T typically one duplicate was measured per station (Fig. 3.5). Also Certified Reference Material (CRM) provided by Andrew Dickson from the Scripps Institution of Oceanography was measured twice per station. The mean offset from CRM values was -1.41 ± 1.34 µmol kg^{-1} for DIC and -0.72 ± 1.73 µmol kg^{-1} for alkalinity (Fig. 3.6). The precision based on duplicate measurements was 0.63 ± 0.50 µmol kg^{-1} for DIC and 1.56 ± 1.44 µmol kg^{-1} for alkalinity. Final corrected DIC and A_T data are available.

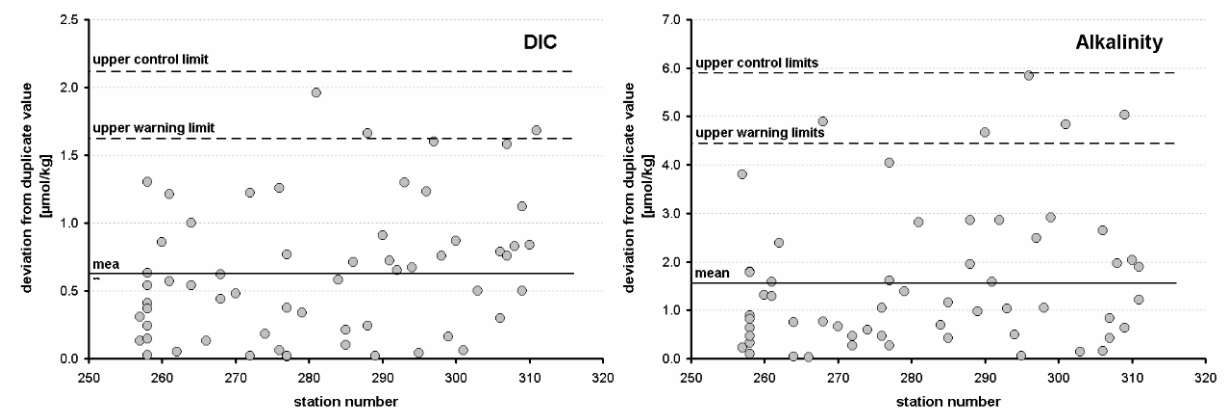

Fig. 3.5 Control charts from measurements of duplicate samples of DIC and alkalinity. Warning and control limits are in accordance with the DOE Handbook (1994)

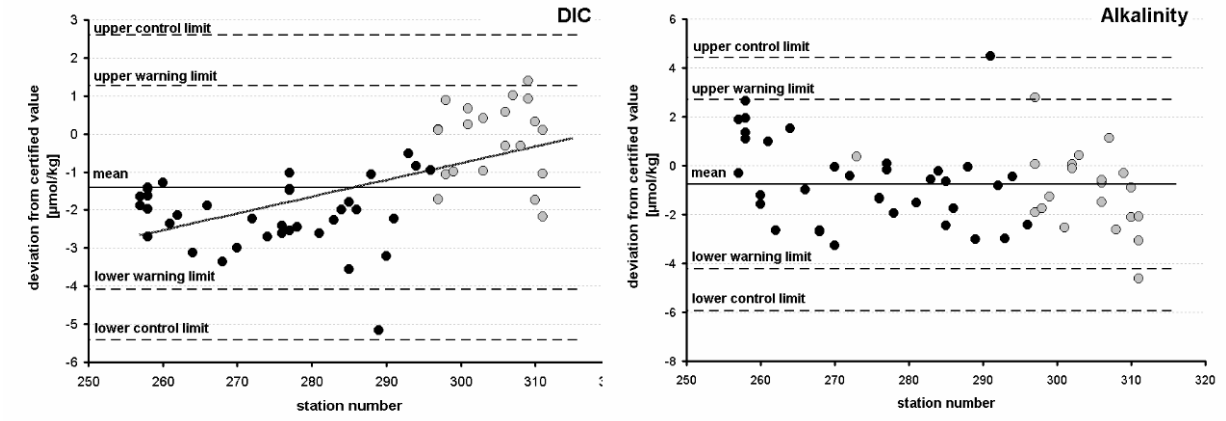

Fig. 3.6 Control charts based on measurements of Certified Reference Material (CRM) for DIC (left) and total alkalinity (right). Two different CRM batches that were used during this cruise (grey: batch 68; black: batch 74). Also shown are warning and control limits as defined in the DOE (1994). A slight drift in DIC measurements was observed. Data were corrected for the observed offsets

Fig. 3.7 provides examples of underway measurements along the coast of Mauritania. We only encountered freshly upwelled waters at the northern end of this section (marked in red), which is indicated by the low SST, high ΔfCO_2 and very low oxygen saturation (and hence gas tension) in this area. The low chlorophyll values show that the biological productivity had not yet started which points at very recent upwelling. In contrast a few kilometers further south we observed a very productive area (marked in blue) which also showed the signatures of upwelling. The SST was still lower than ambient. Due to biological production as evidenced by high chlorophyll values we found much smaller ΔfCO_2 values combined with oxygen supersaturation (and high total gas tension).

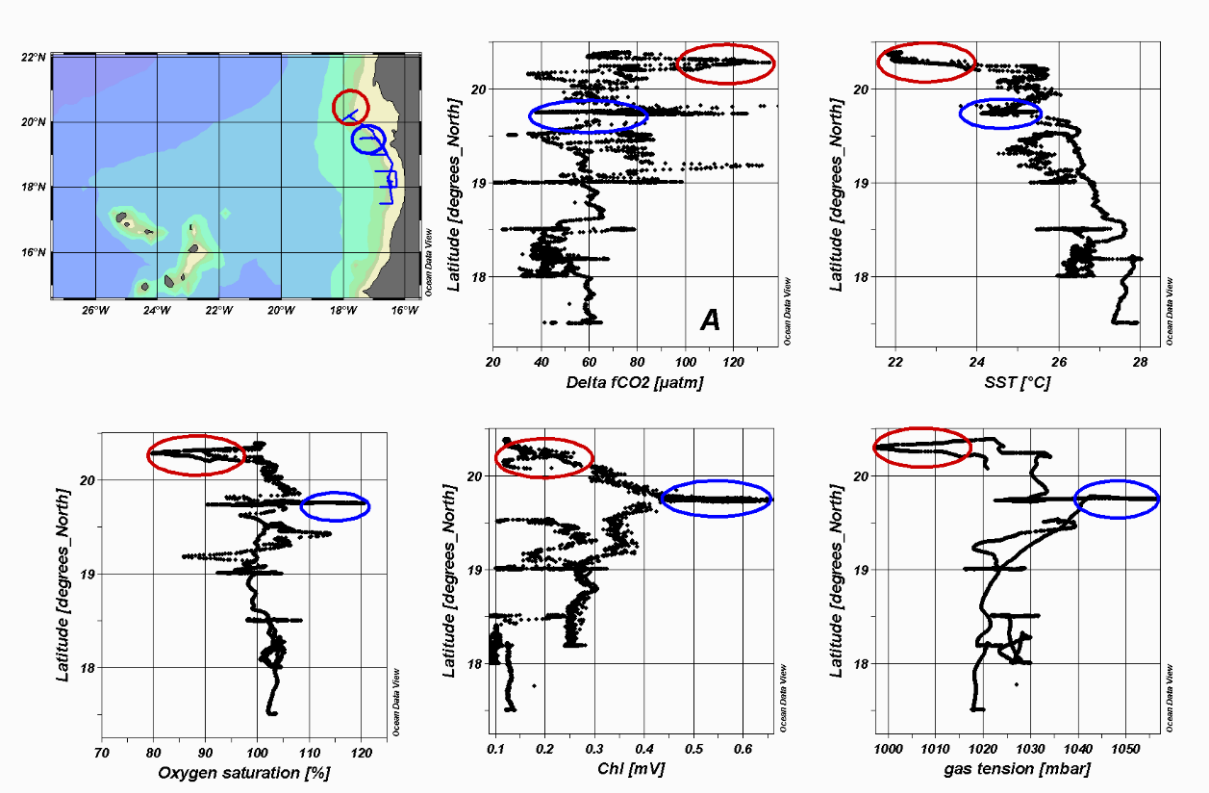

Fig. 3.7 Underway measurements along the Mauritanian coast. Red ellipse denotes area of fresh upwelled water; blue ellipse denotes area of high biological productivity (drift station 406)

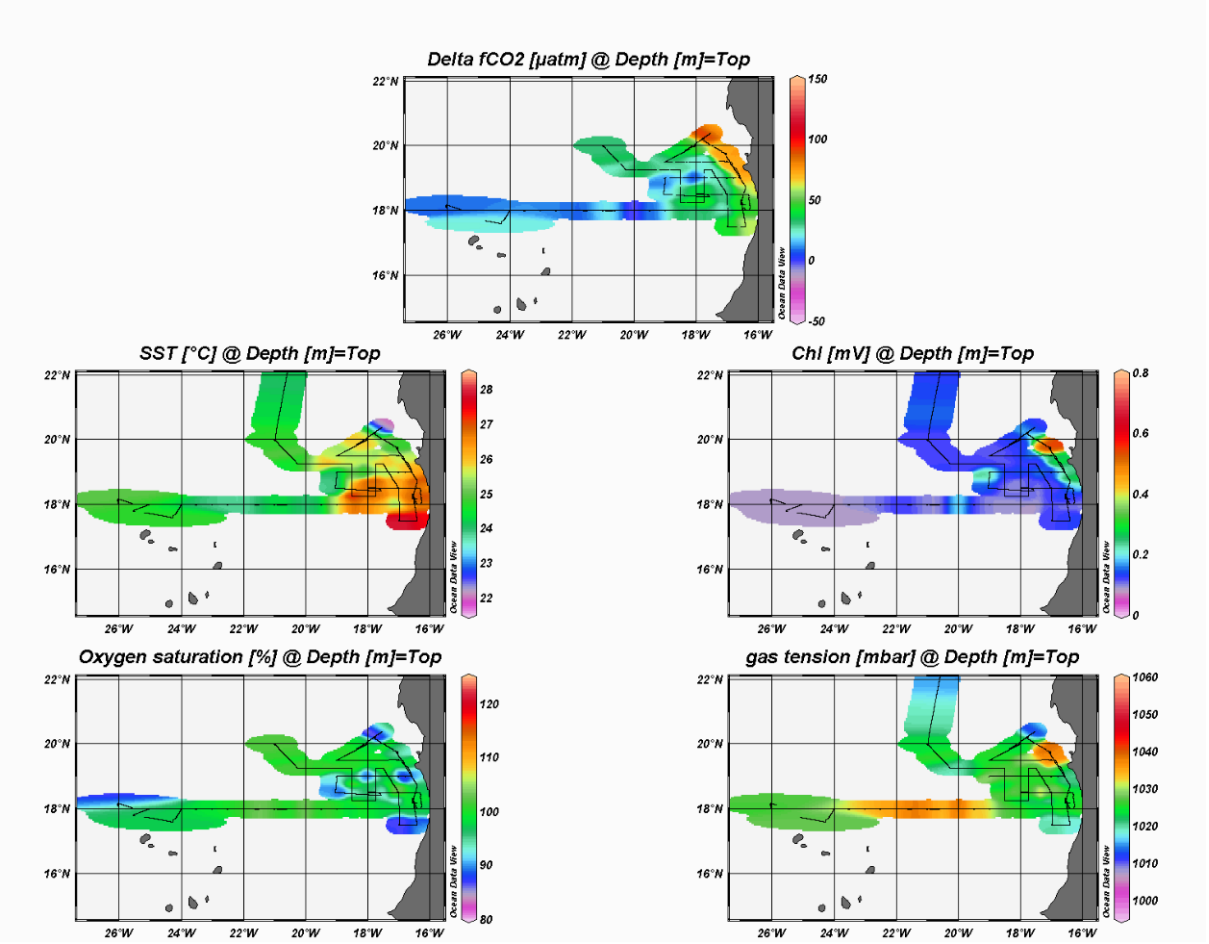

Fig. 3.8 Surface maps of selected parameters measured continuously in surface waters along the cruise of R/V METEOR Cruise 68/3

Surface maps of selected variables from underway measurements are shown in Fig. 3.8. As expected for this time of the year, upwelling was restricted to the northern end of the cruise track which is just south of a region of year-round upwelling activity.

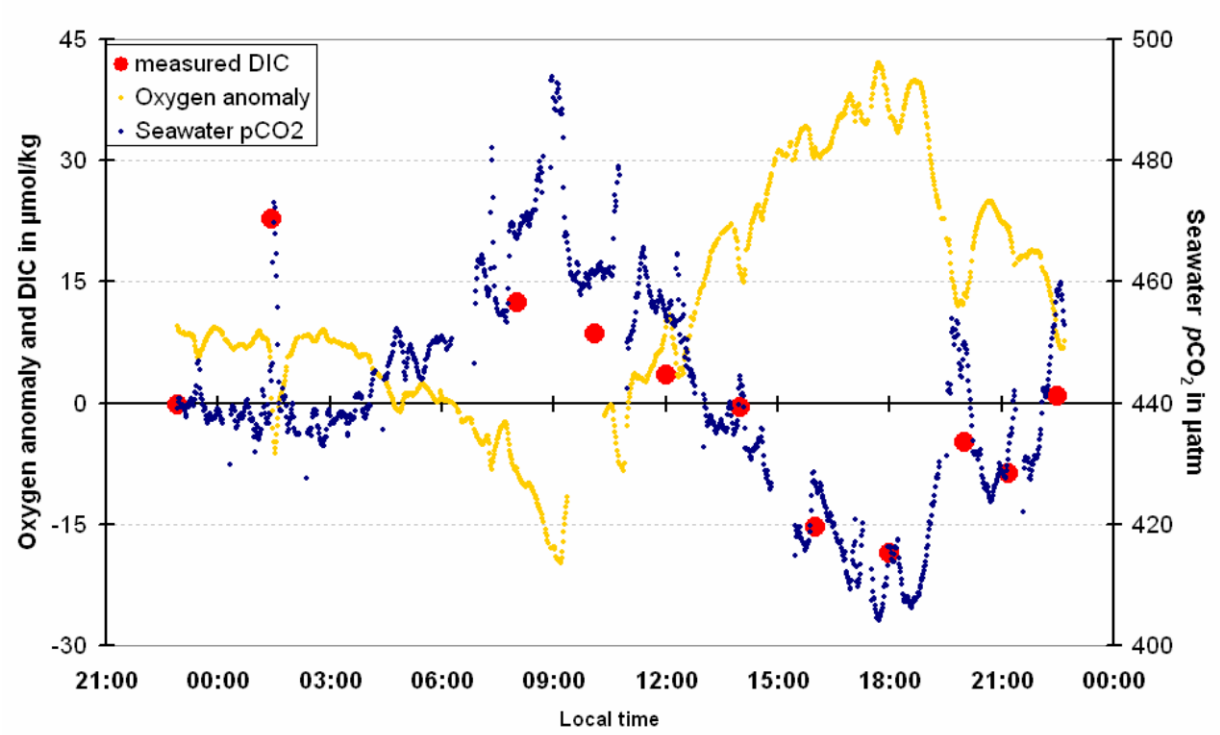

Fig. 3.9 Measurements of seawater pCO_2 (blue, continuous) and anomalies of dissolved oxygen (yellow, continuous) and DIC (red, discrete) during drift station 406 (blue ellipse in Fig. 3.7)

During two drift stations (station 304 and 311), DIC and A_T were sampled every 2 h during he day and at a 6 h interval at night. At station 304 (Fig. 3.9) which was located near the coast in an area of high chlorophyll values we found a strong diurnal DIC cycle with an amplitude of about 40 µmol kg^{-1}. The seawater pCO_2 shows the equivalent amplitude of nearly 100 µatm. The corresponding oxygen values shown are taken from the underway optode data. The oxygen shows an amplitude of similar magnitude but in opposite phase. The second drift station, which took place in oligotrophic waters, also showed a DIC and oxygen diel cycle but with a much smaller amplitude (~3 µmol kg^{-1}).

3.4.3 Production of Organic Trace Gases by Phytoplankton

(Ilka Peeken, Stefano Taddei, Valerie Gros, Sarah Gebhardt, Thomas Custer, Eckart Zöllner, Katrin Bluhm, Manuela Martino)

As part of the European FP6 project OOMPH (Organics over the Ocean Modifying Particles in Both Hemispheres) the following scientific goals were addressed during METEOR cruise 68/3:

- Determine which organic species are produced by ocean biology and released into seawater and eventually into the air.
- Determine fluxes for key organic species between sea and air.

- Determine main driving factors for organic species emission in the marine boundary layer.
- Differentiate between oligotrophic and upwelling waters based on changes in chemical mixing ratios and fluxes measured in the atmosphere.
- Characterize the biology of a summer upwelling situation off the coast of Mauritania.
- Investigate the role of CDOM as a precursor for VOC production (see also 3.4.5.2).

We approached these goals through a combination of seawater analyses, determination of gas-phase mixing ratios, and micrometeorological measurements onboard the Meteor. Measurements along repeated transects between oligotrophic an upwelling regions were made to identify possible correlations between emissions of VOCs and characteristics of different biological systems. Incubation measurements were performed to gain insight into factors driving gas exchange fluxes under controlled and well-characterized conditions. Such experiments seek to link specific water properties or their changes to patterns in trace gas emission. Micrometeorological flux measurements represent a different approach which allowed us to measure fluxes directly and to correlate these fluxes with other environmental observations. This search for correlations between fluxes and environmental factors is the basis of our “empirical approach”.

3.4.3.1 Empirical Approach

Routine phytoplankton measurements of CTD samples were performed as part of the empirical approach to determine biological drivers of ocean-atmosphere gas exchange and to characterize the biology of a weak summer upwelling scenario off the coast of Mauritania. Our group also was interested in the diurnal cycle of production rates which are being compared to trace gas production. These parameters will be correlated with flux and mixing ratio data after analyses are performed.

Sampling

At each station, 8 depths were sampled from CTD casts for biological variables in the upper ocean at standard depths (5, 10, 20, 30, 40, 60, 80, 120 m). Samples for the following variables were collected usually every morning and sometimes midday or in the evening from CTD casts: photosynthetic efficiency (Phytopam), pytoplankton pigments (determination by HPLC), flow cytometrie (bacteria and pico- and nanoplankton), Utermöhl (microphyto- and zooplankton), particulate organic carbon (POC) and nitrogen (PON), stable isotope signal of ^{15}N and ^{13}C in particulate matter, and occasionally bacterial community composition (CARD-FISH). To determine the general role of zooplankton in the investigation area, net hauls of the upper 100 m were taken and preserved for further analysis at the AWI (S. Schiel). A second net was separated in the following size classes (>4000, >2000, >1000, >500 and >202 µm) which were frozen for ^{15}N analysis at the Georgia Tech. University (J. Montoya). In total 35 stations were sampled for the plankton communities and a few less for the zooplankton samples.

Additional CDOM samples were taken in the surface and occasionally from depth profiles in the upper 120 m. These samples and the microscopic samples were kept at 5°C, while samples

for all variables were stored frozen, except for POC/PON, which were dried. Except for photosynthetic efficiency, which was measured on board and CARD-FISH, for which additional funding is needed, all analyses will be carried out at shore within the next 6-12 months.

During the 24 h drift stations we also measured on three 3 occasions diurnal cycles of bacteria (^{3}H-leucine uptake) and primary production (^{14}C-uptake) from the surface water supply system ("moon pool"). The ^{3}H-leucine uptake measurements were complemented by regular samplings for pico-/nanoplankton abundances (analysis at home by flow cytometry) in order to calculate cell-specific incorporation rates. For total phytoplankton chlorophyll *a* subsamples where taken during the entire light cycle to calculate assimilation rates.

Preliminary Results

Preliminary results indicate that bacteria display distinct diel activity patterns: at the first, oligotrophic site lowest uptake rates of 25 pM h^{-1} were found in the morning at 9:00 LT and maxima of 500 pM h^{-1} were reached between noon and at 15:00 LT. The second more eutrophic station showed minimal values at noon (160 pM h^{-1}) and highest rates at 18:00 LT (340 pM h^{-1}). Primary production varied between a maximum of 2-16 mg C m^{-3} h^{-1} (Fig. 3.10) and showed a diurnal cycle, however, maximum production seemed to be more correlated with the available light then with an internal daily production cycle. On overcast days, maximum of primary production occurred in the afternoon (Exp. 3 and 6, Fig. 3.10), while on sunny days, the maximum was found before midday (Exp 4, Fig. 3.10).

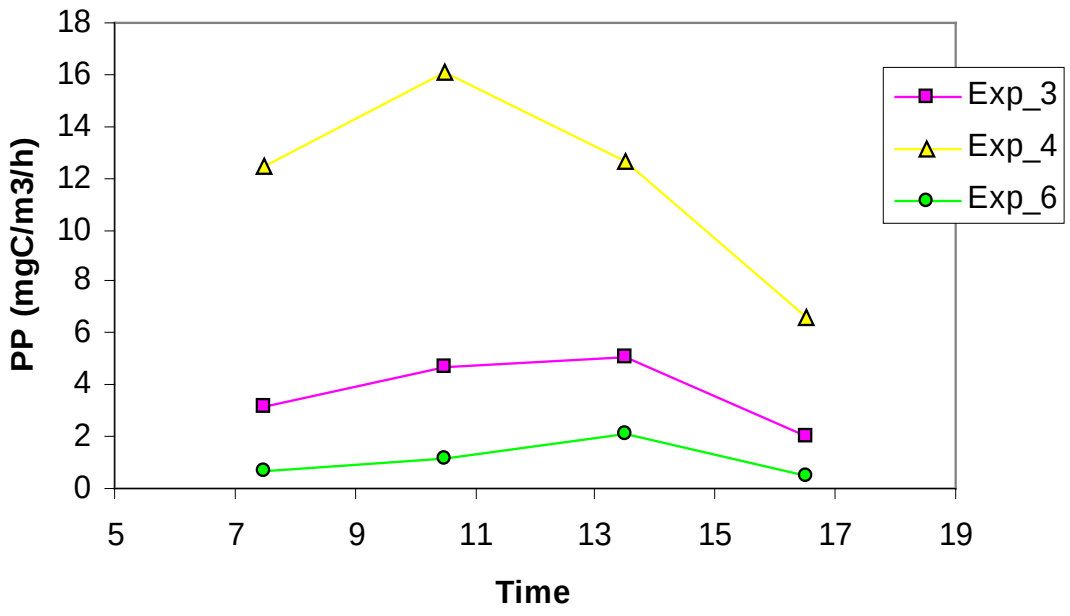

Fig. 3.10 Diurnal cycles of primary production (PP) during the various experiments (Exp)

3.4.3.2 Experimental Approach

Three different types of experiments were carried out (Table 3.2, Fig. 3.11) to study:

- Role of heterotrophic communities on trace gas production;
- Possible pathways of organic iodine compound production including volatile species;
- Role of light and different oceanic plankton communities for the trace gas production.

Table 3.2 Details of experimental set up of light incubation experiments during METEOR 68/3

Experiment (Bedford number)	Water collection date	Water sample depth	Incubator measurement date	Light conditions	Measurements
1 (105457)	15/07/06	10 m	16-17 July	50%	CO, NMHC, cartridge
1b (105457)		10 m	17 July	50%	CO
2 (105617)	17/07/06	Chlorophyll maximum	18-21 July	20% (18-19) 50% (20-21)	CO, NMHC, cartridge
3 (St. 285, cast 48)	21/07/06	26 m	22-23 July	50%	CO, NMHC, cartridge
3b (106188)	24/07/06	10 m	24 July	50%	CO
4 (106278)	24/07/06	Chlorophyll Maximum	25-27 July	50% (25-26) 20% (27)	CO, NMHC, cartridge
4b (106585)	28/07/06	5 m	28 July	50%	CO
5 (106608)	28/07/06	Chlorophyll maximum	29 July-1 Aug	20% (29-30) 50% (31-01)	CO, NMHC, cartridge, halocarbon
6 (106813)	1/08/06	Chlorophyll Maximum	2-3 Aug	20% (02) 50% (03)	CO, NMHC, cartridge, halocarbon

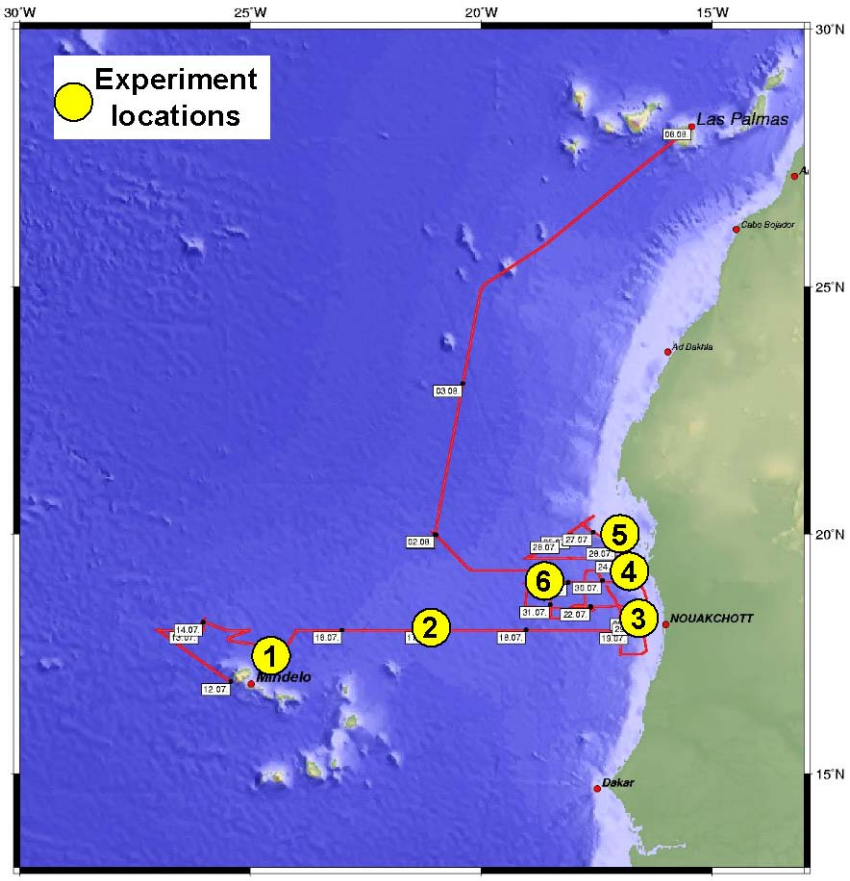

Fig. 3.11
Locations where water was collected for the various experiments (see Table 3.2)

Experiment Type 1

Two long-term (10 d) dark experiments were performed to investigate the potential impact of heterotrophs of different size fractions on the biogenic production of various organic trace gases. Samples from the chlorophyll maximum of oligotrophic (Exp. 1) and late upwelling filament waters (Exp. 2) were incubated in complete darkness to inactivate phytoplankton and allow for heterotrophic processes to dominate. Therefore, six bottles were filled with water containing organisms <1.2 µm (mainly bacteria). Three of these received an addition of water containing heterotrophic protist grazers of the size up to 63 µm, whereas the others were inoculated with the 1.2 µm-filtrate of this plankton community (no grazers). Then, for one week various biological and biogeochemical (nutrients, POC, DOC) parameters were measured with parallel repeated headspace sampling (cartridges) for later GC-MS analyses of VOCs. Biological measurements onboard mainly consisted of daily samplings and different fixation protocols (Lugol´s solution, paraformaldehyde, formol, glutaraldehyde) for later analyses of viruses, bacteria, auto- and heterotrophic pico- and nanoplankton as well as microzooplankton (by flow cytometry, epi-fluorescence and inverted microscopy, HPLC). Between 18 and 50 samples per parameter and experiment were taken. Furthermore, microbial activity was determined by ^{3}H-leucine uptake measurements and CTC-assays (proportion of respiratory active bacterial cells). For later molecular analyses of microbial community composition and dynamics (e.g. by Denaturing Gradient Gel Electrophoresis (DGGE), Sequencing and Catalyzed Reporter Deposition-Fluorescence In Situ Hybridisation, CARD-FISH; dependent on additional funding), samples were taken from different periods of the experiments.

Experiment Type 2

Iodine is present in seawater as iodate and iodide. While iodate is regarded as the stable form of iodine, there are significant amounts of iodide in surface waters. Thus in open oceans the concentration of iodate increases with depth to an approximately constant level while that of iodide decreases with depth to around the detection limit (0.1-0.2 nM) below the euphotic zone. This suggests that biological processes may be involved in the transformation of iodate to iodide. Nitrate reductase has been implicated in the reduction of iodate to iodide because of the similarity between iodate and nitrate. Two hypotheses were followed here:

- Chemistry and biology of iodine are coupled.
- The concentration of nitrate influences the reduction of iodate to iodide.

To test the first hypothesis, 8 vertical profiles were carried out for the distribution of iodate and iodide. Four profiles were taken in the oligotrophic regions and the other four profiles in the more eutrophic upwelling regions. Eight depth were sampled from the CTD Niskin bottles (5, 20, 40, 80, 120, 200, 300 m and deepest depth of the cast).

The second hypothesis was tested using incubation experiments which were carried out in incubation chambers holding eight 1L polycarbonate bottles. The first experiment followed the time course of change from iodate to iodide over a period of 10 d. Seawater samples were sampled from the CTD Niskin bottles and collected from the chlorophyll maximum. Eight bottles were kept in a 50 % light regime and two controls were kept in the dark. Sampling was

performed every day collecting a 1L liter bottle and analyzing it for flow cytometry, microscopy, chl-a and iodine speciation.

A second experiment was carried out with the same initial conditions as mentioned above. One series of bottles was treated with approx. 7.5 µM of nitrate. The other series was left untreated. Sampling was performed every second day over a period of 10 d for the parameters named above. After 5 days the nitrate enriched sample received a second 7.5 µM nitrate addition.

Samples were run in parallel with each experiment and controls were always kept in the dark. The iodine species will be measured via cathodic stripping square wave voltammetry. Samples were filtered over 0.2 µm cellulose acetate filters and the filtrate will be stored frozen until analyzing. Aliquots for the flow cytometry and microscopy will give information about the phytoplankton community within the samples. All parameters taken will be measured and analyzed within the next 6-8 months. The concentration of total free iodine (iodate + iodide) is about 550 nM in surface waters and 520 nM in bottom waters. On the shelf and in the upwelling regions iodine concentrations were slightly lower (Fig. 3.12).

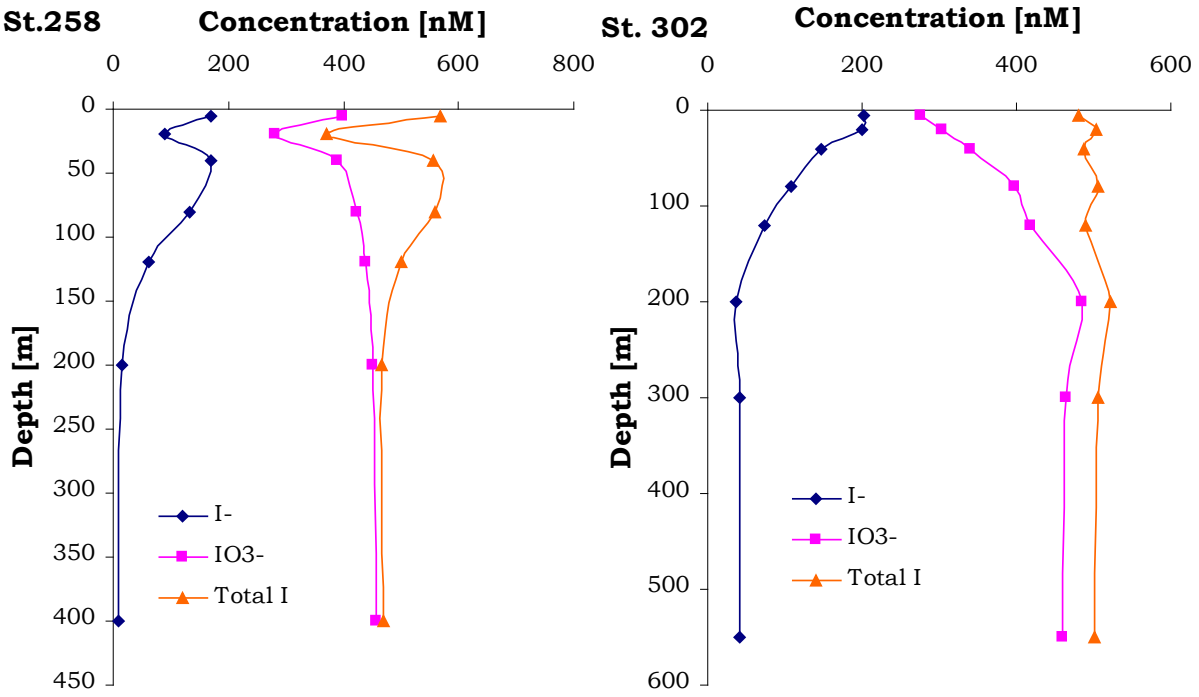

Fig. 3.12 Vertical profiles of iodide, iodate and total iodine. St. 258 is an open ocean oligotrophic station and St. 302 is a shelf station

In the incubation chambers no changes were observed in the samples taken. Iodide and Iodate concentrations stayed constant throughout the experiment.

Experiment Type 3

Incubator Setup: Several incubators were set up on the forecastle for a combination of atmospheric and biological sampling. Incubators consisted of two Plexiglas cubes and two PVC cubes covered with neutral density foil in order to reach approximately 50 % and 20 % of the surface irradiance. Up to nine 2.5 L Duran glass bottles could be tied to the bottom of each incubator and contained CTD water samples, either from the surface or from the chlorophyll maximum, to be analyzed. The lids of the incubators were equipped with holes for inlets and outlets of sampling and flushing gases whose use will be described later. Seawater was constantly pumped through the incubators in order to avoid heating. For a routine sample, 10 bottles placed in the incubators were reserved for measurement of biological parameters while the remaining bottles were used for measurements of chemicals partitioning into the scrubbed air constantly flushing through the bottle headspace. A control bottle was also produced by first filtering CTD water through a 0.2 µm filter. A more detailed overview of experiments can be found in Table 3.2. Light conditions were monitored continuously outside the incubators and inside the chosen light intensity incubator with a LiCor 4pi sensor.

Biological Measurements: The setup of these experiments was to allow investigation of the impact of different light conditions on the formations of trace gases. The experiments started usually at 18:00 LT of a given day and inital values for all biological variables mentioned above, except POC/PON were determined While bacterial production was determined immediately, primary production samples were kept overnight in the dark and a full light cycle was performed the following day for the following size fractions: >0.2 µm, >5 µm and >20 µm. In total 10 biological bottles were available and kept in the start light condition (see table 3.2). While nine of the bottles underwent the following sampling scheme, one bottle was left for 2 h sub-sampling of chlorophyll *a* during day 1 and 3, which where also the cartridge sampling days. After 48 h three bottles were sub-sampled for biological variables, while three bottles were kept at initial light conditions, while the other three bottles were changed to the new light conditions, similar to the gas flushed bottles. From the sub sampling after 48 h, again, bacterial production was performed immediately and primary production was carried out the next day with the modified light conditions (Tab. 3.2). After 96 h the experiment was terminated and biological and CDOM samples were taken from all biological and flushed air bottles. Additional, the controls were sampled for bacteria. For experiments 4 and 6 additional a daily cycle of primary production every 3 h was performed, either with the starting community or with surface water from the drift station. From experiment 3 on CDOM samples have been taken from samples and controls.

CO Measurements: Compressed air whose CO content was reduced by circulation through a filter was flushed through water samples at ~10 mL min^{-1} following an initial passivation period where flushing occurred at ~100 mL min^{-1}. Although both sample and control were always flushed, CO mixing ratios were measured in only a single flask at any given time. As it exited the bottle, air was pulled continuously into the sampling loop of a gas chromatograph-mercury reduction instrument for measurement of CO. Measurements alternated between sample and calibration gas every 5 min. Additional sampling of entirely empty flasks was also performed. For these blanks, values of 4 ± 2 ppb with no diurnal cycle were observed as expected.

Non-Methane Hydrocarbons (NMHC) Measurements: Low NMHC level compressed air was flushed through samples at about 100 mL min^{-1}. A 4-port valve allowed switching of

measurements between sample and control bottles. Air was analyzed for NMHCs by gas chromatography-flame ionization detection with a detection limit of about 20 ppt and a precision of ~10 %. Flushing air composition and a calibrated gas standard were also measured once a day.

Cartridge Volatile Organic Carbon (VOC) Measurements: Low VOC level synthetic was flushed through incubation flasks at ~80 ml min^{-1}. Air exiting the bottles was then sampled through a 0.2 µm filter and through graphitized carbon VOC collection cartridges at a flow rate of 50 mL min^{-1} for a period of 1 h. Sample and control measurements were made simultaneously. Cartridges were sampled for the two different light regimes for one entire light cycle starting at 6:00 LT and continuing hourly until 19:00 LT and the next day at noon. Additionally the flushing gas was measured every other day to establish background values. Sampled cartridges were stored at 5°C and will be analyzed at the MPI in Mainz.

Halocarbon Measurements: Low VOC level synthetic air was flushed through flasks at ~80 ml min^{-1}. Air exiting the bottles was then sampled and analyzed by gas chromatography-mass spectrometry (GC-MS) equipped with a cryogenic pre-concentration system for halogenated VOCs. The air was pumped into a sampling loop by a metal bellows pump at a flow rate of approximately 30 mL min^{-1}. Before entering the cryotrap the sample passed a $MgClO_4$ dryer heated to 100°C. About 300 mL of air were flushed through a stainless steel tube filled with glass beads at -70°C to trap the target components. The measurements of sample, control and blank were performed over a period of 5 d.

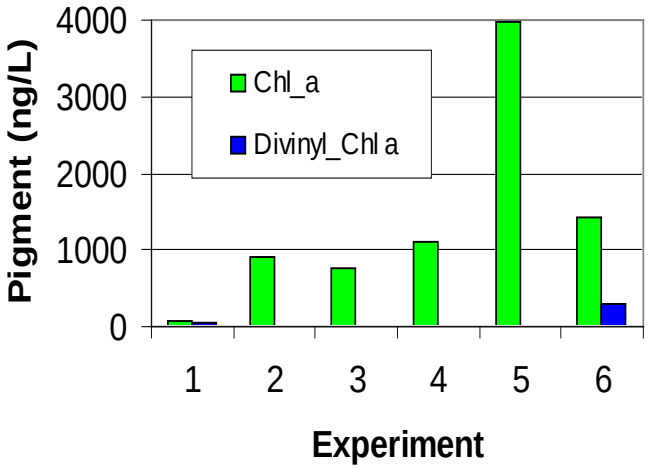

Fig. 3.13
Initial conditions of the phytoplankton biomass (chl a) and prochlorophyte biomass (divinyl chl a) of the various experiments

Preliminary Results

Different initial conditions were observed in the various experiments (Fig. 3.13). While experiment 1 showed lowest phytoplankton biomass, it had the highest contribution of divinyl Chl a, the marker of prochlorophytes. This group was found again only in experiment 6, but at a smaller proportion to total phytoplankton biomass. Highest biomass, however, was observed in experiment 5, close to the African coast with up to 4000 ng Chl a L^{-1}. This community was clearly dominated by diatoms, based on marker pigments (Fig. 3.14). Marker pigments reveal the extreme heterogeneity of phytoplankton starting communities in the various experiments with the most mixed community during experiment 6 (for further details see Fig. 3.14). It is hoped that these differences are also reflected in the VOC composition.

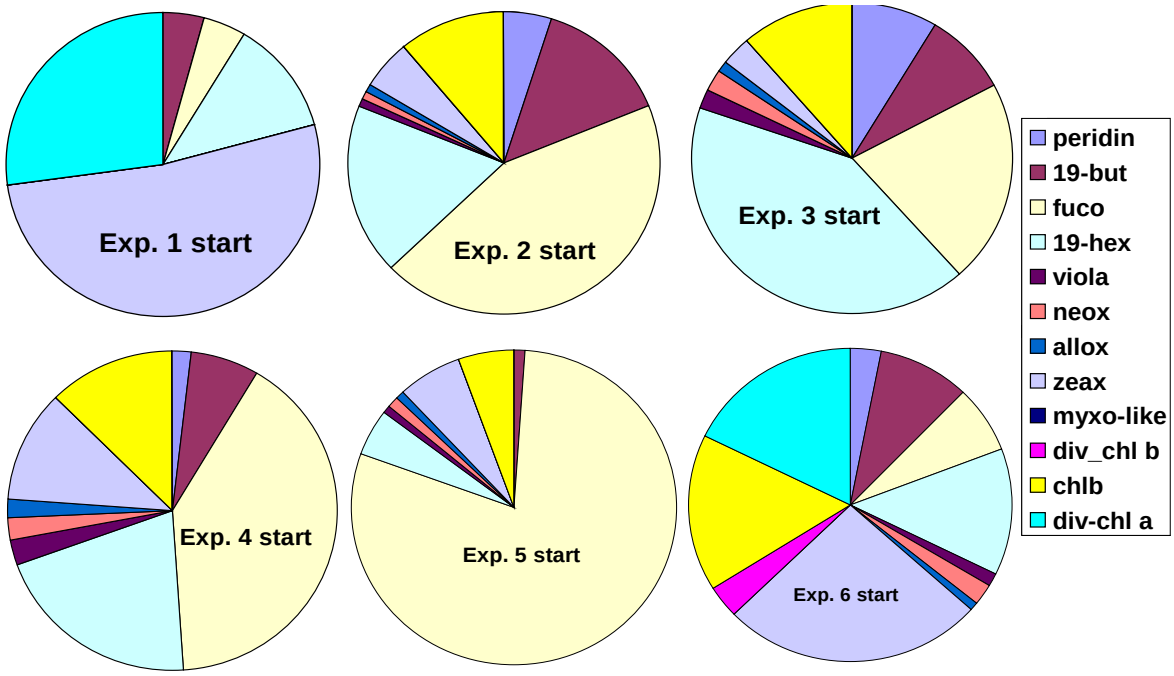

Fig. 3.14 Initial phytoplankton assemblages of the various experiments based on marker pigments that represent different phytoplankton groups (peridinin = autotroph dinoflagellates, 19-but = pelagophytes, fuco = diatoms, 19-hex = prymnesiophytes, viola + neox + chlb = chloro-phytes, allox = cryptophytes, zeax = cyanobateria, myxo-like = unknown, div_chlb + div-chl a = prochlorophytes)

Figure 3.15 shows CO measurements during the experiments 1, 2 and 3 (raw data, outliers not removed). In these experiments, global radiation amplitude was quite similar every day, except for experiment 3 for which the radiation maximum was significantly reduced.

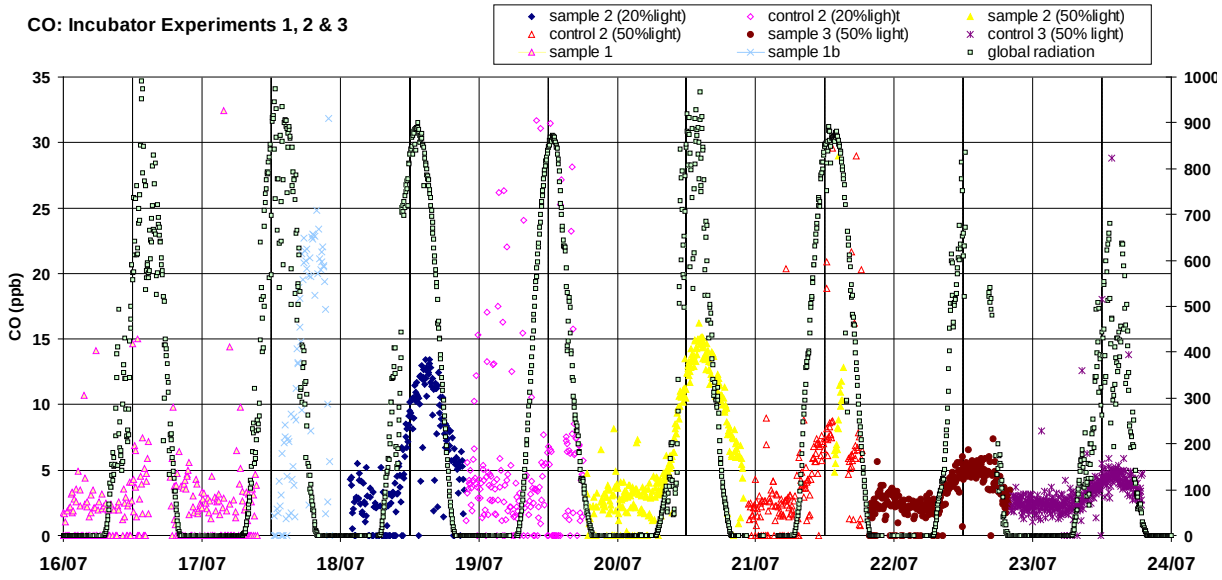

Fig. 3.15 CO measurements for experiments 1, 2 and 3

Sample 1 shows a very light diurnal cycle with enhanced CO values during the day time. Sample 1b showed clearly enhanced values when the flask was placed outside the incubator, directly influenced by solar radiation. Sample 2 was at first placed in the incubator with low light (20 %) conditions and showed a clear diurnal pattern, with CO levels rising in parallel with the global radiation and showed a maximum value of 13 ppb around 15:00 LT. Control 2 showed slightly enhanced values during the day, up to 8 ppb. Sample 2 was then placed in the incubator with higher light (50 %) conditions and showed a similar cycle as when placed in the 20 % light incubator, with a slightly higher maximum (15 ppb). Control 2 also placed in the incubator with higher light (50 %) conditions also showed a similar cycle as when placed in the 20 % light incubator, with a slightly higher maximum (9 ppb). During the measurement of control 2 (50 % light), the measuring line was shortly disconnected to measure sample 2 which showed (although not yet at equilibrium) values as high as 13 ppb. Sample 3 and control 3 showed a light diurnal cycle with maximum values of 6 ppb. For all primary production daily cycle measurements, also a clear diurnal cycle with maxima either in the morning or at noon were observed.

The result suggest two CO production mechanisms, one dependant on biomass and light (biological production), the other one only light dependant (possibly via photochemical production from the dissolved organic matter). The results of July 21, when switching from control to sample flask, illustrates these two different mechanisms. Whereas the control showed maximum levels of about 9 ppb, the sample rapidly reached the value of 13 ppb. When the biomass is too low (experiment 1), or when the light signal is too low (experiment 3), only the second mechanism seems to be operative. From experiment 4, it seems that once the sample has been placed in high light conditions, weaker light conditions are not sufficient to initiate the CO production mechanism. Non-Methane Hydrocarbons data analysis requires analysis of around 50 chromatograms/day and will be performed over the next few months. Cartridge samples will also be analyzed in the months following the voyage at the laboratory in Mainz. Analysis of halocarbon compounds turned out to be problematic due to clogging of the water trap and subsequent water saturation of the sampling apparatus and GC column.

3.4.3.3 Micrometeorological and Atmospheric Measurements

A handful of techniques are available to directly measure atmospheric fluxes above small, undisturbed ecosystems. Such measurements rely on swift, simultaneous measurement of micro-meteorological and chemical parameters in a specific location. Among these techniques are the disjunct eddy covariance, relaxed eddy accumulation, and so-called virtual disjunct eddy covariance methods. Although it has long been possible to measure atmospheric abundances of chemicals such as CO_2 and water vapor in the air with sufficient speed and precision to obtain fluxes, only recently has it become technically feasible to determine fluxes of a wider range volatile organic compounds in a like manner. Additional complications arise in attempting to determine micrometeorological parameters on a moving platform such as a rocking ship.

Disjunct Eddy Covariance (DEC)

Two half-liter stainless steel flasks equipped with fast opening valves along with a sonic anemometer (METEK, USA-1) and a Inertial Navigation System combined with a global positioning system (INS/GPS platform, Migits III) were positioned at the top of the forward mast along with teflon sampling and pumping lines for transporting air to the air chemistry container on the forecastle for fast chemical analysis. Every 30 s air is swiftly sampled (duration ~0.3 s) into one of the stainless steel containers and is immediately sampled by a Proton transfer reaction mass spectrometer (PTRMS) housed in the laboratory container. While one stainless steel flask is being sampled, the second is being evacuated in preparation for the next sampling cycle 30 s later. Within this sampling routine, mixing ratios of methanol, acetonitrile, acetaldehyde, acetone/propanal, dimethyl sulfide, isoprene, and methacrolein/methylvinyl ketone, and benzene were measured with a time resolution of approximately 0.3 Hz over each 30 s sampling interval. The sonic anemometer and INS/GPS sensor continuously record wind and anemometer velocities and position at 10 Hz to provide micrometeorological data with which the air mixing ratio information from the canisters can be correlated and a flux determined. Due to large number of data points collected, total analysis is not yet completed.

Virtual Disjunct Eddy Covariance (VDEC)

A second sample line in the vicinity of the anemometer continuously pulled air for immediate sampling by a second PTRMS instrument measuring identical chemicals at the same sampling speed as the first PTRMS. In this case, the flow-drift tube of the mass spectrometer is used as a sampling flask in lieu of those at the top of the mast and correlations with micrometeorological parameters to determine fluxes will be made in a way similar to the disjunct method. Also connected to this line is a Licor-7000 instrument measuring atmospheric CO_2 and H_2O mixing ratios at 10 Hz which, via eddy covariance, can be used to calculate fluxes of these species.

Relaxed Eddy Accumulation (REA)

In order to increase sensitivity of chemical measurements, air can also be accumulated in reservoirs for a longer period of time than in disjunct or virtual disjunct sampling. To accomplish this, a computer was programmed to calculate in real-time the true wind velocity as measured by anemometer and INS/GPS device. If the wind was above or below a given threshold wind velocity, air was collected in either of two cartridges and otherwise discarded. For these experiments, air was collected on the same graphitized carbon VOC trapping cartridges that were used with the incubations. The sampling system consisting of solenoid and teflon needle valves was hoisted up the mast by a rope and pulley periodically to sample air from the proximity of the micrometeorological instrumentation.

Although this system was operational and appeared to be operate successfully for many hours, eventual problems in communication between computers and a specialized circuit board controlling solenoid valve switching for air collection caused repeated crashes that could not be remedied while on-board the ship. These crashes prevented collection of extensive REA data sets. However, future measurements using this system look promising and the journey served as a useful test run for future expeditions.

General Atmospheric Measurements

In addition to micrometeorological flux measurements, a variety of other important atmospheric measurements were also performed. Attempts were made to use gas-chromatography mass spectrometry (GC-MS) equipped with cryogenic pre-concentration capabilities and a water trap to measure mixing ratios of halogenated compounds (chemicals such as CH_3Br, CH_3I, CH_3Cl) as well as a variety of oxygenated volatile organic compounds. Such measurements were intended to provide chemical identification information unavailable using PTRMS measurements and the other gas chromatographic techniques available, provide a much broader record or atmospheric chemical composition, and to make selected incubation and REA measurements as described previously. Power failures early in the experiments, likely caused by spikes in the unstable power supply to which all of the instruments in our container were connected, crippled the use of a water trap that would have greatly facilitated measurements in a humid marine environment and incubation flasks.

An aethelometer was used to measure black carbon from a sampling inlet placed on the top deck of the ship. This instrument should show the background aerosol in a marine environment and will help to identify, if relevant, the influence of the ship stack. Radon in air sampled from the top deck of the ship was measured using a thorium daughter detection system and should provide information on when air-masses were influenced by continental air masses. Data from this system will be downloaded from the instrument upon return to Mainz. A second CO instrument (GC-RGD), identical to that described in the incubation section, was used for continuous monitoring of atmospheric air and sampled from the top deck of the ship. The mixing ratio of methane in the atmosphere was successfully monitored by GC-FID. The air inlet was installed at the front of the Heli-Deck.

Relative humidity and temperature were measured from the top deck. Data from this instrument will be retrieved upon the return of the instrumentation to Mainz. Ozone measurements were attempted although instrumental problems made these measurements impossible in the end.

Preliminary Results

Preliminary data indicates that the micrometeorological system was fully operational and that wind vectors could be successfully corrected for ship movement. For example, Fig. 3.16 indicates a clear correlation between water mixing ratio and the vertical component of the true vertical wind velocity which is directly proportional to the flux. Based on this and other correlation analyses we hope to see fluxes in other chemicals as well as determine the variation of fluxes over time. Full synchronization of the raw data is currently underway to extract final fluxes of a range of different species. Flow distortion due to the ship will be corrected by numerical fluid dynamics calculations.

A first glimpse of synchronized data has been obtained for latent and sensible heat flux and should provide a preview of what is to come for other flux measurements. In general, the signal to noise ratio for the fluxes at the air-sea interface is very low. This is due both to the inherently low values of the fluxes themselves and to the high noise caused by flow distortions related to

the ship superstructure. Accurate synchronization of signals acquired by different instruments serves to reduce the noise as much as possible.

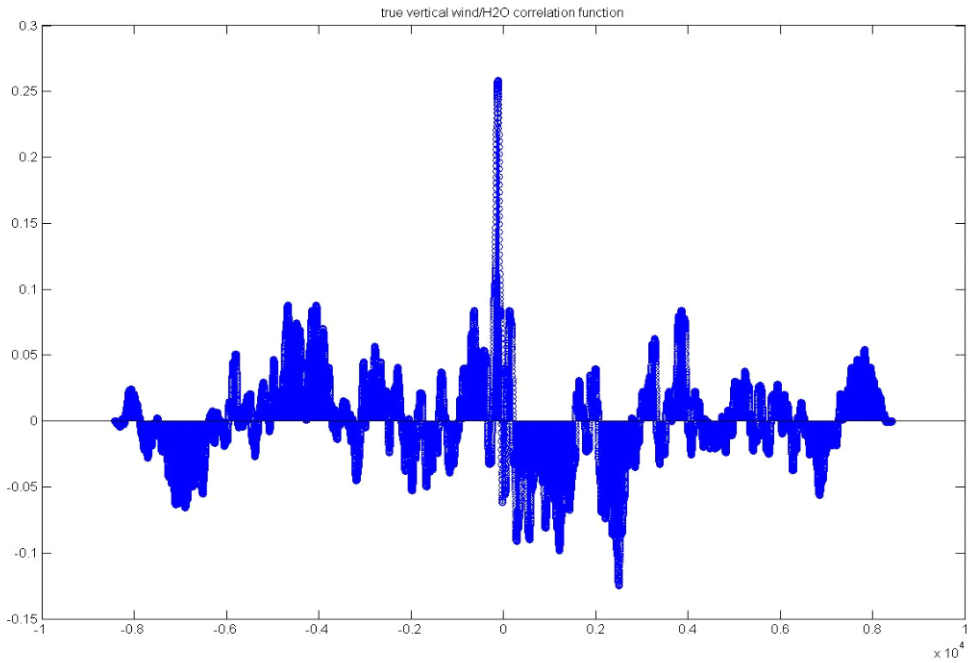

Fig. 3.16 Correlation function between the specific humidity and the vertical component of the true wind velocity (one hour of data)

In Fig. 3.17 latent and sensible heat fluxes obtained by the EC method are compared with the same fluxes calculated by a bulk method (Fairall et al., 2003). The bulk method is based on empirical relationships between the turbulent fluxes, the wind speed, and the temperature and humidity differences between air and sea. In contrast with direct methods, the bulk method derives fluxes starting from the average values instead of from fluctuations. Since fluxes derived from these two methods are based on completely different physical principles, good agreement between the flux data calculated with the EC method and the bulk method shows the quality of the collected data and suggests our ability to reliably measure fluxes under the conditions presented aboard the METEOR.

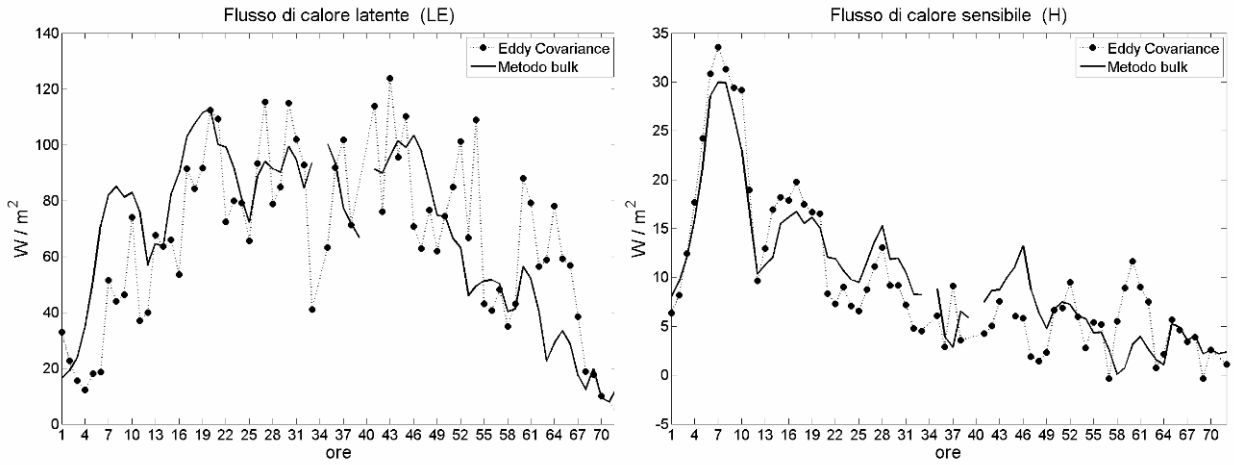

Fig. 3.17 Flux of latent (left) and sensible heat (right) based eddy covariance measurements and bulk calculations

PTR-MS data has been converted to mixing ratios and now needs to be synchronized with micrometeorological parameters and final fluxes calculated and corrected for flow distortions. Calibration results indicate that sensitivity was good. Early in the measurements, problems related to connection with unstable power supply of the ship caused certain increase in noise as well as numerous crashes of computers and instrumentation that made it difficult to generate continuous data sets for flux calculations. These problems were largely alleviated by connection of instrumentation to the stable power supply of the ship. Instabilities in the ion source of one instrument also caused certain jumpiness to the data and was not eliminated by changing to stable power.

Atmospheric measurements employing the GC-MS with cryogenic trapping were extremely difficult following the death of a transformer used to heat the cryotrap and severe damage in the controlling unit due to power spikes in the ship's power supply. This breakage was followed by the breakage of a GC column and the blowing of multiple fuses in a pump controlling unit that had also to be remedied. Further measurements following repair of these breakdowns and placing the instrumentation on a stable power supply allowed some measurements to be collected. However, the chemical record is limited to specific days where instrumentation was fully operational.

Atmospheric records for methane are of high quality as are records of CO and black carbon. Ozone measurements were never fully operational. Radon, temperature, and humidity measurements will be downloaded in Mainz and are presumably complete.

3.4.4 Production of Volatile Organic Halocarbons

(Gert Petrick, Christian Albers, Douglas Wallace)

The vertical distribution of volatile halogenated organics (bromomethane and chlorobromomethane) has been studied extensively in the tropical and subtropical North Atlantic Ocean during the Meteor Cruises M55 and M60/5. Building on these results (e.g. Richter and Wallace, 2004; Quack et al., 2004), work carried out during M68/3 was focused on experiments to study:

- the light dependence on the production of volatile halogenated compounds (bromo-, bromoiodo-, chlorobromocompounds and iodinated compounds),
- possible biogenic pathways and/or the role of "dissolved" organic matter for the production of these compounds.

One major aspect of the work was to test procedures, blanks, etc. for in situ incubation experiments during 24 h drift experiments. For this purpose, a newly constructed Lagrangian surface drifter (equipped with radar reflector, flashlight and radio beacon) was tethered to sub-surface in situ incubator "wheels" (see Fig. 3.18). The "wheels" supported quartz flasks (250 mL) in which the incubation experiments were conducted. Seawater collected from 400 m depth (a single CTD-Niskin bottle) was used as an "initial" sample for filling the incubation flasks.

For a full deployment/experiment, a total of 28 quartz bottles were filled with water from this "initial" sample. Of these, 12 bottles each were incubated at in situ light-levels on the two

incubation wheels and 4 bottles were kept as dark controls. Of the 12 incubation bottles per light level, 6 were untreated, 3 had been nano-filtered through a 150 KD ceramic filter, the remaining had been filtered through a 3 to 15 KD filter. The nano-filtration was intended to remove particulate and colloidal matter and a significant fraction of the material that is traditionally considered "dissolved" using the operational 0.4 µm cut-off would have been removed. An incubation at 20 m (max. 20 % of surface light level) serves as reference. All incubations were performed over 24 h starting and ending at dark, i.e. they covered a full daily light cycle.

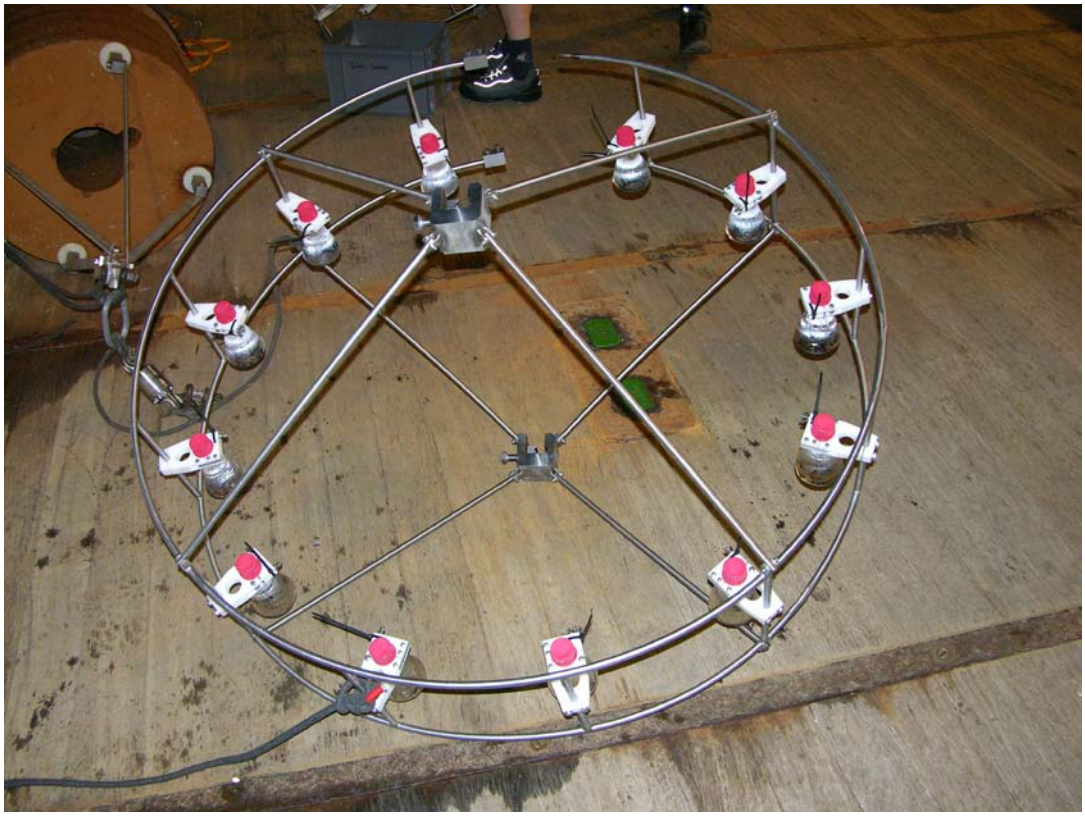

Fig. 3.18 Sub-surface in situ incubator with quartz bottles that was tethered to a Lagrangian surface drifter (equipped with radar reflector, flashlight and radio beacon)

The following deployments/experiments were carried out during the cruise:

(1) Single incubation wheel (12 bottles) at 10 m depth;

(2) Wheels at 5 m and 20 m depth;

(3) Single wheel at 2 m depth;

(4) Wheels at 2 m and 20 m depth;

(5) Deck incubation.

All samples were analyzed by purge and trap GC-ECD and GC-MS. Preliminary results showed a clear light dependence of the production of several halogenated organic compounds. The light-dependent production rates varied with substance. The presence of particulate,

colloidal and high-molecular weight dissolved matter also appeared to have an impact on the production rates.

In addition to the above mentioned experiment, four vertical profiles were taken (5-60 m) for comparison with the results of the Poseidon Cruise 320/1 conducted in spring 2005.

3.4.5 Production of Volatile Organoiodine Compounds (VIOC) and CDOM

(Manuela Martino)

3.4.5.1 Volatile Organoiodine Compounds

The GC-MS system was up and running with a very good vacuum and low N_2/O_2, when, due to a power surge, the Mass Spectrometer broke down on the July 14. It was tried to repair the MS, but it became clear that there was a major problem with the high energy dynode, which involved major replacement parts that would have to be provided from the manufacturer. Therefore, regrettably there are no measurements of halocarbon concentrations in water, nor results from incubations with molecular iodine.

3.4.5.2 Chromophoric Dissolved Organic Matter (CDOM)

Samples for CDOM were collected from July 23 onwards, from both CTDs and underway non-toxic supply (surface samples). A total of 13 CTDs was sampled, most of which shallow (max depth 120 m), with samples collected from 200-1000 m in three occasions. Also 45 surface samples were collected from either the underway non-toxic supply or the shallowest CTD bottle. Also 47 samples for CDOM from incubations of natural phytoplankton assemblages were processed in collaboration with Drs. Peeken, Zöllner and Gros. Samples were generally collected in 250 mL glass bottles and filtered through 0.2 µm pore-size filters, using and acid-washed all-glass filtration unit. The samples were analyzed by Dr. Rüdiger Röttgers at the Institut für Küstenforschung/GKSS-Forschungszentrum immediately upon return to Germany.

Preliminary Results

Preliminary results of CDOM absorption coefficients (m^{-1}) at 312 nm are shown in Figs. 3.19 and 3.20. For surface samples (Fig. 3.19), highest absorption coefficients (0.55-0.70 m^{-1}) were observed in the region of highest chlorophyll abundance, which was driven by active or recent upwelling. Similarly, high absorption coefficients were observed through the water column in the shallow areas of coastal upwelling (e.g. casts 294/62 and 301/73), and sub-surface maxima in CDOM absorption coefficients were observed in correspondence with the chlorophyll maxima.

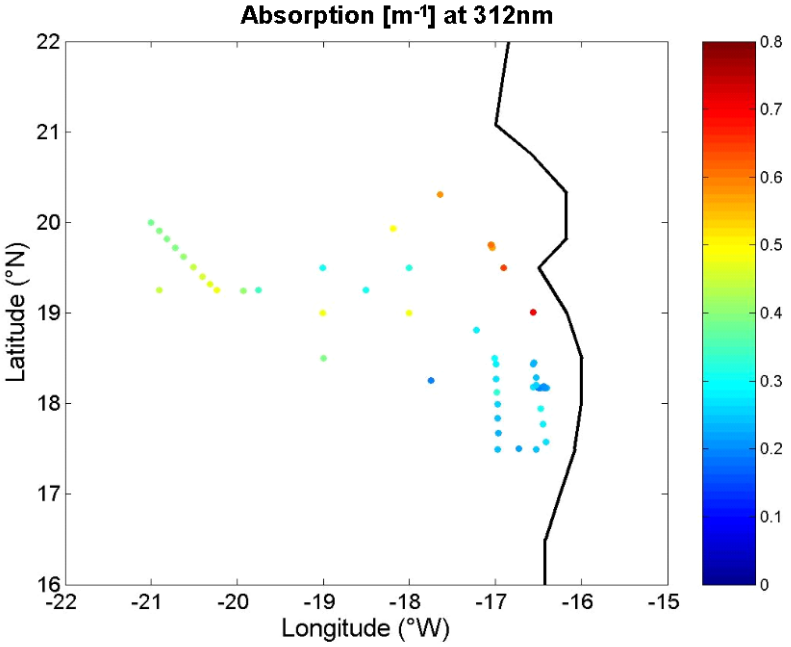

Fig. 3.19
Surface CDOM absorption coefficients at 312 nm (m^{-1})

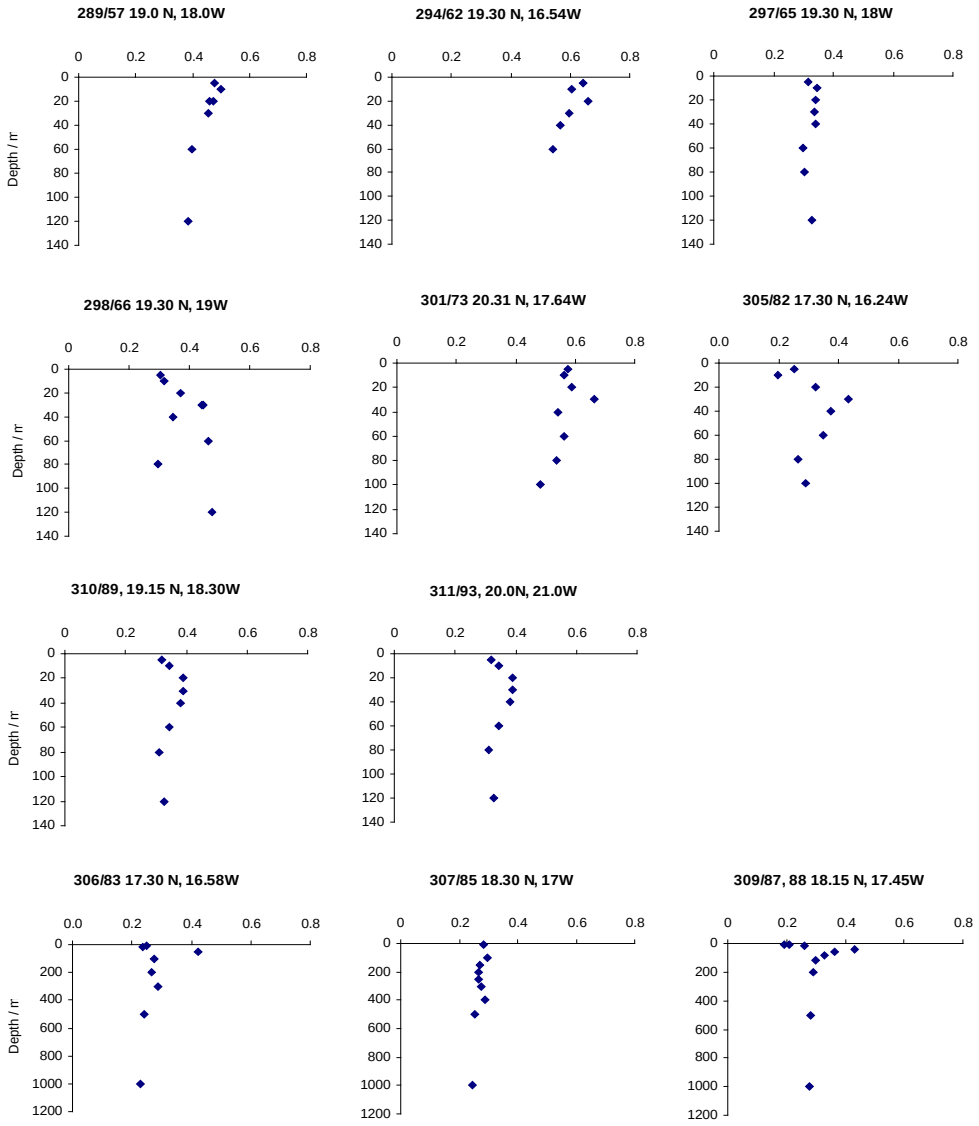

Fig. 3.20 Depth-profiles for CDOM absorption coefficients at 312 nm

3.4.6 DMS/DMSP Production and Phytoplankton Composition

(Daniel Franklin, Gareth Lee)

The major objective of the project was to investigate the relationship between phytoplankton species composition and dimethylsulphoniopropionate (DMSP) in the particulate and dissolved phase ($DMSP_p$ and $DMSP_d$), as well as the concentration of the product of DMSP cleavage, the volatile trace-gas dimethylsulphide (DMS), in surface waters. DMSP is a significant compatible solute in some phytoplankton cells, and can account for a large proportion of cell carbon. DMS, along with its oxidation products, can have a significant role in atmospheric chemistry and the formation of clouds. This ocean-atmosphere link is important in the global sulphur cycle and has been studied due to its potential geophysiological/Gaian role. DMSP-lyases are enzymes that cleave DMSP to DMS. DMSP-lyases have been found in haptophytes, dinophytes and bacteria. In higher latitudes, enormous coccolithophore blooms can release large amounts of DMS to the atmosphere. We wanted to study the situation in lower latitudes, where coccolithophores can be a significant component of the 'steady-state' phytoplankton assemblage, rather than seasonal and ephemeral bloom species. This was a compliment to our laboratory work where we have been investigating differences between coccolithophore species. The inshore waters off Mauritania, subject to year-round upwelling at 20°N, were contrasted with lower-productivity offshore stations.

Sampling

We used CTD casts and sampling from Niskin bottles to generate depth profiles of DMS, $DMSP_d$, $DMSP_p$ and DMSP-lyase. We sampled 32 stations and typically analyzed 6 depths per station in the first 60 m. The deep chlorophyll maxima (DCM) were typically found at 30-40 m; coccolithophore biomass is often found concentrated at the DCM. We sampled from approximately 180 Niskins for the analysis of a range of parameters.

We measured DMS, $DMSP_d$ and $DMSP_p$ in Niskin-sampled seawater via gas chromatography with flame photometric detection (GC-FPD). All DMS/P measurements followed pre-concentration with a cryogenic purge-and-trap preparation system. After the cruise we analyzed phytoplankton species composition and biovolume with acidic Lugol's iodine-fixed water samples. Calcareous/coccolithophore species abundance and distribution was analyzed by collecting cells on polycarbonate filters and analysis by light and electron microscopy. All taxonomic work was carried out by Alex Poulton and Jeremy Young at the Natural History Museum, London. DMSP-lyase activity (DLA), filtered onto GF/F filters (enzyme activity in microalgae and surface-associated bacteria), was measured with GC-FPD. Photosynthetic pigments, via HPLC, were analyzed by Ilka Peeken (IfM-GEOMAR).

Preliminary Results

Figure 3.21 shows stations sampled for DMS/DMSP. Not all measurements were achieved at every station: due to a technical problem, $DMSP_p$ and $DMSP_d$ measurements were only possible in the last part of the cruise.

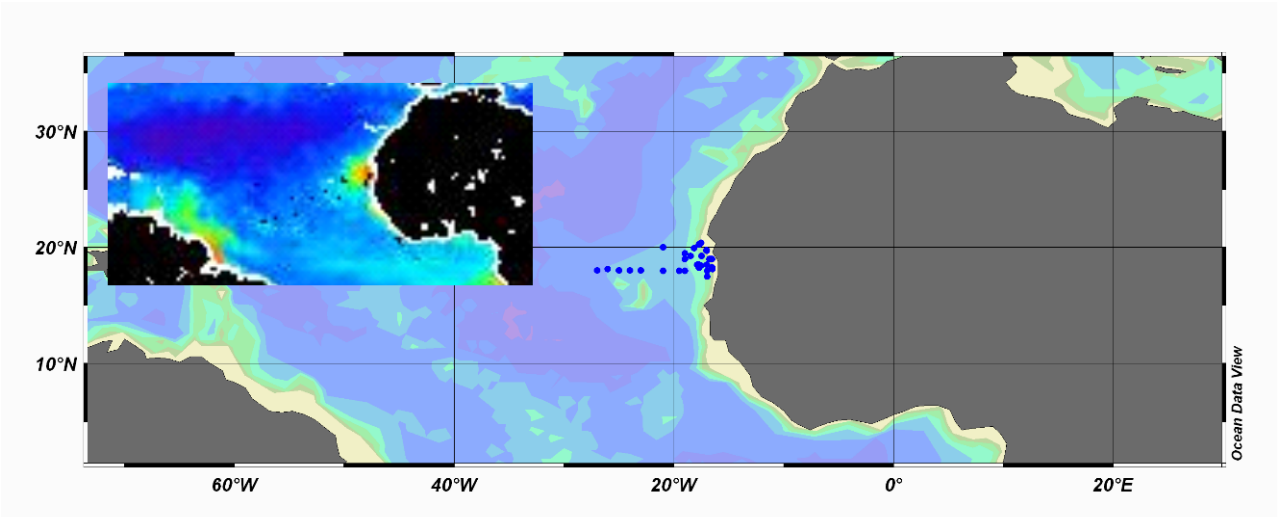

Fig. 3.21 DMSP/DMS sampling stations during METEOR Cruise M68/3. Inset shows SeaWiFS image of surface chlorophyll in June 2006

Figure 3.22 shows DMS concentrations along the 18°N transect. DMS ranged from below detection to 14 nM (mean 1.9 nM, n = 171). Notably elevated DMS concentrations occurred at 3 stations, and at 2 of these stations, DMS was associated with an upwelling event. $DMSP_d$ showed a close relationship with DMS (mean 2.3 nM, n = 64) whilst $DMSP_p$ was higher (mean 7.5 nM, n = 64). Naturally, all DMS/P parameters showed a distinct relationship with phytoplankton biomass, i.e. elevated concentrations above the mixed layer depth. DMSP-lyase showed a similar pattern, and was concentrated above the mixed layer depth, with a maximal concentration of 45 nM DMS/h (Figure 3.22).

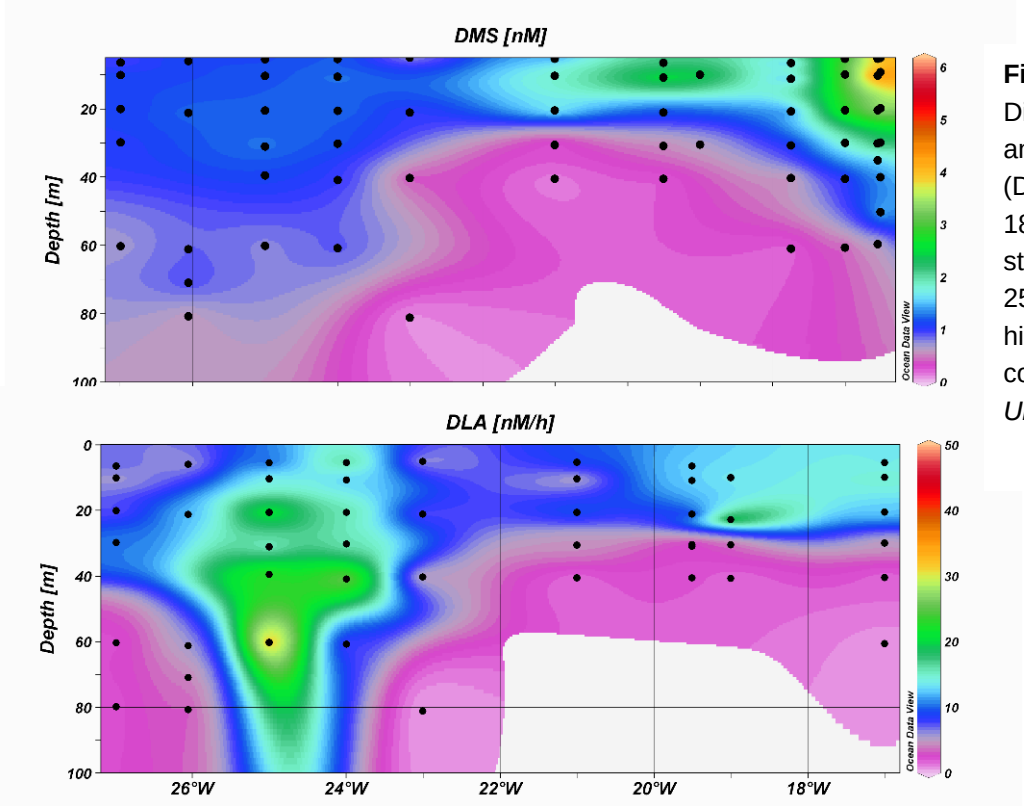

Fig. 3.22 Dimethylsulphide (top) and DMSP-lyase activity (DLA, bottom) along the 18°N transect. The strong peak in DLA at 25°W corresponds to high numbers of the coccolithophore *Umbellosphaera*

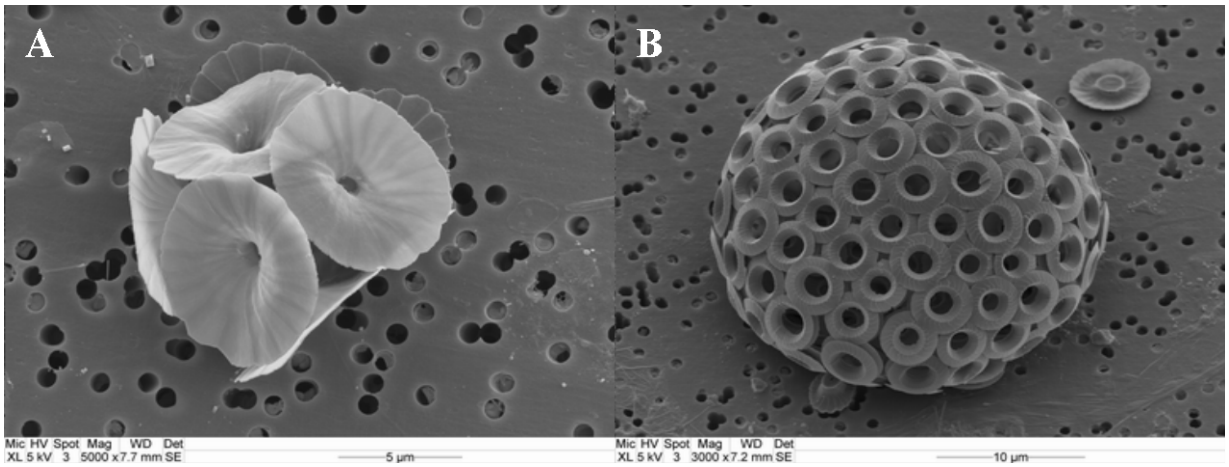

Fig. 3.23 Open-ocean coccolithophores important at 25°W. A - *Umbellosphaera irregularis*; B - *Umbilicosphaera sibogae*. These two species were important components of the biomass in oceanic waters, whereas other species, such as *Emiliania huxleyi*, were important closer to the coast

We recorded a distinct change in the phytoplankton community along the 18°N transect. Offshore, at around 25°W, open ocean coccolithophores such as *Umbellosphaera* and *Umbilicosphaera* (Figure 3.23) showed a strong subsurface peak in biomass, in waters which were otherwise quite low in phytoplankton biomass. East of 22°W on the 18°N transect, species composition became more diverse, with higher abundances of ciliates, flagellates, dinoflagellates, diatoms, cyanobacteria and coccolithophores recorded.

According to the underway data, the most distinct upwelling event was encountered at 20°N at a series of stations analyzed on an outward transect. This corresponds to the point where the Canary current leaves the coast and is a location of year-round upwelling. We recorded a peak in DMS early on in the transect where the underway system later indicated maximal upwelling. The upwelling event was confirmed in our diatom counts, which indicated biomasses of up to 150 mg C m^{-3}, in the upwelled water. At the point earlier on in the transect where DMS was maximal, biomass was spread more evenly between taxa.

3.4.7 Production of Hydroxylamine, Nitrous Oxide and Methane

(Alina Freing, Hermann W. Bange)

The scope of this field program can be summarized as follows:

- Determination of the N_2O surface distribution in the area off Mauritania during the non-upwelling season;
- Determination of the N_2O distribution in the water column;
- Functional gene analysis of the N_2O formation pathways;
- Comparison with results from the POSEIDON cruise P320/1 off Mauritania during the upwelling season in March/April 2005;
- Quantification of the N_2O emissions off Mauritania;
- Identification of the major N_2O formation pathway;
- Quantification of the physical contribution to the N_2O emissions.

Sampling

In order to achieve these goals, the following approaches were used:

- Continuous surface measurements of N_2O (atmosphere and ocean) north of 18°N;
- Measurements of N_2O/NH_2OH depth profiles along zonal transect at 18°N;
- Filter sampling (3 depths: surface, O_2 minimum, deep waters) for functional gene analysis at selected stations.

Methods

N_2O was measured on board with a GC/ECD system. For the determination of N_2O in the water column, triplicate samples (at each depth) were drawn from the rosette and equilibrated with helium. After equilibration, a sub-sample of the headspace was injected manually into the GC/ECD with a gas tight syringe. Continuous measurements in the surface mixed layer were performed with a seawater-gas equilibrator (Weiss-type) connected to the GC/ECD system. Ambient air was pumped continuously from the "Peildeck". The measurements were calibrated by using two certified standard gas mixtures of N_2O in synthetic air.

For the determination of NH_2OH, also triplicate samples were drawn from the rosette. After sampling, NH_2OH was converted to N_2O with Fe^{3+}(aq.) and then the samples were equilibrated with helium. After equilibration, a sub-sample of the headspace was injected manually with a gas tight syringe. NH_2OH was determined as the difference between background N_2O (measured as described above) and N_2O resulting from the conversion of NH_2OH. Recovery factors were determined at each station where NH_2OH was measured.

For filter sampling, four liters of seawater were filtered through polycarbonate filters (2 µm pore size, 47 mm diameter) and frozen for later analysis at IFM-GEOMAR in Kiel.

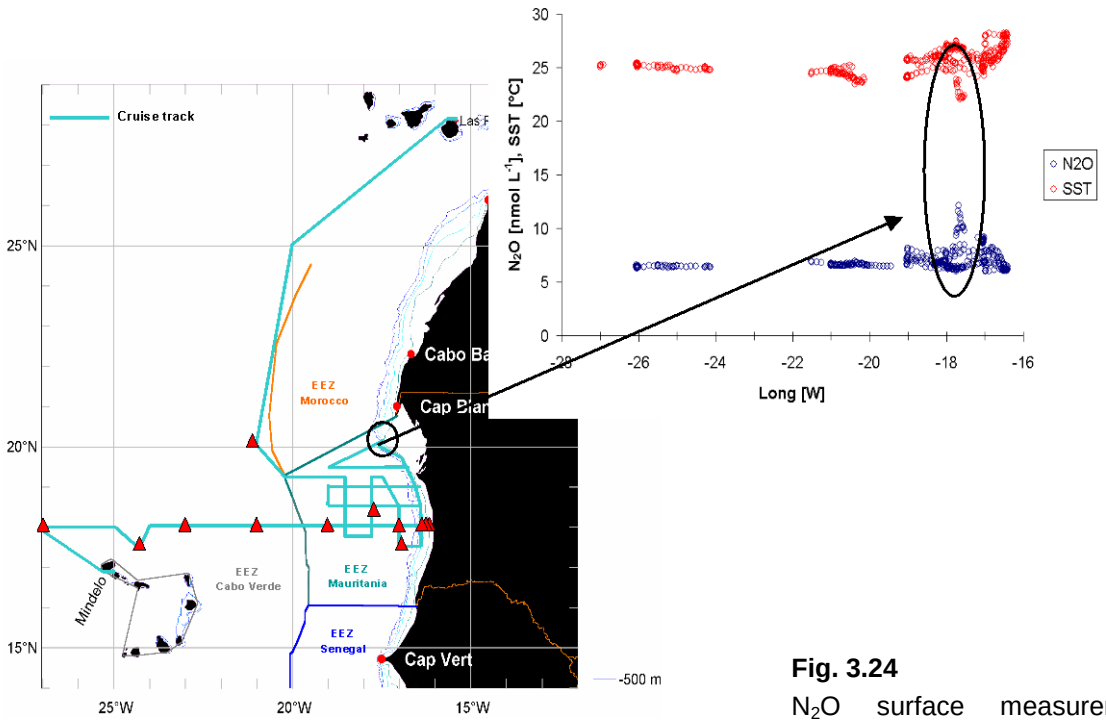

Fig. 3.24
N_2O surface measurements along the cruise track of M68/3

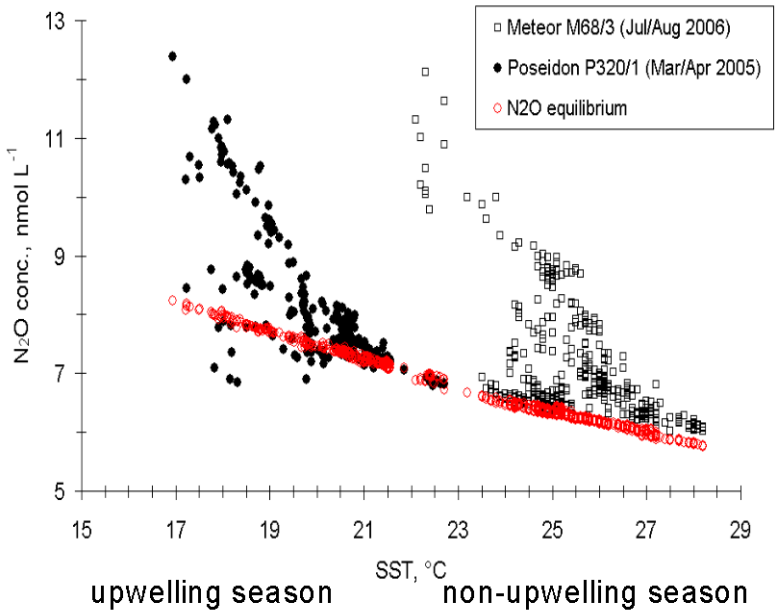

Fig. 3.25 Comparison of N_2O surface measurements off Mauritania during upwelling (data from cruise P320/1, Gebhardt and Bange, unpublished) and non-upwelling (M68/3)

Preliminary Results

The mean atmospheric N_2O dry mole fraction during the cruise was 319 ± 2 ppb. This is in agreement with N_2O measurements from the AGAGE and WMO-GAW global greenhouse gas monitoring networks. N_2O surface concentrations were generally low, except in areas with weak upwelling. Enhanced N_2O concentrations were associated with decreased sea surface temperatures (Fig. 3.24). The mean N_2O surface saturation in the open ocean was 104 ± 3 %. The maximum saturation of up to 177 % was observed in the coastal upwelling region. The N_2O surface concentrations measured during the non-upwelling season (M68/3) are in the same range as those measured during the upwelling season in March/April 2005 (P320/1) (Fig. 3.25).

The water column distributions of N_2O and NH_2OH at stations along the 18°N transect are shown in Fig. 3.26. Maximum N_2O concentrations (up to 35 nmol L^{-1}) were found in the oxygen minimum zone (OMZ). In general, N_2O concentrations were well correlated with oxygen (O_2) concentrations. NH_2OH concentrations were highly variable and ranged from not detectable to about 50 nmol L^{-1}. Enhanced NH_2OH concentrations were usually observed in the OMZ, whereas NH_2OH concentrations in the surface and deep layers tend to be very low. We found no relationships between NH_2OH and O_2 or N_2O. A simple water mass analysis of the main water masses found in the OMZ of the eastern tropical North Atlantic Ocean (i.e. North/South Atlantic Central Waters) revealed that the enhanced NH_2OH concentrations were only found within a narrow range of NACW/SACW mixtures (Fig. 3.27).

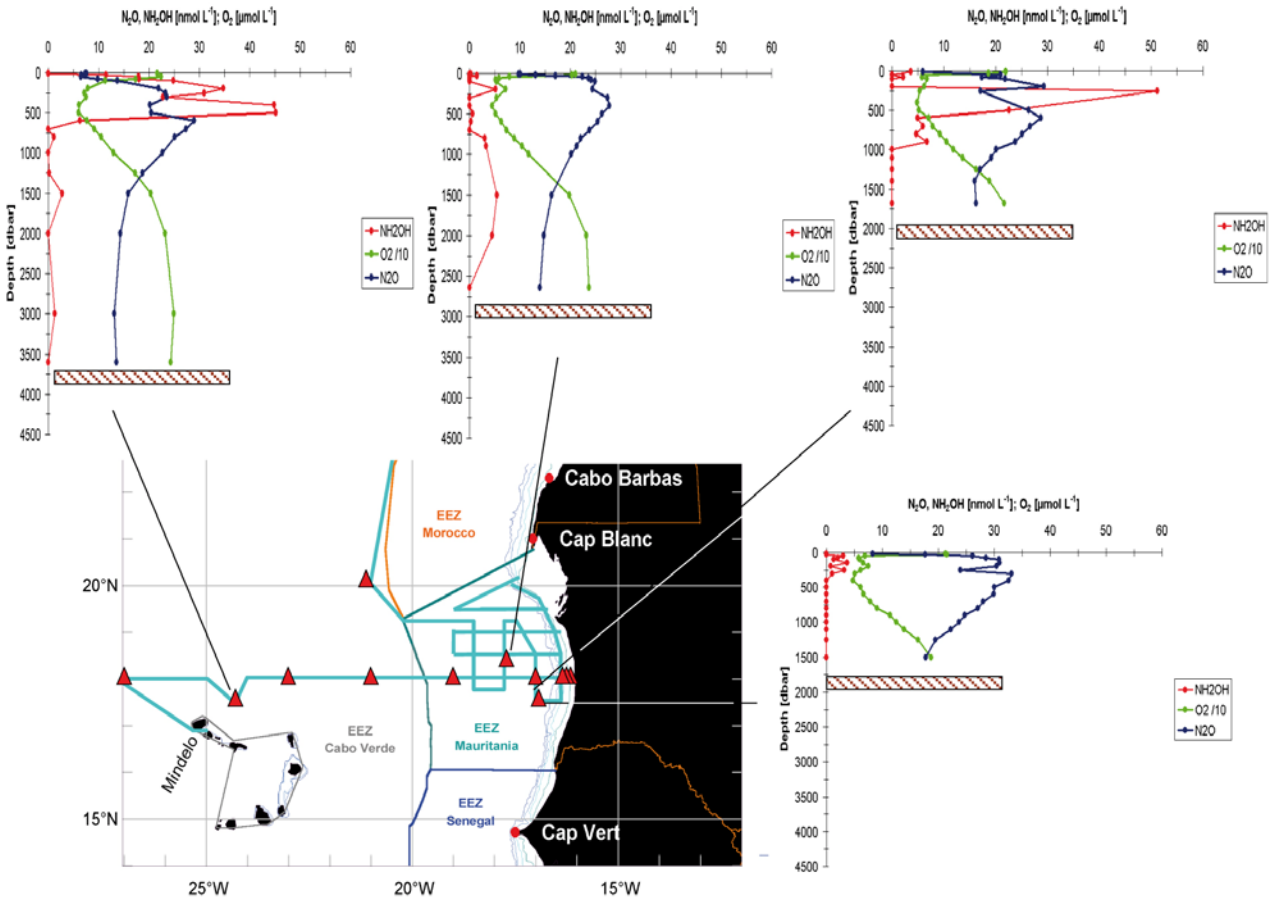

Fig. 3.26 N_2O, NH_2OH and O_2 depth profiles along the 18°N zonal transect. Green line: O_2 conc. in µmol L^{-1} divided by 10; blue line: N_2O conc. in nmol L^{-1}; red line: NH_2OH conc. in nmol L^{-1}

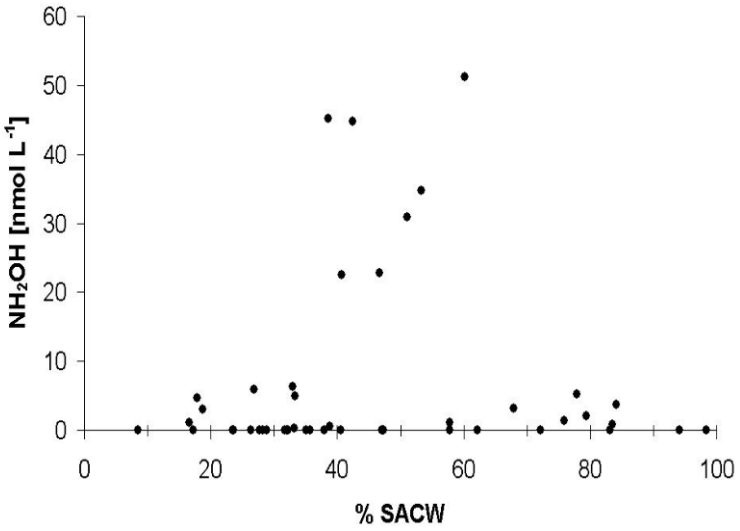

Fig. 3.27 NH_2OH concentrations vs. contribution of SACW in the OMZ during M68/3

The functional gene analysis (carried out jointly with Jörg Süling, IFM-GEOMAR) is ongoing and results are not yet available.

3.4.8 Surface Ocean Diel Cycling of H_2O_2

(Peter Croot, Christian Schlosser, Peter Streu)

Hydrogen peroxide (H_2O_2) is the most stable intermediate in the four-electron reduction of O_2 to H_2O and may function as an oxidant or a reductant. H_2O_2 is principally produced in the water column by photochemical reactions involving dissolved organic matter (DOM) and O_2. Open ocean H_2O_2 concentrations show a distinct exponential profile with a maximum at the surface consistent with the photochemical flux. Concentrations can reach up to 300 nmol L^{-1} in equatorial and tropical regions with high DOM concentrations such as in the Amazon plume in the Atlantic (Yuan and Shiller, 2001). In regions of low DOM and low sunlight, surface H_2O_2 levels are much lower with values in the Southern Ocean of 10-20 nmol L^{-1} (Sarthou et al., 1997). Rainwater is a major potential source for H_2O_2 to surface seawater as it is preferentially removed from the atmosphere, relative to other peroxides, during convective events (Croot et al., 2004).

H_2O_2 can also be produced by biological processes in the ocean with observations from the Sargasso Sea (Palenik and Morel, 1988) and in phytoplankton cultures (Palenik et al., 1987) of production in the dark. Most studies to date suggest that the major production pathway for H_2O_2 in the water column is photochemical production, however in a few cases in the Southern Ocean, distinct H_2O_2 maximums at depth, corresponding to the chlorophyll maximum, suggest a significant biological source of H_2O_2 (Croot et al., 2005). The 'dark decay life-time' of H_2O_2 can vary from hours to weeks in the ocean, but typically may be around 4 days in the open ocean (Plane et al., 1987). Overall the decay rate of H_2O_2 is apparently controlled by several factors: H_2O_2 concentration, colloid concentration, bacteria/cyanobacteria numbers and temperature.

Sampling

During M68-3 samples were taken predominantly from the upper 200 m during most CTD casts and samples were concentrated over the euphotic zone. Deeper samples were often also analyzed to examine the effect of mixing processes bringing H_2O_2 deeper into the water column.

Methods

Seawater samples were obtained using Niskin bottles on a standard CTD rosette. Samples were drawn into 100 mL low density brown polyethylene bottles which were impervious to light. Samples were analyzed within 1-2 h of collection where possible and were not filtered. In the present work H_2O_2 was measured using a flow injection chemiluminescence (FIA-CL) reagent injection method (Yuan and Shiller, 1999). In brief, the chemiluminescence of luminol is catalyzed by the reaction of H_2O_2 present in the sample with Co^{2+} at alkaline pH. H_2O_2 standards were made by serial dilution from a primary stock solution (30 % Fluka - Trace Select). The concentration of the primary standard was determined by direct spectrophotometry of the solution (ε = 40.9 mol L^{-1} cm^{-1}). Secondary standards were analyzed with a spectrophotometric method using Cu(II) and 2,9-dimethyl-1,10-phenanthroline (Kosaka et al., 1998). Seawater samples were measured directly by FIA-CL, while rainwaters were diluted, up to 1:100, with ultrapure water (18 MΩ). Sample concentrations were corrected daily for the reagent blank (Yuan and Shiller, 1999) and for H_2O_2 in the ultrapure water (20-60 nmol L^{-1}).

Samples were analyzed using 5 replicates: typical precision was 2-3 % through the concentration range 1-100 nM, the detection limit (3σ) was typically 0.6 nmol L^{-1}.

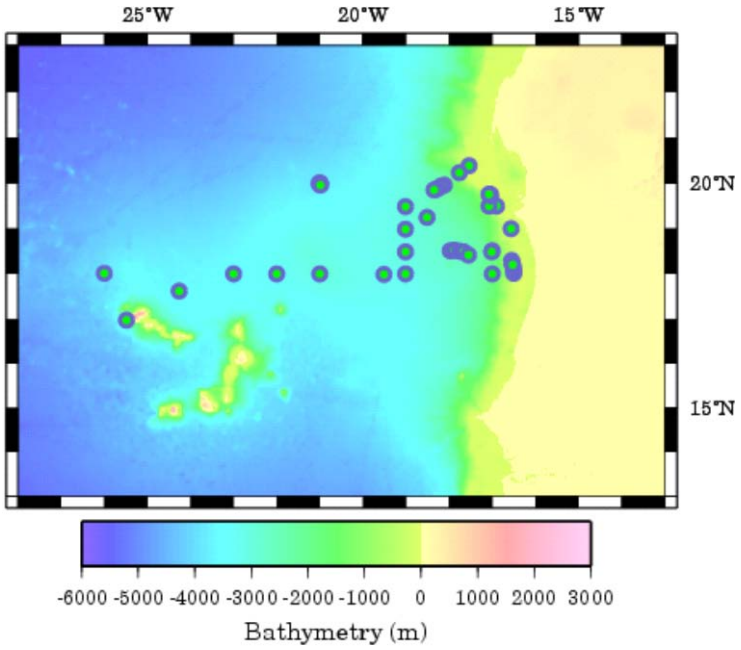

Fig. 3.28 Location of stations sampled for H_2O_2 during M68-3

Preliminary Results

H_2O_2 profiles were measured at 44 stations during the course of M68-3 from a wide range of upper ocean environments (Fig. 3.28). Initial analyses suggest that mixing processes strongly controlled the vertical distribution of H_2O_2 more so than the light attenuation, though presently the influence of the CDOM concentrations on the production has not been factored in. Highest surface concentrations were found in the l shallow coastal waters of the Mauritanian shelf due to significant photochemical production from the higher levels of CDOM found here.

Diel cycles of H_2O_2 were examined during four of the five 24 h drift experiments. These experiments ranged in environments from high productivity waters associated with the shallow shelf regions and upwelling, through to the shelf edge and oligotrophic conditions. Fig. 3.29 shows a strong diel cycle for H_2O_2 in waters along the edge of the Mauritanian continental shelf.

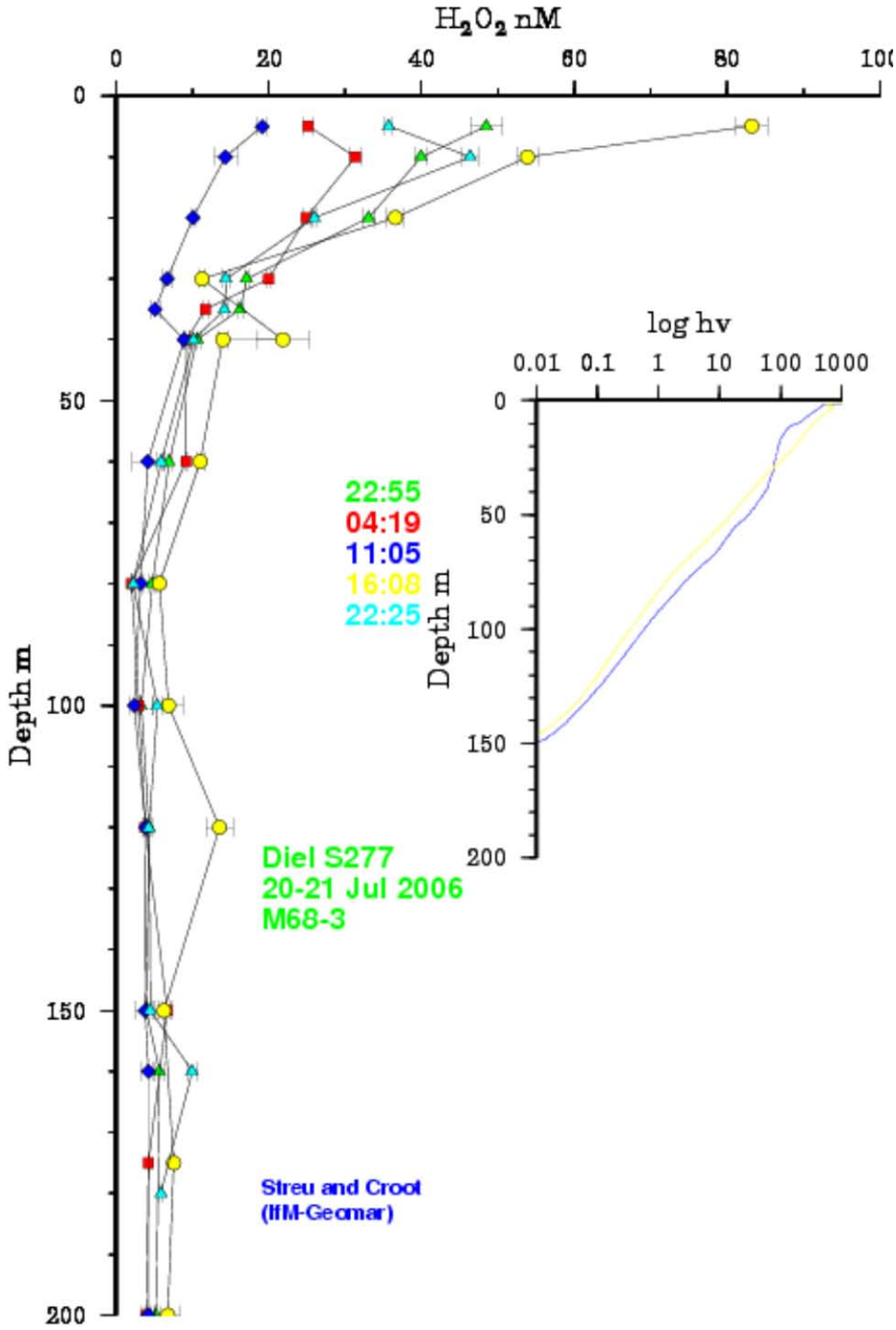

Fig. 3.29 Location of stations sampled for H_2O_2 during M68-3

Later work will include comparing the H_2O_2 profiles with the simultaneous bio-optical measurements made during each CTD cast with the Biospherical Instruments QSP2300 light sensor and the mixing information provided by the CTD and MSS measurements. Using this approach it should be possible to determine the major processes (e.g. active mixing and upwelling, production via photolysis or phytoplankton production of H_2O_2) controlling the distribution of H_2O_2 in the upper water column across the Mauritanian shelf and in the adjacent oligotrophic waters.

3.4.9 Aerosol Iodine Chemistry

(Alex Baker, Manuela Martino)

The aim of the sampling was to collect size-segregated aerosol samples for analysis of soluble nutrient species (Fe, N, P, Si). This complements our on-going UK-SOLAS study in which we are examining the role of the atmosphere in supplying nutrients to the Tropical Atlantic Ocean. The Saharan dust is the largest source of mineral dust to the atmosphere and this dust constitutes an important source of Fe, and to a lesser extent of P and Si, to the remote ocean. Dust inputs to the tropical Atlantic are highest close to the coast of West Africa so that M68/3 offers the possibility to study a system where atmospheric inputs are relatively high.

Sampling

Samples were collected daily throughout the cruise with two two-stage cascade impactors, allowing separation of the aerosol in size of <1 µm and >1 µm. Filters were changed approx. every 23 h, and stored frozen. The determination of aerosol composition is currently on-going at UEA. Aqueous extraction methods are employed for the determination of soluble trace metals (Fe, Al, Mn, Zn), major ions (Na^+, Mg^{2+}, K^+, Ca^{2+}, NH_4^+, Cl^-, NO_3^-, SO_4^{2-}, organic acids) and phosphate and silicate. Soluble trace metal analysis is almost completed and major ion analysis is in progress. Samples will also be analyzed for total trace metal content, and possibly iodine speciation in a subset of the samples too. It is expected that the analyses will be completed in six months. A second collector was operated on behalf of colleagues from the University of Crete (Prof. Nikos Mihailopoulos). These samples will be analyzed for organic nitrogen speciation and tracers of combustion. This analysis is also in progress.

3.4.10 Trace Metals

3.4.10.1 Measurements of Al, Fe and Ti

(Peter Croot, Christian Schlosser, Peter Streu)

It is now well established that Fe can be a limiting nutrient for phytoplankton in High Nutrient Low Chlorophyll (HNLC) regions of the world. It has also been shown recently that Fe can also have an important influence on nitrogen fixation in macronutrient poor oligotrophic regions. Despite the recognition of the importance of iron for primary productivity in the oceans we still know little about the mechanism by which Fe is supplied to the ocean and how processes within the ocean scavenge/uptake or remineralized dissolved Fe.

In many cases examination of other elements similar in chemistry to iron reveals more information on the key processes involved – such elements include Ti(IV) and Al(III). By comparison of the concentrations of these 2 strongly hydrolyzed elements in the soluble, dissolved and particulate phases we hope to be able to better understand the processes affecting dust dissolution and particle scavenging in the surface ocean. The Mauritanian shelf receives the highest dust loading of any oceanic region being strongly affected by dust blown from the adjacent Saharan Desert.

By comparison of the chemistries and distributions of Ti, Al and Fe this study is aiming to improve our knowledge of the processes effecting trace metal distributions in the ocean with emphasis on a severely dust impacted region. The Mauritanian upwelling region is unique in combining high dust deposition with high productivity and gives a perfect opportunity to examine the interaction between organic ligands and iron, and their overall effect on iron solubility. This work follows up early work performed in the same region during M55 (German-SOLAS) and more recently ANTXXIII-1 (German GEOTRACES). The work performed during M68-3 is a further direct contribution to the international programs SOLAS and GEOTRACES.

Sampling

As Fe exists at extremely low levels in seawater, extreme caution is needed in taking samples at sea, because of the potential for contamination from the ubiquitous steel construction of modern research vessels. Thus for the purposes of the present work we employed a variety of techniques for obtaining clean water samples:

- Discrete water samples from depth were obtained via GO-FLO samplers deployed on a Kevlar line. Dissolved samples were collected after filtration through 0.2 µm cartridge filters with slight N_2 overpressure. All sample collection was carried out in a Class 100 Clean Air Container situated on the working deck. Samples were taken from the following depths: 20, 40, 60, 80 m. The working range of the hydrowire was limited to these depths as the wire had become squeezed in places causing the messengers to stick on the wire, particularly in places where the bottles had been secured previously;
- Surface water samples were collected from the IFM-GEOMAR towed fish deployed from a winch on the working deck some 3-4 m from the side of the ship and a depth of 2-3 m. From the fish samples were pumped to the clean lab via a totally enclosed system with suction provided by Teflon diaphragm pumps. The water was then sent to several 20 or 50 L carboys for collection and use for the bioassay experiments carried out during M68-3. Filtered samples were also obtained by drawing a sample through a 0.2 µm cartridge filter during pumping.

Samples for Ti and Al were taken from the CTD (after previous experience during ANTXXIII-1) because in spite of the potential for contamination from Ti and Al components of the CTD itself, initial comparisons of samples from the Niskins from the CTD rosette and the GOFLOs using the Kevlar wire showed no discernable differences between sampling methods. This may be due to the poor solubility, a lack of appreciable redox chemistry under ambient seawater conditions and durability of the oxide coatings on these metals in comparison to iron.

Methods

Samples were analyzed using a combination of online flow injection analysis (FIA) systems: Total Fe as Fe(III) by luminol/H_2O_2 chemiluminescence. Al(III) and Ti(IV) were measured via new voltammetric methods developed at IFM-GEOMAR (Croot, in preparation). For solubility experiments an aliquot of 70 µl of a 15.1 µM ^{55}Fe standard was added to 50 mL of seawater (resulting in a Fe 20 nM solution). The Fe_T and dissolved (<0.02 µm) fraction was then

measured over time: t_0 (0 h), t_1 (3 h), t_2 (6 h), t_3 (24 h), t_4 (48 h) and t_5 (72 h). Samples were filtered using (i) 0.02 µm filter (Antotop) or (ii) Vivaflow® 50 filtration system (100,000 kD, 10,000 kD, 0.2 µm). Samples for ^{55}Fe were measured onboard via liquid scintillation counting.

Fe uptake experiments were performed in collaboration with the Bioassay experiments conducted during M68-3. ^{55}Fe was added to 500 ml of seawater using the same experimental design as for the bioassay work. After 48 h samples were filtered through 0.2 µm filters (Polycarbonate) and the ^{55}Fe content of the particulate and dissolved phases was measured via liquid scintillation counting.

Preliminary Results

The distribution of samples is shown in Fig 3.30. Samples were analyzed for Fe, Al and Ti from 8 GO-FLO stations, with a smaller set of samples for other dissolved elements (Cd, Zn, Pb, Cu, Co, Mn) collected and acidified for return to the laboratory in Kiel for later analysis. The samples for Fe were limited to the upper 80 m while Ti and Al samples from the CTD were also utilized allowing a full depth profile to be obtained.

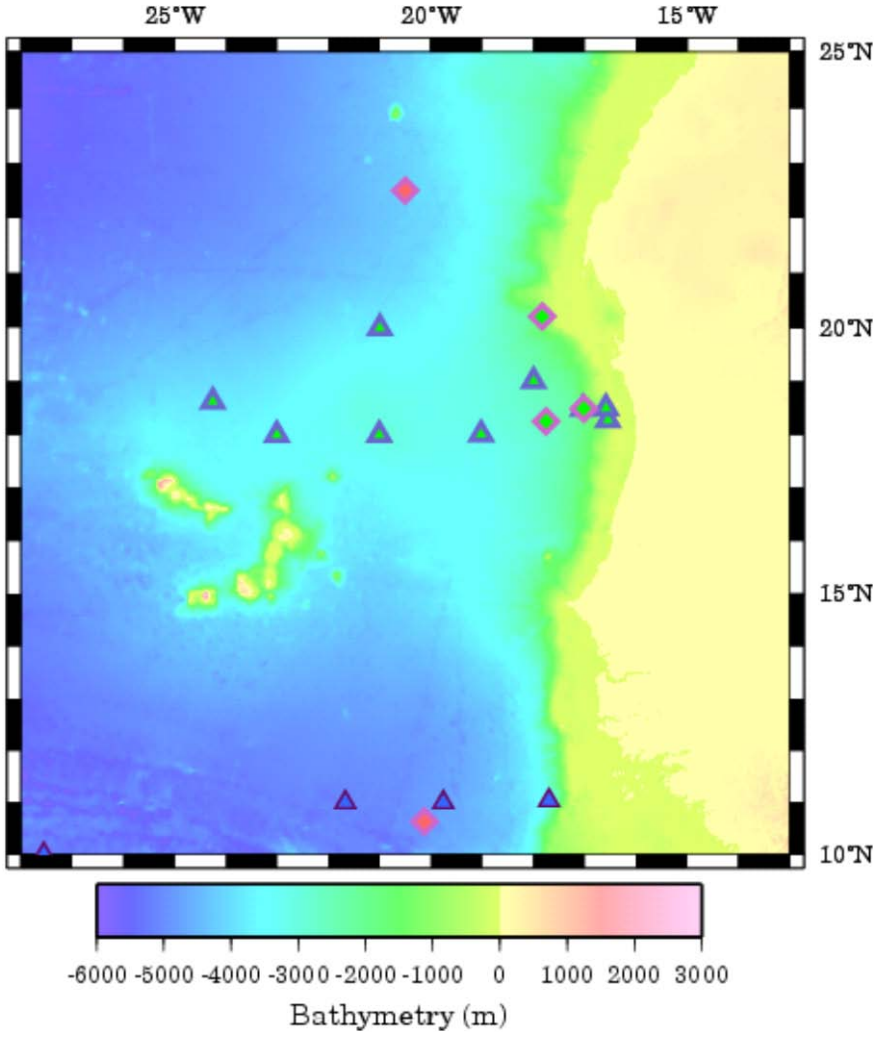

Fig. 3.30
Position of sampling stations for near surface waters for Fe, Al and Ti (GO-FLO casts: green/blue triangles) during M68-3. Deep stations for Al and Ti from M68-3 are also shown (CTD casts: green/maroon diamonds). For comparison to other recent sampling campaigns in the same region, stations from both GEOTRACES (ANTXXIII-1: red/maroon diamonds) cruise and M55 (German SOLAS: blue/purple triangles) are also located on the map

Iron solubility data (Fig. 3.31) showed increases with depth and with proximity to the Mauritanian coast. Preliminary data indicates that soluble Fe in the mixed layer is enhanced in productive waters and is low in oligotrophic waters.

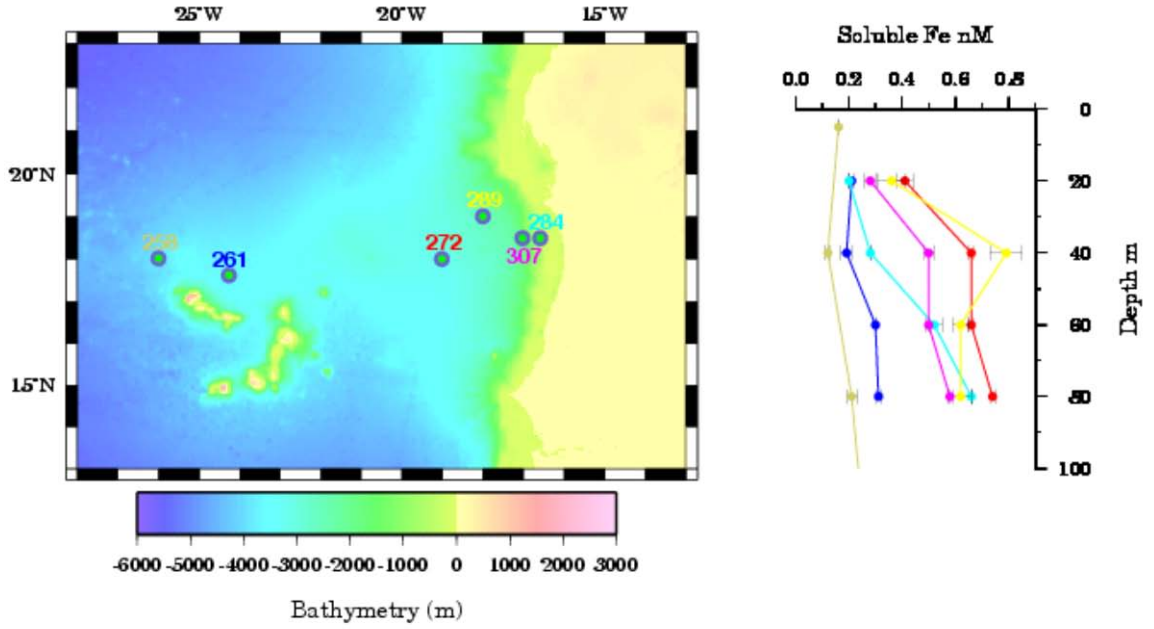

Fig. 3.31 Location of stations (left) sampled during M68-3 for iron solubility (right). Preliminary data from M68-3 for maximum Soluble Fe (source: C Schlosser)

3.4.10.2 Elemental Ratios in Particles

(Peter Croot, Christian Schlosser, Rob Sherrell)

The elemental ratios in surface water particulate matter reflect the nature and formation pathways of the particles themselves and provide valuable information on the processes that formed them. In regions of high productivity the content of the mostly organic particles reflects the concentrations of the bioavailable fraction of the metals in seawater; this may include changes in the Cd:P or Zn:P ratio or in the Fe:P ratio. In contrast in regions with a high dust load, the particles may reflect more the inorganic/crustal signature of the aerosol source regions. By measuring elemental ratios in particles collected during M68-3 we hope to gather further information on how particle supply and production, scavenging and dissolution control dissolved metal concentrations in the open ocean and in turn how this may effect primary productivity.

Sampling

In the present work we obtained surface and near surface samples across the Mauritanian shelf and during the transect from Cape Verde. Sampling was conducted in two modes:

- A limited number of samples (n = 11) were obtained using surface sampling from the IFM-GEOMAR FISH with a trace metal clean Teflon diaphragm pump, This involved collecting 20 L of seawater into a trace metal clean carboy and filtering through either 47 mm quartz or polycarbonate filters. All sample manipulations and filtration took place in a class 100 clean container. The filters were then later dried on the laminar flow bench and stored for later analysis at Rutgers.
- Depth resolved sampling was performed at eight of the SOPRAN stations during M68-3. This involved filtering 2 L of seawater collected from the GO-FLO samplers through 13 mm quartz fibre filters under low N_2 overpressure in a class 100 clean container. Samples were obtained from 20, 40, 60 and 80 m. The filters were then dried in the clean room using a small incubator and stored for later analysis at Rutgers.

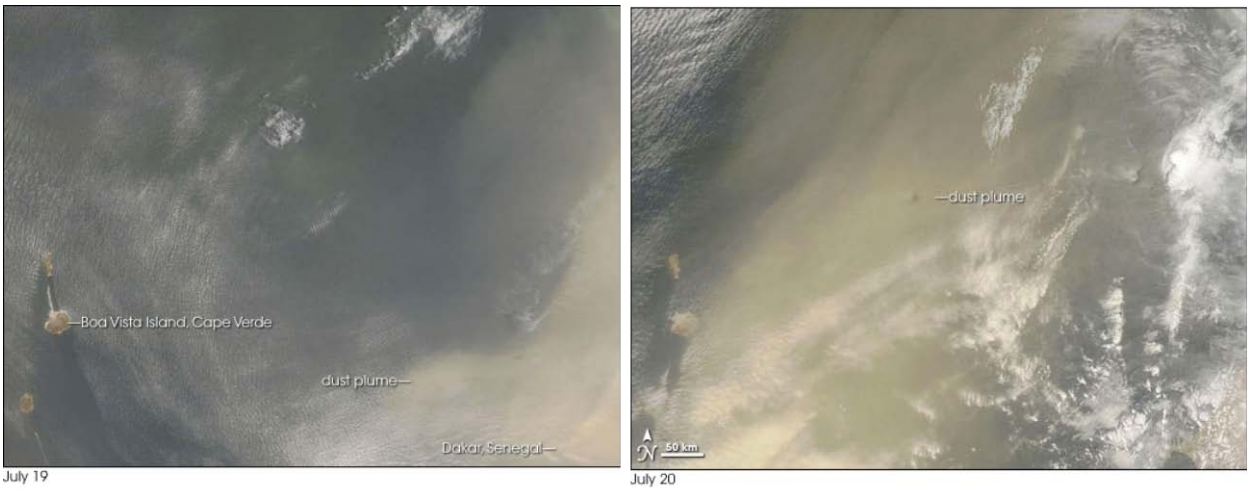

Fig. 3.32 Major dust deposition event encountered in M68-3 over July19-20, 2006. NASA MODIS Terra Satellite images from over Cape Verde (http://earthobservatory.nasa.gov/NaturalHazards/natural_hazards_v2.php3?img_id=13725)

Preliminary Results

During M68-3 a major dust deposition event was observed over 24 h from July 19-20, 2006. This major outbreak of Saharan dust over the study region was clearly seen in Satellite images (Fig. 3.32) and was observed on the METEOR as a decrease in the visibility (Fig. 3.33). The dust was transported in the SAL (Saharan Air Layer) some 1500-4000 m above sea level and so the dust observed at sea level by the Meteor were predominantly larger particles settling out of the overhead dust cloud. These particles were clearly visible on the deck of the ship on the morning of July 20 as coarse red sand covered the entire ship. The same particles were also observed on the filters used for water particle sampling (Fig. 3.34) as observed by microscopy.

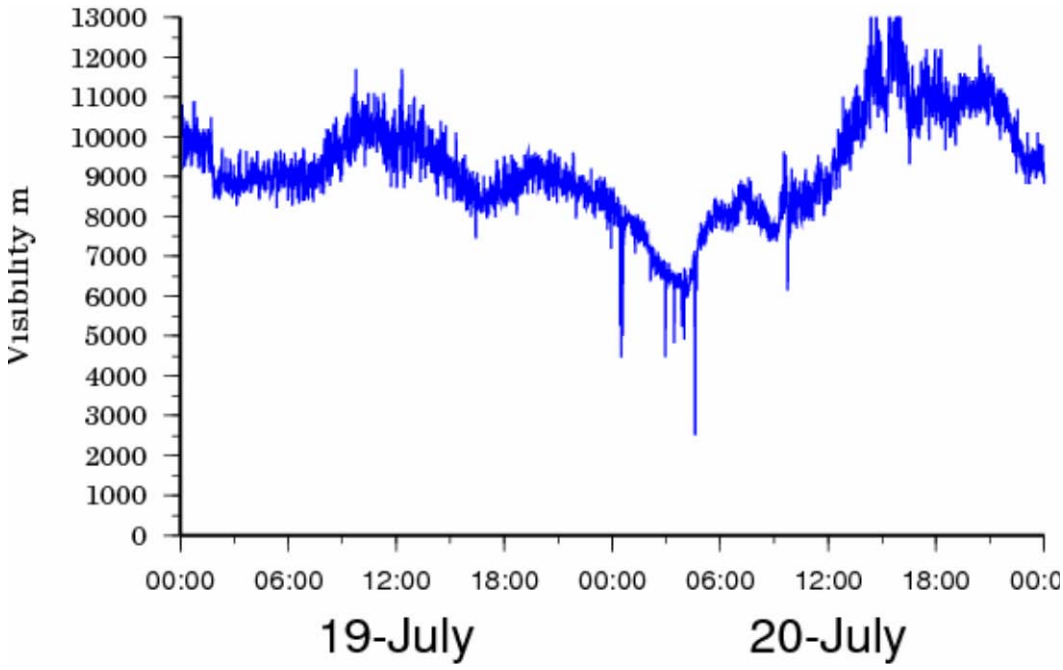

Fig. 3.33 Visibility during a major dust deposition event encountered in M68-3 over July 19-20, 2006

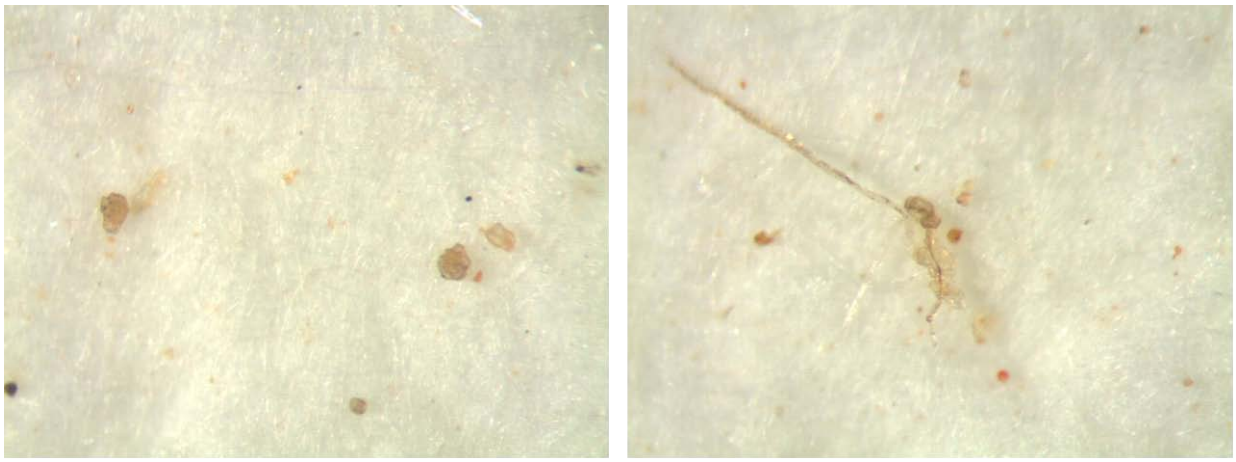

Fig. 3.34 Microscopic 0bservations of Saharan sand particles collected from the water column over July19-20, 2006 (Photos: Rob Sherrell)

Preliminary water column data for dissolved metals also suggests differences in trace metal dissolution rates from this rapid deposition of large particles with elevated concentrations of Pb, Zn and Cu in surface waters and contrastingly higher values of Fe at depth.

The collected samples will be analyzed by ICP-MS in the laboratory at Rutgers. The present study is part of the continuation of a pilot study, begun during the first German GEOTRACES cruise (ANTXXIII-1, Oct-Nov 2005), to examine the feasibility of combining this type of sampling with work on the dissolved metals in the water column carried out by the trace metal group at the IFM-GEOMAR. This is an international collaboration between Germany and the USA as an initial contribution to both German GEOTRACES and SOLAS/SOPRAN.

3.4.11 Nitrogen Fixation and Nutrient Limitations

(Rebecca Langlois, Orly Levitan, Stefanie Pröbst, Christian Schlosser, Peter Croot, Ilana Berman-Frank, Julie LaRoche)

The Nitrogen Fixation Bioassay Group had two main objectives during the M68-3 cruise:

- Assess the limitation of nutrients and effects of CO_2 enrichment on several biological processes and communities;
- Measure size fractionated nitrogen fixation rates and nitrogenase activity throughout one day/night cycle during 24 h drift experiments including vertical distribution and activity of diazotrophs.

In the Atlantic Ocean there is long-standing debate as to whether or not phosphorus is the nutrient limiting phytoplankton productivity. Nutrient enrichment experiments in oligotrophic waters indicate that N limits the rate of primary productivity in many regions of the modern ocean (Graziano et al., 1996; Mills et al., 2004; Moore et al., 2006). However, on geological time scales, nitrogen fixation can increase the nitrogen inventory of the ocean, thus increasing primary production. In turn, nitrogen fixation may be limited by either P (Sanudo-Wilhelmy et al., 2001), Fe (Falkowski, 1997), or both (Mills et al., 2004). Upwelling areas are characterized by seasonal pulses of N-replete waters, however may also experience N-limitation between upwelling events. In recent work, bioassay experiments aboard the Meteor 55 and 60 cruises in the sub-tropical and tropical North Atlantic showed that phytoplankton productivity and biomass were nitrogen limited while the active diazotrophic (N_2 fixing) community was phosphorus and iron co-limited and bacterial productivity was nitrogen and phosphorous co-limited (Mills et al., 2004; Moore et al., 2006; Mills et al., submitted).

Using the Meteor 55 and 60 cruises as a framework, we carried out similar bioassay experiments investigating the nutrient limitation of CO_2 fixation, chlorophyll a biomass, and N_2 fixation during Meteor 68-3. In most experiments we also tested the effects of elevated CO_2 conditions on the parameters listed above. As nitrogen is fixed diurnally by some bacteria and nocturnally by others, we used the 24 h drift stations as an opportunity to investigate when nitrogen is being fixed and by who through ^{15}N nitrogen fixation rate measurements and nitrogenase activity. Additionally, samples were collected from CTD casts in order to characterize and compare the diazotrophic community and photosynthetic parameters in upwelling and oligotrophic areas.

Sampling and Measurements: Nutrient Bioassay Experiments

Trace metal clean techniques were used throughout the preparation and execution of the experiments. Surface seawater was collected (~2-5 m) after dark using a trace metal clean diaphragm pump. Seawater was pumped into one 60 L carboy from which it was siphoned into 4.5 L acid-washed polycarbonate bottles. Nutrients were added alone and in combination to nominal final concentrations of 1.0 µM NH_4^+ + 1.0 µM NO_3^- (N), 0.2 µM NaH_2PO_4, 2.0 nM $FeCl_3$ and 2 µM NO_3^-. An atmospherically processed Moroccan dust and a soil sample from Glomar Chall were added to an additional set of bottles to concentrations of ~2 mg L^{-1}. After filling, bottles were sealed and placed in on-deck incubators with circulating surface seawater.

For each treatment, incubations were run in quadruplicate over 48 h with nitrogen fixation and primary productivity rate measurements made during the final 24 h. Samples from three of the quadruplicates were taken and measured on-board for fluorescence parameters (using the Satlantic Fluorescence Induction and Relaxation, or FIRe, instrument), chlorophyll, nutrients, ammonium, ^{3}H Bacterial productivity, and iron. Fluorescence parameters such as F_0, F_m, variable fluorescence, maximum photosynthetic yield, absorption cross sections, turnover times of the electron acceptors were measured with the FIRe instrument. Samples for analytical flow cytometry, $^{15}N_2$ Fixation, and $^{13}CO_2$ assimilation were collected in triplicate for measurement in the laboratory. One sample for *nifH*, 16s, and 18s gene analyses was taken from each treatment to be measured in the laboratory. Simulated in situ incubations were conducted in Perspex flow-through incubators cooled by flowing surface seawater. Light was attenuated to 30 % of incident surface values by blue filters.

Three bioassay experiments looked at the effects of higher CO_2 levels in addition to added nutrients. The water was collected and amended in the same way as described previously, except that either ambient air or 900 ppm CO_2 in an air mixture was bubbled through the bottles for roughly 40 h prior to the initiation of the tracer incubations. Once the water samples were equilibrated with ambient air or higher CO_2 levels, rate measurements were initiated and all other parameters were measured, as described previously. The samples from these experiments, except those for FIRe, chlorophyll, nutrient and bacterial productivity need to be analyzed in the lab or are waiting to be worked up (Fig. 3.35).

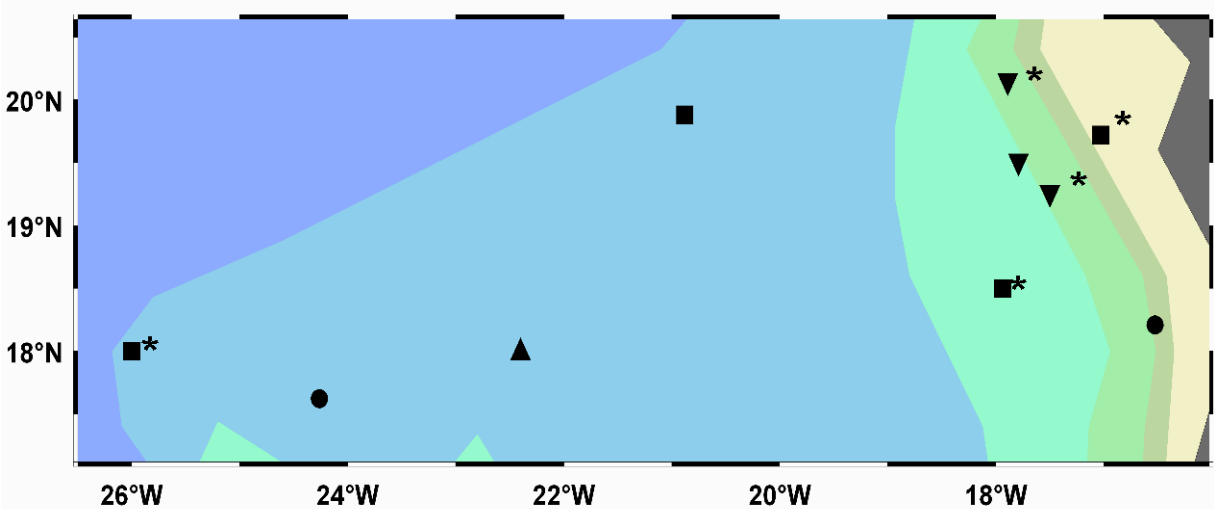

Fig. 3.35 Locations of bioassay experiments. Symbols are as follows: ■ 24 h drift station, ▲ nutrient addition bioassay, ▼ CO_2 bioassay, ● CTD station. Symbols marked with '*' indicate locations where samples were cloned

Sampling and Measurements

We took part in four 24 h drift experiments. Sampling was done in two parts: for $^{15}N_2$ fixation and $^{13}CO_2$ assimilation rates water was collected as for bioassay experiments and profiles were made using the CTD casts for diazotroph activity and distribution. The light cycle was split into four 6-h time periods (21:00-3:00, 3:00-9:00, 9:00-15:00, 15:00-21:00 LT). Profiles were

collected in the middle of these time periods. These times were based on the maximum activity of the nitrogenase enzyme in *Trichodesmium*. Samples for FIRe, POC/PON, and HPLC were collected in addition to the parameters measured for the bioassay experiments. As with the bioassay experiments, most samples still need to be analyzed (Fig. 3.35).

We conducted four bioassay experiments, three of which were CO_2 enrichment experiments, and measured four 24 h drift stations (Fig 3.35). From both program parts we collected a total of 150 analytical flow cytometry samples and chlorophyll samples, 80 HPLC and POC/PON samples, 150 samples for stable isotope (^{15}N and ^{13}C) analysis, 200 samples for genetic analysis including samples from two plankton tows, and made FIRe measurements. We also collected one filter from about 200 L seawater for a metagenomics project. In order to build depth profiles for fluorescence parameters along the cruise track, FIRe profiles and several underway surface FIRe measurements were made throughout the cruise, totaling 738 measurements.

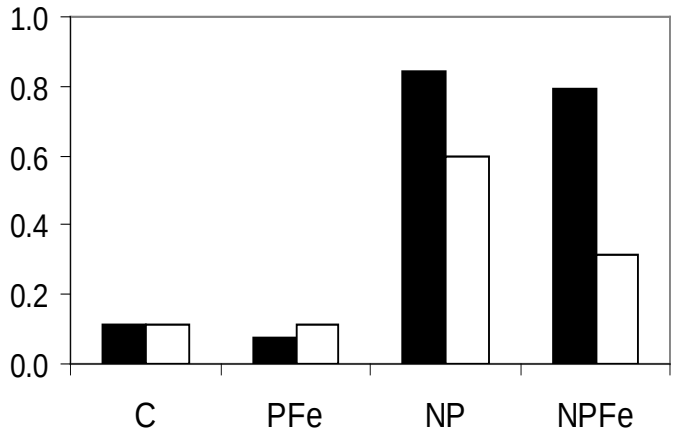

Fig. 3.36 Chlorophyll a (mg L^{-1}) data from CO_2 bioassay experiment 1. Black bars indicate treatments with high CO_2 and white bars have ambient CO_2 levels

Preliminary Results

All experiments were conducted in oligotrophic waters (initial NO_3 conc. of 0.09, 0.19, and 0.10 µmol L^{-1}) and indicated that the plankton and bacterial communities were N or NP limited (Fig 3.35). Both chlorophyll *a* (Fig. 3.36) and intrinsic fluorescence (F_0) measurements (Fig 3.37) showed a slight increase with higher CO_2 levels. Dissolved inorganic carbon (DIC) was measured during the third CO_2 experiment and increased in high CO_2 treated bottles, however it seems that the change in biomass was mainly due to NP additions, as seen by F_0 and maximal fluorescence (F_m, Fig. 3.37). Conversely, bacterial productivity data from the first CO_2 experiment showed a repression of production with higher CO_2 levels (Fig. 3.38). Chlorophyll *a* analysis from two CTD casts and the drift stations showed that the deep chlorophyll max was around 30-40 m (Fig. 3.39a) and between 50-80 m for stations in the far western part of the cruise track. FIRe data (F_v/F_m) from the mooring station showed peaks in the surface and at 80 m (Fig. 3.39b). Genetic material has been extracted and isolated from all CO_2 bioassay and 24 h drift samples. To date the *nifH* gene was found to be present in all experiments, except for CO_2 bioassay 1 and drift experiment 4. At present *nifH* clone libraries are being produced from the

initial samples of each experiment in order to characterize the diazotroph community. Remaining molecular analyses (such as phylogenetic analysis and real-time qPCR) should be completed in the next five months. FIRe data for the bioassay experiments has been analyzed and the remaining depth profiles will be analyzed upon request. Stable isotope measurements will be completed next month. About three months of work remain for analyzing the HPLC and POC/PON samples. The flow cytometry samples will take about six months to analyze.

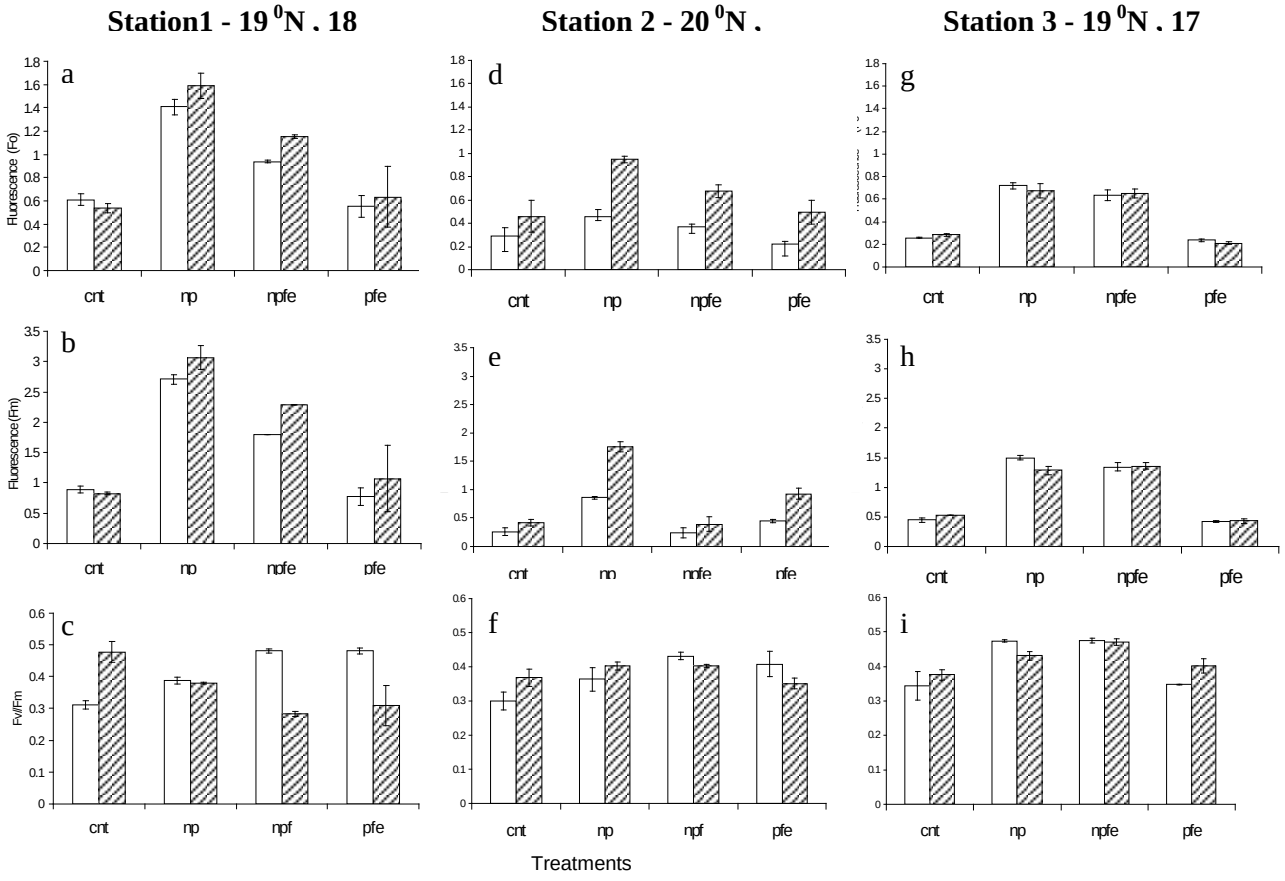

Fig. 3.37 FIRe results from the three CO_2 bioassay experiments: C01 (a-c); C02 (d-f) and C03 (g-i). Panels (a), (d) and (g) show the intrinsic fluorescence (F_0), panels (b), (e) and (h) show the maximal fluorescence (F_m), and panels (c), (f) and (i) are maximal photosynthetic yields as calculated by F_v/F_m. All variables shown are an average of two samples from one treatment bottle. Error bars represent ±1 standard deviation. White bars indicate ambient CO_2 treatments, while striped bars are high CO_2 treatments

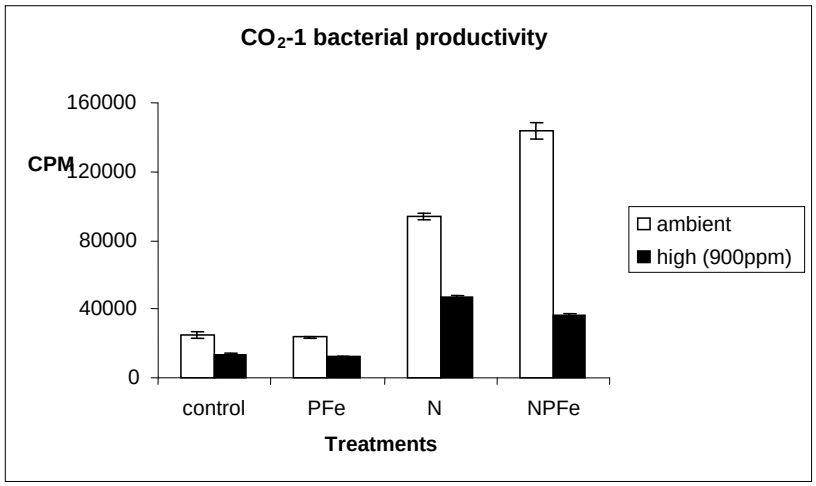

Fig. 3.38 Bacterial productivity results from the first CO_2 experiment

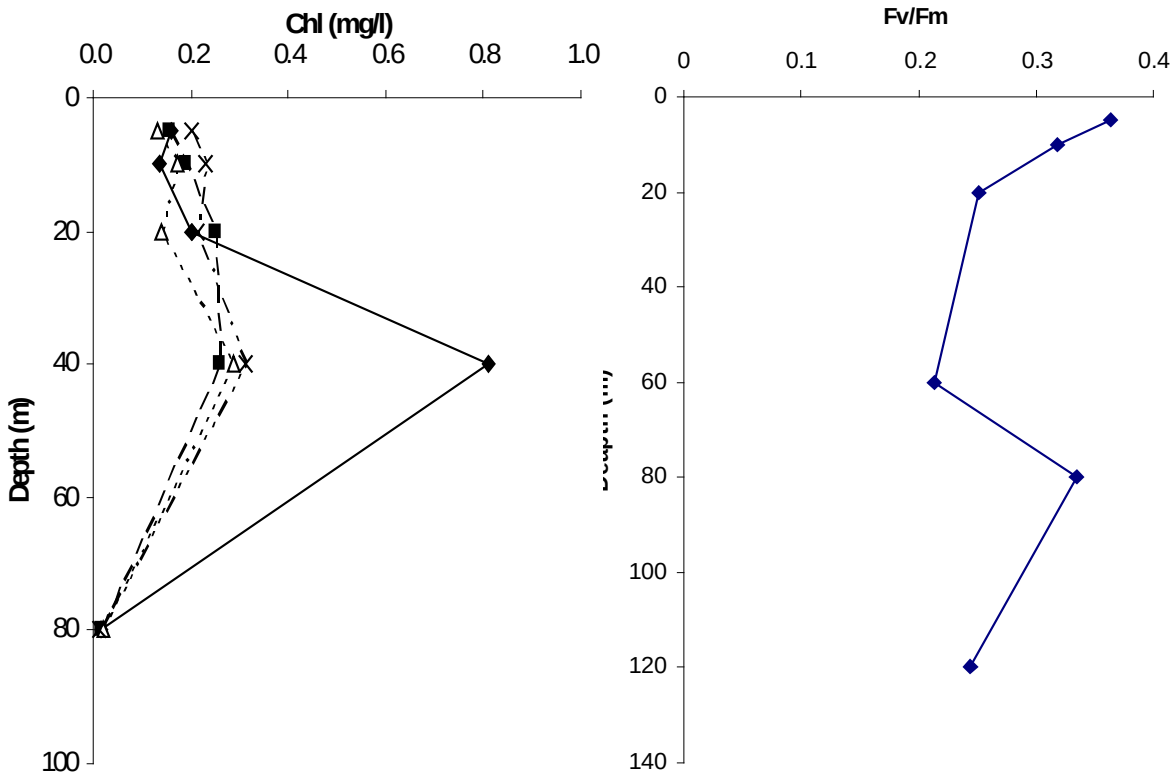

Fig. 3.39 (a) Chlorophyll *a* (mg L^{-1}) from a typical drift experiment. Profiles were collected at the following times: ◊-0000, ■-0600, ∆-1200, x-1800. (b) Profile of the maximum photosynthetic yield, calculated as F_v/F_m, from the Cape Verde times series site (15.07.06)

3.4.12 Upwelling Velocities from Helium Isotopes

(Jan Aschmann, Monika Rhein)

Upwelling regions are important for the supply of trace gases, nutrients and trace metals from the ocean's interior into the mixed layer. Upwelling is also a key process for the air-sea flux of organohalogen species, produced below the mixed layer (e.g. bromoform). It also plays an important role for the maintaining of the equatorial cold tongue, influencing the West African climate. Direct measurements of the upwelling have been hampered by the small speeds involved. Instead, vertical motion has to be estimated by indirect methods. Klein and Rhein (2004) proposed a new approach to infer upwelling velocities by exploiting the helium isotope disequilibrium between atmosphere and oceanic mixed layer. During M68/3, on every other station, 6-8 helium samples have been taken in the upper 150 to 300 m to obtain a data set, suitable for the estimate of the upwelling velocites. In total, about 270 samples have been taken. Preparation and analysis of the samples are carried out in the dedicated mass spectrometer in our department at the University Bremen. The gases have been already extracted from the water samples, and the analysis are being carried out in June/July 2007.

3.5 Station List M68/3 and Instrument Deployments

Table 3.3 CTD casts during R/V METEOR cruise M68/3

Ship expocode	Station No.	CTD Profile No.	Date Start UTC	Time Start UTC	Lat. Degrees Start	Lat. Minutes Start	Lon. Degrees Start	Lon Minutes Start	Water depth	Max Press	No. of Bottles
06ME68/3	**256**	1	7/12/2006	20:29	16° N	58.2'	25° W	29.6'	1977.0	301.0	21
06ME68/3	**257**	2	7/13/2006	6:50	17° N	59.9'	27 °W	0.1'	4326.0	401.0	21
06ME68/3	**257**	3	7/13/2006	8:27	17° N	59.9'	27 °W	0.1'	4325.0	4256.0	21
06ME68/3	**258**	4	7/13/2006	21:20	18 °N	0.1'	26 °W	0.1'	3892.0	1006.0	21
06ME68/3	**258**	5	7/14/2006	0:34	18 °N	2.6'	26 °W	1.8'	3891.0	202.0	21
06ME68/3	**258**	6	7/14/2006	6:35	18 °N	4.8'	26 °W	2.1'	3911.0	198.0	21
06ME68/3	**258**	7	7/14/2006	9:32	18 °N	5.6'	26 °W	3.1'	3920.0	200.0	21
06ME68/3	**258**	8	7/14/2006	12:34	18 °N	7.6'	26 °W	3.3'	3924.0	201.0	21
06ME68/3	**258**	9	7/14/2006	15:31	18 °N	9.7'	26 °W	2.7'	3927.0	201.0	21
06ME68/3	**258**	10	7/14/2006	18:29	18 °N	10.1'	26 °W	2.3'	3925.0	200.0	21
06ME68/3	**258**	11	7/14/2006	21:31	18 °N	10.8'	26 °W	2.0'	3932.0	200.0	21
06ME68/3	**259**	12	7/15/2006	2:12	18 °N	0.1'	25 °W	30.0'	3464.0	1003.0	21
06ME68/3	**260**	13	7/15/2006	6:37	18 °N	0.0'	25 °W	0.1'	3649.0	997.0	21
06ME68/3	**261**	14	7/15/2006	20:01	17 °N	36.5'	24 °W	16.2'	3604.0	11.0	21
06ME68/3	**261**	15	7/15/2006	20:17	17 °N	36.8'	24 °W	16.0'	3606.0	401.0	21
06ME68/3	**261**	16	7/15/2006	21:52	17 °N	37.4'	24 °W	15.7'	3606.0	3584.0	21
06ME68/3	**262**	17	7/16/2006	6:55	18 °N	60.0'	24 °W	0.0'	3651.0	1006.0	21
06ME68/3	**263**	18	7/16/2006	13:00	17 °N	59.5'	23 °W	30.2'	3797.0	1001.0	21
06ME68/3	**264**	19	7/16/2006	17:05	18 °N	0.1'	23 °W	0.2'	3501.0	400.0	21
06ME68/3	**264**	20	7/16/2006	18:25	18 °N	0.1'	23 °W	0.6'	3505.0	3501.0	21
06ME68/3	**265**	21	7/17/2006	1:00	17 °N	59.8'	23 °W	30.3'	3333.0	1001.0	21
06ME68/3	**266**	22	7/17/2006	6:30	18 °N	0.1'	22 °W	0.1'	3296.0	1002.0	21
06ME68/3	**267**	23	7/17/2006	13:00	17 °N	59.7'	21 °W	30.2'	3185.0	991.0	21
06ME68/3	**268**	24	7/17/2006	17:00	17 °N	60.0'	21 °W	0.1'	3075.0	399.0	21
06ME68/3	**268**	25	7/17/2006	18:23	18 °N	0.3'	21 °W	0.7'	3071.0	3040.0	21
06ME68/3	**269**	26	7/18/2006	0:39	18 °N	0.0'	20 °W	30.0'	3120.0	998.0	21
06ME68/3	**270**	27	7/18/2006	6:03	18 °N	0.2'	20 °W	1.1'	3200.0	994.0	21
06ME68/3	**271**	28	7/18/2006	12:00	17 °N	59.4'	19 °W	30.3'	3227.0	989.0	21
06ME68/3	**272**	29	7/18/2006	17:00	18° N	0.0'	19° W	0.0'	3139.0	387.0	21
06ME68/3	**272**	30	7/18/2006	18:20	18 °N	0.5'	19 °W	1.0'	3151.0	3156.0	21
06ME68/3	**273**	31	7/19/2006	0:42	17 °N	60.0'	18 °W	30.0'	3028.0	1001.0	21
06ME68/3	**274**	32	7/19/2006	6:18	17 °N	59.9'	18 °W	0.0'	2804.0	1005.0	21
06ME68/3	**275**	33	7/19/2006	11:50	17 °N	60.0'	17 °W	30.2'	2517.0	1003.0	21
06ME68/3	**276**	34	7/19/2006	16:00	18 °N	0.0'	17 °W	0.0'	1712.0	401.0	21
06ME68/3	**276**	35	7/19/2006	17:16	17 °N	59.9'	17 °W	0.4'	1730.0	1700.0	21
06ME68/3	**277**	36	7/19/2006	22:35	18 °N	0.5'	16 °W	29.9'	193.0	182.0	21
06ME68/3	**277**	37	7/20/2006	4:00	18 °N	3.7'	16 °W	29.9'	190.0	178.0	21
06ME68/3	**277**	38	7/20/2006	10:45	18 °N	9.1'	16 °W	30.8'	185.0	161.0	21
06ME68/3	**277**	39	7/20/2006	15:52	18 °N	13.8'	16 °W	32.1'	199.0	192.0	21
06ME68/3	**277**	40	7/20/2006	22:07	18 °N	18.0'	16 °W	33.1'	202.0	181.0	21
06ME68/3	**278**	41	7/21/2006	1:15	18 °N	0.3'	16° W	25.1'	107.0	101.0	21
06ME68/3	**279**	42	7/21/2006	2:47	18 °N	0.2'	16° W	20.0'	72.0	75.0	21
06ME68/3	**280**	43	7/21/2006	4:20	18 °N	3.1'	16 °W	16.4'	39.0	37.0	21
06ME68/3	**281**	44	7/21/2006	7:09	18 °N	30.0'	16 °W	19.0'	39.0	26.0	21
06ME68/3	**282**	45	7/21/2006	8:14	18 °N	30.1'	16 °W	24.1'	56.0	50.0	21
06ME68/3	**283**	46	7/21/2006	9:25	18 °N	30.1'	16 °W	29.1'	85.0	80.0	21

Ship expocode	Station No.	CTD Profile No.	Date Start UTC	Time Start UTC	Lat. Degrees Start	Lat. Minutes Start	Lon. Degrees Start	Lon Minutes Start	Water depth	Max Press	No. of Bottles
06ME68/3	**284**	47	7/21/2006	11:18	18 °N	29.6'	16 °W	34.6'	182.0	160.0	21
06ME68/3	**285**	48	7/21/2006	15:29	18 °N	30.0'	17 °W	0.0'	1611.0	47.0	21
06ME68/3	**285**	49	7/21/2006	16:01	18 °N	30.4'	17 °W	0.0'	2686.0	992.0	21
06ME68/3	**286**	50	7/22/2006	0:34	18 °N	30.7'	17° W	58.6'	2624.0	1001.0	21
06ME68/3	**286**	51	7/22/2006	6:30	18 °N	31.5'	17° W	53.0'	2484.0	206.0	21
06ME68/3	**286**	52	7/22/2006	13:59	18 °N	30.7'	17 °W	44.6'	2517.0	199.0	21
06ME68/3	**286**	53	7/22/2006	18:58	18 °N	29.4'	17 °W	39.8'	2433.0	245.0	21
06ME68/3	**286**	54	7/22/2006	23:41	18 °N	25.4'	17 °W	33.1'	2433.0	199.0	21
06ME68/3	**287**	55	7/23/2006	9:06	18 °N	29.9'	19 °W	0.0'	3046.0	996.0	21
06ME68/3	**288**	56	7/23/2006	14:21	18 °N	59.8'	19 °W	0.4'	3005.0	1001.0	21
06ME68/3	**289**	57	7/23/2006	20:37	19 °N	0.1'	17 °W	60.0'	2551.0	1003.0	21
06ME68/3	**290**	58	7/24/2006	4:05	19 °N	0.2'	17 °W	0.1'	1172.0	801.0	21
06ME68/3	**291**	59	7/24/2006	6:39	19 °N	0.1'	16 °W	47.1'	194.0	180.0	21
06ME68/3	**292**	60	7/24/2006	9:36	19 °N	0.1'	16 °W	38.0'	85.0	80.0	21
06ME68/3	**293**	61	7/24/2006	12:39	19 °N	0.4'	16 °W	33.8'	67.0	61.0	21
06ME68/3	**294**	62	7/24/2006	20:22	19 °N	30.0'	16 °W	54.1'	72.0	71.0	21
06ME68/3	**295**	63	7/24/2006	21:49	19 °N	30.0'	16 °W	59.1'	103.0	98.0	21
06ME68/3	**296**	64	7/24/2006	23:25	19 °N	30.1'	17 °W	4.0'	552.0	449.0	21
06ME68/3	**297**	65	7/25/2006	6:29	19 °N	30.0'	18 °W	0.3'	2322.0	1001.0	21
06ME68/3	**298**	66	7/25/2006	12:56	19 °N	30.1'	19 °W	0.1'	2975.0	1003.0	21
06ME68/3	**299**	67	7/26/2006	0:32	19 °N	59.7'	18 °W	2.6'	1943.0	1020.0	21
06ME68/3	**299**	68	7/26/2006	6:31	19 °N	57.8'	18 °W	6.0'	2002.0	200.0	21
06ME68/3	**299**	69	7/26/2006	13:01	19 °N	56.1'	18 °W	11.2'	2164.0	200.0	21
06ME68/3	**299**	70	7/26/2006	19:06	19 °N	53.0'	18° W	16.0'	2289.0	201.0	21
06ME68/3	**299**	71	7/26/2006	23:29	19 °N	51.7'	18 °W	20.7'	2401.0	201.0	21
06ME68/3	**300**	72	7/27/2006	12:35	20 °N	23.1'	17 °W	32.0'	64.0	50.0	21
06ME68/3	**301**	73	7/27/2006	13:53	20 °N	18.5'	17 °W	38.4'	117.0	100.0	21
06ME68/3	**302**	74	7/27/2006	15:07	20 °N	14.2'	17 °W	45.1'	728.0	551.0	21
06ME68/3	**303**	75	7/27/2006	16:59	20 °N	11.7'	17 °W	49.3'	1266.0	1000.0	21
06ME68/3	**304**	76	7/28/2006	0:05	19 °N	44.0'	17 °W	3.2'	87.0	79.0	21
06ME68/3	**304**	77	7/28/2006	6:32	19 °N	43.5'	17° W	2.4'	96.0	82.0	21
06ME68/3	**304**	78	7/28/2006	12:58	19 °N	45.0'	17 °W	2.1'	63.0	56.0	21
06ME68/3	**304**	79	7/28/2006	16:00	19 °N	45.2'	17 °W	2.9'	66.0	59.0	21
06ME68/3	**304**	80	7/28/2006	18:58	19 °N	44.7'	17 °W	3.6'	73.0	70.0	21
06ME68/3	**304**	81	7/28/2006	23:31	19 °N	45.9'	17 °W	4.4'	73.0	73.0	21
06ME68/3	**305**	82	7/29/2006	21:14	18 °N	12.3'	16 °W	31.5'	188.0	170.0	21
06ME68/3	**306**	83	7/30/2006	4:19	17 °N	30.0'	16 °W	58.1'	1500.0	1451.0	21
06ME68/3	**306**	84	7/30/2006	6:36	17 °N	29.8'	16 °W	59.1'	1523.0	203.0	21
06ME68/3	**307**	85	7/30/2006	13:51	18 °N	29.9'	17 °W	0.5'	1644.0	1501.0	21
06ME68/3	**308**	86	7/31/2006	0:30	19 °N	15.1'	17 °W	30.2'	1910.0	989.0	21
06ME68/3	**309**	87	7/31/2006	9:40	18 °N	14.8'	17 °W	45.0'	2703.0	2651.0	21
06ME68/3	**309**	88	7/31/2006	12:52	18 °N	15.2'	17 °W	45.0'	2640.0	202.0	21
06ME68/3	**310**	89	8/1/2006	0:59	19 °N	15.0'	18 °W	30.2'	2686.0	801.0	21
06ME68/3	**311**	90	8/1/2006	20:26	20 °N	0.0'	20 °W	60.0'	3734.0	101.0	21
06ME68/3	**311**	91	8/1/2006	22:19	20 °N	0.2'	20 °W	59.8'	3733.0	3737.0	21
06ME68/3	**311**	92	8/2/2006	2:38	19 °N	59.4'	20 °W	59.9'	3741.0	101.0	21
06ME68/3	**311**	93	8/2/2006	7:18	19 °N	60.0'	21 °W	0.4'	3724.0	228.0	21
06ME68/3	**311**	94	8/2/2006	13:00	19 °N	59.8'	20 °W	59.8'	3729.0	201.0	21
06ME68/3	**311**	95	8/2/2006	19:40	19 °N	59.1'	20 °W	59.5'	3727.0	201.0	21
06ME68/3	**311**	96	8/2/2006	23:34	19 °N	57.8'	20 °W	59.3'	3722.0	201.0	21

Table 3.4 Microstructure measurements during R/V METEOR cruise M68/3

Date	Station	CTD cast	Water depth	Time	Start latitude		Start longitude		MSS profiles	max pressure
[UTC]	No.	No.	[m]	[UTC]	degrees N	minutes N	degrees W	minutes W	No.	[dbar]
7/13/2006	**257**	3	4317	11:49	18	1.24	26	59.27	1_3	249
7/13/2006	**258**	4	3891	22:40	18	1.17	25	59.83	4-6	234
7/14/2006	**258**	5	3903	1:15	18	2.90	26	1.90	7-9	245
7/14/2006	**258**	6	3915	7:20	18	5.27	26	2.27	10-12	261
7/14/2006	**258**	7	3924	10:18	18	6.05	26	3.47	13-15	276
7/14/2006	**258**	8	3921	13:15	18	8.01	26	2.90	16-18	251
7/14/2006	**258**	9	3923	16:11	18	9.70	26	2.00	19-21	253
7/14/2006	**258**	10	3928	19:15	18	10.36	26	1.94	22-24	308
7/19/2006	**277**	36	195	23:14	18	0.64	16	29.86	25-27	185
7/20/2006	**277**	36	124	2:39	18	2.97	16	29.19	28-30	124
7/20/2006	**277**	37	189	4:35	18	4.30	16	30.00	31-33	168
7/20/2006	**277**	38	179	10:05	18	8.90	16	30.68	34-36	167
7/20/2006	**277**	38	206	14:30	18	12.60	16	32.10	37-39	212
7/20/2006	**277**	39	212	18:00	18	15.70	16	32.81	40-42	213
7/21/2006	**278**	41	106	1:35	18	0.80	16	24.90	43-46	98
7/21/2006	**279**	42	78	3:07	18	0.80	16	20.10	47-49	72.9
7/21/2006	**282**	45	55	8:32	18	30.49	16	24.15	50-52	53
7/21/2006	**283**	46	88	9:46	18	30.46	16	29.33	53-55	85
7/21/2006	**284**	47	172	10:45	18	29.55	16	33.98	56-58	170
7/24/2006	**291**	59	219	7:35	19	0.11	16	47.79	59-62	170
7/24/2006	**292**	60	84	9:59	19	0.16	16	38.02	63-66	78.8
7/24/2006	**293**	61	66	13:02	19	0.39	16	33.91	67-71	63
7/24/2006	**294**	62	73	20:44	19	30.03	16	54.16	72-76	68
7/24/2006	**295**	63	102	22:14	19	30.21	16	59.44	77-80	99
7/25/2006	**296**	64	550	0:17	19	30.85	17	4.29	81-83	258
7/27/2006	**after 299**	Transect 1	522	5:44	20	15.18	17	44.06	84-89	278
7/27/2006	**after 299**	Transect 1	396	7:38	20	16.68	17	41.48	90-103	231
7/27/2006	**after 299**	Transect 1	89	9:52	20	19.50	17	37.28	104-117	84.1
7/27/2006	**after 299**	Transect 1	72	11:26	20	21.76	17	33.88	118_131	66.8
7/28/2006	**304**	80	81	19:17	19	44.67	17	3.67	132-145	80.2
7/29/2006	**after 305**	Transect 2	416	12:40	18	11.01	16	33.39	146-150	229
7/29/2006	**after 305**	Transect 2	83	16:38	18	11.00	16	25.20	151-175	93
7/29/2006	**after 305**	Transect 2	122	19:10	18	10.78	16	29.07	176-178	124
7/29/2006	**after 305**	Transect 2	152	19:46	18	10.88	16	30.16	179-181	153.4
7/29/2006	**after 305**	Transect 2	176	20:28	18	11.39	16	30.99	182-184	201.9
8/1/2006	**311**	90	3735	21:06	20	0.38	20	59.87	185-187	341
8/2/2006	**311**	91	2729	1:28	19	59.80	20	59.60	188.19	309
8/2/2006	**311**	92	3727	3:08	19	59.20	21	0.20	191-193	311
8/2/2006	**311**	93	3733	6:21	19	59.66	21	1.31	194-196	311.5
8/2/2006	**311**	93	3737	9:19	19	59.94	21	1.16	197-199	274.1
8/2/2006	**311**	94	3736	12:17	20	0.11	21	0.27	200-202	190
8/2/2006	**311**	94	3736	14:14	20	0.10	20	59.50	203-205	299
8/2/2006	**311**	95	3727	18:30	19	59.39	20	59.78	206-208	294
8/2/2006	**311**	96	3724	21:20	19	58.35	20	54.46	209-211	250

Table 3.5 Vertical phytoplankton and zooplankton net hauls during R/V Meteor Cruise M68/3

Station no.	*PN*	*ZPN*	*Latitude*			*Longitude*		
			°	'	*N/S*	°	'	*W/E*
256	X		18	0.02	N	26	59.96	W
	X		18	0.08	N	26	59.89	W
260	X		18	0.59	N	25	0.08	W
		X	18	0.78	N	25	0.32	W
		X	18	0.82	N	25	0.45	W
266	X		18	0.20	N	21	59.96	W
		X	18	0.20	N	21	59.91	W
		X	18	0.25	N	21	59.94	W
270	X		17	59.97	N	20	0.42	W
		X	18	0.13	N	20	0.66	W
		X	18	0.22	N	20	0.81	W
274		X	17	59.95	N	18	0.06	W
		X	18	59.98	N	18	0.01	W
	X		17	59.95	N	17	59.99	W
277	X		18	13.60	N	16	32.20	W
284	X		18	29.92	N	16	35.37	W
		X	18	30.00	N	16	35.44	W
		X	18	30.10	N	16	35.50	W
286	X		18	32.20	N	17	46.31	W
287		X	18	30.15	N	19	2.11	W
		X	18	30.13	N	19	2.52	W
288	X		18	59.90	N	19	0.20	W
	X		18	59.90	N	19	0.30	W
293	X		19	0.21	N	16	33.80	W
		X	19	0.22	N	16	33.82	W
		X	19	0.29	N	16	33.81	W
297	X		19	30.10	N	18	0.07	W
		X	19	30.02	N	18	0.17	W
		X	19	29.99	N	18	0.21	W
299	X		19	54.05	N	18	14.53	W
		X	19	52.63	N	18	17.60	W
		X	19	52.60	N	18	17.82	W
303	X		20	12.47	N	17	43.67	W
305	X		18	11.41	N	16	34.23	W
	X		18	11.10	N	16	33.60	W
306		X	17	29.86	N	16	58.80	W
		X	17	29.77	N	16	58.88	W
307	X		18	29.90	N	17	0.30	W
308		X	19	15.05	N	17	30.24	W
		X	19	15.10	N	17	30.25	W
309	X		18	15.18	N	17	45.14	W
		X	18	15.07	N	17	45.10	W
		X	18	15.02	N	17	45.09	W
311		X	20	0.10	N	21	0.10	W
		X	20	0.10	N	21	0.30	W
		X	19	58.10	N	20	58.02	W

Table 3.6 GoFlo casts (trace metal clean water sampling) during R/V Meteor Cruise M68/3

Station no.	Bottle depths				Latitude			Longitude		
					°	'	N/S	°	'	W/E
261	20	40	60	80	17	37.36	N	24	15.68	W
264	20	40	60	80	18	0.12	N	23	0.59	W
268	20	40	60	80	18	0.19	N	21	0.68	W
272	20	40	60	80	18	0.48	N	19	0.90	W
277	20	40	60	80	18	16.71	N	16	32.68	W
284	20	40	60	80	18	29.81	N	16	35.25	W
289	20	40	60	80	19	0.13	N	18	0.02	W
307	20	40	60	80	18	29.30	N	17	1.70	W
311	20	40	60	80	19	59.20	N	20	59.96	W

Table 3.7 Surface drifter deployments during R/V Meteor Cruise M68/3

Argos ID	WMO #	Date dd.mm.yy	Time UTC	Longitude	Latitude	Sensors
62279	13640	14.07.06	00:12	26 ° 01,50 ' W	18 ° 02,28 ' N	T
62278	13639	19.07.06	22:15	18 ° 29,92 ' W	18 ° 00,30 ' N	T
62277	13638	21.07.06	22:10	17 ° 59,82 ' W	18 ° 30.20 ' N	T
62276	13637	25.07.06	21:16	18 ° 00,33 ' W	19 ° 59.96 ' N	T
62275	13636	27.07.06	23:21	17 ° 03,27 ' W	19 ° 4,15 ' N	T

Table 3.8 Profiling float deployments (ARGO) during R/V Meteor Cruise M68/3

Float S/N	WMO	ID (DEC)	Date dd.mm.yy	Time UTC	Longitude	Latitude	Sensors	Depth	
								Park	Profile
604	WHOI SOLO		18.07.06	16:30	19 ° 01,00 ' W	18 ° 00,00 ' N	T/S/P	1000	1100
551	WHOI SOLO		02.08.06	23:52	20 ° 59.43 ' W	19 ° 58,03 ' N	T/S/P	1000	1100

3.6 Acknowledgements

We would like to express our sincere thanks to

- the RV METEOR Crew for outstanding performance and cooperativeness well beyond the call of duty, and
- Mr. Jemal Ould Abed, our Mauritanian observer, for good cooperation and spirit.

On the occasion of the very last cruise of Captain Martin Kull we address to him our sincere thanks for a great service to the German and international oceanographic community and our very best wishes for the upcoming years – less stressful, more easygoing but still with the same unfailing energy and motivation.

3.7 References

Croot, P.L., Laan, P., Nishioka, J., Strass, V., Cisewski, B., Boye, M., Timmermans, K., Bellerby, R., Goldson, L., de Baar, H.J.W., 2005. Spatial and Temporal distribution of Fe(II) and H2O2 during EISENEX, an open ocean mesoscale iron enrichment. Mar. Chem., 95: 65-88.

Croot, P.L., Streu, P., Peeken, I., Lochte, K., Baker, A.R., 2004. Influence of ITCZ on H2O2 in near surface waters in the equatorial Atlantic Ocean, Geophys. Res. Lett., 31, L23S04.

Fairall, C.W. et al., 2003. Bulk parametrization of air-sea fluxes: updates and verification for the COARE algorithm. J. Clim., 16: 571-591.

Falkowski, P.G., 1997. Evolution of the nitrogen cycle and its influence on the biological sequestration of CO2 in the ocean. Nature, 387: 272-275.

Graziano, L.M., Geider, R.J., Li, W.K.W., Olaizola, M., 1996. Nitrogen limitation of North Atlantic phytoplankton: Analysis of physiological condition in nutrient enrichment experiments. Aquatic Microbial Ecol., 11: 53-64.

Johnson, K.M., Wills, K.D., Butler, D.B., Johnson, W.K., Wong, C.S., 1993. Coulometric total carbon dioxide analysis for marine studies: maximizing the performance of an automated gas extraction system and coulometric detector. Mar. Chem., 44: 167-187.

Kosaka, K., Yamada, H., Matsui, S., Echigo, S., Shishida, K., 1998. Comparison among the methods for hydrogen peroxide measurements to evaluate advanced oxidation processes: Application of a spectrophotometric method using copper(II) ion and 2.9 dimethyl-1,10-phenanthroline. Env. Sci. Techn., 32: 3821-3824.

Mills, M.M., Ridame, C., Davey, M., La Roche, J., Geider, R.J., 2004. Iron and phosphorus co-limit nitrogen fixation in the eastern tropical North Atlantic. Nature, 429: 292-294.

Mintrop, L., Pérez, F.F., González-Davila, M., Santana-Casiano, J.M., Körtzinger, A., 2000. Alkalinity determination by potentiometry - intercalibration using three different methods. Cienc. Mar. 26: 23-37.

Moore, C.M., Mills, M., Milne, A., Langlois, R.J., Achterberg, E.P., Lochte, K., Geider, R., La Roche, J., 2006. Iron limits primary productivity during spring bloom development in the central North Atlantic. Global Change Biol., 12: 626-634.

Palenik, B., Morel, F.M.M., 1988. Dark production of H2O2 in the Sargasso Sea. Limnol. Oceanogr., 33: 1606-1611.

Palenik, B., Zafiriou, O.C., Morel, F.M.M., 1987. Hydrogen peroxide production by a marine phytoplankter. Limnol. Oceanogr., 32: 1365-1369.

Plane, J.M.C., Zika, R.G., Zepp, R.C., Burns, L.A., 1987. Photochemical modeling applied to natural waters. In: Zika, R.G., Cooper, W.J. (eds.), Photochemistry of environmental aquatic systems. American Chemical Society, Washington D.C., pp. 215-224.

Quack, B., Atlas, E., Petrick, G., Schauffler, S., Wallace, D.W.R., 2004. Oceanic bromoform sources for the tropical atmosphere, Geophys. Res. Lett., 31 (23), L23S05.

Richter, U., Wallace, D.W.R., 2004. Photochemical production of methyl iodide in the tropical Atlantic Ocean. Geophys. Res. Lett., 31 (23), L23S03.

Sanudo-Wilhelmy, S.A., Kustka, A.B., Gobler, C.J., Hutchins, D.A., Yang, M., Lwiza, K., Burns, J., Capone, D.C., Raven, J.A., Carpenter, E.J., 2001. Phosphorus limitation of nitrogen fixation by *Trichodesmium* in the central Atlantic Ocean, Nature, 411: 66-69.

Sarthou, G., Jeandel, C., Brisset, L., Amouroux, D., Besson, T., Donard, O.F.X., 1997. Fe and H2O2 distributions in the upper water column in the Indian sector of the Southern Ocean. Earth Planet. Sci. Lett., 147: 83-92.

Yuan, J., Shiller, A.M., 1999. Determination of Subnanomolar Levels of Hydrogen Peroxide in Seawater by Reagent-Injection Chemiluminescence Detection. Anal. Chem., 71: 1975-1980.

Yuan, J., Shiller, A.M., 2001. The distribution of hydrogen peroxide in the southern and central Atlantic ocean. Deep-Sea Res. II, 48: 2947-2970.

CCHDO Data Processing Notes

Date	Person	Data Type	Action	Summary
2013-03-07	Staff, CCHDO	BTL Legs 1 & 2	Website Update	Available under 'Files as received'

The following files are now available online under 'Files as received', unprocessed by the CCHDO.
06MT20060606.exc.csv

2013-03-07	Staff, CCHDO	CrsRpt all legs	Website Update	Available under 'Files as received'

The following files are now available online under 'Files as received', unprocessed by the CCHDO.
Meteor-Bericht_M68.pdf

2013-08-27	Kappa, Jerry	CrsRpt all legs	Website Update	Final PDF version online

I've placed new PDF versions of the cruise report:
06MT20060606do.pdf and
06MT20060712do.pdf
into the directories:
co2clivar/atlantic/meteor/06MT20060606/ (leg 2) and
co2clivar/atlantic/meteor/06MT20060712/ (leg 3).
There is no directory for leg 1 at this time.
The files include all the reports provided by the cruise PIs, summary pages and CCHDO data processing notes for all 3 legs, as well as a linked Table of Contents and links to figures, tables and appendices.